Screening Regulatory Landscape of Sialic Acid Reveals Novel microRNA Biology

by

Faezeh Jamechenarboo

A thesis submitted in partial fulfillment of the requirements for the degree of

Doctor of Philosophy

Department of Chemistry
University of Alberta

Abstract

Sialylation is a crucial post-translational modification that covalently attaches sialic acid to glycoproteins and glycolipids, and is driven by a superfamily of enzymes called sialyltransferases (STs). Alterations in sialylation have been identified in different biological contexts including cancer biology (transformation, progression and malignancies); immunology (cellular communication, cell signaling); infectious dieases (host-pathogen interactions); and neurodegenerative disorders. The expression levels of STs directly impact the cellular sialylation content through which they in turn affect cell normal physiological and pathological status. Protein homeostasis, the balance of proteins, is tuned post-transcriptionally. **mi**cro**RNA** (miRNA, miR) mediate protein expression via direct interactions with corresponding transcript, mainly with 3' untranslated region (3'UTR). In my Ph.D. journey in the Mahal laboratory, I aim to address the query of "how human sialylation is regulated by miRNA?"

In Chapter 2, the miRNA regulatory landscape of α-2,6-sialyltransferases (i.e., ST6GAL1 and ST6GAL2) were profiled using a ratiometric fluorescence assay called "miRFluR". Unexpectedly, the analysis reveals a *bidirectional* tuning of protein expression by miRNA: the *inhibition* of translation and protein *upregulation*. The observed miRNA-mediated protein expressions were validated across different cancer cell lines for their impact on protein, mRNA of ST6GAL1 and ST6GAL2, and α-2,6-sialylation levels. Direct miRNA: 3'UTR interactions, predicted by RNAhybrid or Targetscan, confirmed via mutating the interacting nucleotides and testing WT and mutant pFmiR sensors using miRFluR assay. The scope of the newly discovered miRNA function, protein upregulation in actively dividing cells, were then expanded to co-upregulation of functionally associated proteins by microRNA, a story described in Chapter 3 for

co-*up*regulation of α-2,3-sialyltransferases, ST3GAL1, ST3GAL2 and their glycoprotein substrate CD98hc. The three proteins were recently found to be functionally correlated in melanoma. In Chapter 3, my analysis showed that microRNA *cooperatively upregulate* either CD98hc:ST3GAL1 or CD98hc:ST3GAL2 protein pairs in melanoma cell lines. The direct impacts by miRNA on the protein co-regulation is confirmed by mutational analysis of the corresponding 3'UTRs.

In Chapter 4, the miRNA modulatory axis of another member of α-2,3-sialyltransferases, ST3GAL5, was examined. While its miRNA regulation has been partially investigated by the Mahal laboratory, I screened the potential human miRNA interactome over ST3GAL5 3'UTR via the high-throughput miRFluR assay. ST3GAL5 initiates the ganglioside biosynthetic pathway by providing GM3 substrate for other glycosyltransferases to extend the glycan chain on lipids. Intriguingly, miRNA were identified to mediate both ST3GAL5 expression and cell surface GM3 epitope in different cancer cell lines.

Apart from sialyltransferases, a key enzyme that impacts cellular sialylation levels is CMAS. This enzyme is responsible for providing activated substrate (CMP-sialic acid) for sialyltransferases, accordingly, it can impact both cellular CMP-sialic acid content and sialylation. In Chapter 5, miRNA were identified to both down- and up-regulate CMAS expression as well as sialylation via direct miRNA: CMAS 3'UTR interaction.

Together, my Ph.D. dissertation may help to expand our current understanding of the regulation of sialylation as well as microRNA biology.

Preface

This dissertation is submitted for the degree of Doctor of Philosophy at University of Alberta. The research described in this dissertation was conducted under the supervision of Professor Lara K. Mahal in the Department of Chemistry, University of Alberta within the time frame of September 2019 and August 2024. This Ph.D. dissertation is an original work by Faezeh Jame-Chenarboo.

Research project described in Chapter 2 has been published in the *ACS Central Science Journal* (DOI: 10.1021/acscentsci.2c00748). Under the supervision of Prof. Lara K. Mahal, I was responsible for the performing experiments, conceptualization, data analysis, data visualization as well as the manuscript composition. Hoi Hei Ng assisted with the mutational analysis on Figure 6. Dawn Macdonald advised on the project.

Research project described in Chapter 3 has been deposited on the *bioRxiv* (MS ID # BIORXIV/2024/593635, DOI: 10.1101/2024.05.10.593635). Under the supervision of Prof. Lara K. Mahal, I was responsible for the performing experiments, conceptualization, data analysis, data visualization as well as the manuscript composition. Joseph N. Reyes assisted with the Western blot experiments, mutational analysis, and data visualization in Figures 3 and 8. Nicholas M. Twells assisted with the labeling of diCBM40 lectins. Hoi Hei Ng and Dawn Macdonald assisted with replicating the mutational analysis. Last but not least, Prof. Eva Hernando provides constructive comments and assisted with conceptualization of the project.

Research work conducted in Chapter 4 has not been made publicly available. Under the supervision of Prof. Lara K. Mahal, I was responsible for the performing experiments, conceptualization, data analysis, data visualization. Joseph N. Reyes assisted with Western blot

experiments and mutational analysis. Tigist Tesfaye Batu assisted with conducting RT-qPCR experiments.

Research work performed in Chapter 5 has not been made publicly available. Under the supervision of Prof. Lara K. Mahal, I was responsible for the performing experiments, conceptualization, data analysis, data visualization. Joseph N. Reyes assisted with Western blot experiments and mutational analysis.

Dedication

TO MY PARENTS

for raising me to believe that anything is possible

TO MY LOVE

for your love, presence, and unconditional support

TO MY MENTOR

for your guidance and support

Acknowledgements

First and foremost, I would like to thank my supervisor. I would like to express my gratitude for your support. You are a brilliant person, and it is my tremendous honor to pursue my Ph.D. journey under your mentorship. You always support me to “stay focused” and “motivated” throughout this marathon. Thank you for being an incredible mentor. Thank you for all the science and life lessons and inspiration you always share. Thank you for bringing me to be here which is far higher from where I began. Thank you!

Secondly, I would like to thank my supervisory committee members: Prof. Warren Wakarchuk and Prof. Mathew Macauley, for your tremendously invaluable advice throughout my Ph.D. program.

Thirdly, I would like to thank all of my former and current colleagues in the Mahal laboratory. I would like to express my deep gratitude to all of my friends in the Mahal and other laboratories for all your support, kind words, and providing a serene atmosphere. I would like to acknowledge all of my colleagues and collaborators for strengthening my experience and knowledge.

I would especially like to thank my wonderful parents, thanks for your unwavering belief in me which provides me with the strength and courage to pursue my ambitions and overcome any obstacle that comes my way. Thank you, mom and dad! I would like to thank my siblings, especially, my adorable little sister, Zeinab, who is also my intimate friend. Thank you for always being there for me!

Last but not least, *an exceptional thanks* to the love of my life who is always my best coach, best friend, and my soulmate. Thank you for everything, Majid!

Table of Contents

List of Tables

List of Figures

List of Abbreviations

Abbreviations

Sia	Sialic acid
Neu5Ac	*N*-Acetylneuraminic acid
Neu5Gc	*N*-Glycolylneuraminic acid
CMP	Cytidine monophosphate
CTP	Cytidine triphosphate
UDP	Uridine diphosphate
GNE	Glucosamine(UDP-*N*-acetyl)-2-epimerase/*N*-acetylmannosamine kinase
NANS	*N*-acetylneuraminic acid synthase
NANP	*N*-acetylneuraminate-9-phosphatase
CMAS	Cytidine monophosphate *N*-acetylneuraminic acid synthetase
SLC35A1	Solute carrier family 35 member A1
ST6GAL1	ST6-β-galactoside-α-2,6-sialyltranferase1
ST6GAL2	ST6-β-galactoside-α-2,6-sialyltranferase2
ST3GAL1	ST3-β-galactoside-α-2,3-sialyltranferase1
ST3GAL2	ST3-β-galactoside-α-2,3-sialyltranferase2
ST3GAL4	ST3-β-galactoside-α-2,3-sialyltranferase4
ST3GAL5	ST3-β-galactoside-α-2,3-sialyltranferase5
ST6GALNAc1	ST6-*N*-acetylgalactosaminide-α-2,6-sialyltransferase1
ST6GALNAc5	ST6-*N*-acetylgalactosaminide-α-2,6-sialyltransferase5
ST8SIA	ST8-α-*N*-acetyl-neuraminide-α-2,8-sialyltransferase
STs	Sialyl transferases
SNA	*Sambucus nigra* lectin
Gal	Galactose
GalNAc	*N*-acetylgalactosamine
Glc	Glucose
GlcNAc	*N*-acetylglucosamine
ManNAc	*N*-acetylmannosamine
Siglec	Sialic acid-binding immunoglobulin-like lectins
HCC	Hepatocellular carcinoma
LUAD	Lung adenocarcinoma
OVCA	Ovarian cancer
PDAC	Pancreatic ductal adenocarcinoma
NSLC	Non-small lung cancer
Pca	Prostate cancer
BRCA	Breast cancer

COAD	Colon adenocarcinoma
RNA	Ribonucleic acid
mRNA	Messenger ribonucleic acid
miRNA, miR	microRNA
lncRNA	Long non-coding ribonucleic acid
DNA	Deoxy-ribonucleic acid
RNA Pol II	RNA polymerase II
TF	Transcription factor
AGO	Argonaute
RBP	RNA binding proteins
RISC	RNA-induced silencing complex
AGO1	Argonaute1
AGO2	Argonaute2
AGO3	Argonaute3
AGO4	Argonaute4
TNRC6A	Trinucleotide repeat-containing gene 6A
TNRC6B	Trinucleotide repeat-containing gene 6B
TNRC6C	Trinucleotide repeat-containing gene 6C
FXR1	Fragile X mental retardation syndrome-related protein 1
miRFluR	miR fluorescent ratiometric
CMV	Cytomegalovirus
3'UTR	3'untranslated region
5'UTR	5'untranslated region
poly (A) tail	Polyadenylation tail
EMT	Epithelial to mesenchymal transition
RT-qPCR	Real-time quantitative polymerase chain reaction
PCR	Polymerase chain reaction
W.B.	Western blot
ER	Endoplasmic reticulum
diCBM40	Dicarbohydrate binding module40
Cy3	Cyanine3
Cy5	Cyanine5
FITC	Fluorescein isothiocyanate
FWD	forward
REV	reverse
Gal	Galectin
WT	Wild type
MUT	Mutant
CD98hc	Cluster of differentiation 98 heavy chain
SLC3A2	Solute carrier family3member2

LAT-1	L-type amino acid transporter-1
MFI	Median fluorescence intensity
Cer/mCh	Cerulean over mCherry ratio
MW, M	Molecular weight
LacCer	Lactosylceramide

Glossary of Terms

Sialic acid	nine-carbon keto sugars that terminate *N*-, *O*-glycans and gangliosides.
Neuraminidase, Sialidase	A large family of glycoside hydrolase that cleaves the glycosidic linkages of neuraminic acids.
microRNA	Small non-coding RNA with ~22 nucletotides which regulated gene expression post-transcriptionally.
RISC complex	RNA-induced silencing complex compromise RBPs, cognate miRNA:mRNA functioning in gene regulation.
miRNA seed sequence, seed region	A conserved heptametrical sequence which is mostly situated at positions 2-7 from the miRNA 5′-end.
Non-canonical miRNA:3'UTR interaction	miRNA:3'UTR binding patterns that do not follow seed binding patterns.
miRNA regulatory network	miRNA(s) tune the expression of functionally correlated proteins.
OncomiR	A microRNA that is associated with cancer.
Fluorescence	Emission of photons by an electron returning to ground state from excited state.
Bioluminescence	A chemical reaction between luciferase enzyme and its substrate to produce light.
LAT-1/CD98hc	A light chain protein, LAT-1 is covalently linked with CD98 heavy chain via a disulfide bond, forming a heterodimeric LAT-1/CD98hc complex that belongs to the heteromeric amino acid transporters (HAT) family.
Integrin signaling	Integrins are transmembrane receptors that help cell-cell interactions and cell-extracellular matrix adhesion. Upon ligand binding, integrins activate signal transduction pathways that mediate cellular signals.
Ganglioside	A molecule composed of a glycosphingolipid (ceramide and oligosaccharide) with one or more sialic acids.

Chapter 1

Introduction

1.1 Introduction to sialic acid

Alterations in glycosylation patterns as a hallmark of disease was first described in 1951, however, the molecular details and underlying mechanisms were poorly understood[1,2]. Advances in genomics, proteomics and glycomics have enabled the association of specific glycan structures with disease states. Among the glycans whose changes are associated with transformation between physiological and pathological states are *Sialic acid* (SA, sia, Neu5Ac). Sialic acid is named after its acidity ($pK_a = 2.6$) derived from the salvia[3,4]. This term is given to three parental molecules *N*-acetyl neuraminic acid (Neu5Ac), *N*- glycolylneuraminic acid (Neu5Gc), and 2-Keto-3-

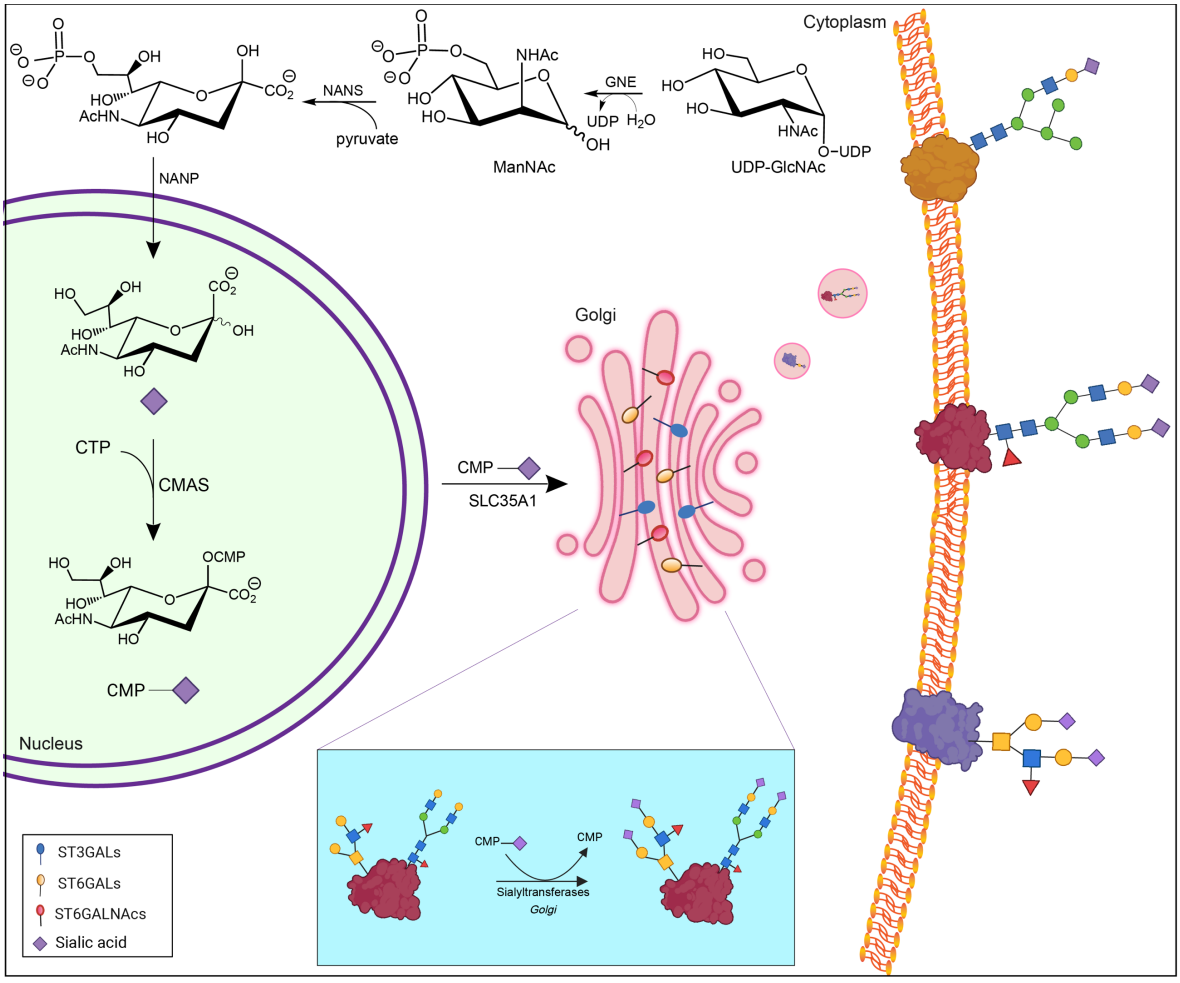

Figure 1.1 Biosynthetic pathway of sialic acid in human.

deoxynononic acid (KDN). The family of sialic acids includes 50 different derivatives, the most prevalent derivative in humans is Neu5Ac[4,5]. Of note, the ability to biosynthesize Neu5Gc is lost due to a mutation in the CMP-Neu5Ac hydroxylase (CMAH) gene in human[6]. In my Ph.D. thesis, I focused on human biology, thus, the term "sialic acid" will be used in this thesis to refer to Neu5Ac, rather than other derivatives. Sialic acid, a nine-carbon glycan, is biosynthesized through multi-step enzymatic reactions (**Figure 1.1**). **G**lucosamine (UDP-***N***-acetyl)-2-**e**pimerase/*N*-acetylmannosamine kinase (GNE) is a bifunctional enzyme catalyzing the conversion of UDP-GlcNAc to *N*-acetylmannosamine-6-P. This reaction comprises two steps: 1- epimerization of GlcNAc of UDP-GlcNAc at C-2 and cleavage of the UDP moiety to result in *N*-acetylmannosamine (ManNAc); 2- Formation of ManNAc-6-P, which consumes adenosine triphosphate (ATP). ***N*-acetylneuraminic acid Synthase** (NANS) facilitates the condensation of phosphoenolpyruvate with ManNAc-6-P through an aldol condensation to form *N*-acetylneuraminic acid-9-P. Next, the phosphate is removed by ***N*-acetylneuraminate-9-phosphatase** (NANP). Finally, the sialic acid is transported to the nucleus where **C**ytidine **m**onophosphate *N*-**a**cetylneuraminic acid **s**ynthetase (CMAS) activates sialic acid, forming **C**ytidine **m**ono**p**hosphate sialic acid (CMP-sialic acid, CMP-Neu5Ac). The activated precursor is then imported into the Golgi by an energy-independent nucleotide sugar antiporter called **S**o**l**ute **c**arrier family **35** member **A1** (SLC35A1)[6] (**Figure 1.1**).

1.1.1 Regulation of enzymes involved in sialic acid biosynthetic pathway

Gene regulation occurs across central dogma: DNA (i.e., epigenetics) transcribed to RNA (post-transcriptional control), RNA translated to protein (post-translational control), ultimately impacting cellular phenotypes[7-9] (**Figure 1.2**).

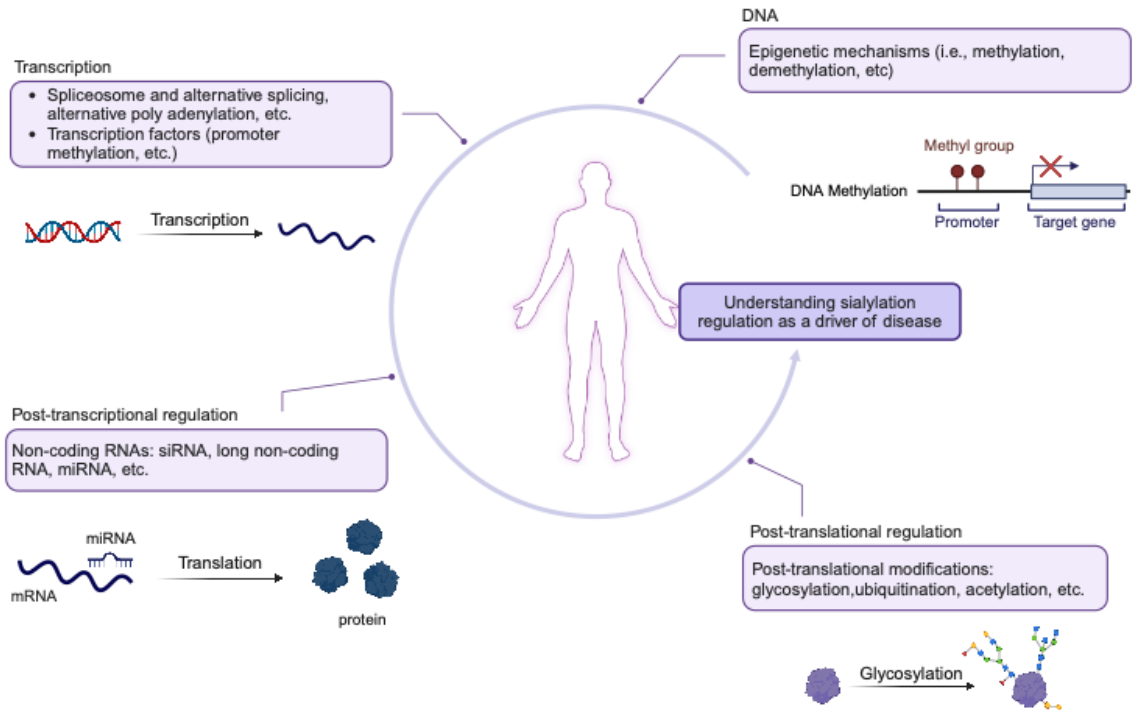

Figure 1.2 Several gene regulation levels across central dogma.

Numerous evidence indicates that the expression levels of enzymes involved in SA pathway impact cellular content of sialic acid, accordingly, the protein expression regulation of these enzymes can directly affect cell sialylation status and corresponding biological processes. For example, in adult-onset GNE myopathy (caused by mutation in enzymatic domains of GNE), reduced sialylation is observed in mouse models. One could argue that salvage pathways can provide sialic acid from degraded glycoproteins. *GNE*-deficient mice have early embryonic lethality, indicating the significance of sialylation during development[10,11]. Oetke, C., *et. al.,* showed that a hypo-sialylated phenotype is caused by downregulation of *GNE* messenger RNA (mRNA) through DNA methylation of its promoter region (e.g., CpG island) in two human hematopoietic cell lines. In this work, the *GNE* mRNA, GNE enzymatic activity and cell surface sialic acid are repaired using "5-aza-dC" compound which is a DNA methylation inhibitor (5'-aza-2'-deoxycytidine)[12]. The hypermethylation of *GNE* CpG promoter is also reported in HIV-1-infected CEM T cells[13]. Also, *nans* is an essential gene for brain development as well as skeletal

growth. Mutations in *nans* impairs NANS enzymatic activity, leading to accumulation of *N*-acetylmannosamine *in vivo*[14]. Together, these examples indicate the prominent roles of epigenetics regulation of enzymes involved in the SA metabolic pathway. To date, there is no report on miRNA-mediated expression regulation of SA biosynthetic enzymes. For the first time, I will discuss miRNA-mediated regulation of CMAS expression in Chapter 5.

1.1.2 Sialylation by Sialyltransferases

Sialylation is a major biosynthetic pathway through which CMP-Neu5Ac is transferred onto oligosaccharide acceptors to generate *N*- or *O*-glycans and gangliosides. In human, 20 different sialyltransferases (STs) use CMP-Neu5Ac served as their donor to transfer Neu5Ac to glycan acceptors terminated with Gal, GalNAc, or Neu5Ac residues[15] (**Figure 1.3**). Mammalian sialic acids can be linked to the 3- or 6-hydroxy group on Gal, 6-hydroxy group on GalNAc and 8-hydroxy group on Neu5Ac. The position of hydroxyl group on Gal, GalNAc, or Neu5Ac residues where sialic acid is bound defines three different linkages: α-2-3, α-2-6, and α-2-8, based on which STs are categorized into 4 main families: ST3-β-galactoside-α-2,3-sialyltransferases (ST3GALs with 6 members), ST6-β-galactoside-α-2,6-sialyltransferases (ST6GALs with 2 members), ST6-*N*-acetylgalactosaminidase-α-2,6-sialyltransferases (ST6GALNAcs with 6 members), and ST8 α-*N*-acetyl-neuraminide α-2,8-sialyltransferase (ST8SIAs with 6 members)[15,16]. Each of the sialyltransferases has distinct expression profiles even within a sub-family, for instance, ST6GAL1 is expressed throughout the human body, whereas ST6GAL2 expression is known to be limited to brain, breast, and colon[17,18]. Different structures of sialosides resulting from STs activities play specific biophysical roles in biological processes including masking recognition sites[19] and/ or recognized by receptor proteins and serve as ligands[20], which can impact the cell physiological and pathological states.

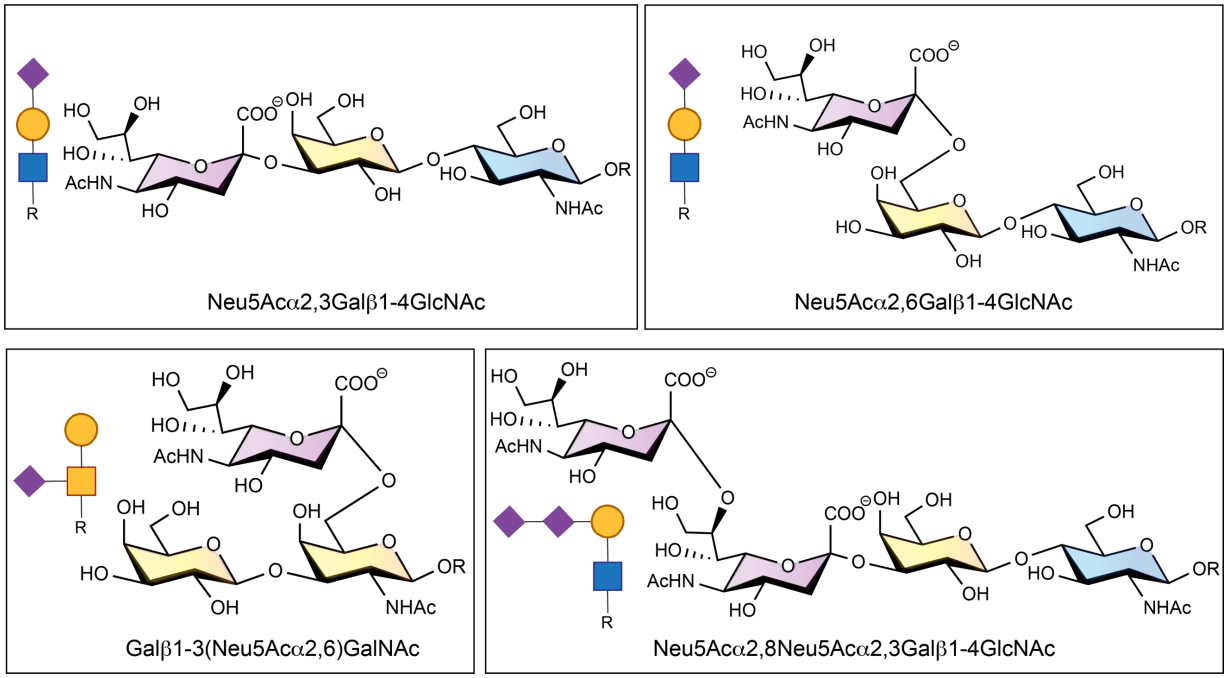

Figure 1.3 General sialoside linkages in human.

1.1.3 Regulation of Sialyltransferases

Gene regulation provides cell-specific expression patterns of proteins, herein, sialyltransferases[21]. In this section, a few key works were briefly described to show roles of transcriptional regulation in defining sialyltransferases expression patterns in different biological contexts (e.g., cancer and immunology). The transcription of *st6gal1*, as one of the most cancer-associated sialyltransferases, is coordinated by four cell type-specific promoters (P1-P4), driving different 5' untranslated regions (5'UTR)[21]. P1 and P3 are shown to drive ST6GAL1 upregulation in cancer cells[22,23]. Dorsett, K. A., *et. al.*, reports that transcription factor, *Sox2*, upregulate ST6GAL1 expression by binding to its P3 promoter in ovarian cancer cell lines[23]. In another work, the Bertozzi laboratory demonstrated that *Myc* transcription factor drives *st6galnac4* expression. ST6GALNAc4 transfers sialic acid to sialyl-T antigen, forming disialyl-T antigen which causes tumor immune escape by engaging human Siglec-7 on macrophages, suggesting *Myc* contributes to tumorigenesis via controlling host immune response[24].

1.2 Sialic acids as regulators of molecular and cellular interactions

The biological function of sialic acid is mainly driven by their intrinsic structural properties. Carrying a negatively charged carboxyl group contributes to the degree of hydrophilicity of cellular membrane, thereby regulating different biological processes including cell-cell communication. This makes cells use sialic acid as a tool to contact with their microenvironment. While there are biophysical effects, the sialic acid linkages provide specificity in biology and pathology. Glycome profiling of normal versus disease (e.g., tumor or infected patients) samples using lectin microarrays clearly shows distinct patterns of sialic acid linkages, showing that sialylation patterns are context dependent[25,26]. The pivotal role of sialylation is known in almost every aspect of cell biology[5,27], therefore, changes in cellular sialic acid content, in a linkage specific manner, can have a substantial impact in the mechanisms of disease pathogenesis, including those operating in nervous system embryogenesis and disease[28,29], inflammation[30,31], infection[32,33], autoimmunity[34,35], and cancer biology[26,36]. In addition, a compelling body of evidence highlights the tremendous potential of sialic acid as valuable diagnostic, predictive and prognostic biomarkers in several clinical applications. Some of them will be discussed.

1.2.1 Examples of sialic acid regulation in cancer biology and immunology

Sialyltransferases contribute to the definition of the sialylation patterns of normal and tumor cells. High levels of sialic acid suggest high metastatic capacity in many types of cancers[37]. **Figure 1.4** shows some of roles of sialyltransferases in cancer: transformation (ST6GAL1 in Pancreatic Ductal Adenocarcinoma (PDAC)[26,38]; ST3GAL4 in Cervical cancer[39]), progression (ST3GAL2 in Colon Adenocarcinoma (COAD)[40]; ST3GAL1 and ST3GAL2 in melanoma[41]), metastasis (ST6GAL1 in: Breast Cancer (BRCA)[42], Non-small Lung Cancer (NSLC)[43], Ovarian Cancer (OVCA)[23,44], Prostate Cancer (PCa)[45], and Hepatocellular Carcinoma (HCC)[46]; ST3GAL1

in melanoma[47] and OVCA[48]; ST6GALNAc1 in Gastric cancer[49]), survival (ST6GAL1 in COAD[50]; ST3GAL5 in Lung Cancer (LUAD)[51]; ST3GAL1 & ST3GAL4 in PDAC[36]), and breast metastasis to brain (ST6GALNAc5[52]). Some of these studies will be discussed in Chapters 2-5. In this Chapter, I describe examples of sialyltransferases' roles in cancer biology and immunology. Functional analysis of clinical samples identified α-2,6-sialyltransferase ST6GALNAc5 as a mediator for brain metastasis of breast cancer. ST6GALNAc5 is known to be highly expressed in brain both in human and mice[52]. This study shows 50% of brain metastatic samples from breast cancer patients (MDA231-BrM2 and CN34-BrM2 cells) are enriched in *Sambucus Nigra* lectin (SNA) staining in compared to parental MDA231 and CN34 cells. Of note, *st6galnac5* messenger RNA level was found to be higher in brain metastatic derivatives in compared to parental cell lines, which could result from differential post-transcriptionally regulation in normal and brain metastasis states[52]. Another regulatory axis driven by sialic acid is Sialic acid-binding immunoglobulin-like lectins (Siglec)/sialic acid thay are considered as a glycoimmune checkpoint[20]. Tumor cells upregulate sialic acid on their surface, as an inhibitory marker, to engage Siglec on immune cells, dampening host immune response and promoting tumor cell survival. For instance, the Kooyk laboratory reports that monocyte to macrophage differentiation is induced by the upregulation of tumor-derived sialic acid (by the action of ST3GAL1 and ST3GAL4) and their interactions with Siglec-7 and Siglec-9 in PDAC cells[36] (**Figure 1.4**).

1.2.2 Therapeutic aspect of sialic acid in cancer

Cell surface sialylation patterns undergo selective changes in normal physiology and pathological states. Sialic acid, as terminal glycans on glycoconjugates, coordinate cellular interactions via binding to different receptors[53]. Siglecs are a family of immunomodulatory

receptors which are predominantly express on immune cells and modulate their communications with cellular microenvironment via binding to the terminal sialic acid-containing ligands expressed

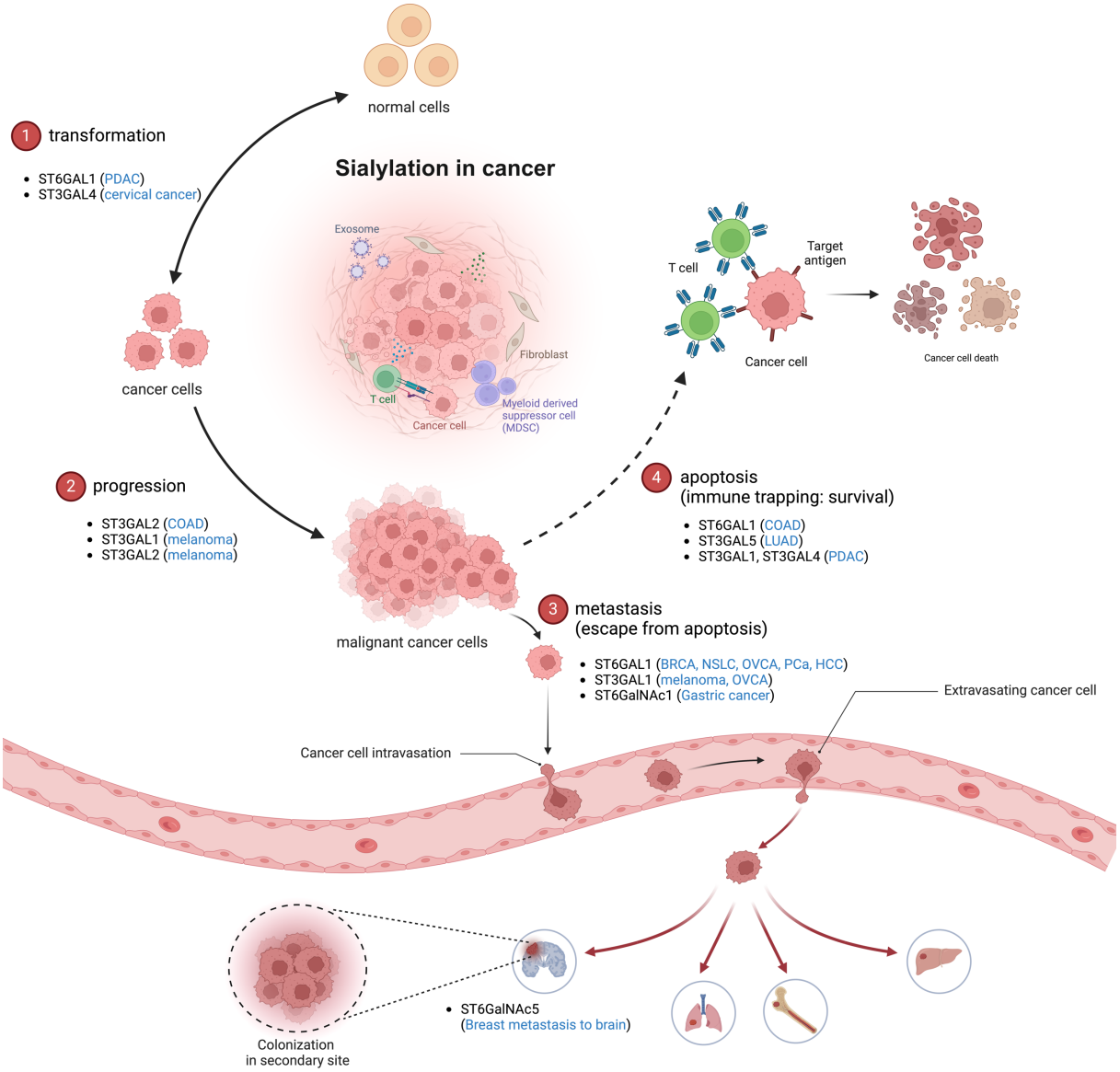

Figure 1.4 Identified roles of sialyltransferases in cancer. Sialyltransferases roles in cancer developmental process from normal cells to cancer cells (transformation), progression, and either invasion/ migration to a secondary site (metastasis) or immune trapping (apoptosis).

on either the same (*cis*) or different (*trans*) cells. The majority of Siglecs: sialic acid interactions provoke immune cell signaling through Siglecs' cytoplasmic immunoreceptor tyrosine-based inhibitory motif (ITIM) domains[54]. Such interactions are considered as self-associated molecular

patterns which occur under normal physiology. As mentioned earlier, tumor cells can trick immune cells via expressing sialic acid on their surface, and engaging Siglec receptors on the immune cell surface, resulting in immune scape and tumor survival[36,55].

From therapeutic standpoint, tumor immune evasion drived by Siglec: sialic acid interactions have drawn specific attentions. Gangliosides, sialylated glycosphingolipids, comprise ~75% of sialic-acid containing ligands in human brain[28]. GD2 is a disialoganglioside, which is highly expressed on tumor cells in neuroblastoma[56]. This epitope binds to Siglec-7 which is expressed on immune cells (e.g., macrophages and NK cells). GD2: Siglec-7 axis suppresses immune cell activity via its cytoplasmic ITIM domain. This interaction is blocked using anti-GD2 antibody, inhibiting Siglec-7's suppressive effects on the immune system[57].

Moreover, sialic acid can mask the ligands for other regulatory proteins called "galectins" which are a family of soluble glycan-binding proteins, and can reprogram innate and adaptive immune systems[58,59]. Galectin-1 (Gal-1) binds to the *N*-acetyllactosamine [Galβ(1-4)GlcNAc, LacNAc] moiety on cell surface glycosylated ligands, controlling several immune cell processes including activation, differentiation, trafficking, and survival. ST6Gal1 counteracts Gal-1 activity through α-2,6-sialylation, and masking Gal-1 ligands. Therefore, the altered expression of ST6Gal1 impacts Gal-1 activity, potentially altering intestinal inflammatory status[19]. Given that sialoside levels with distinct patterns (α-2,3, α-2,6, α-2,8; with or without further modifications, such as acetylation[60,61]) drives various events within cellular microenvironment, understating the regulation of these motifs is vitally important. As shown earlier in **Figure 1.2**, gene regulation occurs in the flow of transferring genetic information in central dogma, one of them is post-transcriptional miRNA-mediate protein expression regulation.

1.3 Introduction to microRNA

micro**RNA**s (miRNA, miR), small (~ 22 nucleotides (nt)) non-coding RNAs, are master regulators of protein expression[62]. In human, the canonical miRNA biogenesis comprise a multi-step pathway which starts in the nucleus (**Figure 1.5**). RNA polymerase II transcribes primary miRNAs (pri-miRNA) from protein coding region of a transcript or a non-coding region[63]. It next converts to a stem-loop structure called ‘‘pre-miRNA” through the actions of a complex of proteins[64], followed by exporting to the cytoplasm by Exportin-5. In the cytoplasm, Dicer cuts the loop, generating a miRNA duplex with two strands: “*star strand”* and “*passenger strand”*[65]. The resulting duplex is loaded into an **Argo**naute (AGO) protein which is concomitant with changes in AGO conformation, and requires Hsp70/Hsp90 chaperone machinery and their ATP hydrolysis. AGO retains one strand called “guide strand”, and discards the second one called “ passenger strand”, resulting in a functional mature miRNA within a complex called **R**NA **i**nduced **s**ilencing **c**omplex (RISC). Now, miRNA within the RISC complex binds to its cognate mRNA (mainly on its 3' untranslated region (3'UTR)) to result in post-transcriptional regulatory impact[66].

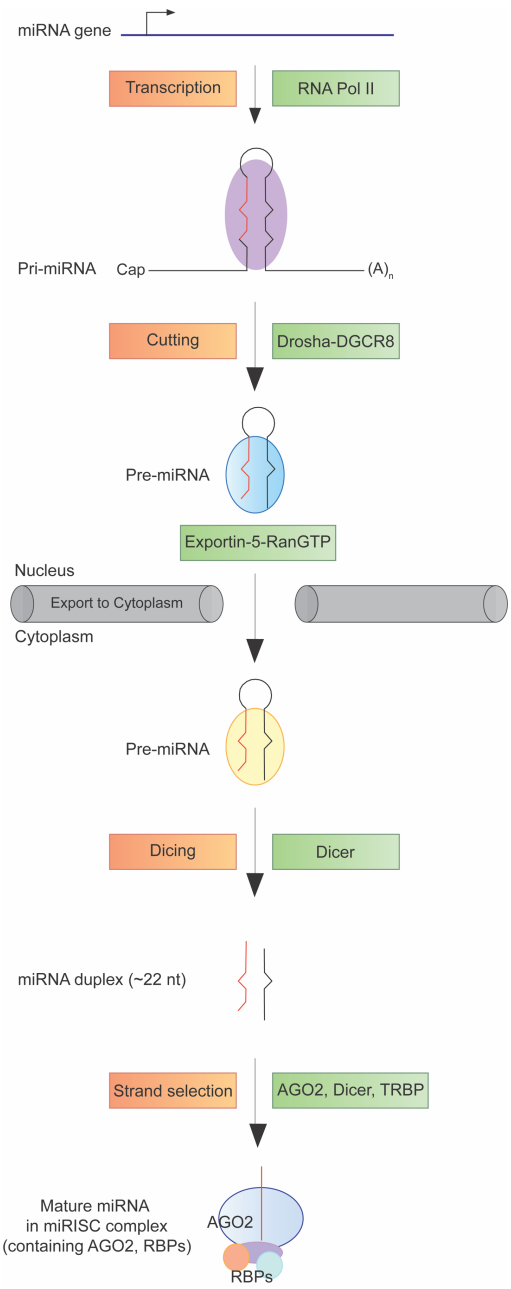

Figure 1.5 miRNA biogenesis pathway in the metazoan.

1.3.1 AGO2 and TNRC6A: the two core components of RISC complex

The RISC complex comprises different components: guide strand of miRNA, target mRNA, AGO2 protein, and other **R**NA **b**inding **p**roteins (RBP). Our current knowledge about the RBPs involved in the RISC function is incomplete. I describe the two most-studied RBPs associated with the RISC complex: AGO and TNRC6 proteins. Human cells have four different isoforms of AGO proteins which share ~80% amino acid sequence identity[67]. AGO2 is the most well-studied paralog due to its unique features: it is the most abundant AGO paralog in different cell types[68], and is thought to be the only AGO paralog with the "slicing" function[69]. The miRNA:AGO complex binds to a scaffolding protein which is the second well-known RISC complex RBP called **t**ri**n**ucleotide **r**epeat **c**ontaining **6** (TNRC6, also known as GW182). This protein has three different human paralogs: TNRC6A, TNRC6B, and TNRC6C which have ~40% amino acid sequence identity[70]. All paralogs bind to AGO2 via three AGO-binding domains, each contains >2 tryptophan (Trp, W) amino acids, and are separated by ≥10 amino acids. TNRC6, as a scaffolding protein, recruits other proteins, constructing the high molecular weight RISC complex[71-73]. miRNA loaded in the RISC complex mediate post-transcriptional regulation of target transcript via either target mRNA degradation or translation inhibition[62,66]. Of note, in Chapter 2, I tested AGO2 and TNRC6A impacts within the context of a novel story that we found.

1.3.2 Cognate microRNA: 3'UTR interactions

The interaction between miRNA and its cognate 3'UTR is thought to rely on specific binding patterns and are considered to drive mRNA destabilization or translation inhibition[66]. The complementarity between cognate miRNA: mRNA pair is primarily thought to be the 7–8 nt at the 5'-end of the mature miRNA, known as the "seed region" which is the most likely predictor of cognate miRNA: mRNA interactions[74] (**Figure 1.6**). Soon after, miRNA scientists found that

complementarity binding between target mRNA and miRNA 3'-end can occur within positions 13–16 of the mature miRNA, compensating for imperfect pairing at the seed region (3'-end of miRNA)[75]. To this end, prediction algorithms including targetscan, RNAhybrid, miRanda consider seed complementarity and/or the thermodynamic stability of miRNA: mRNA interactions. Scientists use bioinformatics to identify transcript targets of a single miRNA. The miRNA is then introduced (either *in vitro* or *in vivo*) to a target and further analysis can be performed using different experimental techniques.

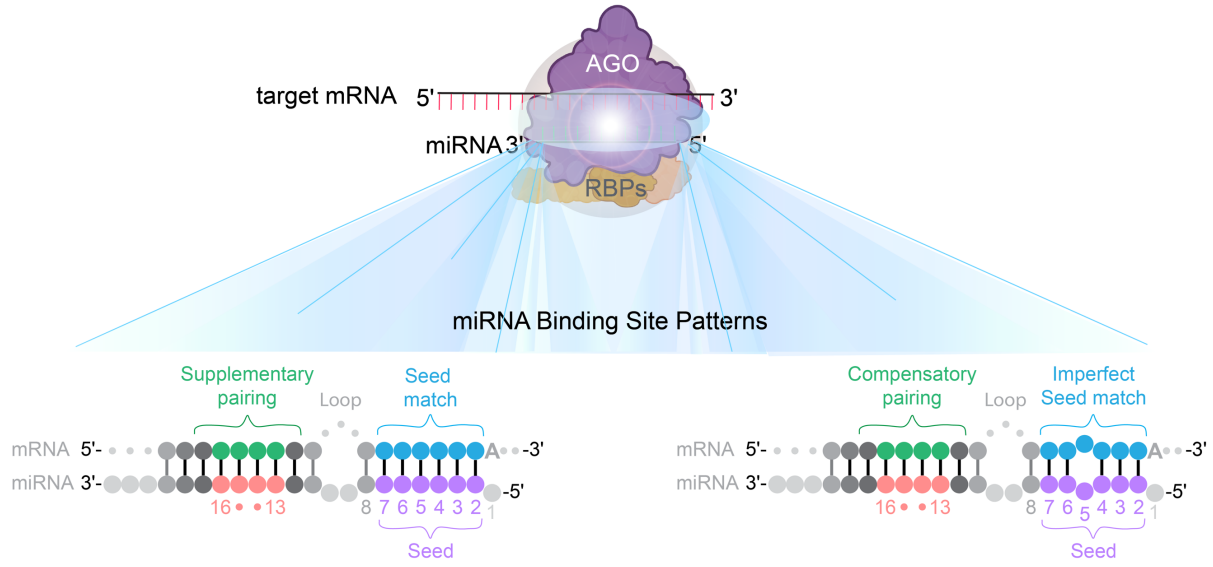

Figure 1.6 miRNA: 3'UTR interaction patterns for miRNA-mediated downregulation.

1.3.3 Investigation of microRNA: 3'UTR interaction

Human cells express 2654 mature miRNAs (miRbase v. 22[76]), each can bind to hundreds of messenger RNAs, predominantly to 3'UTR regions[66]. Given the importance of post-transcriptional regulation in controlling cellular homeostasis, for instance, by maintaining protein expression, it is crucial to understand the miRNA regulatory landscape. To this end, research groups employ different methods to survey miRNA-mediated gene regulation. *The luciferase assay* is the first reporter assay that was designed, and widely used by many researchers for

studying cognate miRNA: mRNA direct interactions. This system requires Luciferase vector construction containing Renilla luciferase vector (*rLuc*) cloned downstream of either Sp6 or T7 RNA polymerase binding sites for *in vitro* transcription. The target 3'UTR is cloned downstream of *rLuc*, co-transfected with the miRNA into mammalian cells[77]. Although this method is widely used for investigating miRNA: 3'UTR interactions, it can only be operated in a moderate throughput format due to the intrinsically laborious steps, such as cell lysis and expensive reagents. A need for mapping miRNA-mediated regulation of a target transcript, in a high throughput format, motivates research groups to design new platforms. The high throughput *miRFluR* assay is a recently introduced dual fluorescence ratiometric method created by the Mahal laboratory, by which we can test the entire human miRNAome against a target 3'UTR[78]. This assay contains three main components: a dual fluorescence sensor called "pFmiR" embedded with target 3'UTR (pFmiR-3'UTR), human miRNA library, HEK293T cells (**Figure 1.7**). In the pFmiR-3'UTR sensor, the target 3'UTR is cloned downstream of the reporter fluorescence protein, Cerulean. A second fluorescent protein, mCherry, is also integrated in the sensor as a control for transfection. The Cerulean fluorescence intensity is lower for those miRNAs hitting target 3'UTR, with a concomitant reduction in the normalized fluorescence ratio. This assay is conducted in a 384-well plate format which enables us to analyze the complex regulatory landscape of the entire known human miRNAome for a single gene in a high-throughput format without further experimental manipulation[78]. I took advantage of this assay in my Ph.D. projects, and will further discuss this in the rest of this dissertation. It is worth noting that for each target transcript, I tested the most prevalent 3'UTR as denoted in the Targetscan database[74].

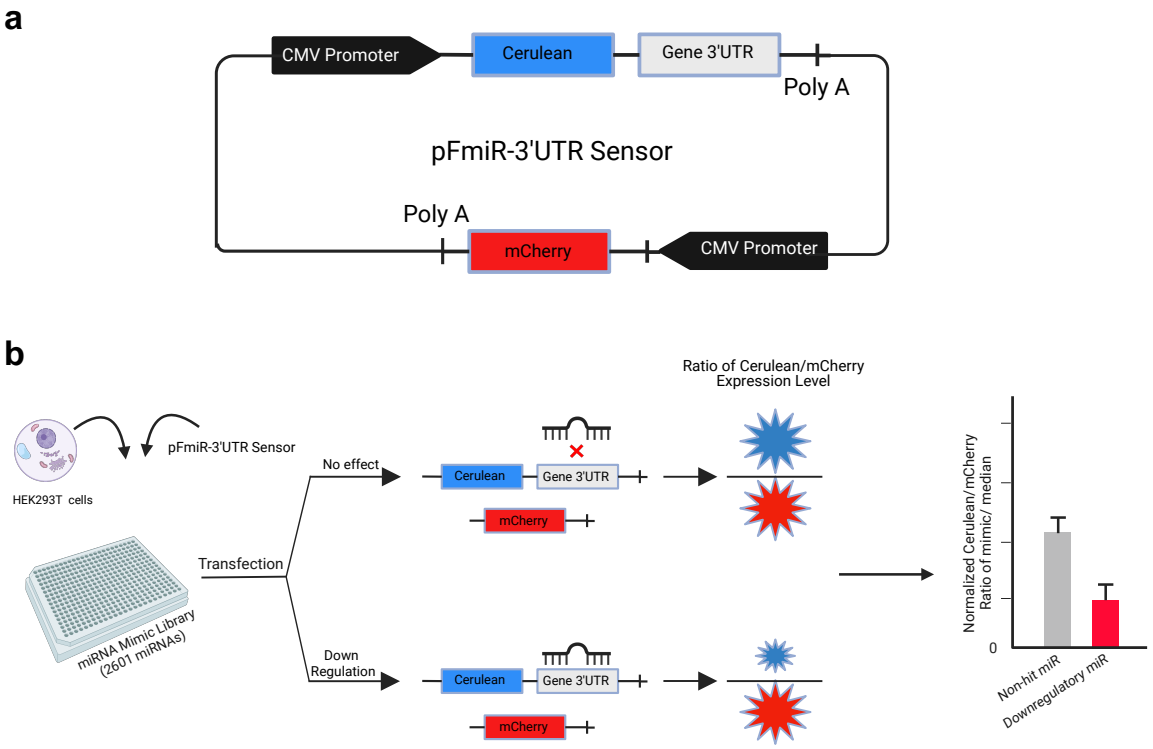

Figure 1.7 miRFluR assay components. This assay contains (a) pFmiR-3'UTR sensor and (b) human miRNA library which will be transfected to HEK293T cells.

1.4 microRNA modes of actions in normal physiology and pathology

microRNA are found to have different modes of action through which they mediate various biological processes in normal physiology and disease state. From a functional standpoint, miRNA activity is pleiotropic. They can act as a tumor suppressor or an oncomiR (oncogenic miRNA) in different biological contexts. These tiny RNAs can act either individually or can they control protein expression in cooperation with other miRNAs. **1**- *Act in a singular manner*: miR-155-5p (processed from *BIG* transcripts) acts with distinct functional roles as both oncomiR and tumor suppressor[79,80]. As an oncomiR, it was first discovered to be upregulated in B-cell lymphoma[81,82]. Activated B cells showed on average 3-fold higher tumor cells positive for *BIG* transcript in comparison with germinal center B cells[81,82]. As a tumor suppressor, miR-155-5p downregulates CLDN1 (claudin-1) via direct interaction with its 3'UTR, inhibiting proliferation and invasion of Ovarian cancer cells[83]. **2**- *Act within a network with other miRNAs*: several miRNAs can act

cooperatively to exert their impacts on expression levels of functionally associated proteins. A standout example of this can be miR-200 family cooperative roles in controlling epithelial to mesenchymal transition (EMT). This is a family of 5 members (encoded by two separate genomic loci, resulting in two subfamilies: miRs: -141, -200a and miRs: -200b, -200c, -429). In each sub-family, miRNAs have an identical seed region. The miR-200 family is expressed in most epithelial cells and their expression is dampened in order for EMT to ensue. EMT, an embryonic development program, is a mechanism by which many cancer cells increase their migratory and invasive capacities[84]. Peng, F., *et. al.*, showed miR-200b/200c inhibit the invasion and migration of cholangiocarcinoma cancer (Bile Duct Cancer) by downregulating rho-kinase-2 via direct miRNA: 3'UTR interactions[85]. **3**- *Act within a network with alternative molecules*: miRNA can be involved in functional networks with other regulatory molecules including long non-coding RNAs (lncRNAs)[86] and transcription factors[87,88]. For example, Cdr1as is a circular RNA whose function is known to dampen neuronal activity in mice[89]. miR-7 and miR-671 cooperatively mediate the inhibition of Cdr1as expression. Cyrano is a lncRNA which can trigger the miR-7 degradation in the brain, leading to the accumulation of miR-7 target, Cdr1as[89]. These examples clearly highlight the functional roles of microRNAs in regulating protein expression in both normal and disease states. In my Ph.D. dissertation, we asked whether miRNA regulate sialosides. In seeking understanding the regulation of sialylation, I focused on the profiling miRNA regulatory landscape of human sialic acid-related genes.

1.4.1 microRNA as a proxy approach for identifying roles of glycosylation

Unlike nucleic acids and proteins, glycan biosynthesis is not directly template-driven. Rather, it is intrinsically controlled at multiple levels including monosaccharide compositions, linkage patterns, and further modifications (phosphorylation, sulphation, etc.)[90]. Glycosylation

regulates central pathways in human physiology and diseases[91]. A better understanding of glycosylation regulation can provide useful insights of underlying mechanisms in human health and disease. An integrated analysis for glycomics and miRNA expression datasets identified regulatory networks between miRNA and different glycosylation patterns (Tn and T-antigens, terminal β-GalNAc, hybrid-*N*-glycans, and blood group B), suggesting functional impacts by miRNAs on glycosylation patterns[92,93]. In 2015, the Mahal laboratory proposed miRNA proxy hypothesis, stating that miRNA and its cognate target(s) may drive the same biological phenocopies. This hypothesis was first tested for uncovering the glycosylation network regulation in breast cancer[94]. In this work, the Mahal laboratory showed that miR-200b-3p, EMT mediator, controls the protein expression of B3GlcT (Beta-3-glucosyltransferase), ST3GAL5, ST6GALNAc5[95]. Knocking down each of the glycogenes phenocopies the overexpression of miR-200b-3p including returning mesenchymal to epithelial states[95]. This work shows miRNA-mediated regulation can be considered as a proxy approach to identify the biological functions of glycosylation proteins.

1.5 Aims of dissertation

In the Mahal laboratory, my Ph.D. journey is focused on investigating miRNA-mediated regulation of sialylation. It begins with a simple question of "whether miRNA regulate α-2,6-sialic acid" (Chapter 2), then extended to address "do they control α-2,3-sialic acid" (Chapters 3 & 4), and ultimately, to further explore miRNA-mediated sialylation, I target the key enzyme in sialic acid biosynthetic pathway, CMAS (Chapter 5).

In Chapter 2, using miRFluR assay, the 3'UTRs (the most predominant miRNA binding sites) of ST6GAL1 and ST6GAL2 were screened over the human miRNAome in a high throughput format. The canonical view of miRNA function in proliferating cells is that miRNA destabilize

mRNA or inhibit protein translation via direct interaction with 3'UTR. During my analysis, we serendipitously found that miRNA predominantly upregulate ST6GAL1 expression. I found that miRNA upregulating ST6GAL1 level also increases α-2,6-sialic acid on target cell surface. This study showed ST6GAL2 is mostly downregulated by miRNA. The binding sites for a subset of upregulatory miRNAs were validated by mutating nucleotides on predicted miRNA binding sites on target 3'UTRs, indicating that the observed upregulation is via direct miRNA: 3'UTR interactions. Furthermore, I identified that AGO2 and FXR1 (RNA binding proteins) are indispensable for upregulatory machinery of miRNA.

In Chapter 3, I expanded our understanding of the newly discovered role of miRNA, protein upregulation, during studying the miRNA-mediated gene regulation of ST3GAL1 and ST3GAL2. The miRNA regulation was tested in different levels: mRNA, protein, and functional assay for ST3GAL1/2 (lectin staining of α-2,3-sialylation). Previous collaborative work from the Mahal and Hernando laboratories identified CD98hc (*slc3a2*) as an essential gene in melanoma growth whose stability is ensured upon α-2,3-sialylation by ST3GAL1 and ST3GAL2. Given that, I tested a hypothesis whether the observed correlation between three proteins is post-transcriptionally mediated by miRNA. To this end, I mapped the CD98hc, ST3GAL1 and ST3GAL2 miRNA regulatory landscapes. Comparison of all three miRNA datasets: ST3GAL1, ST3GAL2, and CD98hc reveals several upregulatory miRNAs between either CD98hc: ST3GAL1 or CD98hc: ST3GAL2. The miRNA: mRNA interactions were evaluated via mutational analysis.

In Chapter 4, I focused on miRNA regulation of gangliosides. Among different genes modifying gangliosides, we chose to study ST3GAL5 gene regulation using the miRFluR assay. Several miRNA: 3'UTR interactions of ST3GAL5 have been tested using the luciferase assay, providing us with miRNA-mediated ST3GAL5 regulation in metastatic breast cancer: EMT and

migration. Given the newly found role of miRNA, protein upregulation, and the importance of GM3 synthase (ST3GAL5) in different cancer types, I took advantage of the high throughput format of miRFluR assay to examine human miRNA interactome over ST3GAL5 3'UTR.

In Chapter 5, the miRNA regulatory landscape of CMAS was investigated. It is known that the CMAS levels can impact the sialylation patterns in human as it provides the activated precursor for sialyltransferases. The miR hit list identified to regulate CMAS expression was examined over endogenous CMAS expression in different cancer cell lines. This project is further explored for potential impacts by miRNA targeting CMAS on cellular sialylation status.

Chapter 2

High-throughput Analysis Reveals miRNA Upregulating α-2,6 Sialic Acid through Direct miRNA: mRNA Interactions

2.1 Acknowledgment

I would like to thank my colleague Hoi Hei Ng for her help in progressing the mutational analysis of this project. I thank Dr. Dawn MacDonald for advice on this project. I would like to acknowledge Prof. Eva Hernando (NYU Langone) for helpful insights and Prof. Matthew Macauley (University of Alberta) for his generous gift of Neuraminidase.

This chapter is adapted from: "*ACS Cent. Sci.* 2022, 8, 11, 1527–1536".

2.2 Introduction

The terminal monosaccharide α-2,6-sialic acid is one of the most studied glycan motifs, with clear roles in immunology[96,97], infectious disease[32], and cancer biology[26,98-100]. This modification is biosynthesized by a family of two enzymes: ST6-β-galactoside-α-2,6-sialyltransferase-1 (ST6GAL1), expressed throughout the human body, and ST6-β-galactoside-α-2,6-sialyltransferase-2 (ST6GAL2), predominantly seen in brain, thyroid gland and colon[17,18,101-104] (**Figure 2.1**). ST6GAL1 is a well-characterized α-2,6-sialyltransferase that is upregulated in almost all cancer types, except bladder cancer[105]. In addition, it is known that ST6GAL1 and the resulting α-2,6-sialic acid alter the physiological and pathological states in immune system[96,97,106], DNA damage response[107]. Despite the vital roles of α-2,6-sialic acid in the phenotypic features of various diseases[26,99,104,108], insufficient attention has been paid to the mechanisms responsible for the regulation of this motif. To date, different research groups have studied ST6GAL1 regulation by transcription factors[23,109,110], however, the questions that I try to answer in this chapter: How α-2,6-sialyltransferses regulated post-transcriptionally? and How this may impact their post-translational regulation? have not been addressed.

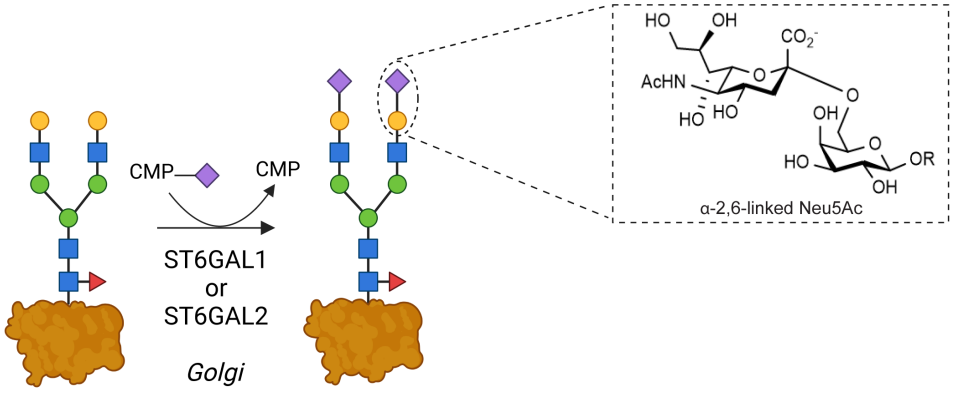

Figure 2.1 α-2,6-sialylation by ST6GAL1 or ST6GAL2.

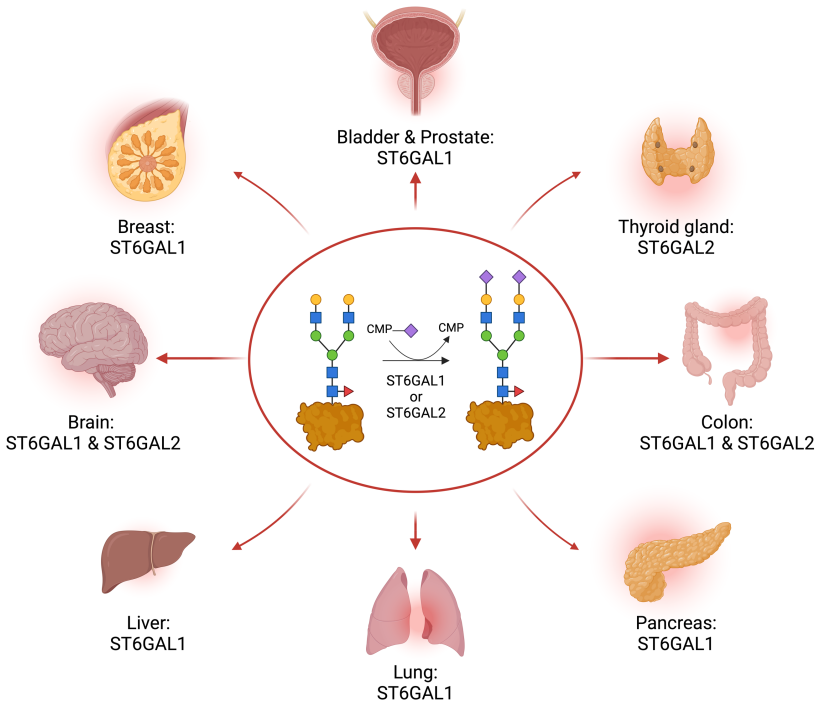

Figure 2.2 Tissue expression map for ST6GAL1 and ST6GAL2.

microRNAs (miRs, miRNAs) are master regulators that tune protein expression through modulation of mRNA. The tiny non-coding RNAs (~22 nucleotides) are thought to be post-transcriptional repressors, binding to the 3'UTR of mRNA and causing mRNA destabilization and/or loss of translation[62,111]. To study miRNA-mediated gene regulation, existing reports generally rely on choosing miRNA predicted by available algorithms (e.g., Targetscan[74], PicTar[112]) for miRNA target identification, and further study of cognate miRNA: mRNA regulation in selected biological contexts is used to validate the inhibition of target protein expression[113-115]. However, this method has two disadvantages: **1-** the prediction tools for miRNA target interactions suffer from a high level of false positive target prediction[78,116], **2-** the method is low-throughput (single miRNA) and cannot provide a comprehensive analysis for miRNA-mediated target regulation. Luciferase assays, which require cell lysis and expensive reagents[117], contain a reporter luciferase mRNA downstream of which a 3'UTR of interest is appended to verify a predicted miRNA:3'UTR interaction site. This method has been used to screen the potential

miRNA regulation at a moderate-throughput[118]. To explore miRNA-mediated gene regulation in a high-throughput format, the Mahal laboratory has recently created a high-throughput **miR**NA **Flu**orescent **R**atiometric reporter assay (miRFluR)[78]. In this assay, the human miRNAome is provided in 24 × 384 well plates containing miRNAs in triplicates. Using the liquid handler equipment, this assay is conducted in a high-throughput format and a time-efficient manner, providing us with a miRNA hit list which results from comprehensively screening the whole human miRNA: 3'UTR interactome (**Figure 2.3**).

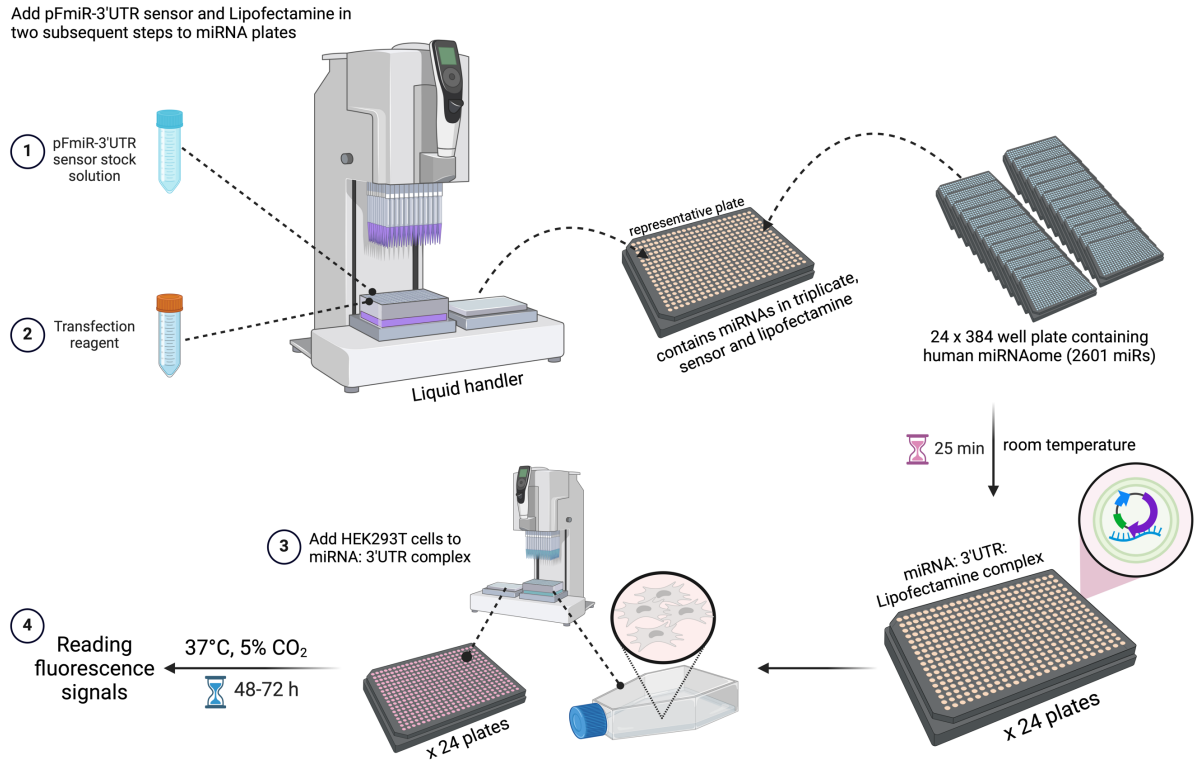

Figure 2.3 miRFluR assay workflow.

This assay uses a genetically-encoded ratiometric sensor called "pFmiR" which contains the fluorescent protein Cerulean under the control of the 3'UTR of the protein of interest, and a control fluorophore mCherry. The pFmiR sensor is transfected into HEK-293T cells along with a human miRNA library in 384 well plates (2,601 miRNA mimics, Dharmacon, v21) (**Figure 2.4**).

In this Chapter, I applied the high-throughput miRFluR assay to map miRNA regulation of ST6GAL1 and ST6GAL2. Together, this chapter provides a comprehensive survey into post-transcriptional gene regulation of α-2,6-sialyltransferases by miRNAs which can be further explored for biomarker discovery and targeting α-2,6-sialic acid in disease state.

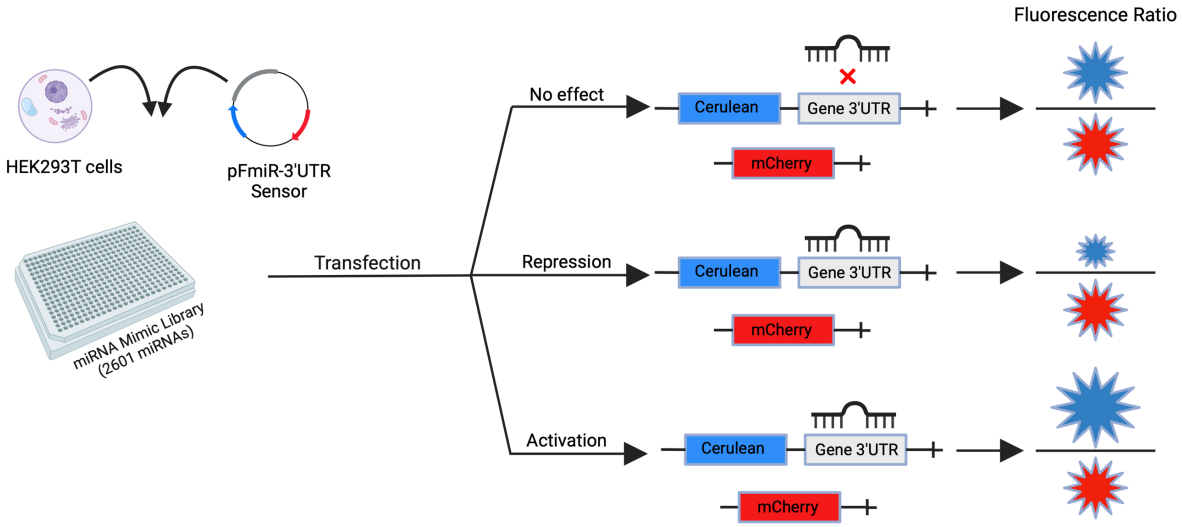

Figure 2.4 miRFluR assay results in three distinct miRNA: 3'UTR interaction outcome. miRFluR assay compromise pFmiR sensor, miRNA library, and HEK293T cells. The assay results are categorized to "No effect", "Repression", or "Activation".

2.3 Results

2.3.1 Mapping gene expression regulation of α-2,6-sialyltransferases

To map miRNA-mediated gene regulation of α-2,6-sialyltransferases, I first cloned the most prevalent 3'UTR of ST6GAL1 (2750 kb) or ST6GAL2 (5078 bp) in the pFmiR sensor, followed by testing human miRNome against each sensor individually through the high-throughput miRFluR assay[78] (**Figure 2.5**). Using the miRFluR assay, miRNA regulatory landscape for ST6GAL1 (**Figure 2.6a-c**) and ST6GAL2 (**Figure 2.6d-f**) were mapped for the most prevalent 3'UTR of the corresponding transcript[74]. Data analysis is discussed in detail in Section 2.6.4. Briefly, miRNAs with high error of measurement (>15% for ST6GAL1 and >14% for ST6GAL2) were all removed, resulting 2,161 miRNAs for ST6GAL1 and 2,166 miRNAs for ST6GAL2 (out

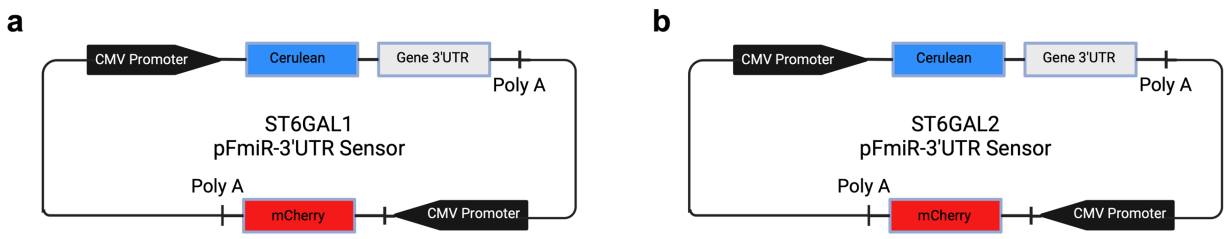

Figure 2.5 pFmiR sensor maps. (a) pFmiR-ST6GAL1 sensor. **(b)** pFmiR-ST6GAL2 sensor.

of 2601 total miRNAs screened). This represents 4% of the miRNA screened over ST6GAL1 3'UTR (**Figure 2.6a**), and 3% of the miRNA tested for ST6GAL2 3'UTR (**Figure 2.6d**) which passed QC. A z-score of ±1.965 (i.e., 95% confidence interval) results in 69 miRNA hits for ST6GAL1 (**Figure 2.6c**) and 62 miRNA hits for ST6GAL2 (**Figure 2.6f**). Surprisingly, data analysis revealed an unexpected result, namely that most miRNAs impacting ST6GAL1 upregulate the enzyme in proliferating cells. Upregulatory miRNAs (up-miRs) were also observed for ST6GAL2, although in this case, it was not their major mode of action. The high-throughput miRFluR assay data indicates that upregulation by miRNA may be a common function of these tiny non-coding RNAs in actively dividing cells.

The majority of miRNA regulating ST6GAL1 (76%, 50 up-miRs, **Figure 2.6b**) were found to be activating (>1.4 fold change), indicating that the primary roles for miRNA are target-dependent. In contrast to ST6GAL1, the majority of hits for ST6GAL2 (69%, 40 down-miRs, **Figure 2.6e**) were downregulatory miRNAs (down-miRs), suggesting the predominant mode of miRNA regulation is target dependent. Given the different expression patterns of ST6GAL1 and ST6GAL2 across the human body, they may have substrate specificity. For example, Siaα2-6Galβ1-4GlcNAc (Sia6LacNAc) trisaccharide results from ST6GAL1 activity. Mice lacking ST6GAL1

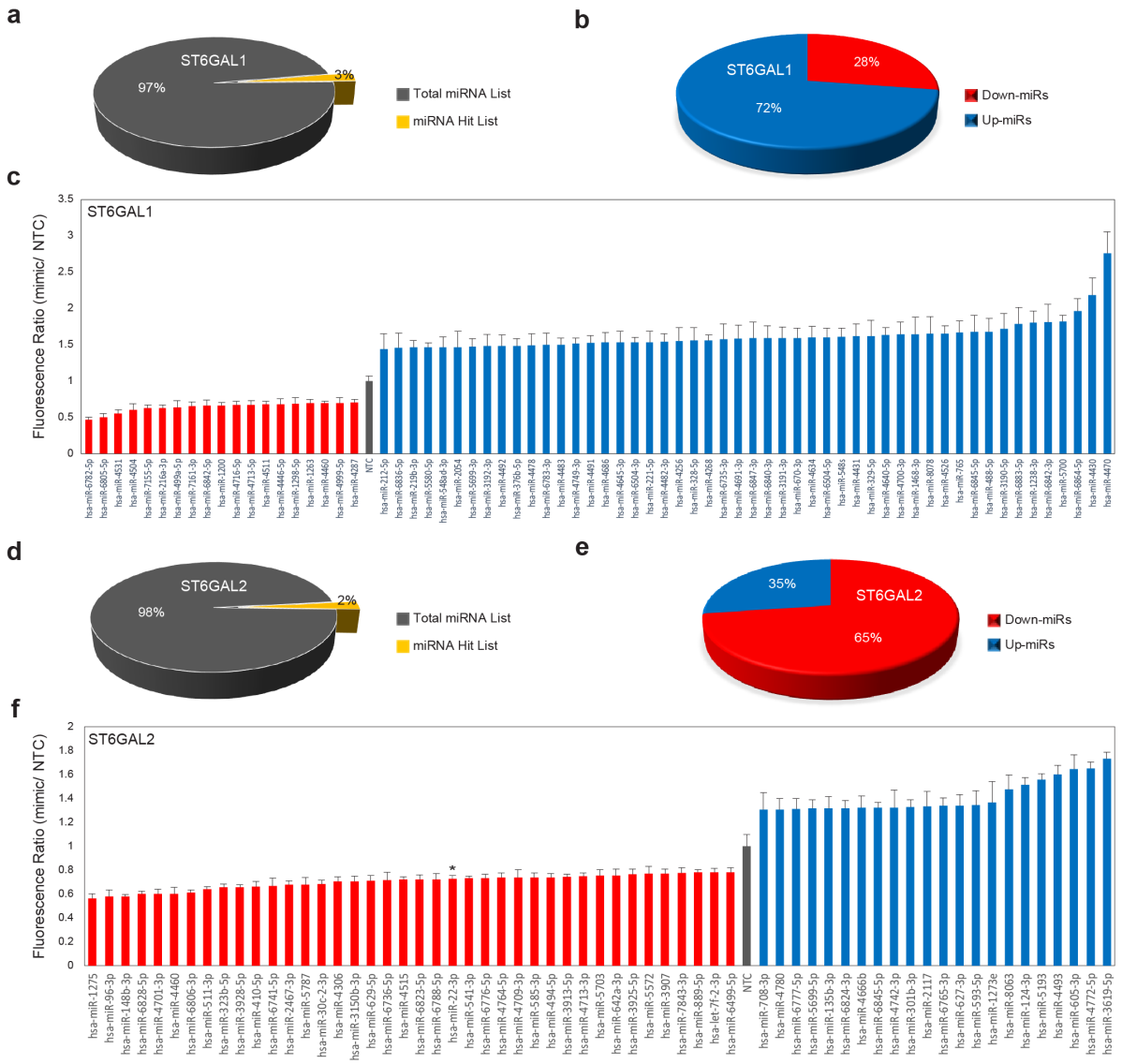

Figure 2.6 miRFluR assay result for α-2,6-sialyltransferases. (a) Pie chart representing percentage of hits observed from miRNA library for ST6GAL1. **(b)** Pie chart representing percentage up- vs. down-miRs seen in hits. **(c)** Bar graph of miRNA hits for ST6GAL1. Data is normalized to non-targeting control (NTC). **(d)** Pie chart representing percentage of hits observed from miRNA library for ST6GAL2. **(e)** Pie chart representing percentage up- vs. down-miRs seen in hits. The miRFluR assay results were obtained 48 hours post-transfection. **(f)** Bar graph of miRNA hits for ST6GAL2. Star represents a known hit[119]. Data is normalized to non-targeting control (NTC). Error bars represent propagated error.

showed severe immunosuppression, revealing an essential immune function of ST6GAL1 via α-2,6-sialylation of *N*-glycan served as a ligand for CD22 (Siglec-2)[97]. While ST6GAL1 is not expressed in brain tissues[120], ST6GAL2 expression is limited mainly to brain[101]. Herein, no overlap in either upregulatory or downregulatory miRNAs (up-miRs and down-miRs, respectively) was

observed between the two enzymes' miRNA hit lists. The distinct lists of miR hits identified for ST6GAL1 and ST6GAL2 may be due to their definite biological functions resulting from their tissue-specific expression patterns[26,99,101,104].

2.3.2 miRNA upregulate ST6GAL1 and α-2,6-sialylation in cancer cells

ST6GAL1 is upregulated in almost all cancer types. It has been shown that both ST6GAL1 and α-2,6-sialic acid level are increased in tumors in compared with normal tissues[26,99,100]. Given the roles of ST6GAL1 and α-2,6-sialylation in tumor initiation and progression, I aimed to test whether up-miRs drive enriched ST6GAL1 expression in cancer cells. To test whether our miRFluR assay is representative of regulation for the actual enzyme ST6GAL1, The miRFluR data is validated for a subset of hits (4 down-miRs, 8 up-miRs). As upregulation was a surprising finding, we validated twice the number of up-miRs and prioritized miRNA with known roles in the literature[121-124]. To ensure that the newly discovered miRNA function is reproducible across cell types, I tested different cancer cell lines including A549 (lung), PANC1 (pancreatic), and HT-29 (colon) (**Figure 2.7**). Consistent with previous work[78], the miRFluR assay accurately identified regulation of ST6GAL1 by miRNA. Overall, up- and down-miRs had the anticipated impact on ST6GAL1 protein levels. Although a few cell-specific differences was observed, most notably for down-miRs (miR-499a-5p, miR-216a-3p), in all cases the expected result was observed in at least one cell line, validating the accuracy of the miRFluR assay.

The regulatory processes occurring post-transcription result in a substantial difference between the abundance of an mRNA and its corresponding protein. miRNA function post-transcriptionally through de/stabilizing of mRNA or bypassing transcription and impacting translation level, meaning that miRNA can potentially affect protein level without having impact on the corresponding mRNA level[125]. I tested ST6GAL1 mRNA regulation by a select subset of

miRNAs in cancer cells (A549, PANC1, HT-29). The results indicate that the response at the mRNA level was often discordant with protein levels and showed a high dependency on the cell (**Figure 2.7**). The results follow data from multiple studies showing discrepancies between mRNA transcript and protein levels[78,95,125,126].

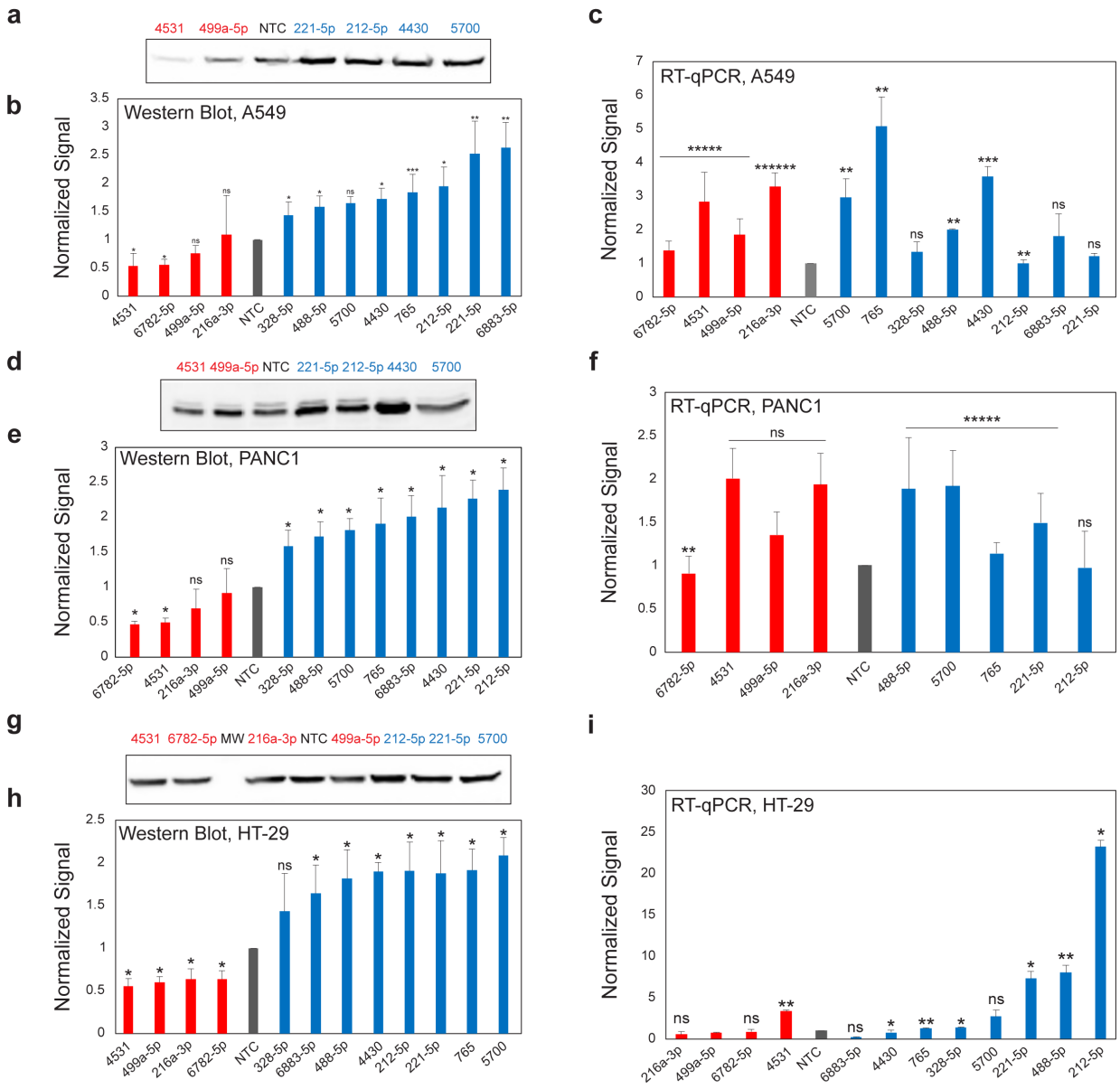

Figure 2.7 miRNAs control ST6GAL1 expression at the protein level. (a-f) Regulation of ST6GAL1 by down- and up-miRs in A549 (a-c), PANC1 (d-f) and HT-29 (g-i) cell lines. **(a, d, g)** Western blot analysis of ST6GAL1 for indicated miRNAs in A549 (a), PANC1 (d), and HT-29 (g, MW: molecular weight) cells. **(b, e, h)** Quantification of Western blots of ST6GAL1 in a, d, g. Cells were transfected with miRNA mimics or non-targeting control (NTC, 50 nM, 48 h). In each cell line, a representative blot is shown. ST6GAL1

expression was normalized by Ponceau and divided by the normalized signal from NTC. miRNAs indicated in figure (blue: up-miR, red: down-miR). **(c, f, i)** RT-qPCR analysis for expression of ST6GAL1 mRNA by individual down- and up-miR in A549 (c), PANC1 (f) and HT-29 (i) cell lines. RT-qPCR samples are normalized to GAPDH as an endogenous housekeeping gene and then to NTC (n=3). All experiments were performed in biological triplicate. Errors shown are standard deviations. Paired *t*-test was used to compare miRs to NTC (ns not significant, * $p < 0.05$, ** < 0.01, *** <0.001, ***** <0.00001, ****** <0.000001).

Given the ST6GAL1 function, I examined whether miRNA regulating protein expression could also impact protein activity (**Figure 2.8**). I tested the potential impact of up-miRs (miR-221-5p, miR-212-5p) and down-miRs (miR-499a-5p, miR-4531) targeting ST6GAL1 on α-2,6-sialylation using the α-2,6-sialic acid specific *Sambucus nigra* lectin (SNA)[127,128].

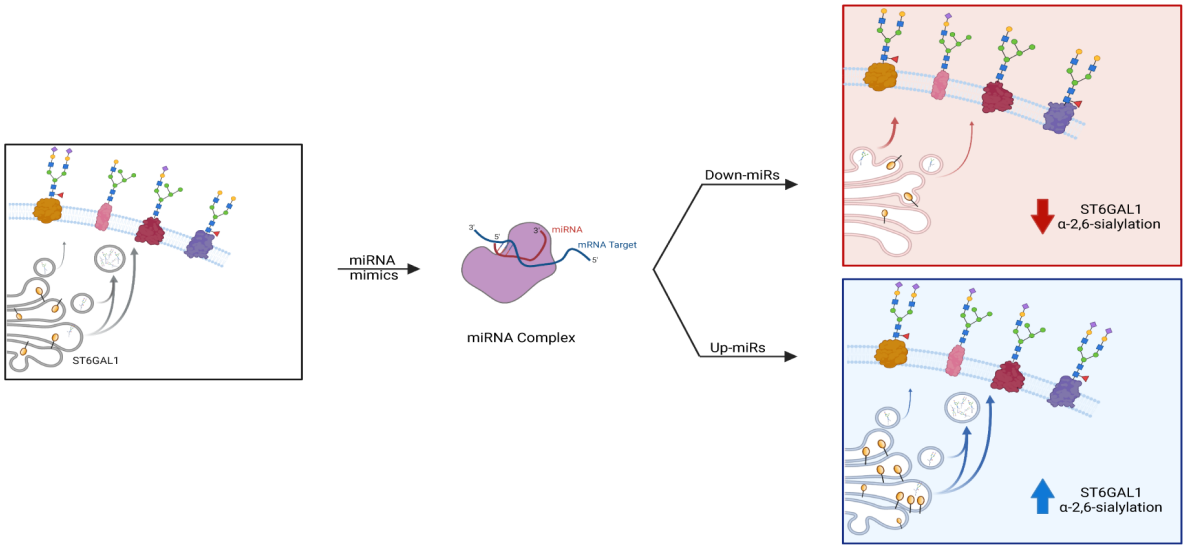

Figure 2.8 miRNA mediate ST6GAL1 and resulting α-2,6-sialylation.

The results were consistent with the effects of miRNA on protein expression, with up-miRs increasing and down-miRs decreasing α-2,6-sialic acid levels in A549 cells (**Figure 2.9**). Intriguingly, the up-miR-221-5p, which has a strong impact on ST6GAL1 and α-2,6-sialylation in A549 cells, is highly expressed in pancreatic cancer, and is associated with decreased survival[122]. In recent work, ST6GAL1 and α-2,6-sialylation have also been shown to be important in pancreatic cancer formation and progression and correlate with decreased survival[26,98,129]. Given the importance

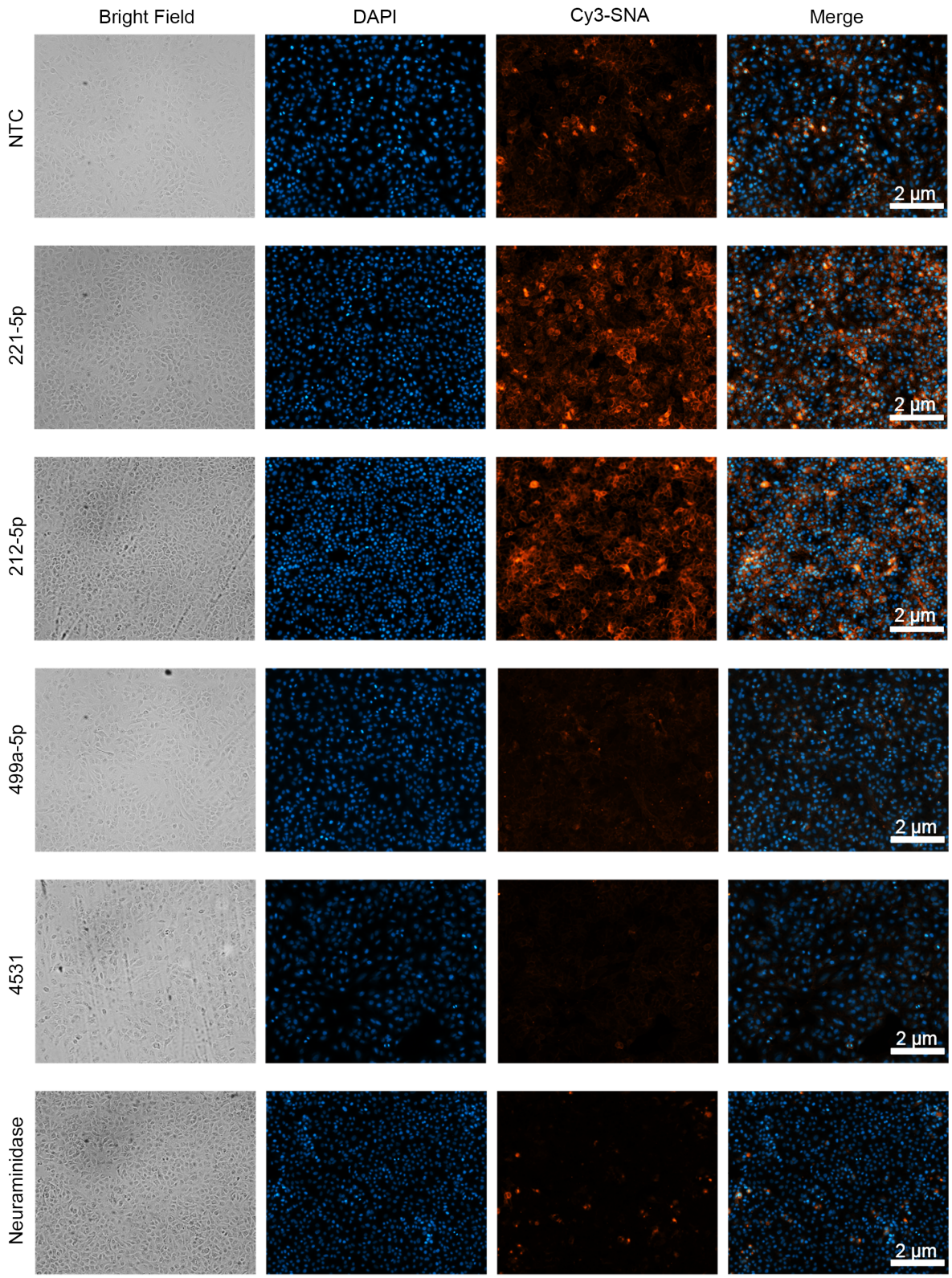

Figure 2.9 miRNAs regulate α-2,6-sialylation via controlling ST6GAL1 expression in A549 cell line. SNA staining of up-miR (miR-221-5p or miR-212-5p) and down-miR (miR-499a-5p, miR-4531) treated in A549 cells. NTC is the control for miRNA and Neuraminidase is a negative control for SNA staining.

Quantification of SNA staining is shown in Figures S4 on published work (PMID: 36439307)[130]. All experiments were performed in biological triplicate.

of both ST6GAL1 and miR-221-5p, miR-212-5p in pancreatic cancer, I also tested the potential impact of these two up-miRs on α-2,6-sialylation in PANC1 cells (**Figures 2.10**). I observed an increase in SNA intensity stained for α-2,6-sialylation. This points towards a potential functional role for upregulatory miRNA in controlling cancer-related proteins and glycan expression (**Figure 2.10**).

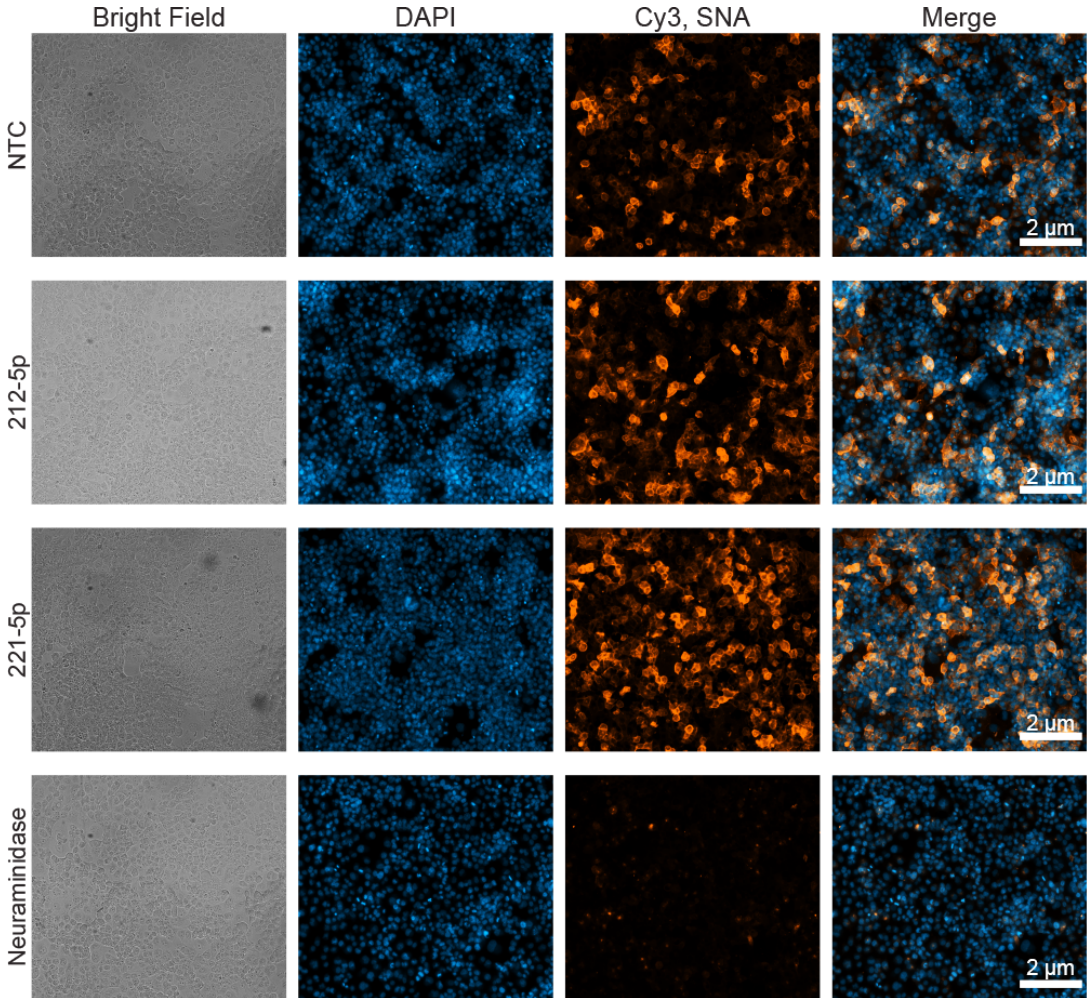

Figure 2.10 Upregulatory miRNAs increase α-2,6-sialylation via upregulating ST6GAL1 expression in PANC1 cell line. SNA staining of up-miR (miR-221-5p or miR-212-5p) treated in the PANC1 cells. NTC is the control for miRNA and Neuraminidase is a negative control for SNA staining. Quantification

of SNA staining is shown in Figures S5 on published work (PMID: 36439307)[130]. All experiments were performed in biological triplicate.

Next, to confirm that the miRNA mimics accurately represent the actions of endogenous miRNA, antimiRs were utilized. These hairpin inhibitors soak up an endogenous miRNA, causing relief of repression for down-miRs. Given their mode of action, it would anticipate that anti-miRs of upregulators would cause repression of protein expression (**Figure 2.11**). A subset of anti-miRs (4 anti-up-miRs: anti-212-5p, -221-5p, -765, -488-5p, and 2 anti-down-miRs: anti-4531, -499a-5p) were tested in A549 cell line (**Figure 2.12a-b**). The anti-up-miRs were also examined in PANC1 cell line (**Figure 2.12c-d**). All anti-miRs chosen had high to moderate levels of miRNA expression in the selected cell lines[121,131-133]. In accordance with expectation, I found that anti-up-miRs downregulated and anti-down-miRs upregulated protein expression for ST6GAL1. For anti-up-miRs a concomitant loss of α-2,6-sialic acid was also observed, supporting a function for these miRNAs in maintenance of sialyltransferases and sialylation levels (**Figure 2.12e**).

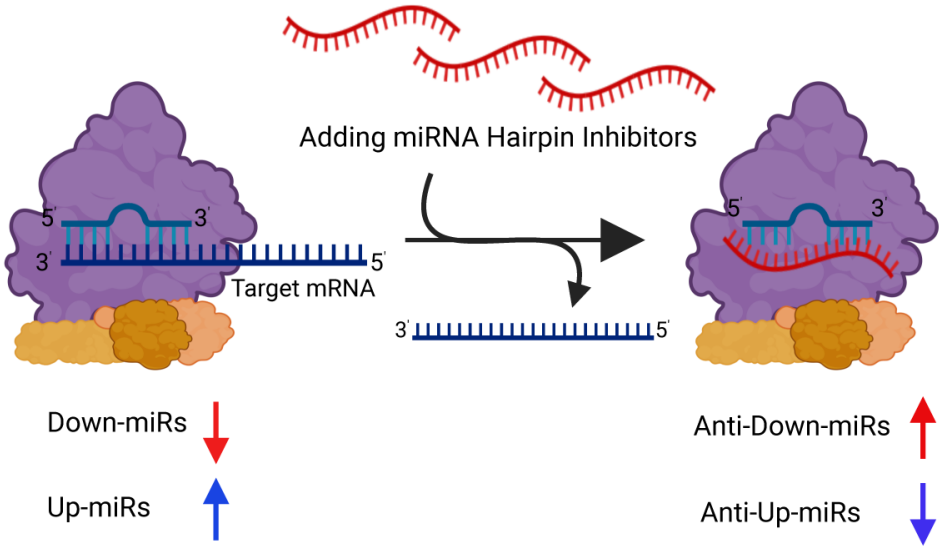

Figure 2.11 Schematic representation of miRNA hairpin inhibitor (anti-miR) function.

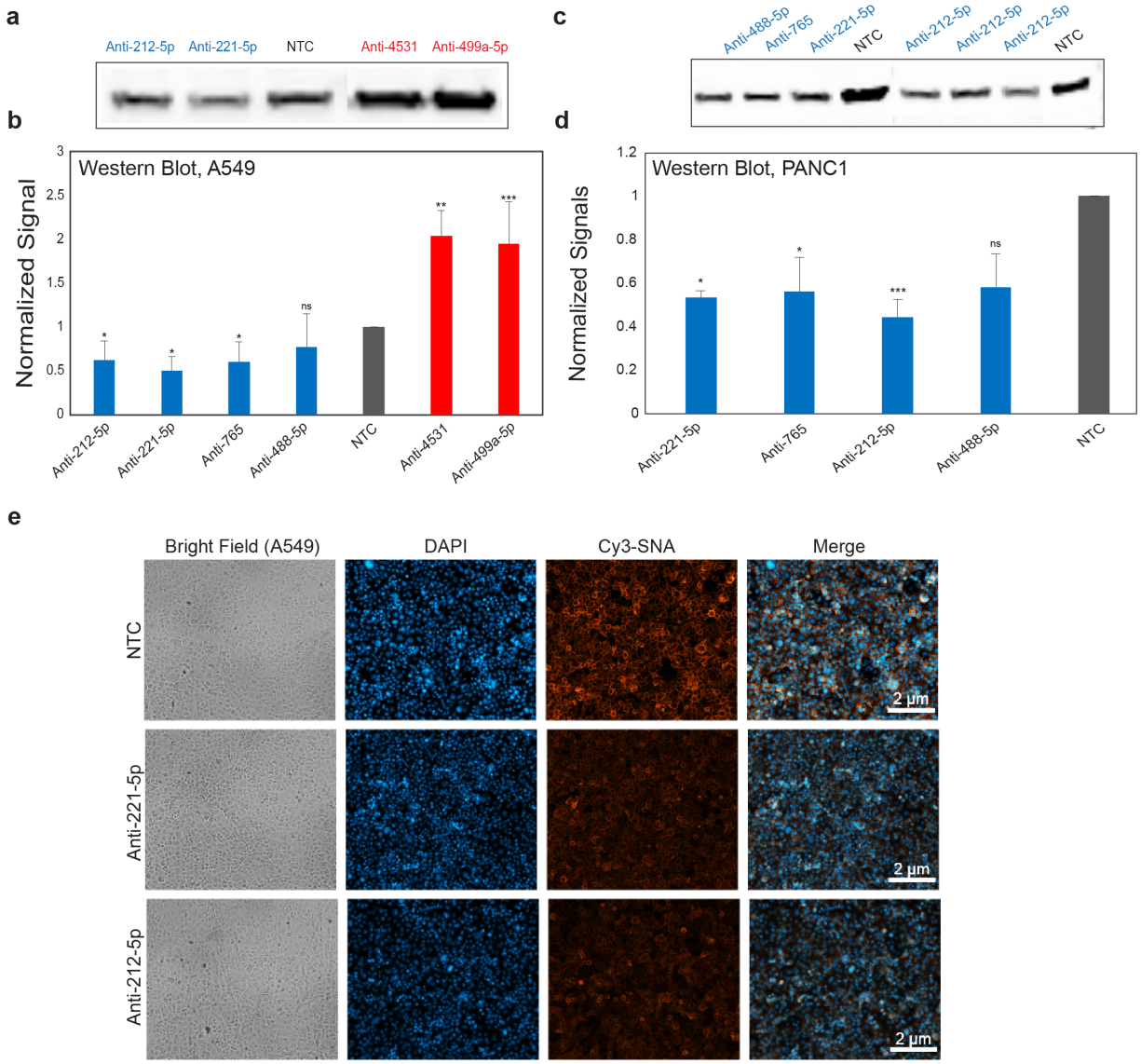

Figure 2.12 Endogenous miRNA both up- and down-regulate ST6GAL1. (a) Western blot analysis of ST6GAL1 for indicated anti-miRs in A549 cells. **(b)** Graph represents normalized data for three biological replicates for samples in a. Inset shows sample Western blot. **(c)** Western blot analysis of ST6GAL1 for indicated anti-miRs in A549 cells. **(d)** Graph represents normalized data for three biological replicates for samples in c. The A549 and PANC1 cells were transfected with anti-miR or non-targeting control for anti-miR (NTC, 50 nM, 48 h). In each cell line, a representative blot is shown. ST6GAL1 expression was normalized by Ponceau and divided by the normalized signal from NTC. Anti-miR indicated in figure (blue: anti-up-miR, red: anti-down-miR). **(e)** SNA staining of cells treated as in b with NTC, anti-miR-221-5p and anti-miR-212-5p. Data for SNA staining for anti-down-miRs are not shown here (PMID: 36439307)[130]. All

experiments were performed in biological triplicate. Errors shown are standard deviations. Paired *t*-test was used to compare miRNAs to NTC (ns not significant, $* p < 0.05$, $** < 0.01$, $*** < 0.001$).

2.3.3 High-throughput analysis of ST6GAL2 shows predominantly downregulation by miRNAs

Mapping the miRNA regulatory landscape for the most prevalent 3′UTR for the *st6gal2* transcript (**Figure 2.5**) indicates that, in contrast to ST6GAL1, 69% of miRNA hits of ST6GAL2 are down-miRs, suggesting the miRNA mode of action is transcript dependent. In choosing the a subset of miRNA to validate, three up-miRs (miRs: -3619-5p, -124-3p, -605-3p) and three down-miRs (miRs: -30c-2-3p, -6828-5p, -22-3p) were selected which is in accordance with their known biological roles in cancer biology[134-137]. The select subset of miRNA hits were validated for their impact on ST6GAL2 expression in two different cancer cell lines: A549 (**Figure 2.13a−b**) and HT-29 (**Figure 2.13d-e**). Consistent with the previous work[78], the impact of miRNA mimics on ST6GAL2 protein expression matched with the impact observed using the pFmiR-ST6GAL2 sensor in the miRFluR assay. The miRNA regulation of *st6gal2* transcript was examined using RT-qPCR in A549 and HT-29 cell lines (**Figure 2.13c, f**). Overall, I observed consistent downregulation of *st6gal2* mRNA by down-miRs and activation of target transcript by up-miRs. To verify the observed protein expression regulation is resulted from endogenous miRNA activity, I used anti-miRs against two up-miRs (anti-3619-5p, anti-124-3p) and two down-miRs (anti-30c-2-3p, anti-6828-5p) in A549 cell line. As expected, inhibiting the endogenous up-miRs caused a loss of protein expression, and inhibiting endogenous down-miRs caused an increase in ST6GAL2 levels (**Figure 2.13g-h**).

In comparison to ST6GAL1, the biological roles of ST6GAL2 are far less studied. Liu, R., *et. al.*, reported that the low expression levels of ST6GAL2 may correlate with liver inflammation in hepatocellular carcinoma (HCC)[108]. The high expression of ST6GAL2 is shown to be associated

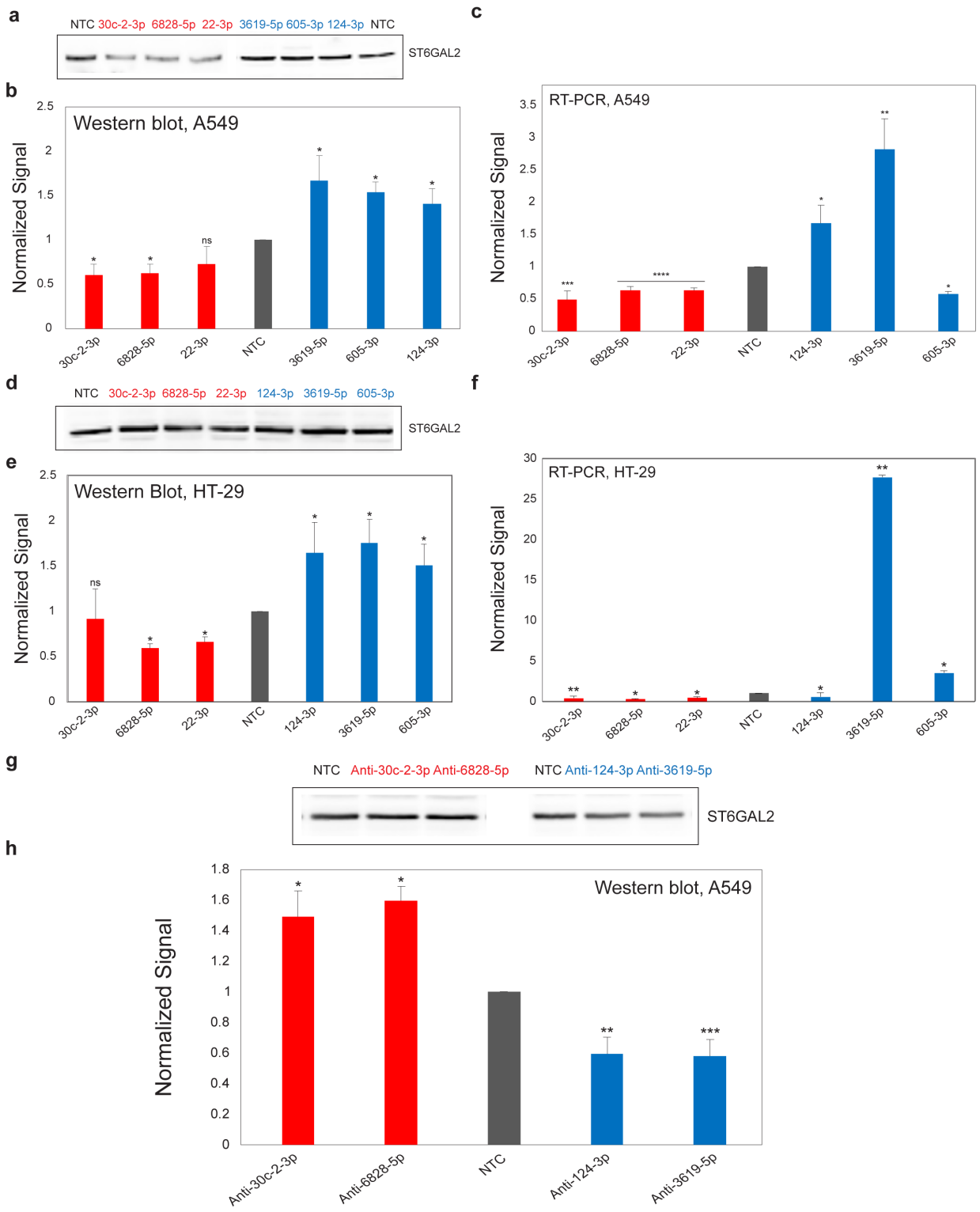

Figure 2.13 miRNAs regulate ST6GAL2 expression at mRNA and protein levels. (a) Western blot analysis of ST6GAL2 in A549 cells. **(b)** Quantitation of Western blot analysis shown in a. **(c)** RT-qPCR analysis for expression of ST6GAL2 mRNA by individual down- and up-miR in A549. **(d)** Western blot analysis of ST6GAL2 in A549 cells. **(e)** Quantitation of Western blot analysis shown in d. **(f)** RT-qPCR analysis for expression of ST6GAL2 mRNA by individual down- and up-miR in HT-29. **(g)** Western blot

analysis of ST6GAL2 for indicated anti-miRs in A549 cells. **(h)** Graph represents normalized data for three biological replicates for samples in g. In each cell line, representative blot is shown. A549 and HT-29 cells were treated with miRNA mimics as in Figure 2.7 and anti-miRs as in Figure 2.12. RT-qPCR samples were normalized to GAPDH and NTC. All experiments were performed in biological triplicate. Paired *t*-test was used to compare miRs to NTC (ns not significant, $* p < 0.05$, $** < 0.01$, $*** < 0.001$).

with tumor progression in follicular thyroid carcinoma (FTC) *in vitro* and *in vivo*[104]. As discussed in Section 1.4, lncRNAs can modulate miRNA levels, altering miRNA regulatory function. Intriguingly, loss of miR-22-3p function, a known down-miR for ST6GAL2, is observed in FTC by the action of lncRNA, HCP5. This results in ST6GAL2 upregulaion in FTC which leads to FTC progression[119]. Herein, miR-22-3p was used as a positive control across miRFluR assay (**Figure 2.6f**), Western blot experiments (**Figure 2.13a-b, d-e**), and RT-qPCR (**Figure 2.13e, f**) for ST6GAL2, showing consistent downregulation of ST6GAL2 through Cerulean channel or endogenous ST6GAL2 protein and mRNA expression, respectively. This points towards the accuracy of miRFluR assay in correctly identifying miR hits for a target 3'UTR. Furthermore, in human, miR-124 is encoded on three loci: *miR-124-1*, *-2*, and *-3*, resulting **pri**mary **miR-124**-1, -2, -3 (pri-miR-124), among which pri-miR-124-1 is dominantly expressed and results in mature miR-124-3p (miR-124-3p-1). This miR-124-3p, identified and validated as an up-miR for ST6GAL2, is a brain-specific miRNA. The Furukawa laboratory showed miR-124-3p functional roles in human and mouse central nervous system (CNS) development (neuronal differentiation, maturation, and survival)[138,139]. Of note, ST6GAL2 is mainly expressed in adult and embryonic brains and plays a functional role in brain development[101]. Together, the miR hit list identified for ST6GAL2 may help to further explore ST6GAL2 roles in different biological contexts.

2.3.4 Upregulation by miRNA is via direct interactions with the 3'UTR and requires AGO2 and FXR1

Multiple mechanisms exist by which miRNA could upregulate protein expression. These include regulation by miRNA of gene promoters and enhancers, competition between miRNA, and other indirect effects[140,141]. The identification of up-miRs via miRFluR precludes that the observed upregulation of endogenous proteins ST6GAL1 and ST6GAL2 is through miRNA modulation of gene promoter or enhancer elements. To test whether competition between miRNA could explain upregulation, I used RNAhybrid[142] to identify potential miRNA binding sites for ST6GAL1 and ST6GAL2 (**Figure 2.14**). As a result, the majority of predicted sites for ST6GAL1 and ST6GAL2 miR hit lists are via non-canonical binding sites, and up-miR predicted sites did not overlap with down-miRs, arguing that the observed upregulation is not predominantly via miRNA competition (**Figure 2.14a-c**). As discussed in Section 1.3.2, miRNA drive their inhibitory functions (as down-miRs) via interacting with their target transcript mainly within seed regions involving two distinct binding patterns: seed match and imperfect seed match with supplementary and compensatory pairing, respectively (**Figure 1.6**). Herein, only 47% (28 out of 59) of downregulatory miRs and 38% (27 out of 72) of upregulatory miRs identified for both ST6GAL1 (down-miRs: 19; up-miRs: 50) and ST6GAL2 (down-miRs: 40; up-miRs: 22) were predicted by Targetscan[74] and followed seed binding patterns, showing ~ 50% and ~ 70% false negative predictions for the down-miRs and up-miRs, respectively (**Figure 2.14d**).

Consistent with this work, miRNAs have been shown to activate expression in select circumstances (e.g. senescent cells[143,144], oocytes[145], and mitochondria[146]) where the mRNA is destabilized, lacking a 5′-cap and a typical poly(A) tail. In actively dividing cells, mRNA do not

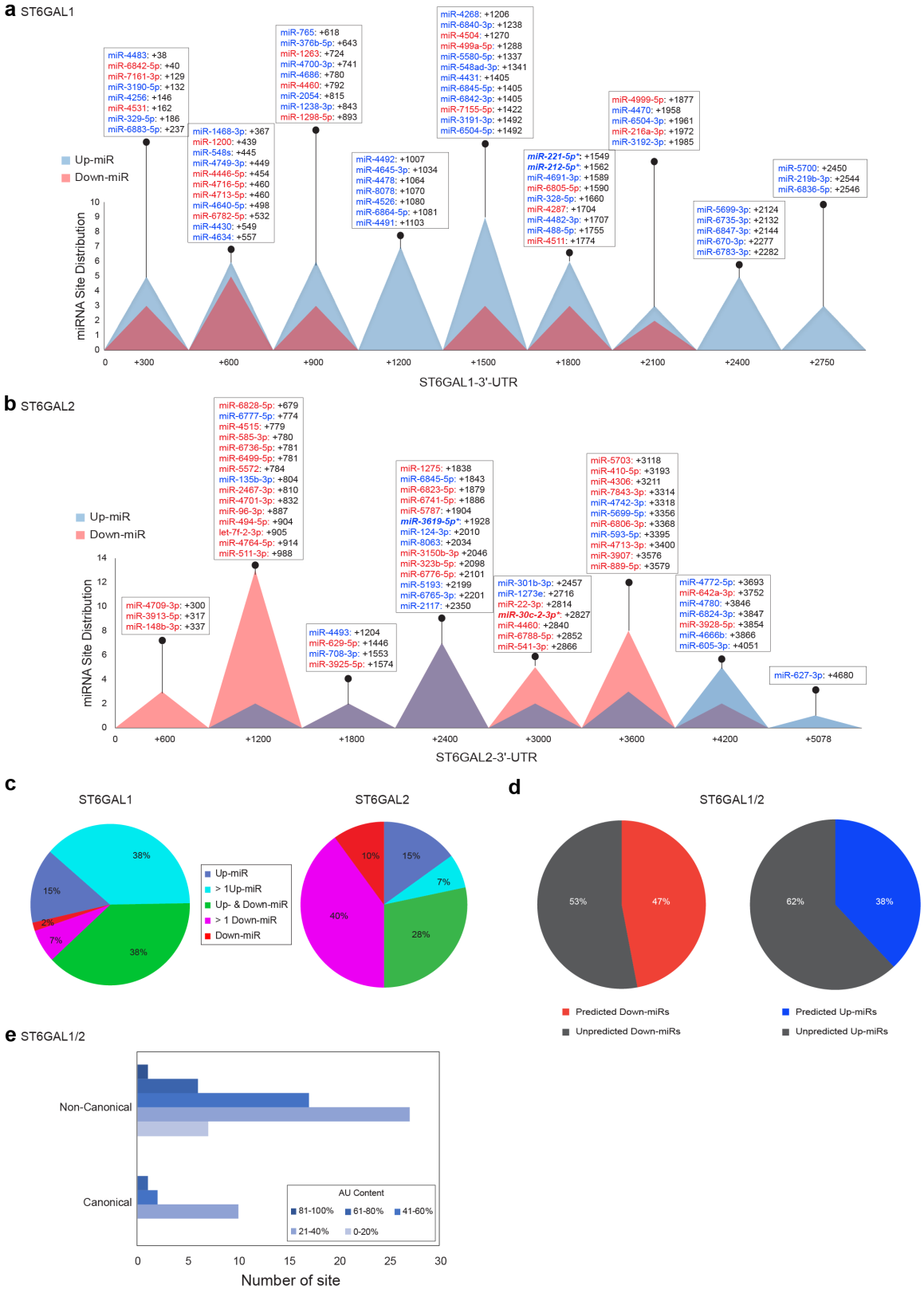

Figure 2.14 Predicted miRNA binding site analysis for α-2,6-sialyltransferases. (a) Map of the binding

sites for miRNA identified as hits by our miRFluR assay. Sites shown are the most stable hybridization sites predicted by RNAhybrid[142]. Annotations are given for every 300 bp. **(b)** Map of the binding sites for miRNA identified as hits for ST6GAL2 by our miRFluR assay. Sites shown are the most stable hybridization sites predicted by RNAhybrid[142]. Annotations are given for every 600 bp. **(c)** Pie charts representing the distribution of miRNA sites overlap within the 3'UTR for ST6GAL1 and ST6GAL2. Sites are defined as overlapping if the annotated hybridization sites share nucleotides. Periwinkle blue: up-miRs with no overlap, turquoise blue: overlap between 2 or more up-miRs, green: overlap between a set of up-miRs and down-miRs, magenta: overlap between 2 or more down-miRs, red: down-miRs with no overlap. Percent is a function of sum of miRNA hits. **(d)** Pie charts show the percentage of down-miRs (left) and up-miRs (right) identified for ST6GAL1/2 predicted by Targetscan[74] **(e)** Bar graphs representing the percentage of AU content of four different predicted miR sites (canonical seed: perfect seed match, supplementary pairing: base pairing near to canonical site, non-canonical seed: imperfect seed match, compensatory pairing: base pairing near to non-canonical site) for all predicted up-miRs sites for ST6GAL1 and ST6GAL2. Sites considered in b are the most stable predicted sites based on RNAhybrid[142] shown in a.

typically meet these requirements and upregulation of expression by miRNA is not thought to occur.

The observed upregulation of protein expression via direct miRNA: mRNA interactions in non-dividing (quiescent) cells or in mitochondria was thought to require AU rich elements and unstable mRNA, respectively[144-146]. In this Chapter, the miRNA-mediated upregulation is observed in *dividing cancer cells*. To gain more insight into the requirements for upregulation observed in this work, I classified the predicted sites for the up-miRs on ST6GAL1 and ST6GAL2 by two categories: site motif and AU content. Currently, contiguous binding of at least 6−8 base pairs in the seed region (5′-end of the miRNA), is thought to be required for strong binding by RISC complexes which mediates miRNA effects Section 1.3.2[74,111,147]. However, imperfect seed miRNA, in which non-contiguous binding is observed at the 5′-end and cases with compensatory interactions at the 3′-end of the miRNA can downregulate, as well. For up-miRs, the vast majority were predicted to have non-canonical binding (without seed binding patterns) and were not AU rich (**Figure 2.14e**). Of the three validated up-miR sites, only one has a perfect seed pairing (miR-221-5p, **Figure 2.15b**), and none are AU rich or contain the AU rich element sequence (AUUUA).

This contradicts the earlier proposal by Steitz and co-workers[144] that this motif is required for the activation of protein expression by miRNA, although that work was done in quiescent cells.

I next tested whether up-miRs act via direct base-pairing. RNAhybrid[142] is used to identify the most stable potential binding sites and an additional potential site for two up-miRs of ST6GAL1 (miR-212-5p and miR-221-5p, **Figure 2.15a-b, d**) and one for ST6GAL2 (miR-3619-5p, **Figure 2.15c-d**). All interacting base pairs in the 3′UTRs were mutated to the corresponding miRNA sequence in the pFmiR-ST6GAL1 and pFmiR-ST6GAL2 sensors and tested them against the mimics using the miRFluR assay (**Figure 2.15d**). In all cases, the most stable site predicted by RNAhybrid[142] was the binding site for the up-miRs, the mutation of which caused a significant loss of upregulation in comparison with the wildtype sensor (WT). Mutation of down-miR predicted sites for ST6GAL1: miR-4531 (**Figure 2.15e**); ST6GAL2: miR-30c-2-3p (**Figure 2.15f**) also gave the expected results (**Figure 2.15g**). The data confirmed upregulation as a direct effect via binding of the miRNA to the 3′UTR.

In quiescent cells, Argonaute 2 (AGO2), an important part of the machinery for miRNA-mediated protein repression, and Fragile-X-mental retardation related protein 1 (FXR1) were found to be required for upregulation[143,144]. However, upregulation was not found in actively dividing cells such as cancer cells. I next tested whether the upregulation I observe in cancer cells might use the same machinery required for upregulation in quiescent cells. To this end, pooled siRNAs were used to deplete FXR1 and AGO2 in A549 cells. I also knocked down the TNRC6A (aka GW182), a scaffolding protein that directly interacts with AGO2 leading to miR-mediated repression[70,148]. Silenced cells (control (NTP), si-AGO2, si-FXR1, si-TNRC6A) were next transfected with either non-targeting control (NTC) or individual up-miRs: miR-212-5p or miR-221-5p and examined their impact on ST6GAL1 protein expression.

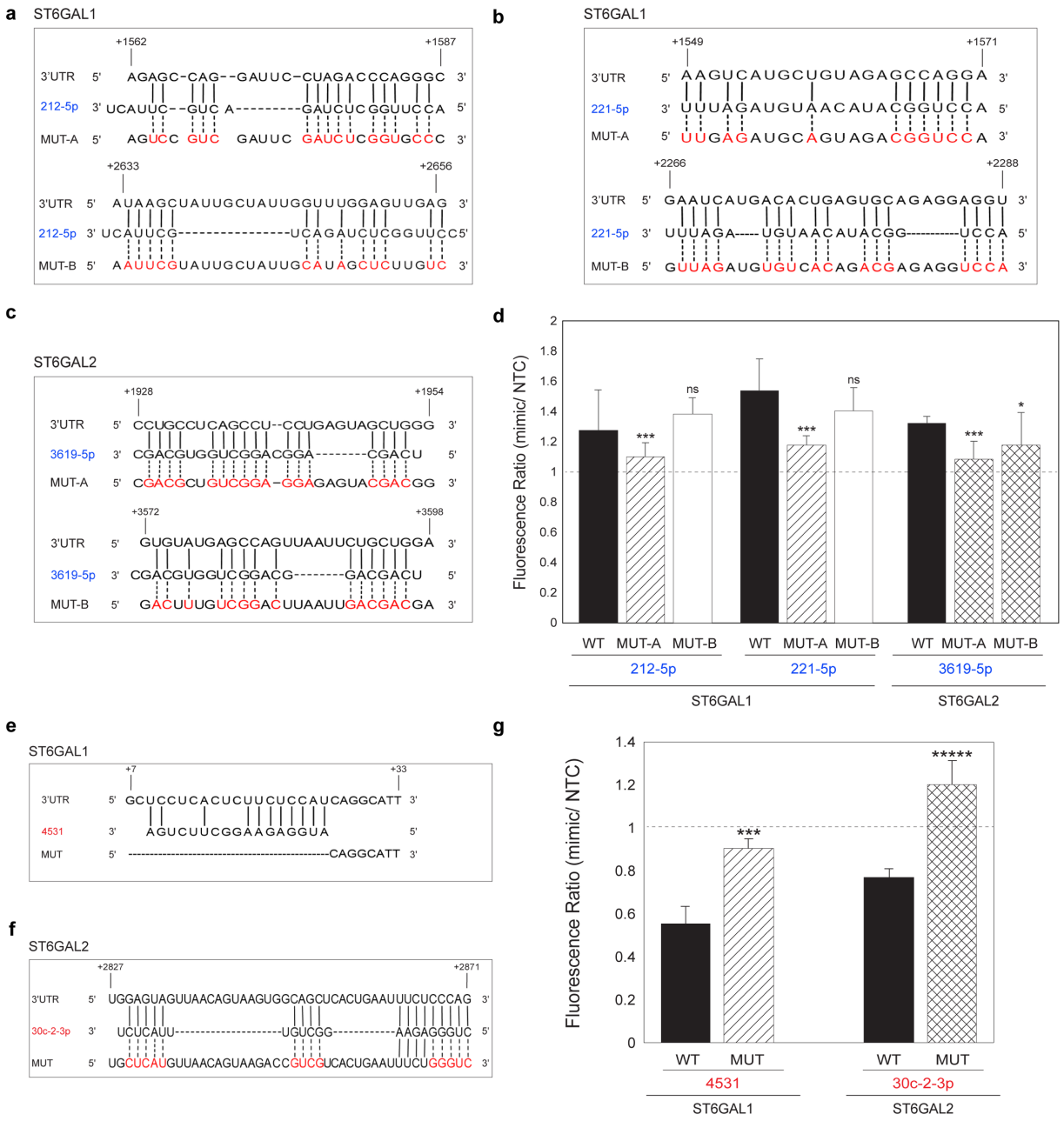

Figure 2.15 Upregulation of expression by miRNAs requires direct interaction with 3′UTR. (a and b) Alignment of miRs (a: 212-5p, b: 221-5p) with predicted ST6GAL1-3′UTR sites and their corresponding mutants. **(c)** Alignment of miR-3619-5p with predicted ST6GAL2-3′UTR sites and their corresponding mutants. **(d)** Bar graph of data from mutant miRFluR sensors as in b and c. **(e and f)** Alignment of miRs (a: 4531, b: 30c-2-3p) with predicted ST6GAL1-3′UTR and ST6GAL2-3′UTR sites, respectively, and their corresponding mutants. **(g)** Bar graph of data from mutant miRFluR sensors as in e and f. Mutated nucleotides are shown in red. Data were normalized over NTC in each sensor. Statistical analysis using the standard t test compared the impact of each miRNA in the wild-type (WT) sensor with the corresponding mutant. Errors are standard deviations. Standard *t*-test was used to compare the impact of miRNA in knockdowns with impact in NTP (ns not significant, *$p < 0.05$, *** < 0.001, ***** < 0.00001).

AGO2 and FXR1 were found to be required for upregulation of ST6GAL1 by up-miRs (**Figure 2.16**). In contrast, depletion of TNRC6A mildly enhanced upregulation by miR- 221-5p compared to the control (~23% increase, $p < 0.01$), in line with a proposed role for TNRC6A as a repressor[146]. Similar results were seen with miR-212-5p, but they did not meet the statistical threshold. This data precludes the "RISC dissociation/relief of repression[149,150]" as desired mechanism as in such circumstances, TNRC6A depletion should not give increased levels of protein upregulation. In mitochondria, the absence of TNRC6A was noted as a critical requirement for miRNA-mediated activation[146], showing a distinct miRNA regulatory machinery drives protein upregulation which does not require TNRC6A, and it is not through relief of repression.

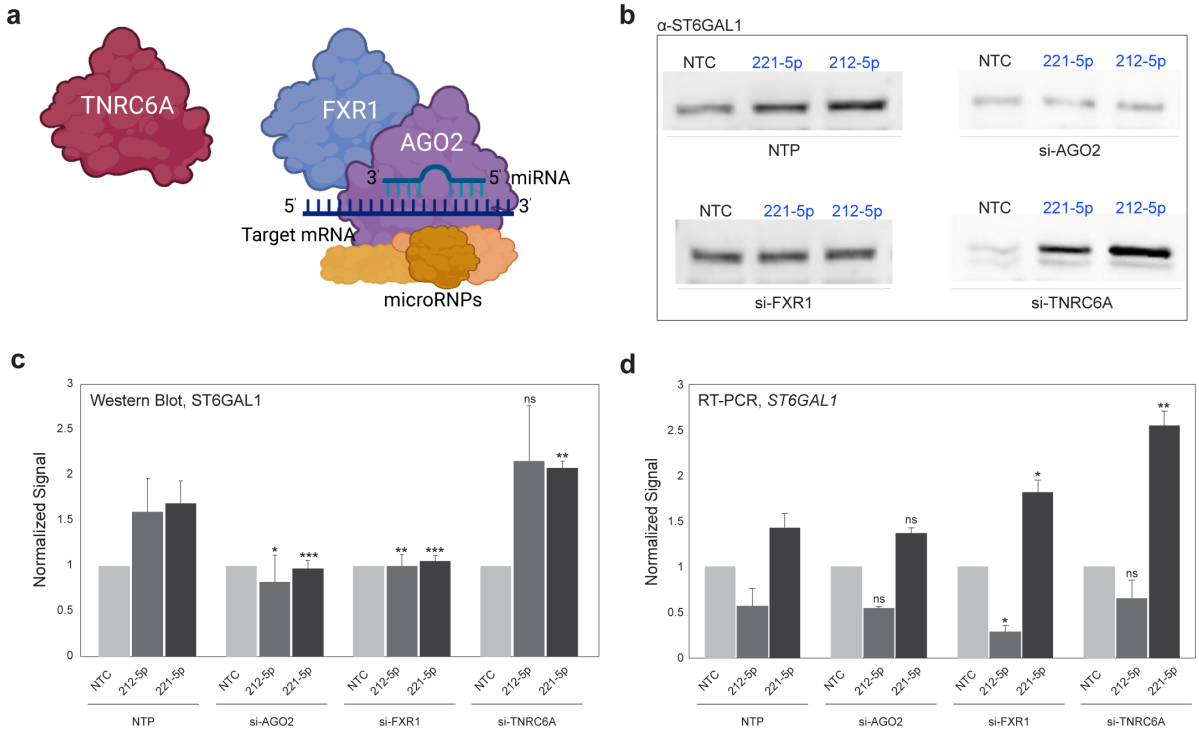

Figure 2.16 Upregulation of expression by miRNAs occurs within a complex containing AGO2 and FXR1. (a) Schematic representation of potential miRNA complex. **(b)** Representative Western blot of ST6GAL1. A549 cells were treated with pools of siRNA (non targeting (NTP), si-AGO2, si-FXR1, si-TNRC6A, 48 h) prior to treatment with miRNA mimics (NTC, miR-212-5p, miR-221-5p, 48 h) and analysis. **(c)** Quantitative Western blot analysis of experiment shown in b. Western blot analysis of ST6GAL1 expression normalized as before. **(d)** RT-qPCR analysis for samples as in c. All RT-qPCR samples are normalized to GAPDH and NTC. All experiments were performed in biological triplicate.

Errors are standard deviations. Standard *t*-test was used to compare the impact of miRNA in knockdowns with impact in NTP (ns not significant, *$p < 0.05$, ** < 0.01, *** < 0.001).

2.4 Discussion

In many cancers, α-2,6-linked sialic acids are overexpressed, and dysregulation of this glycan is emerging as a crucial driver of cancer formation, metastasis, and immune recognition[26,96,97,99,100,151]. miRNA are major regulators of the glycome, but their role in controlling α-2,6-linked sialic acid has not been well studied[92,94,95,152-154]. The comprehensive analysis of the miRNA regulatory landscape for the α-2,6-linked sialylation enzymes ST6GAL1 and ST6GAL2, described in this Chapter, has revealed new potential links between miRNA and the upregulation of α-2,6-linked sialosides observed in cancer. The dominant view of miRNA regulation is that in proliferating cells the direct impact of miRNA on protein expression is downregulatory. The high-throughput analysis of ST6GAL1 and ST6GAL2 contradicts this, revealing that upregulatory interactions may be commonplace. Consistent with this, a smaller high-throughput luciferase assay for POT1, PTEN, MXI1, and other cancer-related genes also identified a number of upregulatory miRNA interactions, but these were ignored as noise[155]. The previous miRFluR analysis of miRNA mediated regulation for B3GLCT also identified potential up-miRs for that enzyme[78]. These interactions have been missed by the scientific community because the current pathway for identifying miRNA interactions has depended on validating potential targets of miRNAs predicted by Targetscan and other algorithms that are focused on downregulation[74]. Recent work knocking out AGO complexes found that removal of the miRNA machinery caused most genes to lose expression, consistent with upregulation being a primary function of miRNA, rather than the expected gain that would come from loss of a repressor[156]. Taken together, the data support upregulation as part of the broader landscape of miRNA regulatory mechanisms in both dividing and quiescent cells.

For ST6GAL1, which is known to be upregulated in many cancers[99], upregulation appears to be the major mode of action of miRNA, although these same miRNAs have downregulatory activity for other genes. Given the importance of miRNA in tuning the expression of genes, it is perhaps unsurprising that regulation by miRNA would be in both directions. Precise control over protein expression is critical for low abundance proteins, where noise becomes an increasing problem[62]. This class of proteins includes many glycosylation enzymes, GPCRs, and most cell surface receptors. These proteins, which often act as initiators of amplified signals, would be important to tightly regulate. The expanded understanding of the miRNA regulatory landscape provided by our work opens new possibilities for miRNA mechanisms to modulate protein expression and exposes our need to create tools to further explore the impact of these noncoding RNA. Validation of our results shows that upregulation by miRNA occurs through direct binding between the miRNA and 3'UTR. My data challenges our current understanding of miRNA regulation, implying that upregulation is a normal mode of miRNA function, suggesting that upregulation of protein expression might not be limited to non-dividing cells. This Chapter may help explain why α-2,6-sialylation is commonly upregulated in cancer, as miRNA that upregulate ST6GAL1 are high in cancers, such as pancreatic cancer, that have high levels of α-2,6-sialylation (**Figure 2.17**)[99,123,157].

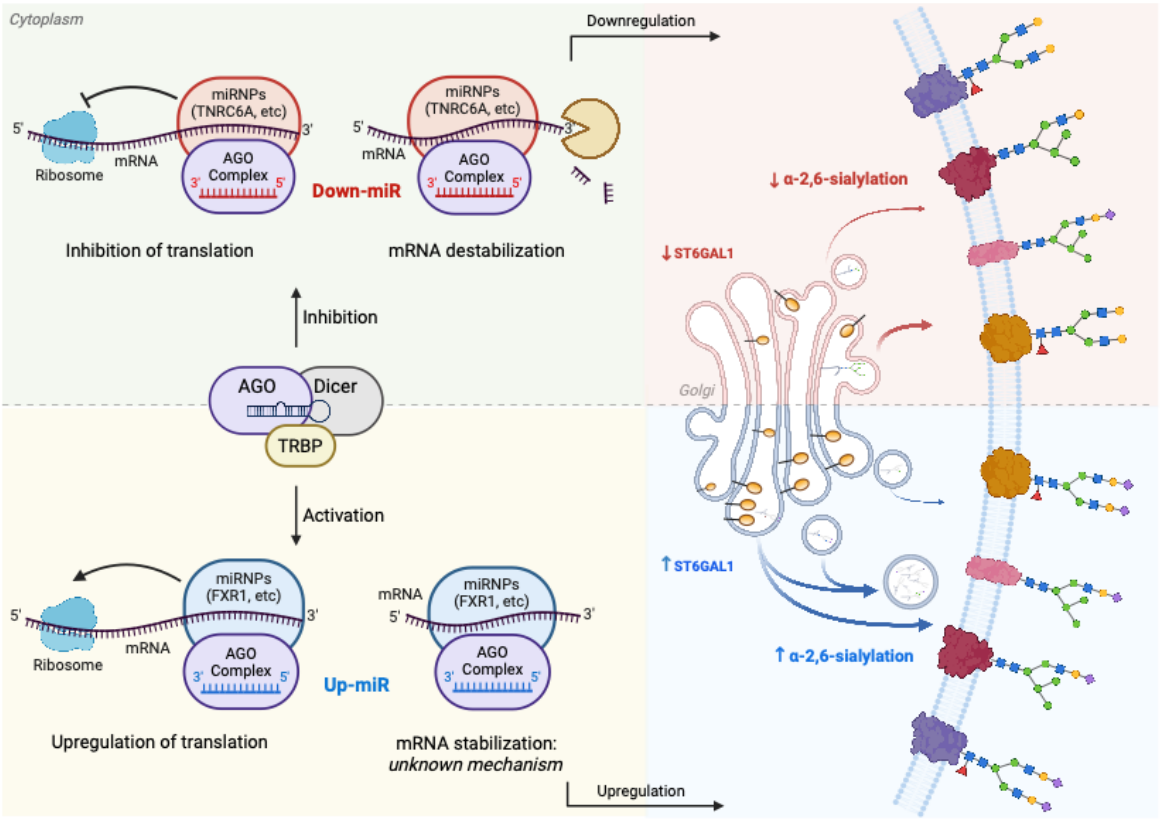

Figure 2.17 Bidirectional tuning by microRNA. Contrary to the dominant model, miRNA upregulates the expression of ST6GAL1/2 enzymes and α-2,6-sialylation. Upregulation requires FXR1 and AGO2 and occurs via a direct miRNA−mRNA interaction.

2.5 Conclusion

Currently, the common presumption is that in proliferating cells the direct impact of miRNA on protein expression is downregulatory. Steitz and coworkers were the first to propose a miRNA mediated upregulation pathway, in which miRNA bound to AU-rich elements (AREs) could activate translation in senescent cells[143,144]. In this Chapter, my work confirms a novel role for miRNAs, protein upregulation in actively dividing cells which is validated to occur through direct miRNA: mRNA interactions. My data further suggests the FXR1/AGO2 proteins are involved in complexes with miRNAs to drive upregulation by miRNA in proliferating cells,

arguing that distinct AGO2 complexes may mediate up- and down-regulation by miRNA. In Chapter 3, I expand the miRNA-mediate protein upregulation to a cooperative upregulation by miRNAs of functionally associated proteins.

2.6 Experimental methods

2.6.1 Cloning

ST6GAL1 and ST6GAL2 3'UTRs were cloned from genomic DNA (gDNA) extracted from HEK293T cell line using QIAquick gel extraction kit (catalog #: 28706) and primers shown in **Table 2.1**. The amplicons were cleaned up using the PCR clean-up kit (catalog #: KTS1115). The 3'UTR fragments were cloned using the NheI and BamHI restriction sites downstream of Cerulean in the pFmiR-empty backbone[78] using standard ligation protocols (NEB) and verified by Sanger sequencing (Molecular Biology Services Unit, University of Alberta). Large-scale endotoxin free DNA preparations were made for sequence-verified constructs (pFmiR-ST6GAL1 and pFmiR-ST6GAL2) using QIAGEN maxi-prep (catalog #: 12362 and catalog #: 19048). Plasmid maps for pFmiR-ST6GAL1 and pFmiR-ST6GAL2 and the glycogenes' 3'UTR sequences can be found in **Appendix A**.

2.6.2 Cell lines

All cell lines (HEK-293T, A549, PANC1, HT-29, OVCAR-3) were purchased directly from the American Type Culture Collection (ATCC) and cultured using suggested media (HT-29 & HEK-293T: Dulbecco's Modified Eagle Medium (DMEM), 10% FBS; A549: FK-12, 10%, FBS; PANC1: DMEM* (catalog # 30-2002), 10% FBS; OVCAR3: RPMI-1640, 20% FBS with 0.01 mg/mL bovine insulin) under standard conditions (5% CO_2, 37°C). All cells used were below passage number 15.

2.6.3 miRFluR high-throughput assay

The Human miRNA mimic library version 21 (MISSION, Sigma) was resuspended in ultrapure nuclease-free water (REF. #: 10977-015, Invitrogen) and aliquoted into black 384-well, clear optical bottom tissue-culture treated plates (Nunc). Each plate contained three replicate wells of each miRNA in that plate (1.8 pmol/well). In addition, each plate contained a minimum of 6 wells containing non-targeting control (NTC). To each well was added 20 ng of pFmiR-ST6GAL1 or pFmiR-ST6GAL2 plasmids in 5 µl Opti-MEM (Gibco) and 0.1 µl Lipofectamine™ 2000 (Life Technologies) in 5 µl Opti-MEM (Gibco). The solution was allowed to incubate at room temperature for 20 min. HEK293T cells (25 µl per well, 400 cells/µl in phenol red free DMEM with FBS 10%) were then added to the plate. Plates were incubated at 37°C, 5% CO_2. After 48 hours, the fluorescence signals of Cerulean (excitation: 433 nm; emission: 475 nm) and mCherry (excitation: 587 nm; emission: 610 nm) were measured using the clear bottom read option (SYNERGY H1, BioTek, Gen 5 software, version 3.08.01).

2.6.4 Data analysis

We calculated the ratio of Cerulean fluorescence over mCherry fluorescence (Cer/mCh) for each well in each plate. For each miRNA, triplicate values of the ratios were averaged, and the standard deviation (S.D.) obtained. We calculated % error of measurement for each miRNA (100 × S.D./mean). As a quality control measurement (QC), we removed any plates or miRNAs that had high errors in the measurement (median error±2 S.D. across all plates) and/or a high median error of measurement for the plate (>15% for ST6GAL1 and >14% for ST6GAL2). After QC we obtained data for 2,161 miRNAs for ST6GAL1 and 2,166 miRNAs for ST6GAL2 out of 2601 total miRNAs screened. The Cer/mCh ratio for each miRNA was then normalized to the Cer/mCh ratio for the NTC within that plate and error was propagated. Data from all plates were then

combined and z-scores calculated. A z-score of ±1.965, corresponding to a two-tailed *p*-value of 0.05, was used as a threshold for significance. Post-analysis we identified 69 miRNA hits for ST6GAL1 and 62 for ST6GAL2 (see **Figure 2.6** and **Datasets 2.1-2.2** (.xls sheets)).

2.6.5 Western blots: ST6GAL1 and ST6GAL2

Cells were seeded in six-well plates (80,000 cells/well) and cultured for 24 h in appropriate media. Cells were then washed with HBSS and transfected with miRNA mimics (50 nM mimic, Dharmacon, Horizon Discovery, 5 μL Lipofectamine 2000, Life Technologies in 250 μL OptiMEM). The media was changed to standard media 12 hours post-transfection. Cells were then lysed at 48 h post-transfection in cold RIPA lysis buffer supplemented with protease inhibitors. For Western blot analysis, 50 μg of protein was run on 10% gels (SDS-PAGE) and transferred to iBlot2 Transfer Stacks (nitrocellulose, Invitrogen, catalog number: IB23002) using the iBlot2 transfer device (Invitrogen). Blots were incubated with Ponceau S Solution (Boston BioProdcuts, catalog #ST-180) for 10 min and the total protein levels were imaged using protein gel mode (Azure 600, Azure Biosystems Inc.). Blots were then blocked with 5% (PANC1, HT-29. OVCAR3) or 10% (A549) non-fat dry milk in TBST buffer (TBS buffer plus 0.1% Tween 20) for 1.5 hours at 55 rpm on rocker (LSE platform rocker, Corning) at room temperature. For ST6GAL1 blots were incubated with rabbit α-human-ST6GAL1 1° antibody (1:900 in TBST with 10% non-fat dry milk, catalog #: 14355-1-AP, Proteintech). For ST6GAL2, rabbit α- human-ST6GAL2 1° antibody (1:900 in TBST with 10% non-fat dry milk, catalog #: 28367-1- AP, Proteintech) was used. After overnight incubation at 4°C, blots were washed 4× for 2 min each with 0.1% TBST buffer. After washing, a secondary antibody was added (α- rabbit IgG HRP, 1: 10,000 in TBST with 10% non-fat dry milk, Abcam). After incubation for 1 h at room temperature with shaking (60 rpm), blots were washed 4× for 2 min each with 0.1% TBST buffer. The blots were then

developed using Clarity and Clarity Max Western ECL substrate according to the manufacturer's instructions (Bio-Rad). Membranes were imaged chemiluminescent mode (Azure 600, Azure Biosystems Inc.). Western blot analysis was conducted for ST6GAL1 up-miRs in four cell lines (A549, PANC1, HT-29, OVCAR3; miRs: miR-328-5p, -488-5p, -221-5p, -6883-5p, -5700, -765, -212-5p, -4430) and for ST6GAL1 down-miRs in three cell lines (A549, PANC1, HT-29; miRs: miR-6782-5p, -499a-5p, -216a-3p, -4531). For ST6GAL2, both up- and down-miRs were tested in two cell lines (A549, HT-29; up-miRs: miR-3619-5p, -124-3p, -605-3p, down-miR: miR-30c-2-3p, -6828-5p, -22-3p). All analysis was done in biological triplicate. The α-human-ST6GAL1, 1° gave multiple bands in some cell lines. Therefore, we validated the antibody using the ON-TARGET plus siRNA reagent against ST6GAL1 in a smart pool format (Dharmacon, Horizon Discovery, CA) in PANC1 and A549 using the manufacturer's protocol (**Appendix B**).

2.6.6 RT-qPCR

Total RNA was isolated from cells treated as in Western blot experiments using TRIzol reagent (catalog #: 15596018, Invitrogen) according to the manufacturer's instructions. RNA concentrations were measured using NanoDrop, and high-quality isolated total RNA was reverse-transcribed to cDNA using Superscript III Cells Direct cDNA synthesis kit (catalog #: 18080300, Invitrogen). Reverse transcription quantitative PCR (RT-qPCR) was performed using the SYBR Green method and cycle threshold values (Ct) were obtained using an Applied Biosystem (ABI) 7500 Real-Time PCR machine and normalized to housekeeping gene GAPDH. The primer sequences used in RT-qPCR can be found in **Table 2.1**. All analysis was done in biological triplicate.

2.6.7 SNA staining assay

Cells were seeded onto sterile 22 × 22 no. 1 coverslips placed into 35 mm dishes at a density of 5×10^4 cells/ml in standard media. After 24h, cells were transfected with miRNA mimics or anti-miRs as in Section 2.6.5. At 48 h post-transfection, cells were washed with PBS (3×, 2 mL) and fixed with 4 % paraformaldehyde for 15 min. Cells were again washed with PBS (3×, 2 mL). blocked using 10 % BSA in PBS for 1h in incubator (37℃, 5% CO_2) and Cy3-SNA was added (1:300 in 10 mM HEPES, 0.15 M NaCl, 0.1 mM $CaCl_2$, pH 7.5, Vector Laboratories, catalog # CL-1303). After 1 h in the incubator, coverslips were washed (PBS, 3×), and cells were counterstained with Hoechst 33342 (1 μg/mL in PBS, 15 min in incubator). The coverslips were then mounted onto slides with 60 μl of mounting media (90% glycerol in PBS) and imaged with a Zeiss fluorescent microscope (Camera: Axiocam 305 mono, software: ZEN 3.2 pro). For each biological replicate, 5 fields were obtained. Specificity of SNA staining was confirmed by using Neuraminidase (gift from Dr. Matthew Macauley) prior to SNA staining. All analysis was done in biological triplicate. For data analysis, the ZOI method in the ZEN 3.2 pro software was used to quantify the fluorescence signal in membrane of all cells. Signal was normalized to cell count using the Hoechst staining to count nuclei in the software. Final data was normalized to the NTC for each biological replicate. A paired *t*-test was used to compare NTC with miRNA or anti-miR.

2.6.8 Endogenous miRNA activity validation

miRIDIAN microRNA Hairpin Inhibitors (ST6GAL1: anti-miR-221-5p, anti-miR-212-5p, anti-miR- 488-5p, anti-miR-765, anti-miR-499a-5p, anti-miR-4531; ST6GAL2: anti-miR-3619-5p, anti-miR-124-3p, anti-miR-6828-5p, anti-miR-30c-2-3p) and miRIDIAN microRNA Hairpin Inhibitor Negative Control (NTC) were purchased from Dharmacon (Horizon Discovery, Cambridge, UK). A549 cells were seeded and incubated as described for Western blot. A549 cells

were transfected with anti-miRNAs, 50 nM using Lipofectamine™ 2000 transfection reagent in OptiMEM following the manufacturer's instructions (Life Technologies). After 12 h media was changed to standard culture media. 48 h post-transfection A549 cells were lysed and analyzed for ST6GAL1 and ST6GAL2 protein and mRNA levels as previously described. For ST6GAL1, anti-up-miRs (anti-miR-221-5p, anti-miR-212-5p, anti-miR-488-5p, anti-miR-765) were also tested in the PANC1 cell line. All analysis was done in biological triplicate.

2.6.9 Multi-site mutagenesis: ST6GAL1

The 3'UTR sequence of ST6GAL1 and the three miRNA sequences (miR-221-5p, miR-212-5p, miR-4531) were analyzed with the RNAhybrid tool[142] which calculates a minimal free energy hybridization of target RNA sequence and miRNA. The two stable predicted miRNA: mRNA interaction sites were selected for designing mutant pFmiR-sensors. Multiple mutation sites were designed and mutant sequences were ordered for synthesis from GenScript Biotech or Integrated DNA Technologies (IDT). Each synthesized mutant fragment (221-MUTA-gBlock, 221 MUTB-gBlock, 212-MUTA-gBlock, 212-MUTB-gBlock) was amplified by standard PCR machine (Bio-Rad), using the primer sequences found in **Table 2.1**. Amplicons were cleaned up using Monarch PCR & DNA cleanup kit (catalog #: T1030S, NEB). The NucleoSpin Gel and PCR Clean-up XS kit (REF. #: 740611.50) was used for DNA gel extraction when needed to exclude non-specific bands. The amplicons were ligated into the empty pFmiR plasmid[78] after enzymatic digestion using a pair of restriction enzymes for each gBlock (221-MUTA: NheI, PasI; 221-MUTB: PasI, BamHI; 212-MUTA: NheI, PasI; 212-MUTB: SwaI, BamHI). Sequences for the mutant pFmiR-ST6GAL1 sensors were then verified by sequencing and used in the miRFluR assay as described previously. A minimum of 3-wells were transfected per sensor and the analysis was done in 2 independent experiments.

2.6.10 Multi-site mutagenesis: ST6GAL2

The 3'UTR sequence of ST6GAL2 and the two miRNA sequences (miR-3619-5p, miR-30c-2-3p) were analyzed with the RNAhybrid tool[142] which calculates a minimal free energy hybridization of target RNA sequence and miRNA. The two stable predicted miRNA: mRNA interaction sites were selected for designing mutant pFmiR-sensors. Multiple mutation sites were designed, and mutant sequences were ordered for synthesis from GenScript Biotech or Integrated DNA Technologies (IDT). Each synthesized mutant fragment (3619-MUTA-gBlock, 3619-MUTB-gBlock, 30c-MUT-gBlock) was amplified by standard PCR machine (Bio-Rad), using the primer sequences found in **Table 2.1**. Amplicons were cleaned up using Monarch PCR & DNA cleanup kit (catalog #: T1030S, NEB). The NucleoSpin Gel and PCR Clean-up XS kit (REF. #: 740611.50) was used for DNA gel extraction when needed to exclude non-specific bands. The amplicons were ligated into the empty pFmiR plasmid after enzymatic digestion using a pair of restriction enzymes for each gBlock (3619-MUTA: AjuI, PasI; 3619-MUTB: Psilv2, PasI; 30c-MUT: AjuI, PasI). Sequences for the mutant pFmiR-ST6GAL2 sensors were then verified by sequencing and used in the miRFluR assay as described previously. A minimum of 3- wells were transfected per sensor and the analysis was done in 2 independent experiments. siRNA knockdown of microRNPs: ON-TARGETplus siRNA reagents against AGO2, FXR1, TNRC6A in a smart pool format and ON-TARGETplus Non-Targeting Control Pool (NTP) were purchased from Dharmacon (Horizon Discovery, CA). A549 cells were seeded in six-well plates (50,000 cells/well) and cultured for 24 h in appropriate media. Cells were then washed with HBSS and transfected with each of the siRNA pools (50 nM, NTP, AGO2, FXR1 or TNRC6A, Dharmacon, Horizon Discovery) with Lipofectamine™ RNAiMAX transfection reagent (catalog #: 13778150, Thermofisher) following the manufacturer's instructions. Media was changed 12 hours post-

transfection. After 48 hours, cells were then transfected with miR-221-5p, miR-212-5p, or NTC as previously described. Cells were then harvested for Western blot and RT-qPCR analysis as previously described. The knockdown efficiency for the siRNA was tested by Western blot analysis using 1:1000 dilution of 1° antibodies targeting AGO2 (catalog #: 67934-1-Ig, Proteintech), FXR1 (catalog #: 12295S, Cell Signaling) and TNRC6A (GW182) (catalog #: ab114857, Abcam) in 10 % non-fat dry milk in TBST (Data not shown here. See Figures S13-14 in the published work (PMID: 36439307)[130]). Blots were processed as for ST6GAL1/2.

Table 2.1 Primer sequences for PCR amplification of WT 3'UTRs, RT-qPCR quantification of mRNAs, and for PCR amplification of mutant 3'UTRs for ST6GAL1 and ST6GAL2.

Primer Name	Sequence (5' → 3')	Sample
a. PCR amplification of ST6GAL1 and ST6GAL2 3'UTRs:		
ST6GAL1-FWD[a]	CGGACCATTCACTGCTAAG	gDNA, HEK293T
ST6GAL1-REV[a]	TTAAAGAAACACACACACATTTATTTTA	gDNA, HEK293T
ST6GAL2-FWD	AAAGGGTTTCTTGGGAATC	gDNA, HEK293T
ST6GAL2-REV	TTCTAGACAAATGAAAACATG	gDNA, HEK293T
b. RT-qPCR[a] quantification of ST6GAL1, ST6GAL2 or GAPDH mRNA		
ST6GAL1-FWD1	GAACACCCAAGAAACCATGCA	Total RNA, A549 or HT-29
ST6GAL1-REV1	ACGTGCTCCGCCCATTC	Total RNA, A549 or HT-29
ST6GAL1-FWD2	AACACCCAAGAAACCATGCAA	Total RNA, PANC1 or OVCAR3
ST6GAL1-REV2	CGTGCTCCGCCCATTC	Total RNA, PANC1 or OVCAR3
ST6GAL2-FWD	GAAGGAGCCACGTGTTGGA	Total RNA, A549 or HT-29
ST6GAL2-REV	GCGGGTTCAGCATTTTGG	Total RNA, A549 or HT-29
GAPDH-FWD	GGTGTGAACCATGAGAAGTATGA	Total RNA, all cell lines
GAPDH-REV	GAGTCCTTCCACGATACCAAAG	Total RNA, all cell lines
c. PCR amplification of ST6GAL1 and ST6GAL2 mutant 3'UTRs		
221-MUTA-FWD	CGGACCATTCACTGCTAAG	221-MUTB-gBlock
221-MUTA-REV	TCTAGGAATGGACCGTCTACT	221-MUTB-gBlock

221-MUTB-FWD	CTCTGCACTCTCAAGGC	221-MUTA-gBlock
221-MUTB-REV	TTAAAGAAACACACACACATTTAT	221-MUTA-gBlock
212-MUTA-FWD	CGGACCATTCACTGCTAAG	212-MUTB-gBlock
212-MUTA-REV	AGCTCCGAGATGGTTAGTTTG	212-MUTB-gBlock
212-MUTB-FWD	ATGATTCTGAAGTCTACAGAAC	212-MUTA-gBlock
212-MUTB-REV	TTAAAGAAACACACACACATTTAT	212-MUTA-gBlock
4531-MUT-FWD	CAGGCATTAAATGAATGGTCTCT	pFmiR-ST6GAL1
4531-MUT-REV	TTAAAGAAACACACACACATTTAT	pFmiR-ST6GAL1
3619-MUTA-FWD	CACCCTGTGCTTCTAGGGATGCACGCCT	3619-MUTA-gBlock
3619-MUTA-REV	ACGAGCATCGGTATTCCATGA	3619-MUTA-gBlock
3619-MUTB-FWD	AGCTGACCTTTCTCACTATG	3619-MUTB-gBlock
3619-MUTB-REV	ATGTTAGATTTTAACACCACCAATGC	3619-MUTB-gBlock
30c-MUT-FWD	CTTCTAGGGATGCACGCCTG	30c-MUT-gBlock
30c-MUT-REV	ACGAGCATCGGTATTCCATGAG	30c-MUT-gBlock

[a] FWD, forward; REV, reverse; RT-qPCR, Reverse transcription quantitative polymerase chain reaction.

Chapter 3

Screening the human miRNA interactome reveals coordinated upregulation in melanoma, adding bidirectional regulation to miRNA networks

3.1 Acknowledgment

I would like to thank my undergraduate student, Joseph Reyes, for helping in performing Western blot experiments and mutational analysis. I would like to thank my colleague Nicholas Twells for preparing and labeling the diCBM40 lectin. I would like to appretiate my colleagues Hoi Hei Ng and Dr. Dawn MacDonald for their help in replicating the mutation experiments. I would like to sincerely acknowledge Prof. Eva Hernando (NYU Langone) for her helpful insights to this project.

This chapter is posted on bioRxiv: "*https://doi.org/10.1101/2024.05.10.593635*".

3.2 Introduction

Cells are defined by protein expression patterns that require precise regulation[17,18]. microRNA (miRNA, miR), small non-coding RNA, provide such precision[62,111]. The canonical view of miRNA action is that miRNA dampen protein expression through binding the 3' untranslated region (3'UTR) of a transcript (down-miR)[111]. Chapter 2 has challenged this view, demonstrating that miRNA can also increase protein expression through direct interactions with the 3'UTR within actively dividing cells (up-miR)[78,130]. This work was in concordance with previous reports of enhanced translation via miRNA:mRNA interactions in quiescent cells[143,144]. AGO2, a fundamental part of the miRNA machinery, is required for upregulation by miRNA. In contrast, TNRC6A (aka GW182), which is a crucial component of the complexes required for downregulation, was not required for upregulation – providing strong evidence that up-miRs do not work by a "relief of repression" mechanism[130,146,158]. Given the important role miRNA have in regulating levels of proteins that coordinate specific biological functions, we would expect that upregulatory interactions would act cooperatively to tune protein expression in these regulatory networks. In this Chapter, I show incorporation of upregulation into such networks, providing evidence that miRNA co-upregulate related targets and positioning them as bidirectional tuners of expression.

In a recent study, we identified a functional relationship between the CD98 heavy chain (CD98hc) and the α-2,3-sialyltransferases ST3GAL1 and ST3GAL2 in melanoma[159] (**Figure 3.1**). CD98hc, encoded by *slc3a2*, is a type II transmembrane glycoprotein ubiquitously expressed at high levels on many cell types. It is a part of the neutral amino acid transport complex LAT-1[160,161]. CD98hc has roles in both physiological and pathological contexts, including in B- and T-cell clonal expansion, integrin signaling and cell proliferation[160,162-164]. It is a target of anti-cancer antibodies

in current clinical trials due to its importance in the biology of various solid tumors (e.g., bladder[165], breast[166], lung[167], melanoma[159,168]) and hematological cancers[163,169]. In melanoma, α-2,3-sialylation of CD98hc by the enzymes ST3GAL1 and ST3GAL2 was found to be important in the stability of CD98hc, protecting it from proteasomal degradation[159].

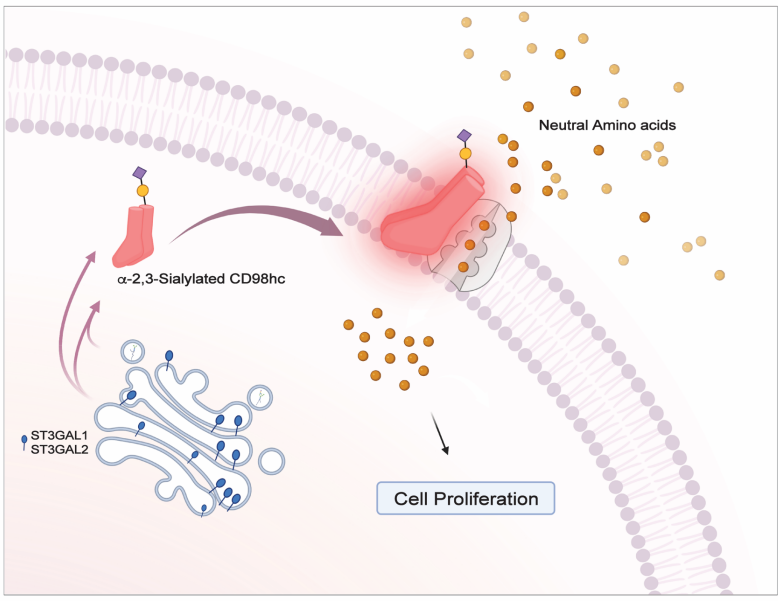

Figure 3.1 α-2,3-Sialylation of CD98hc by ST3GAL1 and ST3GAL2 stabilizes the essential protein, CD98hc, in melanoma[159].

ST3GAL1 and ST3GAL2 transfer sialic acid onto the 3-position of terminal galactose predominantly on *O*-glycans and glycolipids, respectively[170,171]. ST3GAL1, which can biosynthesize the tumor antigen sialyl T (Neu5Acα2-3Galβ1-3GalNAc)[172] plays functional roles in the biology of several cancers including breast cancer[173], ovarian cancer[48], and melanoma[47,159]. It is also an important regulator of cell migration[171] and recently was found to mediate sequestration of CAR-T cells from circulation, inhibiting the cell's ability to home to cancer tissues[174]. In contrast to ST3GAL1, less is known of the function of ST3GAL2. It is associated with transformation in colorectal cancer[40] and is highly expressed in pancreatic cancer compared to normal tissue[175]. We have recently shown that it, along with ST3GAL1 and CD98hc, is an essential gene in melanoma[159].

I posited that, given the functional relationship between CD98hc and both ST3GAL1 and ST3GAL2, that these genes might be co-regulated by miRNA. I screened the human miRNAome for regulatory relationships for all three genes using the high-throughput miRFluR assay. In the previous work and Chapter 2, we have used this assay to uncover miRNA regulation of the glycosylation enzymes B3GLCT[78], ST6GAL1 and ST6GAL2[130], leading to the discovery that miRNA can upregulate protein expression through direct interactions with the 3'UTR of mRNA (upregulatory miRNA or up-miR). In this Chapter, analysis of CD98hc, ST3GAL1 and ST3GAL2 provided a regulatory map of these genes, identifying 10 co-up-miRs: 6 between CD98hc and ST3GAL1 and 4 between CD98hc and ST3GAL2. The majority of these co-upmiRs were associated with either melanoma metastasis or progression[152,176], positioning upregulation as a central part of miRNA regulatory network.

3.3 Results

3.3.1 Mapping miRNA regulation of CD98hc identifies up- and downregulatory interactions

To map the miRNA regulatory landscape of CD98hc, I utilized the previously described miRFluR assay[78] (Chapter 2[130]). In Chapter 2 and previous work by the Mahal laboratory, we analyzed the miRNA regulation of glycosylation enzymes, which are moderate to low abundance proteins[78,130]. In contrast, CD98hc is highly expressed in many cancer (e.g. melanoma)[168] and non-cancer (e.g. immune) cells[163,169].

To assess regulation, I cloned the most prevalent 3'UTR for CD98hc into the pFmiR empty sensor[78] to create pFmiR-CD98hc (**Appendix A**). While the 3'UTRs of the other genes studied in the Mahal lab system were > 1 kilobase in length[78,130]; the 3'UTR of CD98hc is only 190 nucleotides (nt). I co-transfected the pFmiR-CD98hc sensor with a miRNA mimic library (Dharmacon, v. 21, 2601 miRs, arrayed in 384-well plates) into HEK-293T cells. All miRNA were

represented in triplicate and fluorescent signals were analyzed 48 hours post-transfection. Upon data analysis, I found that the "non-targeting" controls (NTCs) provided with the library were significantly shifted from the median signals within the plates, arguing that they impacted sensor expression. These NTCs are two miRNAs (cel-miR-67, cel-miR-239b) from *C. elegans*, and were reported to have minimal sequence identity with known miRNAs from human, mouse and rat (Dharmacon, Horizon Discovery). These *C. elegans* miRNAs (cel-miRs) are assumed to not interact with human, mouse and rat transcriptomes, however, the data provided by the company for supporting their applications as NTCs is limited.

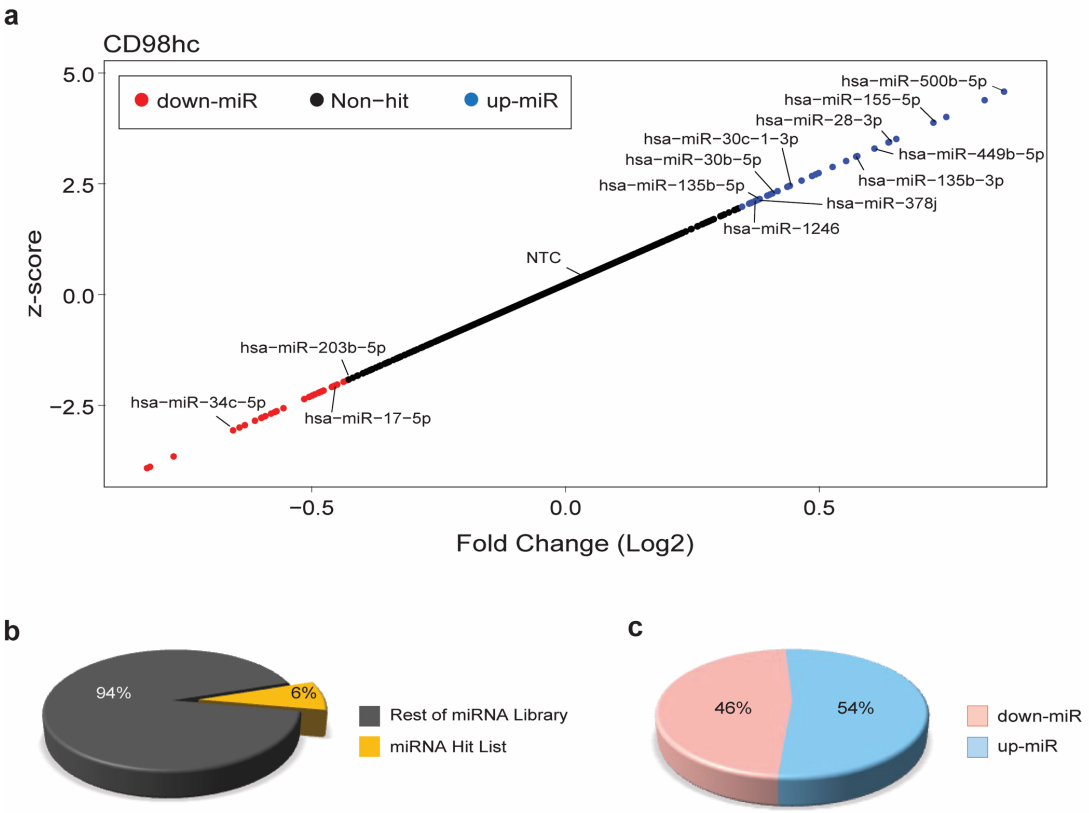

Figure 3.2 Comprehensive map of CD98hc regulation by miRNA. a. Scatter plot of miRFluR data for 3'UTR of CD98hc. miRNA in the 95% confidence interval by z-score are indicated (down-miRs: red, up-

miRs: blue) and validated miRNAs are shown. **b.** Pie chart showing % miRNA hits compared to total library post-QC. **c.** Pie chart indicates % down-miR (48%) vs. up-miR (52%) in CD98hc hit list.

Given that normalization over NTCs (provided with the library) have significantly shifted my miRFluR data from the median signals across the library, and they may have binding sites within human 3'UTRs, I median normalized the data (**Figure 3.2a**). After quality control, I $\log_2$ transformed the data (954 miRs) and then applied a z-score at the 95% confidence interval to identify miR hits. The high-throughput analysis found approximately even numbers of downregulatory (down-miRs, n=30), and upregulatory (up-miRs, n=35) miRNA, representing 6% of miRNA interactions passing QC (**Figure 3.2a-c**). Given that commercial NTCs (cel-miRs) target *slc3a2* transcript, I sought to determine a new non-targeting controls for further validation experiments (**Figure 3.3**). Of the three miRNA tested, miR-548ab was chosen as the new NTC because there are no biological processes currently associated with this miRNA[177].

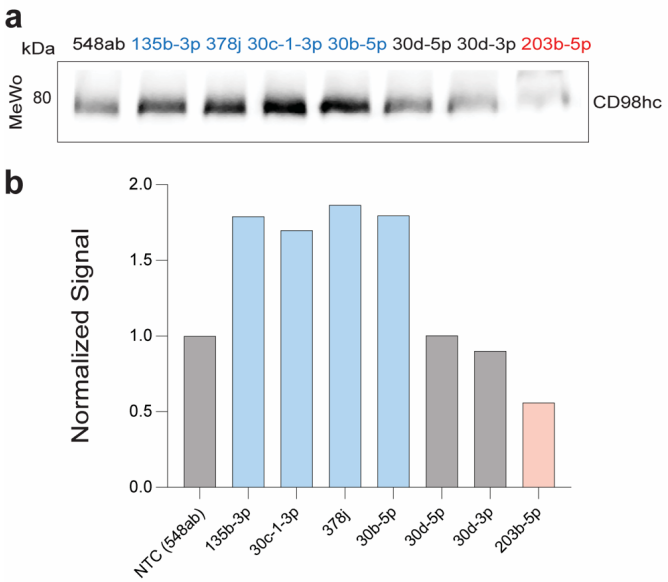

Figure 3.3 Validation of miR-548ab as new NTC. a. miRNA mimics of median controls (miRs: -548ab (NTC), -30d-5p, -30d-3p), down-miRs (miR-203b-5p) and up-miRs (miRs: -135b-3p, -378j, -30c-1-3p, -30b-5p) were transfected into MeWo cells (50 nM miR, 48 h) prior to Western blot analysis. **b**. Bar graph shows quantification of Western blot result shown in a.

3.3.2 CD98hc expression is both up- and downregulated by miRNA in cancer cells

CD98hc is an emerging cancer target, with a therapeutic antibody in Phase I clinical trial[164,166,178,179]. Therefore, I focused my validation on miRNAs associated with cancer biology[180-182] down-miRs: miR-17-5p, miR-34c-5p, miR-203b-5p; up-miRs: miR-135b-5p, miR-155-5p. I

utilized three cancer cell lines from two tissue types: two melanoma: MeWo and 131/4-5B1 (5B1[183]) and one breast: MCF-7. Cells were treated with miRNA mimics for 48h prior to lysis and analysis by Western blot. In line with my miRFluR data, down-miRs resulted in a decrease in endogenous CD98hc expression (~0.5-fold) and up-miRs in an increase in protein levels (**Figure 3.4a-d**, 1.6-2-fold) in melanoma cell lines. I next analyzed CD98hc cell-surface expression in

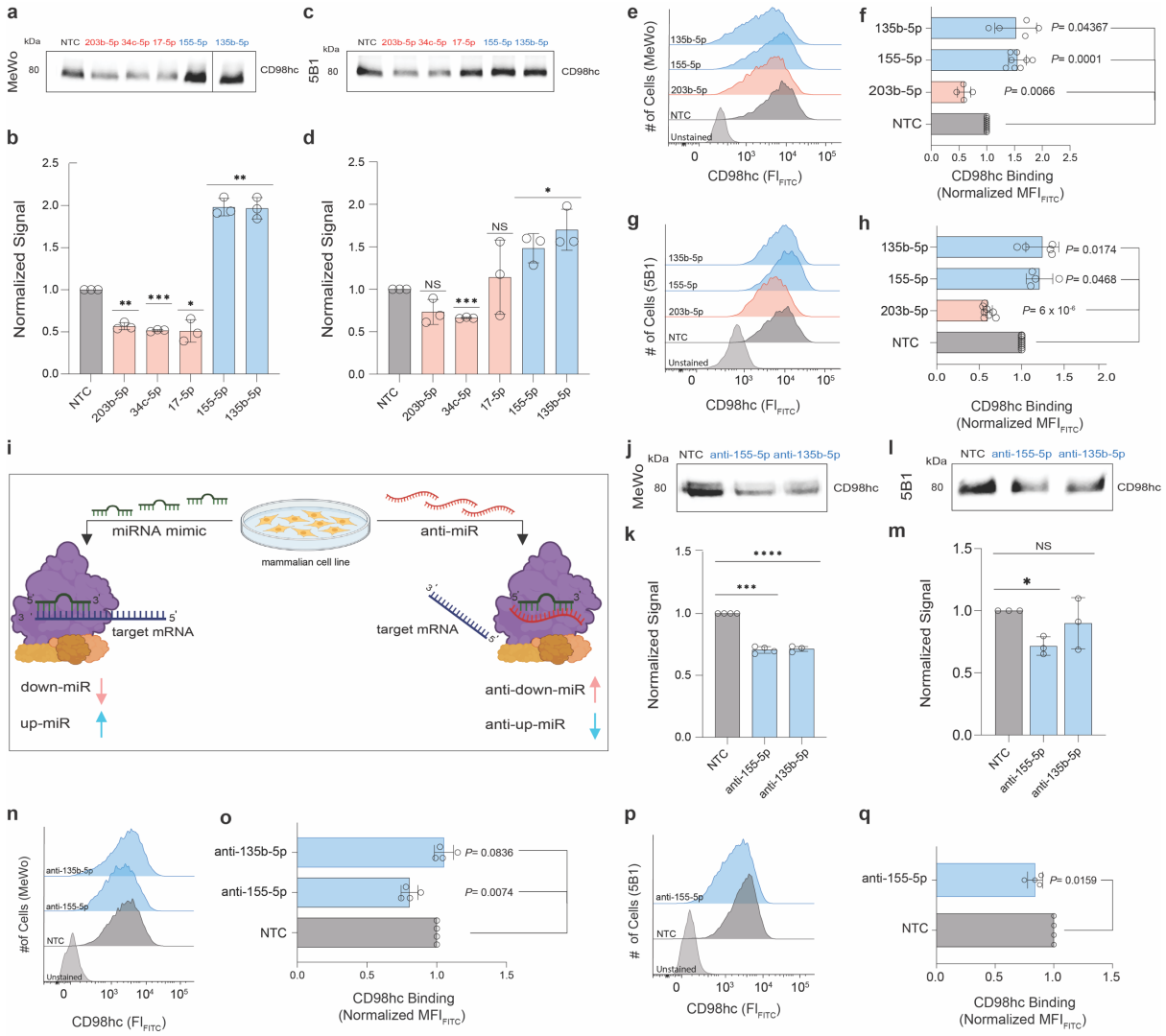

Figure 3.4 CD98hc miRFluR analysis identifies endogenous regulators of expression in MeWo and 5B1 cell lines. Impact of miRNA mimics on CD98hc expression. MeWo (a, b, e, f) or 5B1 (c, d, g, h) cells were treated with miRNA mimics (down-miRs: miR-203b-5p, -34c-5p, -17-5p, upmiRs: miR-155-5p, -135b-5p) or non-targeting control (NTC: miR-548ab was used for all miR mimic experiments) at 50 nM for 48h and analyzed as indicated. **a, c.** Representative Western blot analysis of CD98hc in MeWo (a) and 5B1 (c). **b, d.** Bar graph of Western blot data for MeWo (b) and 5B1 (d). **e, g.** Representative flow cytometry

analysis of CD98hc binding in MeWo (e) and 5B1 (g). **f, h.** Bar graph of flow cytometry data for MeWo (f) and 5B1 (h). Impact of endogenous miRNA on CD98hc expression (i-q). **i.** Anti-miRs sequester the endogenous miRNA by interacting with target in AGO2 complexes, causing loss of protein expression for up-miRs. MeWo (j, k, n, o) or 5B1 (l, m, p, q) cells were treated with anti-miRs (anti-up-miRs: anti-155-5p, anti-135b-5p) or non-targeting control (NTC) at 50 nM for 48h and analyzed as indicated. **j, l.** Representative Western blot analysis of CD98hc in MeWo (j) and 5B1 (l) cells. **k, m.** Bar graph of Western blot data for MeWo (k) and 5B1 (m). **n, p.** Representative flow cytometry analysis of CD98hc binding in MeWo (n) and 5B1 (p). **o, q.** Bar graph of flow cytometry data for MeWo (o) and 5B1 (q). All experiments were performed in ≥ biological triplicate. Errors shown are standard deviations. For Western blot analysis, the One sample *t*-test was used to compare miRs to NTC (ns not significant, * $p < 0.05$, ** < 0.01, *** < 0.001). In flow cytometry analysis, paired *t*-test was used to compare miRs to NTC and *p*-values are indicated on the graph.

MeWo and 5B1cell lines using flow cytometry approach. My data again confirmed that up-miRs (miR-135b-5p, miR-155-5p) enhance cell surface expression of CD98hc, while down-miRs (miR-203b-5p) decrease it (**Figure 3.4e-h**).

To test whether endogenous up-miRs enhanced CD98hc expression, I used miRNA hairpin inhibitors, which displace target mRNA from AGO complexes (anti-miRs, **Figure 3.4i**). These inhibitors should repress expression of proteins whose levels are enhanced by upregulatory miRNA. I focused on up-miRs: -155-5p and -135b-5p, both of which are expressed in melanoma [176,184]. As expected, transfection with anti-up-miRs for miR-155-5p inhibited expression of CD98hc as observed in both Western blot analysis and flow cytometry for MeWo and 5B1 (**Figure 3.4j-q**). However, I observed cell line dependent differences for the anti-miRs of miR-135b-5p, with MeWo showing clear loss of expression and no impact in 5B1. This discrepancy may be due to the expression level of this miRNA in the two cell lines. In addition, I tested the select miR subset for CD98hc in MCF-7 breast cancer cell line, showing consistent result with the two melanoma cell lines (**Figure 3.5a-b**). Overall, my data confirms the validity of our miRFluR assay to identify endogenous miRNA regulating CD98hc.

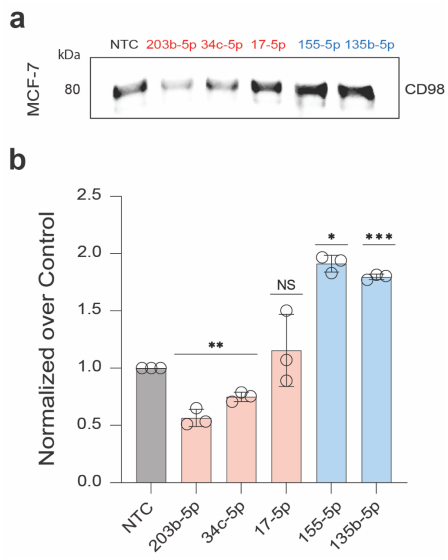

Figure 3.5 Validation of miRFluR data for CD98hc in MCF-7 cell line. Impact of miRNA mimics on CD98hc expression. MCF-7 cells were treated with miRNA mimics (down-miRs: miR-203b-5p, -34c-5p, -17-5p, up-miRs: miR-155-5p, -135b-5p) or non-targeting control (NTC: miR-548ab) at 50 nM for 48h and analyzed as indicated. **a.** Representative Western blot analysis of CD98hc in MCF-7. **b.** Bar graph of Western blot data shown in a. The One sample *t*-test was used to compare miRs to NTC (NS: not significant, * $p < 0.05$, ** < 0.01, *** <0.001). Western blot experiments are performed in independent biological replicates (n=3).

I, and others, have found discordance between the impacts of miRNA on the transcript levels and the observed impacts on protein expression[78,95,125,126,130]. I therefore analyzed the impact of miRNA mimics on transcript levels of CD98hc (*slc3a2*) in 5B1 (**Figure 3.6a**) and MCF-7 (**Figure 3.6b**) cells. In keeping with Chapter 2[130], I found a mixture of impacts on the transcriptome with

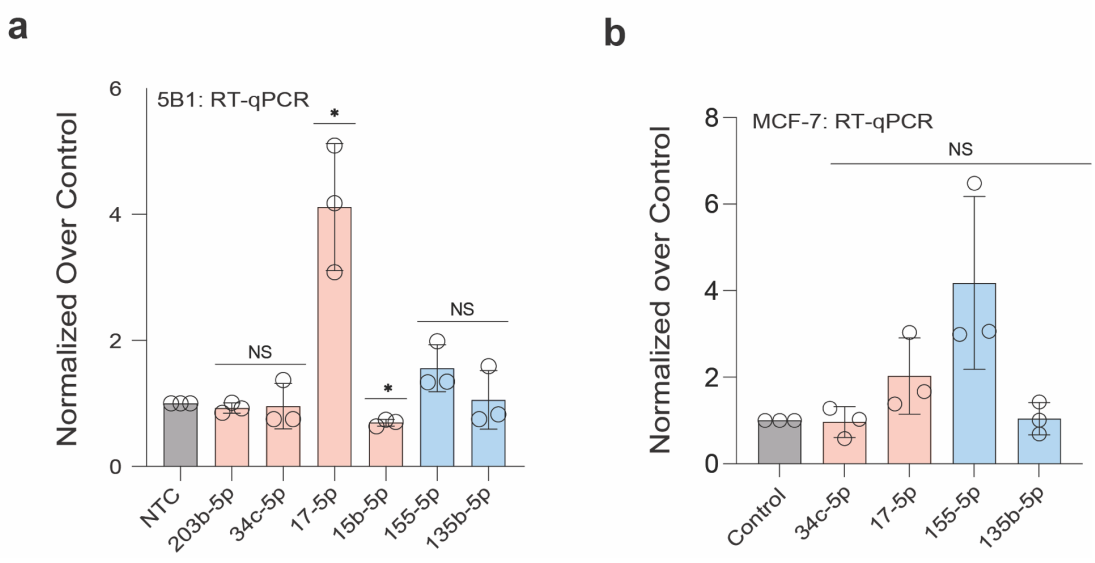

Figure 3.6 Validation of miRFluR data for cd98hc in 5B1 and MCF-7 cell lines. Impact of miRNA mimics on cd98hc expression. Cells were treated with miRNA mimics (down-miRs: miR-203b-5p, -34c-5p, -17-5p, up-miRs: miR-155-5p, -135b-5p) or non-targeting control (NTC: miR-548ab) at 50 nM for 48h

and analyzed as indicated. **a.** RT-qPCR quantitative analysis of slc3a2 in 5B1. **b.** RT-qPCR quantitative analysis of slc3a2 in MCF-7. Samples were normalized to GAPDH and NTC. The One sample *t*-test was used to compare miRs to NTC (NS: not significant, * $p < 0.05$). RT-qPCR experiments are performed in independent biological replicates (n=3).

little concordance between the transcript and protein levels for either down- or up-miRs. This implicates mechanisms beyond transcript degradation or, conversely, stabilization, in the control of protein levels by miRNA[78,95,130].

3.3.3 miR-155-5p upregulates CD98hc via direct miRNA: mRNA interactions

The roles of CD98hc dovetail with those of miR-155-5p, which is highly expressed in many cell types[185,186]. Both are known to be upregulated and functionally important in B-cell lymphoma[82], acute myelogenous leukemia[169,187], and non-small cell lung carcinoma[167,188]. Both are also critical to clonal expansion of B- and T-cells[162-164,189,190]. I anticipated that miR-155-5p would directly bind to the CD98hc 3'UTR to mediate upregulation. To test this, I utilized the miRFluR system (**Figure 3.7a**). In Chapter 2, the RNAhybrid algorithm was able to accurately predict regulatory binding sites for up-miRs[130]. This algorithm predicts the most stable binding site between miRNA and mRNA[142]. A non-canonical miR-155-5p binding site was identified at position-152 in the CD98hc 3'UTR (**Figure 3.7b**). Using site-directed mutagenesis, I mutated all interacting nucleotides at the potential binding site in my pFmiR-CD98hc sensor and tested the mutant in the miRFluR assay (**Figure 3.7c**).

As expected, I lost miR-155-5p mediated upregulation in the mutant sensor, confirming that upregulation of CD98hc by this miRNA is through direct interactions. In line with Chapter 2, the upregulatory sites are not AU rich[143,144] and do not adhere to the seed rules that are often observed in downregulatory sites[111]. My results suggest that miR-155-5p may be directly involved in the upregulation of CD98hc observed in cancer and immunity.

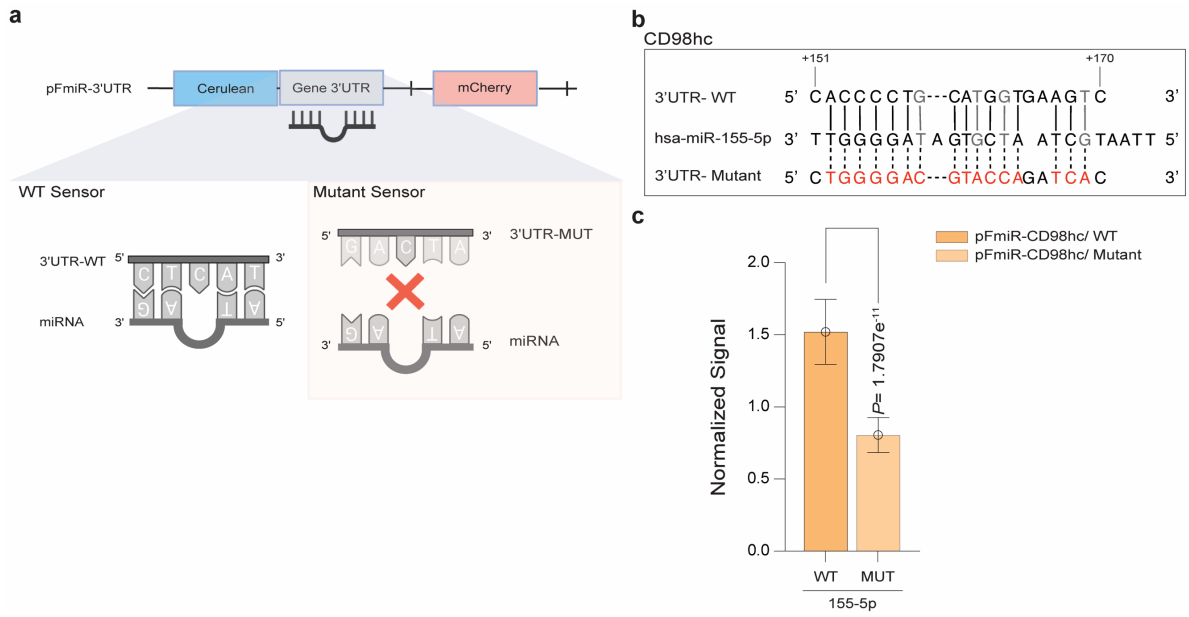

Figure 3.7 Mutational analysis identifies miR-155-5p binding site on CD98hc 3'UTR. a. Comparison of wild-type (WT) and mutant pFmiR-3′UTR interactions with miRNA. **b.** Alignment of miR-155-5p with predicted CD98hc-3′UTR site and corresponding mutant. Mutated residues are shown in red, wobble interactions (G: U) are shown in grey. **c.** Bar graph of data from wildtype (WT) and mutant (MUT) miRFluR sensors. For each sensor, data was normalized over NTC. Experiment was performed in biological duplicate, representative assay with n=8 wells is shown. Standard *t*-test was used for comparison, *p*-value is indicated on the graph.

3.3.4 Mapping miRNA regulation of ST3GAL1&2, mediators of CD98hc stability in melanoma

Co-regulation of critical proteins within a network through coordinated targeting by miRNA has been widely observed for down-miRs[78,95].There are no existing examples of such networks for upregulation by miRNA. In analyzing the up-miRs for CD98hc, I noticed that a significant number of them (15/35, 43%) were associated with melanoma transformation and progression[152] (**Table 3.1**). CD98hc is highly expressed in metastatic melanoma and is associated with lower survival of melanoma patients[168,176]. In recent work, I identified a role for α-2,3-sialylation, mediated by the sialyltransferases ST3GAL1 and ST3GAL2, in the stabilization of CD98hc in melanoma specifically. Inhibition of ST3GAL1 or ST3GAL2 induced enhanced degradation of CD98hc and loss of the protein[159].

Table 3.1 CD98hc up-miR analysis in melanoma dataset.

up-miR	fold change in miRFluR (normalization over control)	signature in melanoma (Log fold-change > 0)
hsa-miR-4640-5p	1.289747317	up
hsa-miR-1246	1.299015856	up
hsa-miR-135b-5p	1.303684609	up
hsa-miR-4436b-3p	1.321963315	up
hsa-miR-30b-5p*	1.326657787	up
hsa-miR-30c-1-3p	1.357529203	up
hsa-miR-6784-5p	1.380467402	up
hsa-miR-34c-3p	1.407505853	up
hsa-miR-199a-3p	1.44020141	up
hsa-miR-660-5p	1.467075023	up
hsa-miR-135b-3p	1.487461446	up
hsa-miR-500a-3p	1.489550747	up
hsa-miR-299-3p	1.554398492	up
hsa-miR-28-3p	1.556006354	up
hsa-miR-155-5p	1.652779561	up

CD98hc up-miR analysis in melanoma dataset. CD98hc co-up-miRs with ST3GAL1 (*purple*), and ST3GAL2 (*green*). (Gómez-Martínez, *et. al.*[32]), (*Gaziel-Sovran, *et. al.*[31]).

Given the impact of ST3GAL1 and ST3GAL2 on CD98hc expression in melanoma, I hypothesized that these genes might be co-upregulated by miRNA. As a first step towards testing this hypothesis, I mapped the miRNA regulation of ST3GAL1 and ST3GAL2 using the miRFluR assay (**Figures 3.8 and 3.9**).

3.3.5 High-throughput analysis shows ST3GAL1 is predominantly up-regulated by miRNA

ST3GAL1, one of six glycosyltransferases that transfer sialic acid to the position-3 of terminal galactose creating the α–2,3-sialyl epitope, predominantly sialylates *O*-glycans such as those found on mucins[171]. It impacts both growth and metastasis in melanoma and alters T-cell migration [47,159,174]. ST3GAL1 upregulation plays a significant role in the development of malignant epithelial ovarian cancer[48] and colon cancer[191,192]. I cloned the most prevalent 3'UTR of ST3GAL1

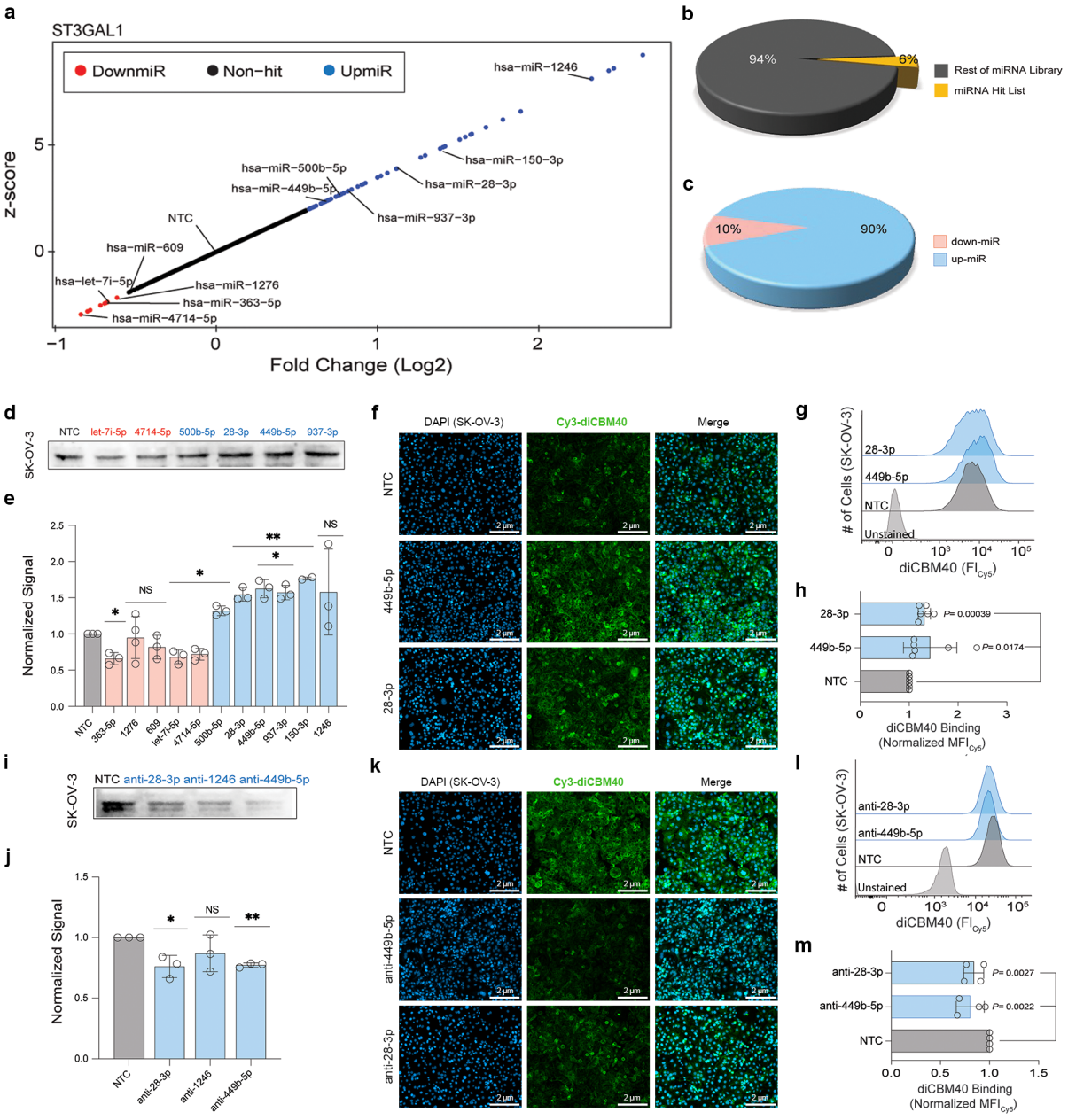

Figure 3.8 miRNA regulation of ST3GAL1 impacts α-2,3-sialylation in SK-OV-3 cell line. **a.** Landscape of miRNA regulation of ST3GAL1 via the 3'UTR is shown via scatterplot of miRFluR data. miRNA in the 95% confidence interval by z-score are indicated (down-miRs: red, up-miRs: blue) and validated miRNAs are labeled. **b.** Pie chart showing % miRNA hits compared to total library post-QC. **c.** Pie chart indicates % down-miR (10%) vs. up-miR (90%) in ST3GAL1 hit list. **d-h.** Impact of miRNA mimics on ST3GAL1 expression. SK-OV-3 cells were treated with miRNA mimics (down-miRs: -363-5p, -1276, -609, let-7i-5p, -4714-5p, up-miRs: -500b-5p, -28-3p, -449b-5p, -937-3p, -150-3p, -1246) or non-targeting control (NTC) at 50 nM for 48h and analyzed as indicated. **d.** Representative Western blot analysis of ST3GAL1. **e.** Bar graph of Western blot data. **f.** Fluorescence microscopy for Cy3- labeled diCBM40 staining of SK-OV-3 treated with NTC or up-miRs: -449b-5p and -28-3p. Representative images are shown. **g.** Flow cytometry analysis of Cy-5 labeled diCBM40 binding for SK-OV-3 treated as in f. **h.** Bar graph of flow cytometry data. MFI: mean fluorescence intensity; FI_{Cy5}: fluorescence intensity. **i-m.** Impact of

endogenous miRNA on ST3GAL1 expression. SK-OV-3 cells were treated with anti-miRs (anti-up-miRs: anti-28-3p, anti-1246, anti-449b-5p) or non-targeting control (NTC) at 50 nM for 48h and analyzed as indicated. **i.** Representative Western blot analysis of ST3GAL1. **j.** Bar graph of Western blot data. **k.** Fluorescence microscopy analysis for diCBM40 staining. **l.** Representative flow cytometry analysis of diCBM40 binding. **m.** Bar graph of flow cytometry data. All experiments were performed in ≥ biological triplicate. Errors shown are standard deviations. For Western blot analysis, the One sample *t*-test was used to compare miRs to NTC (ns not significant, * $p < 0.05$, ** < 0.01). For flow cytometry analysis, the paired t-test was used to compare miRs to NTC and *p*-values are indicated on the graph.

(~5 kb) into the pFmiR sensor (pFmiR-ST3GAL1, **Appendix A**) for analysis in the miRFluR assay. Of the 1807 miRNAs that passed QC, I identified 7 down-miRs and 60 up-miRs within the 95% confidence interval (**Figure 3.8a-c**). Interestingly, the majority (90%) of miRNA hits were upregulatory, which is similar to my observations for ST6GAL1 presented in Chapter 2[130]. I chose miRNA that were biologically significant and spread out within the 95% confidence interval for validation. I focused on 5 down-miRs (miR-363-5p, miR1276, miR-609, miR-4714-5p, let-7i-5p) and 6 up-miRs (miR-937-3p, miR-500b-5p, miR-28-3p, miR-449b-5p, miR-1246, miR-150-3p), the majority of which were associated with various forms of cancer biology[193-196]. I initially tested the miRNA in the ovarian cancer cell line (SK-OV-3) (**Figure 3.8)** for their impact on ST3GAL1.

As expected, Western blot analysis of ST3GAL1 in cells treated with miRNA mimics followed the regulation observed in the miRFluR assay (**Figure 3.8d-e**). I next tested the potential impact of select up-miRs (miRs: -28-3p, -449b-5p) on α-2,3-sialylation in SK-OV-3 using the Cy3-conjugated lectin diCBM40[197]. In line with my expectations, I observed upregulation of α-2,3-sialic acid by both fluorescence microscopy and flow cytometry (**Figure 3.8f-h**). To confirm that ST3GAL1 is regulated by the corresponding endogenous miRNA, I transfected SK-OV-3 cells with anti-up-miRs: -449b-5p, -28-3p and -1246. I observed a loss of both ST3GAL1 protein expression and the corresponding α-2,3-sialic acid (**Figure 3.8i-m**). My data again confirms the validity of the miRFluR assay and provides strong evidence for endogenous upregulation of ST3GAL1. In addition, I examined the select miR subset for ST3GAL1 in the colon cancer cell

line (HT-29) for their impact on ST3GAL1 (**Figure 3.9**), showing consistent miRNA regulatory patterns obtained from the SK-OV-3 cell line (**Figure 3.8**). In keeping with Chapter 2 and previous works by others, transcript levels did not directly follow protein levels (**Figure 3.9c-d**)[78,95,125,126,130].

3.3.6 Mapping the miRNA regulatory landscape of ST3GAL2

ST3GAL2, another member of the α-2,3-sialyltransferase family, is thought to modify both O-glycans and glycolipids[170]. Overexpression of ST3GAL2 may help drive tumorigenesis in several cancers[40,173]. I mapped the miRNA regulation of the most prevalent transcript of ST3GAL2 using the miRFluR assay (pFmiR-ST3GAL2, **Appendix A**). After data processing, I identified 28

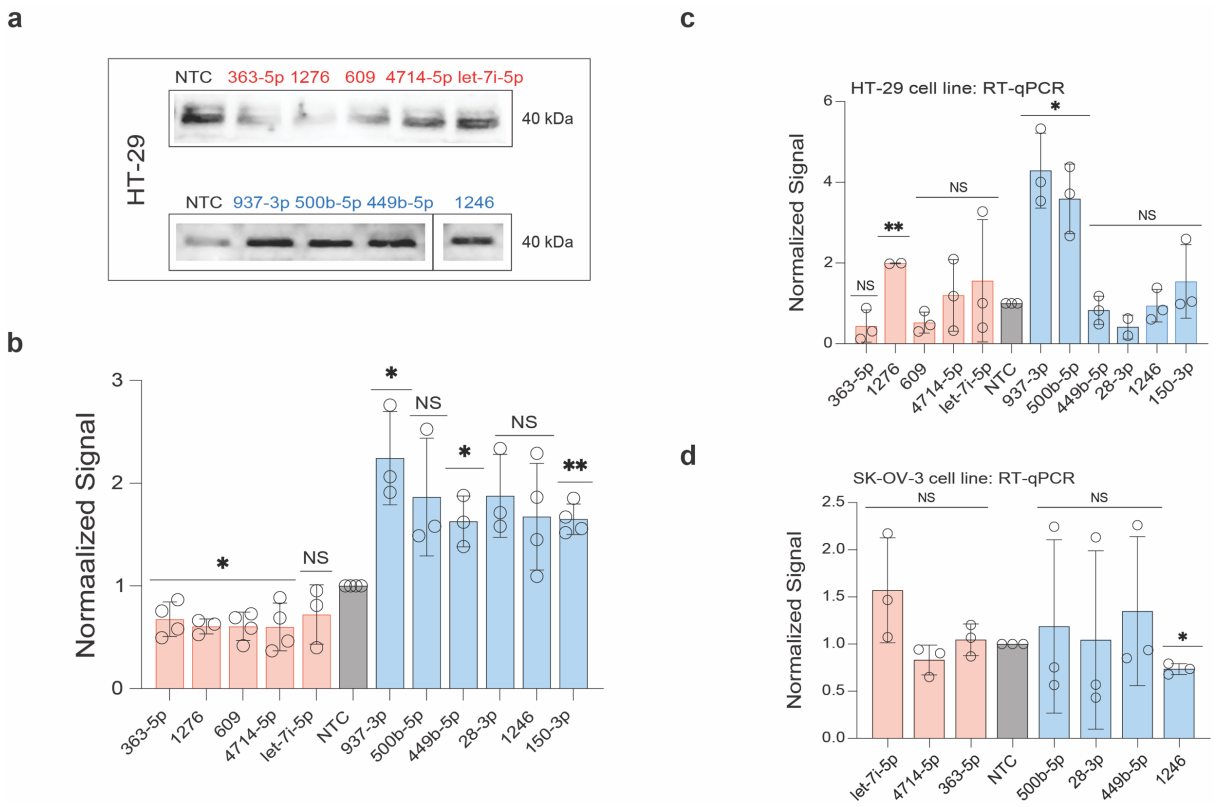

Figure 3.9 miRNA up- and down-regulate ST3GAL1 expression in HT-29 colon and SK-OV-3 ovarian cell lines. Impact of miRNA mimics on ST3GAL1 expression. HT-29 (a, b) cells were treated with miRNA mimics (down-miRs: -363-5p, -1276, -609, let-7i-5p, -4714-5p, up-miRs: -500b-5p, -28-3p, -449b-5p, -937-3p, -150-3p, -1246) or NTC at 50 nM for 48h and analyzed as indicated. **a.** Representative Western blot analysis of ST3GAL1 in HT-29. For simplicity, some wells for upregulators are not shown. **b.** Bar

graph of Western blot data for HT-29. **c, d.** RT-qPCR quantitative analysis of *st3gal1* in HT-29 (c) and SK-OV-3 (d) cells. All experiments were performed in ≥ biological triplicate. Errors shown are standard deviations. The One sample *t*-test was used to compare miRs to NTC for Western blot and RT-qPCR experiments (ns not significant, * $p < 0.05$, ** < 0.01).

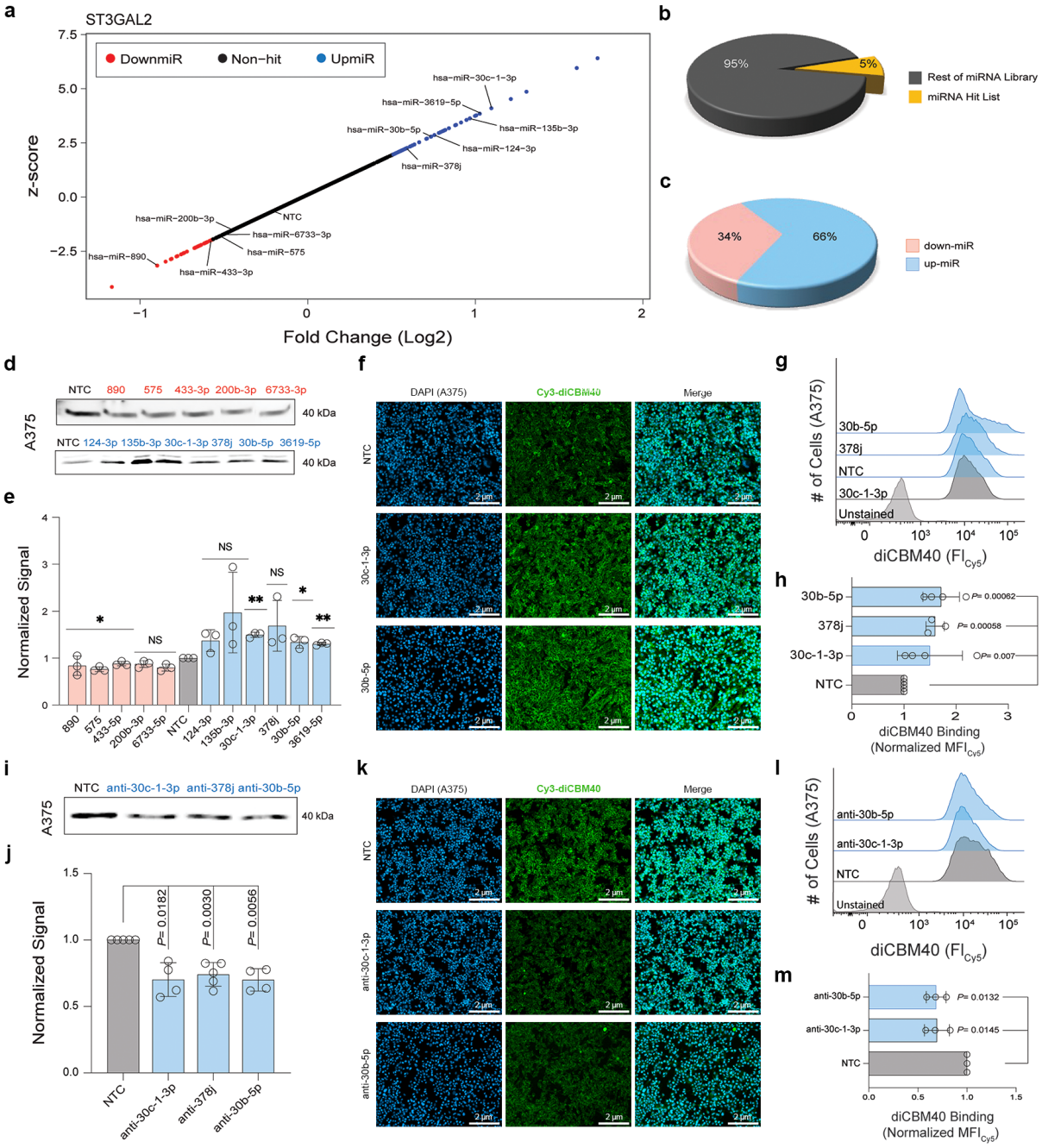

Figure 3.10 miRNA regulation of ST3GAL2 impacts α-2,3-sialylation in A375 melanoma cell line. a. Landscape of miRNA regulation of ST3GAL2 via the 3'UTR is shown via scatterplot of miRFluR data. miRNA in the 95% confidence interval by z-score are indicated (down-miRs: red, up-miRs: blue) and validated miRNAs are labeled. **b.** Pie chart showing % miRNA hits compared to total library post-QC. **c.** Pie chart indicates % down-miR (34%) vs. up-miR (66%) in ST3GAL2 hit list. **d-h.** Impact of miRNA mimics on ST3GAL2 expression. A375 cells were treated with miRNA mimics (down-miRs: -890, -575, -

433-5p, -200b-3p, -6733-5p, upmiRs: -124-3p, -135b-3p, -30c-1-3p, -378j, -30b-5p, -3619-5p) or non-targeting control (NTC) at 50 nM for 48h and analyzed as indicated. **d.** Representative Western blot analysis of ST3GAL2. **e.** Bar graph of Western blot data. **f.** Fluorescence microscopy analysis for Cy3-diCBM40 staining. **g.** Representative flow cytometry analysis of Cy5-diCBM40 binding. **h.** Bar graph of flow cytometry data. **i-m.** Impact of endogenous miRNA on ST3GAL2 expression. A375 cells were treated with anti-miRs (anti-up-miRs: anti-30c-1-3p, anti-378j, anti-30b-5p) or non-targeting control (NTC) at 50 nM for 48h and analyzed as indicated. **i.** Representative Western blot analysis of ST3GAL2. **j.** Bar graph of Western blot data. **k.** Fluorescence microscopy analysis for of Cy3-diCBM40 staining. **l.** Representative flow cytometry analysis of Cy5-diCBM40 binding. **m.** Bar graph of flow cytometry data. All experiments were performed in ≥ biological triplicate. Errors shown are standard deviations. For Western blot analysis, the One sample *t*-test was used to compare miRs to NTC (ns not significant, * $p < 0.05$, ** < 0.01). For flow cytometry analysis, the paired *t*-test was used to compare miRs to NTC and *p*-values are indicated on the graph.

down-miRs and 55 up-miRs within the 95% confidence interval (**Figure 3.10a-c**). I again chose a subset of miRNA (down-miRs: -890, -433-3p, -575, -6733-3p, -200b-3p; up-miRs: -124-3p, -3619-5p, -135b-3p, -30c-1-3p, -378j, -30b-5p) based on the criteria outlined above for validation[152,198]. miRNA mimics were transfected into A375 (melanoma, **Figure 3.10d-e**) and analyzed by Western blot analysis after 48 hours. The resulting impacts on ST3GAL2 protein expression were in line with the miRFluR assay. I next tested the effect of select up-miRs (miRs: -30b-5p, -30c-1-3p, -378j) on α-2,3-sialic acid levels in A375 using fluorescence microscopy and flow cytometry and observed the anticipated increase in sialylation (**Figure 3.10f-h**). I confirmed the impact of endogenous upregulatory miRNA using anti-miRs (anti-up-miRs: -30b-5p, -30c-1-3p, -378j) and observed the expected loss of both protein and glycan expression (**Figure 3.10i-m**). Furthermore, I examined the select miR subset for ST3GAL2 in the A549 lung cancer cell line for their impact on ST3GAL2 (**Figure 3.11a-b**), showing consistent miRNA regulatory patterns obtained from the A375 cell line (**Figure 3.10**). My data again showcases the power of the miRFluR assay to explore the miRNA regulatory landscape. In line with Chapter 2 and previous works by others, the effects of miRNA mimics on the transcript of *st3gal2* was more variable (**Figure 3.11c-d**)[78,95,125,126,130].

3.3.7 miRNA co-upregulate CD98hc and α-2,3-sialylation in melanoma

Given the importance of ST3GAL1 and ST3GAL2 on CD98hc stability in melanoma[159], I examined whether they might be co-regulated by miRNA. Comparison of all three miRNA datasets did not identify miRNA that regulated all three proteins. I also did not observe miRNA that have opposing effects (i.e. up-miR in one, down-miR in another) between any of the three transcripts. However, CD98hc and ST3GAL1 shared 6 up-miRs in common (miRs: -765, -488-5p, -449b-5p, -500b-5p, -28-3p, -1246), 4 of which were associated with melanoma (underlined).

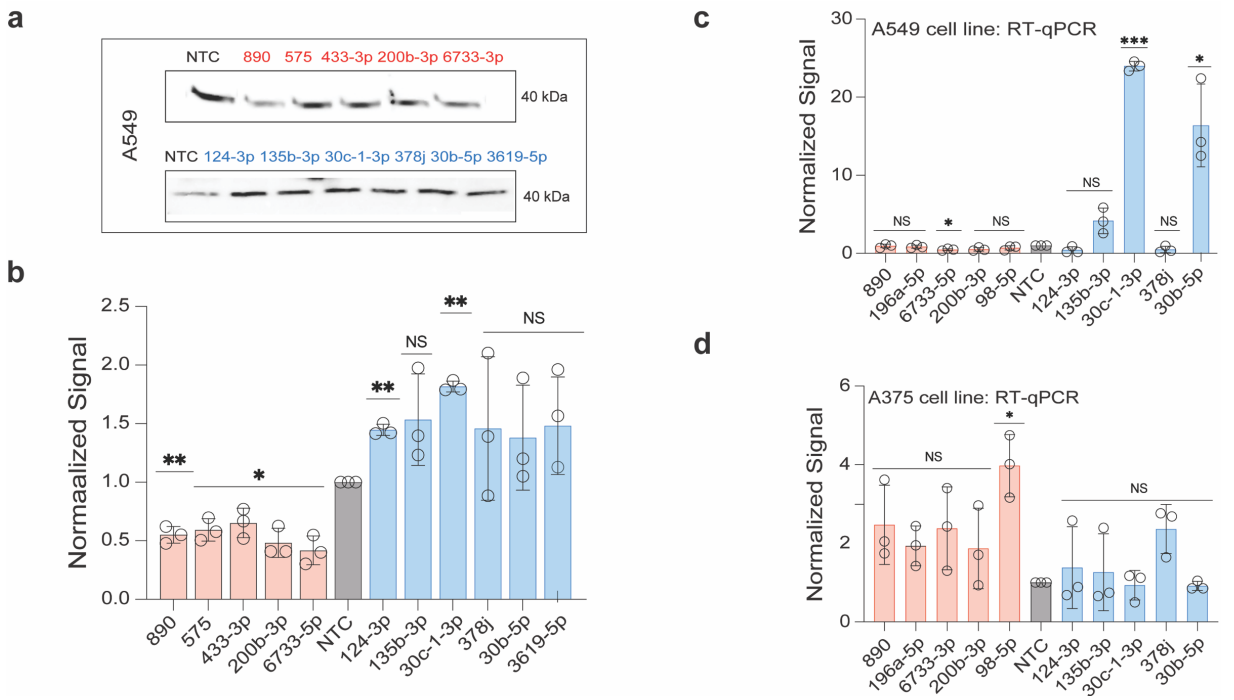

Figure 3.11 miRNA up- and down-regulate ST3GAL2 expression in A549 lung and A375 melanoma cell lines. Impact of miRNA mimics on ST3GAL2 expression. A549 (a, b) cells were treated with miRNA mimics (down-miRs: -890, -575, -433-5p, -200b-3p, -6733-5p, up-miRs: -124-3p, -135b-3p, -30c-1-3p, -378j, -30b-5p, -3619-5p) or NTC at 50 nM for 48h and analyzed as indicated. **a.** Representative Western blot analysis of ST3GAL2 in A549. **b.** Bar graph of Western blot data for A549. **c, d.** RT-qPCR quantitative analysis of st3gal2 in A549 (c) and A375 (d). All experiments were performed in ≥ biological triplicate. Errors shown are standard deviations. The One sample *t*-test was used to compare miRs to NTC for Western blot and RT-qPCR experiments (NS: not significant, * $p < 0.05$, ** < 0.01, *** < 0.001).

In addition, four up-miRs were found to co-regulate CD98hc and ST3GAL2 (miRs: -378j, -135b-3p, -30b-5p, -30c-1-3p), three of which were associated with melanoma[152,176,198](**Table 3.1,**

Figure 3.12). To address whether these miRs might co-regulate CD98hc and sialylation by ST3GAL1 or ST3GAL2, I tested the impact of a select subset of these co-regulatory miRs (ST3GAL1: miRs: -1246, -28-3p, -500b-3p, -449b-5p; ST3GAL2: miRs: -378j, -135b-3p, -30b-5p, -30c-1-3p) on expression in the melanoma cell lines MeWo (**Figures 3.13**) and 5B1 (**Figure 3.14)**, and the breast cancer line MCF-7 (**Figure 3.15**). In line with my miRFluR results, transfection of co-upmiRs upregulated both CD98hc (orange) and either ST3GAL1 (purple) or ST3GAL2 (green) in all three cell lines as seen by Western blot analysis (**Figures 3.13a- d and 3.14a-d**, **Figure 3.15**).

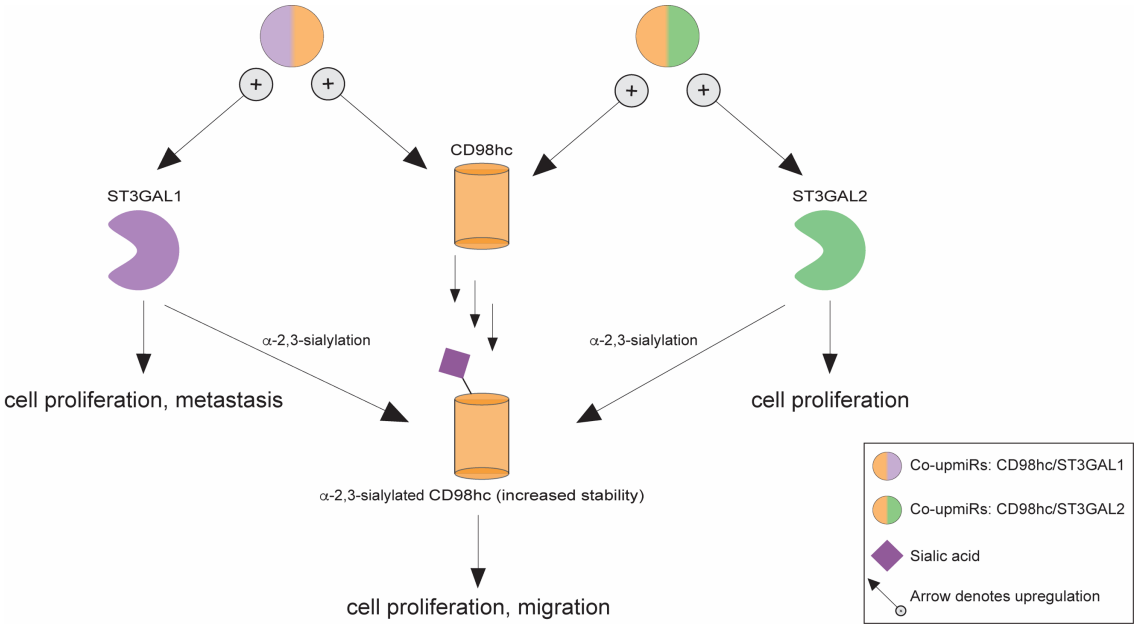

Figure 3.12 Upregulatory miRNAs co-regulate CD98hc/ST3GAL1 or CD98hc/ST3GAL2. Sialylation is required for the stability of CD98hc in melanoma where ST3GAL1, ST3GAL2 and CD98hc are all essential genes.

Flow cytometry analysis of CD98hc confirmed Western blot results (**Figures 3.13e-f and 3.14e-f**). I also observed an increase in α-2-3-sialylation by flow cytometry, in line with upregulation of ST3GAL1 or ST3GAL2 expression by the up-miRs (**Figures 3.13g-h and 3.14g-h**). To confirm that endogenous miRNA could co-regulate these proteins, I utilized the

corresponding anti-miRs to the co-upregulators (**Figures 3.13i-p and 3.14i-p**). All miRNA tested were known to be expressed in melanoma or the MeWo cell line[176,184]. As anticipated, Western blot analysis clearly shows loss of expression for co-regulated proteins upon inhibition of the endogenous miRNA. This data was supported by flow cytometry analysis of CD98hc. I also observed the loss of α-2,3 sialic acid, concordant with the loss of ST3GAL1 or ST3GAL2 expression upon up-miR inhibition, although this was only observed in the 5B1 cell line (**Figure 3.14p**). Overall, my data strongly supports the idea that miRNA regulatory networks include co-upregulation of critical proteins.

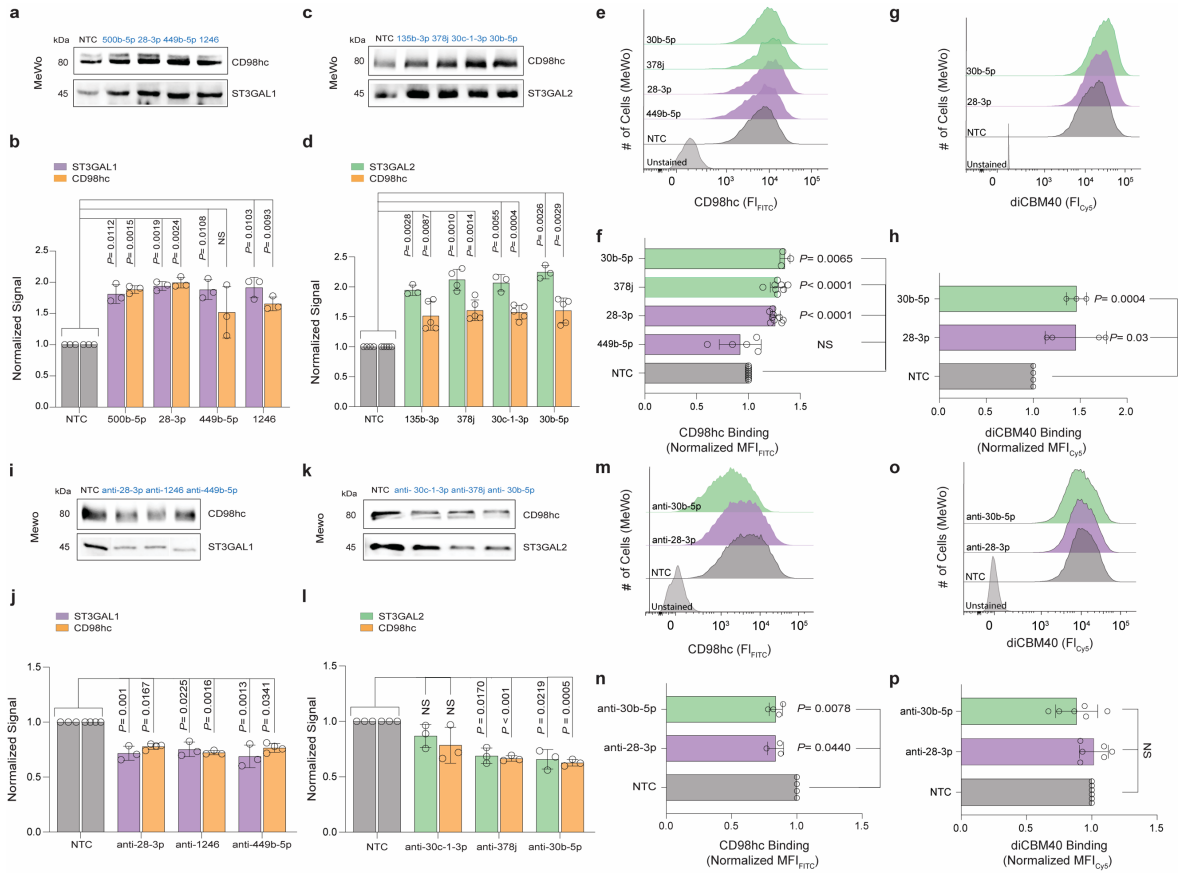

Figure 3.13 Co-upregulation of CD98hc and either ST3GAL1 or ST3GAL2 is observed in MeWo cell line. a-d. Impact of co-up-miR mimics on either CD98hc (orange) & ST3GAL1 (purple, co-up-miRs: -500b-5p, -28-3p, -449b-5p, -1246) or CD98hc (orange) & ST3GAL2 expression (green, co-up-miRs: -135b-3p, -378j, -30c-1-3p, -30b-5p) in MeWo cells treated with corresponding co-up-miRs or non-targeting control (NTC) at 50 nM for 48h and analyzed as indicated. **a.** Representative Western blot analysis of

CD98hc and ST3GAL1. **b.** Bar graph of corresponding Western blot data. **c.** Representative Western blot analysis of CD98hc and ST3GAL2. **d.** Bar graph of corresponding Western blot data. **e.** Representative flow cytometry analysis of CD98hc binding. **f.** Bar graph of flow cytometry data. **g.** Representative flow cytometry analysis of Cy5-diCBM40 binding. **h.** Bar graph of flow cytometry data. **i-o.** Impact of endogenous co-up-miRs on either CD98hc (orange) & ST3GAL1 (purple) or CD98hc (orange) & ST3GAL2 (green) expression. MeWo cells were treated with anti-miRs (anti-up-miRs: anti-28-3p, anti-1246, anti-449b-5p; anti-30c-1-3p, anti-378j, anti-30b-5p) or non-targeting control (NTC) at 50 nM for 48h and analyzed as indicated. **i.** Representative Western blot analysis of CD98hc and ST3GAL1. **j.** Bar graph of Western blot data. **k.** Representative Western blot analysis of CD98hc and ST3GAL2. **l.** Bar graph of Western blot data. **m.** Representative flow cytometry analysis of CD98hc binding. **n.** Bar graph of flow cytometry data for MeWo. **o.** Representative flow cytometry analysis of Cy5-diCBM40 binding. **p.** Bar graph of flow cytometry data. All experiments were performed in ≥ biological triplicate. Errors shown are standard deviations. For Western blot analysis, the One sample *t*-test was used to compare miRs to NTC. For flow cytometry analysis, paired *t*-test was used to compare miRs to NTC. All *p*-values are indicated on the graph (NS not significant).

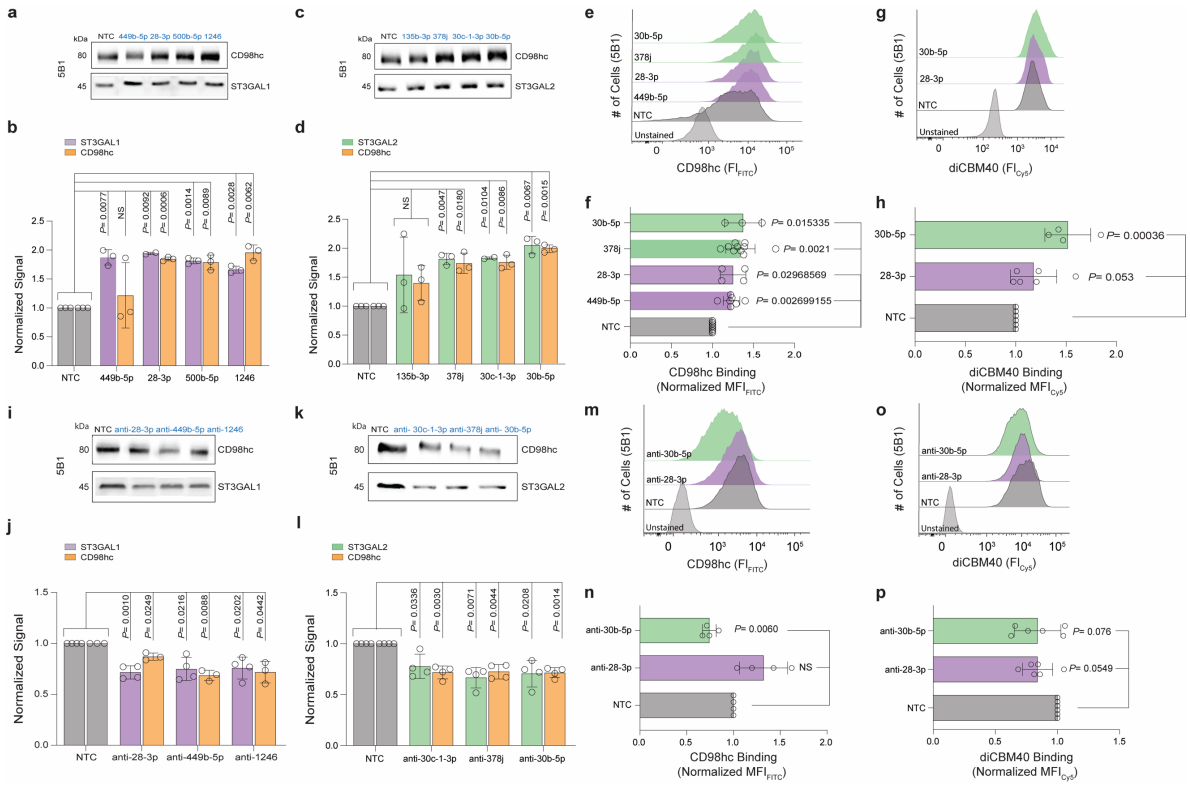

Figure 3.14 Co-upregulation of CD98hc and either ST3GAL1 or ST3GAL2 is observed in 5B1 cell line. a-d. Impact of co-up-miR mimics on either CD98hc (orange) & ST3GAL1 (purple, co-up-miRs: -500b-5p, -28-3p, -449b-5p, -1246) or CD98hc (orange) & ST3GAL2 expression (green, co-up-miRs: -135b-3p, -378j, -30c-1-3p, -30b-5p) in 5B1 cells treated with corresponding co-up-miRs or non-targeting control (NTC) at 50 nM for 48h and analyzed as indicated. **a.** Representative Western blot analysis of CD98hc and ST3GAL1. **b.** Bar graph of corresponding Western blot data. **c.** Representative Western blot analysis of CD98hc and ST3GAL2. **d.** Bar graph of corresponding Western blot data. **e.** Representative flow cytometry analysis of CD98hc binding. **f.** Bar graph of flow cytometry data. **g.** Representative flow cytometry analysis of Cy5-diCBM40 binding. **h.** Bar graph of flow cytometry data. **i-o.** Impact of endogenous co-up-miRs on either CD98hc (orange) & ST3GAL1 (purple) or CD98hc (orange) & ST3GAL2 (green) expression. 5B1 cells were treated with anti-miRs (anti-up-miRs: anti-28-3p, anti-1246,

anti-449b-5p; anti-30c-1-3p, anti-378j, anti-30b-5p) or non-targeting control (NTC) at 50 nM for 48h and analyzed as indicated. **i.** Representative Western blot analysis of CD98hc and ST3GAL1. **j.** Bar graph of Western blot data. **k.** Representative Western blot analysis of CD98hc and ST3GAL2. **l.** Bar graph of Western blot data. **m.** Representative flow cytometry analysis of CD98hc binding. **n.** Bar graph of flow cytometry data for 5B1. **o.** Representative flow cytometry analysis of Cy5-diCBM40 binding. **p.** Bar graph of flow cytometry data. All experiments were performed in ≥ biological triplicate. Errors shown are standard deviations. For Western blot analysis, the One sample *t*-test was used to compare miRs to NTC. For flow cytometry analysis, paired *t*-test was used to compare miRs to NTC. All *p*-values are indicated on the graph (NS not significant).

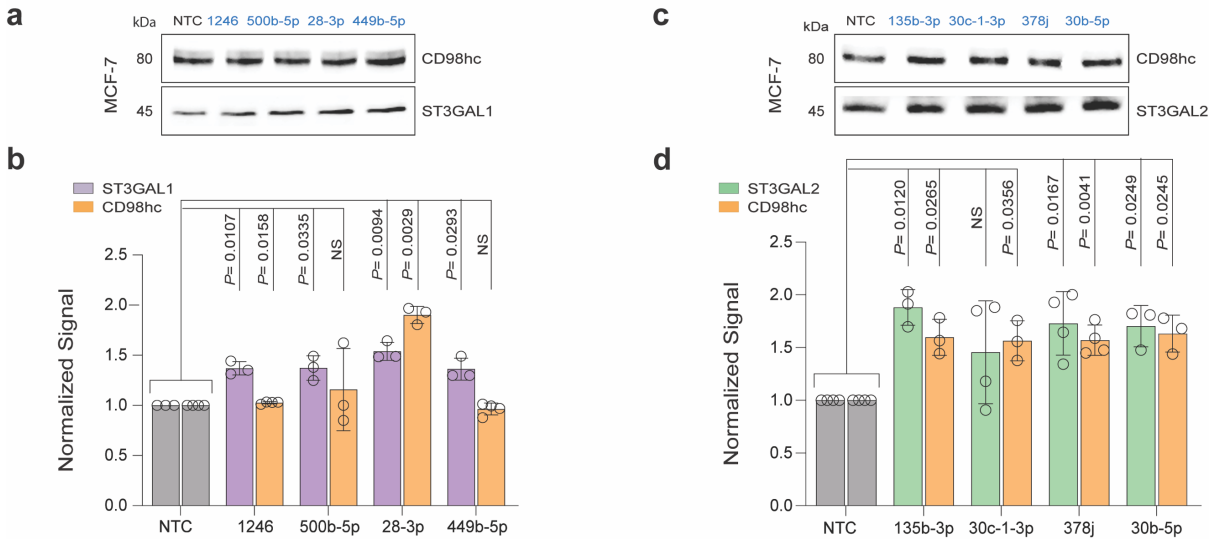

Figure 3.15 miRNA regulation of CD98hc and a-2,3-sialylation in MCF-7 cell line. Impact of co-up-miR mimics on either CD98hc (orange) & ST3GAL1 (purple, co-up-miRs: -500b-5p, -28-3p, -449b-5p, -1246) or CD98hc (orange) & ST3GAL2 expression (green, co-up-miRs: -135b-3p, -378j, -30c-1-3p, -30b-5p) in MCF-7 cells treated with corresponding co-up-miRs or non-targeting control (NTC) at 50 nM for 48h and analyzed as indicated. **a.** Representative Western blot analysis of CD98hc and ST3GAL1. **b.** Bar graph of Western blot data for blots shown in a. **c.** Representative Western blot analysis of CD98hc and ST3GAL2. **d.** Bar graph of Western blot data for blots shown in c. All experiments were performed in ≥ biological triplicate. Errors shown are standard deviations. For Western blot analysis, the One sample *t*-test was used to compare miRs to NTC (NS not significant, and *p*-values are indicated on the graph).

3.3.8 Co-regulation of CD98hc and α-2,3-sialic acid is via direct miRNA:3'UTR interactions

The impact of miRNA on protein expression can be via direct or indirect effects. In Chapter 2[130] and previous work by the Mahal laboratory[78], we established that the miRFluR assay identifies miRNA regulation via direct interactions between the miRNA and the 3'UTR of the transcript of interest. To verify that miRNA co-upregulation of CD98hc and either ST3GAL1 or ST3GAL2 were via direct miRNA: mRNA interactions, I identified the upregulatory sites for two miRNAs: miR-1246 (CD98hc/ST3GAL1) and miR-30b-5p (CD98hc/ST3GAL2) using RNAhybrid[142].

These miRNAs are highly expressed in melanoma and are associated with melanoma progression[152,198]. I then mutated these sites in my pFmiR sensors and tested their impact on miRNA-mediated upregulation (**Figure 3.16**).

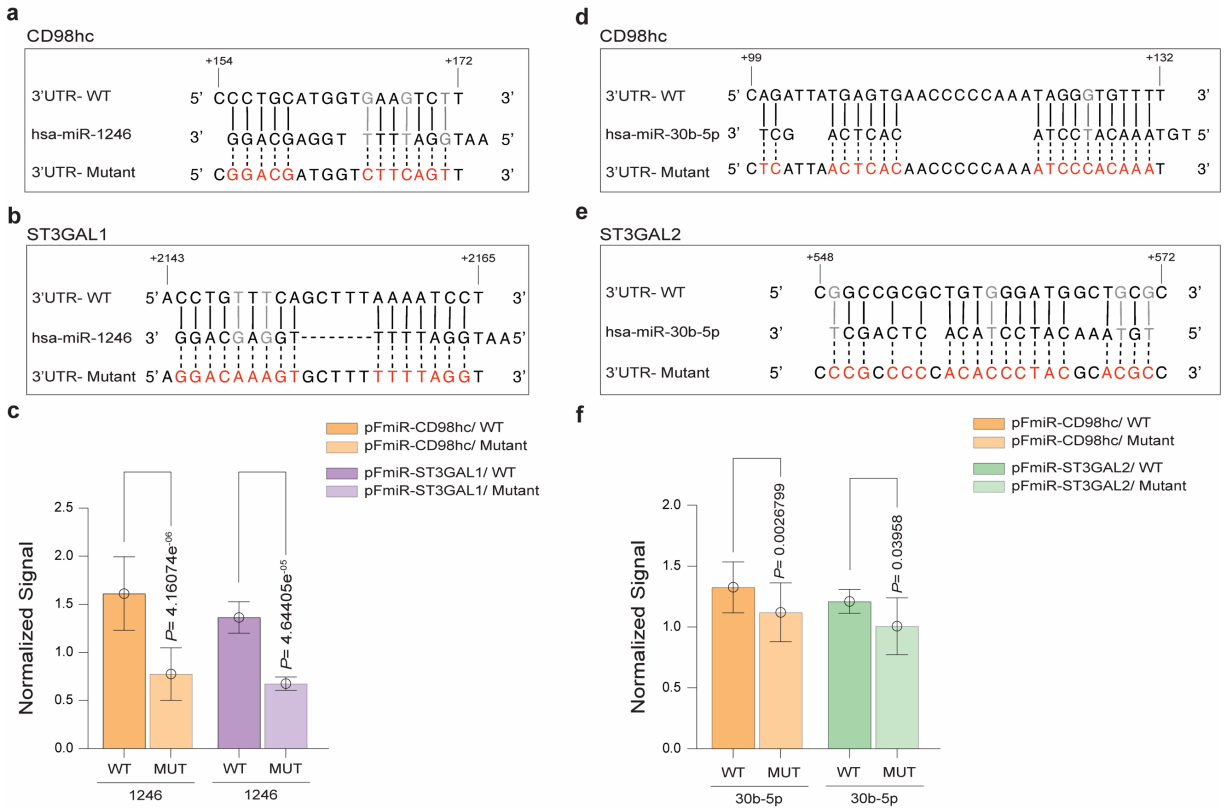

Figure 3.16 Co-upregulation by miRNAs requires direct interactions with 3′UTRs of CD98hc, ST3GAL1 and ST3GAL2. a, b. Alignment of miR-1246 with predicted CD98hc-3′UTR (a) or ST3GAL1-3'UTR (b) sites and their corresponding mutants. Mutated residues are shown in red. Wobble interactions are shown in grey. **c.** Bar graph of data from miRFluR sensors. For each sensor, data was normalized over NTC. **d, e.** Alignment of miR-30b-5p with predicted CD98hc-3′UTR (d) or ST3GAL2-3'UTR (e) sites and their corresponding mutants. Mutated residues are shown in red. Wobble interactions are shown in grey. **f.** Bar graph of data from miRFluR sensors. For each sensor, data was normalized over NTC. A standard *t*-test was used for comparisons and *p*-values are indicated on the graph. All experiments were performed in biological triplicate, a representative experiment with n = 5 wells is shown.

In line with Chapter 2[130], mutation of the RNAhybrid predicted sites abrogated upregulation. None of the four sites identified had canonical seed binding, nor were they AU rich. Taken together, my data strongly supports an alternative binding motif for upregulatory miRNA interactions that has yet to be fully determined.

3.4 Discussion

The canonical view of miRNA, which can have >100 targets each, is that they downregulate the expression of proteins that synergistically control specific cellular pathways and phenotypes. In Chapter 2, I identified and validated that miRNA can upregulate protein expression through direct binding to the 3'UTR in dividing cells [130]. This contradicts the dominant view of miRNA, providing a mechanism for bidirectional tuning of protein expression. In this Chapter, I provide further evidence for upregulation and expand upon its roles in the tuning of protein networks.

In mapping the miRNA landscape for both the sialyltransferases (ST3GAL1, ST3GAL2) and their glycosylation target (CD98hc), I identify up- and downregulatory miRNAs for all three genes (up-miRs: 149 total interactions, down-miRs: 68 total interactions). As expected, biological validation of up- and down-miRs using both miRs and anti-miRs followed the data from the miRFluR assay. Chapter 2 focused on identifying regulators of α-2,6-sialyltransferases, which are often medium to low abundance proteins[130]. In contrast, CD98hc (*slc3a2*) is a component of a neutral amino acid transporter found at the cell surface[160,199]. It is highly abundant in cancer and in proliferating B- and T-cells, where it plays an important role in clonal expansion[162-164]. Of note, one of the strongest hits observed in my miRFluR result for CD98hc was miR-155-5p, a highly abundant miRNA which itself is critical in both cancer and clonal expansion of B- and T-cells[179,189,190]. The concordance of roles for miR-155-5p and CD98hc strongly suggests that CD98hc is a primary target of miR-155-5p in these biological systems.

The majority of miRNA regulation is currently thought to occur at the 3'UTR of transcripts, and the miRFluR assay is focused on such regulation. The length of the 3'UTR has increased as organisms have become more complex and required enhanced regulation of protein expression.

The median 3'UTR length in humans is ~1,200 nucleotides[200,201]. Similar to other genes analyzed using the miRFluR assay to date, the 3'UTRs of ST3GAL1 and ST3GAL2 are both > 2 kb. However, the 3'UTR of CD98hc is notably short, at only 190 nt. Upregulatory miRNAs were seen for all three genes, indicating that upregulation does not require a long 3'UTR. The proportion of up- to down-miRs for these genes was target dependent, with ST3GAL1 biased towards up-miRs (90%, **Figure 3.8c**) and CD98hc almost evenly divided between up- and down-regulators (54:46, up: down, **Figure 3.2c**). Consistent with these differences, in Chapter 2, I observed transcripts biased toward down-regulatory miR interactions (ST6GAL2) and those biased towards upregulation (ST6GAL1)[130]. This hints that the structure of the 3'UTR may influence the consequence of miRNA interactions, changing the predominant mode of regulation.

The local binding between miRNA and their cognate mRNA in downregulatory complexes are highly enriched in seed sequences, in which positions 2-8 at the 5'-end of the miRNA are base paired to the mRNA[202]. Of the five upregulatory binding sites identified in this Chapter (**Figures 3.7 and 3.16**), none follow canonical seed rules. In Chapter 2, I identified 3 upregulatory binding sites, of which only one had a canonical seed. We, and others, found that upregulation by miRNA in both dividing[130] and quiescent[143] cells requires Argonaute 2 (AGO2), but is inhibited by TNRC6A (GW182), an essential component of downregulatory AGO2 complexes[146,158]. In a re-evaluation of miRNA: mRNA target base-pairing within AGO complexes, Helwak, *et. al.,* found that non-canonical binding was highly prevalent and that there were distinct non-canonical base-pairing patterns[203]. The same miRNA were found to engage in both seed and non-canonically patterned binding. They posited that differential binding patterns of miRNA: mRNA complexes might alter AGO2 structures, leading to different complexes and activities. The data to date supports a hypothesis that the interaction rules between a single miRNA and its cognate transcript

are different in up- and downregulation, potentially recruiting distinct components into AGO2 complexes that define the translational fate of the mRNA[130,143].

Within the cell, miRNA cooperatively tune the expression of proteins that act in concert within a biological pathway[62,204,205]. This role has been well established for downregulatory miRNA interactions. Co-regulation of proteins in a network by up-miRs has yet to be reported. In recent work, we identified ST3GAL1 and ST3GAL2 as essential genes in melanoma. Loss of these genes caused apoptosis and enhanced proteasomal degradation of CD98hc, itself an essential gene[159]. In strong concordance with the biological relationship between CD98hc and ST3GAL1/2 in melanoma, I observed co-upregulators for CD98hc with either ST3GAL1 or ST3GAL2 (**Figure 3.12**). I do not observe any overlap between the miRFluR hits for ST3GAL1 and ST3GAL2, nor do I observe either co-down-miRs or opposing miRNA regulation between the three genes. Of the ten co-upregulators identified, six are overexpressed during melanoma progression (CD98hc/ST3GAL1: miR-28-3p, -1246, -449b-5p; CD98hc/ST3GAL2: miR-135b-3p, -30b-5p, -30c-1-3p)[152,176,198]. This is consistent with the increased protein expression of CD98hc, ST3GAL1 and ST3GAL2 observed in melanoma patients[47,168]. Co-upregulation makes biological sense as α2,3-sialylation by these enzymes is required for CD98hc protein stability in melanoma, which is most likely mediated by protein glycosylation, a known regulator of trafficking and stability[159,206]. However, it is highly unlikely that the stability of the Golgi enzymes ST3GAL1 or ST3GAL2 requires CD98hc and the loss of ST3GAL1/2 in melanoma causes loss of CD98hc independent of miRNA, thus tuning through co-downregulation is not required.

Several of the co-upregulators have other known targets in melanoma biology. Proliferation and viability of melanoma cells were enhanced by the expression of miR-1246, which was found to directly target and downregulate the tumor suppressor FOXA2[198]. In earlier work

from the Mahal and Hernando laboratories, miR-30b-5p was identified as overexpressed in melanoma metastasis and was found to inhibit the expression of GALNT7, a GalNAc transferase, increasing the invasive capacity of melanoma cells *in vitro* and the metastatic potential *in vivo*[152]. Taken together with my data, this provides strong evidence for bidirectional tuning by the same miRNA within regulatory networks, with upregulation vs. downregulation determined by the miRNA: mRNA pair. This Chapter positions upregulation as a central part of miRNA regulatory networks and argues for a re-examination of the functions of miRNA.

3.5 Conclusion

Cellular protein expression is coordinated post-transcriptionally by an intricate network of regulation. To date, it has been presumed that miRNA work by coordinating repression of key targets within a network. In recent work, upregulation of protein expression by miRNA has been found in dividing cells[78,130], providing an additional mechanism of regulation. In this Chapter, I demonstrate coordinated upregulation of coupled proteins by miRNA. I focused on CD98hc, the heavy chain of the neutral amino acid transporter LAT1, and two α-2,3-sialyltransferases: ST3GAL1 and ST3GAL2 that are critical for its stability in melanoma and profiled their miRNA regulation using the high-throughput miRFluR assay. I identified independent co-upregulators for CD98hc with both sialyltransferases that were enriched in melanoma datasets. My findings add co-upregulation by miRNA into our understanding of miRNA regulatory networks and add a new twist to the impact miRNA have on glycosylation.

3.6 Experimental methods

3.6.1 Cloning

CD98hc, ST3GAL1 and ST3GAL2 3'UTRs were amplified via PCR from genomic DNA (gDNA, 10 μg, from MCF-7 cell line: CD98hc) or gene synthesis (GenScript Gene Synthesis

company: ST3GAL1 and ST3GAL2) using the primers shown in **Table 3.2**. The amplicons were cleaned up using a Monarch® PCR & DNA cleanup kit (catalog #: T1030S, NEB). The 3'UTR fragments were then cloned into the pFmiR-empty backbone[78], downstream of Cerulean with the following restriction sites (for CD98hc & ST3GAL2: NheI and BamHI; for ST3GAL1: AgeI and BsiWI) using standard ligation protocols (NEB). Plasmids were verified by Sanger sequencing (Molecular Biology Services Unit, University of Alberta). Large-scale endotoxin free DNA preparations were made for sequence-verified constructs (pFmiR-ST3GAL1 and pFmiR-ST3GAL2) using Endotoxin-free plasmid DNA purification (Takara Bio USA, Inc., catalog #: 740548). Plasmid maps (for pFmiRs: -CD98hc, -ST3GAL1 and -ST3GAL2) and their corresponding 3'UTR sequences can be found in **Appendix A**.

3.6.2 Cell lines

Cell lines HEK-293T, SK-OV-3, A549, and MCF-7 were purchased directly from the American Type Culture Collection (ATCC), HT-29 was a gift from lab of Kristi Baker, MeWo, 131/4-5B1, and A375 were gifts from the Hernando Lab. Cells were cultured in media as follows: HT-29 & HEK-293T:Dulbecco's Modified Eagle Medium (DMEM), 10% FBS; A549: FK-12, 10%, FBS; A375 & MeWo: DMEM* (catalog # 30-2002), 10% FBS; 131/4-5B1: RPMI-1640, 10% FBS) ; SK-OV-3: McCoy's 5a Medium Modified (catalog # 30-2007), 10% FBS; MCF-7: DMEM/F12 (catalog #: 11320033), 10% FBS, under standard conditions (5% CO_2, 37°C)

3.6.3 miRFluR high-throughput assay

The Human miRIDIAN miRNA mimic Library 21.0 (Dharmacon) was resuspended in ultrapure nuclease-free water (REF. #: 10977-015, Invitrogen) and aliquoted into black 384-well, clear optical bottom tissue-culture treated plates (Nunc). Each plate contained three replicate wells of each miRNA in that plate (2 pmol/well). In addition, each plate contained a minimum of 6 wells

containing miRIDIAN non-targeting controls. To each well was added target pFmiR plasmid (pFmiR-CD98hc: 30 ng, pFmiR-ST3GAL1: 30 ng, or pFmiR-ST3GAL2: 20 ng) in 5 µl Opti-MEM (Gibco) and 5 µL of transfection solution (0.1 µL Lipofectamine™ 2000 (catalog #: 11668500, Life Technologies) diluted to 5 µl total volume with Opti-MEM (Gibco), premixed 5 min at room temperature). The mixture was allowed to incubate at room temperature in the plate for 20 min. HEK293T cells (25 µl per well, 400 cells/ µl in phenol red free DMEM supplemented with 10 % FBS and Pen/Strep) were then added to the plate. Plates were incubated at 37°C, 5% CO_2. After 48 hours, the fluorescence signals of Cerulean (excitation: 433 nm; emission: 475 nm) and mCherry (excitation: 587 nm; emission: 610 nm) were measured using the clear bottom read option (SYNERGY H1, BioTek, Gen 5 software, version 3.08.01).

3.6.4 Data analysis

I calculated the ratio of Cerulean fluorescence over mCherry fluorescence (Cer/mCh) for each well in each plate. For each miRNA, triplicate values of the ratios were averaged, and the standard deviation (S.D.) obtained. We calculated % error of measurement for each miRNA (100 × S.D./mean). As a quality control measurement (QC), we removed any plates or miRNAs that had high errors in the measurement (median error ±2 S.D. across all plates) and/or a high median error of measurement for the plate (>15%). After QC we obtained data for 954 miRNAs for CD98hc, 1,807 miRNAs for ST3GAL1, and 1,542 miRNAs for ST3GAL2 out of 2601 total miRNAs screened for each target 3'UTR. We checked whether the miRIDIAN non-targeting controls were at the median and found that they were skewed. Therefore, the Cer/mCh ratio for each miRNA was normalized to the median of Cer/mCh ratios within that plate without exclusions of any data in the plate and error was propagated. Data from all plates were then combined and log-transformed z-scores calculated. A z-score of ±1.965, corresponding to a two-tailed *p*-value of

0.05, was used as a threshold for significance. Post-analysis we identified 65 miRNA hits for CD98hc, 67 miRNA hits for ST3GAL1, and 84 for ST3GAL2 within 95% confidence interval (**Figure 3.17,** and corresponding **Figures 3.2a, 3.8a, 3.10a**, and **Datasets 3.1-3.3** (.xls sheets)).

3.6.5 Western blot analysis of CD98hc, ST3GAL1 and ST3GAL2

Western blot analysis was conducted for CD98hc in MeWo, 5B1 and MCF-7 cell lines (down-miRs: miRs -17-5p, -34c-5p, -203b-5p; up-miRs: miRs -135b-5p, -155-5p). For ST3GAL1, Western blot analysis was done in SK-OV-3 and HT-29 cell lines (down-miRs: miRs -363-5p, -1276, -609, -4714-5p, let-7i-5p; up-miRs: miRs -937-3p, -500b-5p, -28-3p, -449b-5p, -1246, -150-3p). For ST3GAL2, the Western blot analysis was performed in A375 and A549 cell lines (down-miRs: miRs -890, -433-3p, -575, -6733-3p, -200b-3p; up-miRs: miRs -124-3p, -3619-5p, -135b-3p, -30c-1-3p, -378j, -30b-5p). For co-up-miRs (CD98hc/ST3GAL1: miRs -1246, -28-3p, -449b-5p, -500b-5p; CD98hc/ST3GAL2: miRs -30b-5p, -30c-1-3p, -378j, -135b-3p), Western blot analysis was tested in the MeWo, 5B1, MCF-7 cell lines for analyzing CD98hc, ST3GAL1 and ST3GAL2 protein levels. For all Western blot analysis using mimics, miR-548ab was used as the non-targeting control (NTC) based on experimental data (**Figure 3.3**). For all experiments, cells were seeded in six-well plates (50,000 cells/well) and cultured for 24 h in appropriate media. Cells were then washed with Hanks buffered salt solution (HBSS, Gibco) and transfected with miRNA mimics: 50 nM mimic (Dharmacon, Horizon Discovery), 5 µl Lipofectamine 2000 (Life Technologies), 250 µl OptiMEM. The media was changed to standard media 12 h post-transfection. Cells were then lysed at 48 h post-transfection in cold RIPA lysis buffer supplemented

with Halt™ protease inhibitors (Thermofisher, catalog #: 89900). For Western blot analysis, 50

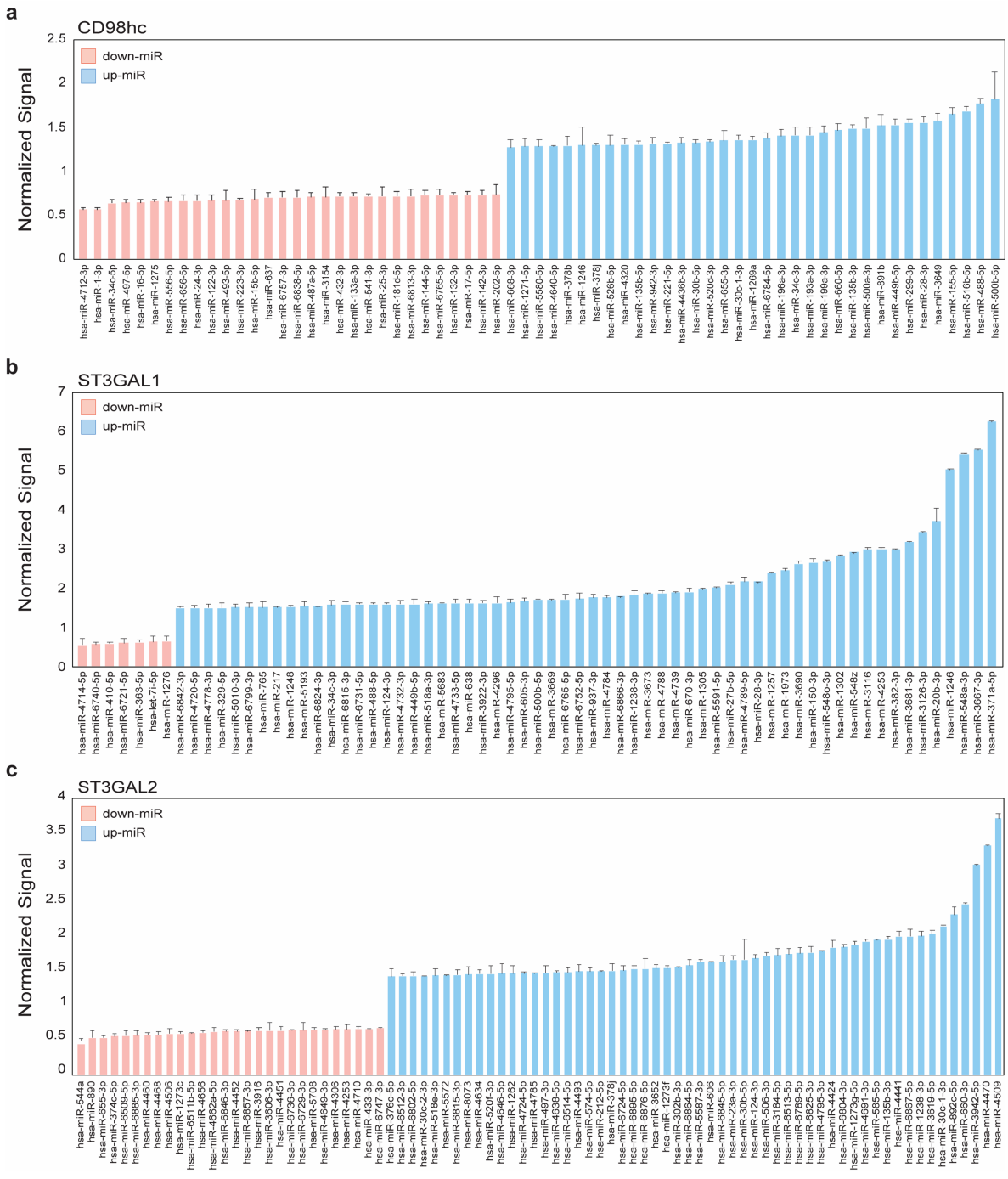

Figure 3.17 miRNA hit lists. Barcharts represent the miRNA hits identified for CD98hc (a), ST3GAL1 (b), and ST3GAL2 (c). Data normalized over median. Error bars represent standard deviation of technical replicates (n=3).

μg of protein was added to 4x loading buffer with DTT (1 mM), heated at 95°C for 10 min and run on a 10% gel (SDS-PAGE) using standard conditions. Proteins were then transferred from the gel to Polyvinylidene fluoride membrane using iBlot2 Transfer Stacks (PVDF, Invitrogen, catalog number: IB24002) and the iBlot2 transfer device (Invitrogen) using the standard protocol (P0). Blots were then incubated with Ponceau S Solution (Boston BioProducts, catalog #ST-180) for 3 min and the total protein levels were imaged using the protein gel mode (Azure 600, Azure Biosystems Inc.). Blots were blocked with 5% BSA (CD98hc and ST3GAL1) or 5% non-fat dry milk (ST3GAL2) in TBST buffer (TBS buffer plus 0.1% Tween 20) for 30 min at room temperature on rocker (LSE platform rocker, Corning) with 60 rpm. For CD98hc, blots were then incubated with Monoclonal mouse α-human-CD98hc 1° antibody (1:500 in TBST with 10% BSA, catalog #: 66883-1-IG, Proteintech). For ST3GAL1, rabbit α-human-ST3GAL1 1° antibody (1:1000 in TBST with 10% BSA, catalog #: HPA040466, Sigma) was used. For ST3GAL2, rabbit α-human-ST3GAL2 1° antibody (1:1000 in TBST with 10% non-fat dry milk, catalog #: ab96028, Abcam) was used. After an overnight incubation at 4ºC, blots were washed 3 × 1 min with 0.1% TBST buffer. A secondary antibody was then added (ST3GAL1/2: α-rabbit IgG-HRP, 1: 6,000 in TBST with 10% BSA (ST3GAL1) or non-fat dry milk (ST3GAL2); CD98hc: α-mouse IgG-HRP, 1: 5000 in TBST with 10% BSA) and incubated for 1 h at room temperature with shaking (60 rpm). Blots were then washed 3 × 1 min with 0.1% TBST buffer. Blots were developed using Clarity and Clarity Max Western ECL substrates according to the manufacturer's instructions (Bio-Rad). Membranes were imaged in chemiluminescent mode (Azure 600, Azure Biosystems Inc.). All analysis was done in a minimum of three biological replicates.3.6.6 Endogenous miRNA activity validation.

miRIDIAN microRNA Hairpin Inhibitors (CD98hc: anti-miRs -155-5p, -135b-5p; ST3GAL1: anti-miRs -1246, -28-3p, -449b-5p; ST3GAL2: anti-miRs -30b-5p, -30c-1-3p, -378j) and miRIDIAN microRNA Hairpin Inhibitor Negative Control (NTC) were purchased from Dharmacon (Horizon Discovery, Cambridge, UK). The selected anti-up-miRs for each protein in different cell lines: CD98hc: MeWo and 5B1 cells; ST3GAL1: SK-OV-3 cells; ST3GAL2: A375 cells. For co-up-miRs (CD98hc/ST3GAL1: anti-miRs -1246, -28-3p, -449b-5p; CD98hc/ST3GAL2: anti-miRs -30b-5p, -30c-1-3p, -378j) were tested in the MeWo, 5B1 cell line for analyzing CD98hc, ST3GAL1 and ST3GAL2 protein levels. Each cell lines were seeded and incubated as described for Western blot analysis. Cells were transfected with anti-miRNAs, 50 nM using Lipofectamine™ 2000 transfection reagent in OptiMEM following the manufacturer's instructions (Life Technologies). After 12 h media was changed to standard culture media. 48 h post-transfection cells were lysed and analyzed for CD98hc, ST3GAL1 and ST3GAL2 protein levels as previously described. All analysis was done in three biological replicates.

3.6.6 RT-qPCR

Total RNA was isolated from cells treated as in Western blot experiments using TRIzol reagent (catalog #: 15596018, Invitrogen) according to the manufacturer's instructions. RNA concentrations were measured using NanoDrop. Isolated total RNA (1 μg) was then reverse transcribed to cDNA using Superscript III Cells Direct cDNA synthesis kit (catalog #: 18080300, Invitrogen). Reverse transcription quantitative PCR (RT-qPCR) was performed using the SYBR Green method and cycle threshold values (Ct) were obtained using an Applied Biosystem (ABI) 7500 Real-Time PCR machine. Values were normalized to the housekeeping gene GAPDH. The primer sequences used for RT-qPCR can be found in **Table 3.2**. All analysis was done in three biological replicates.

3.6.7 Fluorescence microscopy

Cells were seeded onto sterile 22 × 22 glass coverslips placed into 35 mm dishes at a density of 2×10^5 cells/ml in the appropriate media for the cell line (see above). After 24h, cells were transfected with miRNA mimics as previously described (see methods for Western blots). At 48 h post-transfection, cells were washed with TBS (3 × 2 mL) and fixed with 4% paraformaldehyde for 20 min. Cells were again washed with TBS (3 × 2 mL). Incubate with Cy5-diCBM40 (made in Mahal lab) by adding (2 mL total volume, 1:300 (vol: vol) in TBS, 0.1% BSA for 1 hour at room temperature in dark. Coverslips were then washed (TBS, 3 × 2 mL), and cells were counterstained with Hoechst 33342 (2 mL, 1 µg/mL in TBS, 15 min in incubator). The coverslips were then mounted onto slides with 60 µl of mounting media (90% glycerol in PBS) and imaged with a Zeiss fluorescent microscope (Camera: Axiocam 305 mono, software: ZEN 3.2 pro). Specificity of diCBM40 staining was confirmed by using Neuraminidase (catalog #: P0722L, NEB) prior to Cy5-diCBM40 staining. All analysis was done in three biological replicates.

3.6.8 Flow cytometry

Lectin staining and flow cytometry analysis: miRNA or anti-miR transfection to samples for Flow cytometry analysis is prepared with the same method as for Western blot analysis. Post 48 hours-transfection, samples were trypsin digested (100 µl of 0.25 % trypsin per well in 6-well plate format). Up to 1 mL of 1X HBSS was added to remove all the cells from the flask, and cells were pelleted out by centrifugation at 350 × g for 6 min. Cell pellet was resuspended in 1X TBS buffer containing 0.1% BSA and were counted using the cell counter. 100 µL of 5×10^5 cells was counted per sample. As a negative control for lectin staining, Neuraminidase (catalog #: P0722L, NEB) sample (is not transfected with miRNA) was trypsin digested and control sample was prepared with Neuraminidase in HBSS: Gibco buffer (catalog #: P0720L, NEB) in 9:1 ratio and

incubated at 37℃ for 1 hour. 15 μg/ml of Cy5-diCBM40 in 1X TBS buffer was added onto each sample and incubated for 25 min at room temperature in dark. Cells were pelleted out by centrifugation at 350 × g for 6 min. Samples were washed with 1X TBS, 0.1%BSA for two times, and centrifuge at 350 × g, 5 min. Samples were resuspended in 400 µl FACS buffer (PBS, 0.1% BSA, 0.1% EDTA, 5 mM).

Cell surface CD98hc staining and analysis with flow cytometry: miRNA or anti-miR transfection to samples for Flow cytometry analysis is prepared with the same method as for Western blot analysis. Post 48 hours-transfection, samples were trypsin digested (100 µl of 0.25 % trypsin per well in 6-well plate format). Up to 1 mL of 1X HBSS was added to remove all the cells from the flask, and cells were pelleted out by centrifugation at 350 x g for 6 min. Cell pellet was resuspended in 1X TBS buffer containing 0.1% BSA and were counted using the cell counter. 100 µL of 5×10^5 cells was counted per sample. Samples were incubated with FITC labeled anti-CD98 antibody (ab26010, Abcam) in 1: 20 ratio. Mouse monoclonal IgG1 (ab91356, Abcam) was used as an isotype control with this antibody. Cells were pelleted out by centrifugation at 350 x g for 6 min. Samples were washed with 1X TBS, 0.1%BSA for two times, and centrifuge at 350 x g, 5 min. Samples were resuspended in 400 µl FACS buffer (PBS, 0.1% BSA, 0.1% EDTA, 5 mM). All samples were analyzed using Katz Fortessa flow cytometer (core facility, Faculty of Medicine and Dentistry, University of Alberta). Experiments are done in three biological replicates. The data was analyzed using FlowJo (10.5.3) software (BD Biosciences).

3.6.9 Multi-site mutagenesis on pFmiR-CD98hc, pFmiR-ST3GAL1, and pFmiR-ST3GAL2

The 3'UTR sequence of CD98hc, ST3GAL1, ST3GAL2 and the corresponding miRNA sequences (CD98hc: miRs: -1246, -30b-5p, -28-3p, -155-5p; ST3GAL1: miRa: -1246; ST3GAL2: miR-30b-5p) were analyzed with the RNAhybrid tool[142] which calculates a minimal free energy

hybridization of target RNA sequence and miRNA. The most stable predicted miRNA: mRNA interaction sites were selected for designing mutant pFmiR-sensors. Multiple mutation sites were designed, the mutant primers were designed using NEB Base Changer version 1 (https://nebasechangerv1.neb.com) and ordered for synthesis to Integrate DNA Technologies (IDT) which are listed in **Table 3.2**. Multiple mutation sites were achieved according to protocol for Site Directed Mutagenesis (SDM) using Q5® Site-Directed Mutagenesis kit (NEB, catalog #: E0554S). Amplicons were cleaned up using Monarch PCR & DNA cleanup kit (catalog #: T1030S, NEB). Sequences for the mutant pFmiR-ST3GAL1, pFmiR-ST3GAL2, pFmiR-CD98hc sensors were then verified by sequencing and used in the miRFluR assay as described previously. A minimum of 5-wells were transfected per sensor and the analysis was done in three biological experiments. Data was normalized to the NTC (CD98hc, ST3GAL1, ST3GAL2: miR-548ab) used with each sensor.

3.6.10 siRNA knockdown of target gene

ON-TARGETplus siRNA reagents against CD98hc (*slc3a2*), ST3GAL1, and ST3GAL2 in a smart pool format and ON-TARGETplus Non-Targeting Control Pool (NTP) were purchased from Dharmacon (Horizon Discovery, CA). MeWo (CD98hc, ST3GAL2) or HT-29 (ST3GAL1) cells were treated with siRNAs or NTP as described in Chapter 2. Blots were incubated with antibodies and processed as described before (**Appendix B**). The shRNA knock down of the three proteins against the corresponding antibodies were analyzed in previous study[159].

Table 3.2 Primer sequences for PCR amplification of WT 3'UTRs, RT-qPCR quantification of mRNAs, and PCR amplification of mutant 3'UTRs for CD98hc, ST3GAL1 and ST3GAL2.

Primer Name	Sequence (5' → 3')	Sample
a. PCR amplification of CD98hc, ST3GAL1 and ST3GAL2 3'UTRs		
CD98hc-FWD[a]	AGGTAGCTAGCCTTCAGCCTGACATGGAC	gDNA, MCF-7
CD98hc-REV[a]	AGGTAGGATCCTATGAGAGAAGCAGAGGGAA	gDNA, MCF-7
ST36GAL1-FWD	AGTCAACCGGTAGATGACGCAGTGAAGGG	gDNA, MCF-7
ST3GAL1-REV	AGTCACGTACGAACAATAAAATAGCTCTTTGTTTATTCAC	gDNA, MCF-7
ST3GAL2-FWD	AGTCAGCTAGCAAGTCTACCGGGGCAACTGAG	gDNA, MCF-7
ST3GAL2-REV	AGTCAGGATCCCATTATCAGTCACAGCTATCCTACC	gDNA, MCF-7
b. RT-qPCR[a] quantification of CD98hc, ST3GAL1, ST3GAL2 or GAPDH transcript		
ST3GAL1-FWD	TTGGAGGACGACACCTACCGAT	Total RNA, HT-29, SK-OV-3
ST3GAL1-REV	CACCACTCTGAACAGCTCCTTG	Total RNA, HT-29, SK-OV-3
ST3GAL2-FWD	TCCGACTGGTTTGACAGCCACT	Total RNA, A549, A375
ST3GAL2-REV	CTTCTCCAGCACCTCATTGGTG	Total RNA, A549, A375
CD98hc-FWD	CCCACTACCCTTCTCCTTTCCTT	Total RNA, 5B1, MCF-7
CD98hc-REV	GTTCACTCATAATCTGCAACAGTTTG	Total RNA, 5B1, MCF-7
GAPDH-FWD	GGTGTGAACCATGAGAAGTATGA	Total RNA, all cell lines
GAPDH-REV	GAGTCCTTCCACGATACCAAAG	Total RNA, all cell lines
c. PCR amplification of CD98hc, ST3GAL1 and ST3GAL2 mutant 3'UTRs		
155-5p-CD98hc-MUT-FWD	accagatcacTCCCTCTGCTTCTCTCATAC	pFmiR-CD98hc
155-5p-CD98hc-MUT-REV	acgtccccagACTTTTATTTGAAGGCAGAAAAC	pFmiR-CD98hc
28-3p-CD98hc-MUT-FWD	tggctagacaTTTTTCTCTTTTTTAAAAACAAACAAAC	pFmiR-CD98hc
28-3p-CD98hc-MUT-REV	ttcggggaccgAAGGAAAGGAGAAGGGTAG	pFmiR-CD98hc
30b-5p-CD98hc-MUT-FWD	cccaaaatcccacaaatCTGCCTTCAAATAAAAGTCAC	pFmiR-CD98hc
30b-5p-CD98hc-MUT-REV	ggttgtgagttaatctgCAACAGTTTGTTTGTTTGTTTTTAAAAAAG	pFmiR-CD98hc
1246-CD98hc-MUT-FWD	tcttcagatCCCTCTGCTTCTCTCATAC	pFmiR-CD98hc
1246-CD98hc-MUT-REV	ccatcgtccgGTGACTTTTATTTGAAGGCAG	pFmiR-CD98hc
1246-ST3GAL1-MUT-FWD	ttttttaggtCCAAAACTTTAAAGACTTTTCTTTTTTC	pFmiR-ST3GAL1
1246-ST3GAL1-MUT-REV	gcactttgtcctTTTCGGTTTGTTTAACAC	pFmiR-ST3GAL1
30b-5p-ST3GAL2-MUT-FWD	cctacgcacgccCCCCAGGGCTTCCTGCGT	pFmiR-ST3GAL2
30b-5p-ST3GAL2-MUT-REV	gtgtgggggcgggAGGTGGGACTGGGGGTCC	pFmiR-ST3GAL2

[a] FWD, forward; REV, reverse; RT-qPCR, Reverse transcription quantitative polymerase chain reaction.

Chapter 4

miRNA Regulate Ganglioside Biosynthetic Enzyme, ST3GAL5, Expression and Cellular GM3 Content

4.1 Acknowledgment

I would like to warmly appreciate my colleague, Tigist Batu, for performing RT-qPCR experiments. Also, I would like to deeply appreciate my undergraduate student, Joseph Reyes, for his contributions in performing Western blot experiments and mutational analysis.

4.2 Introduction

Gangliosides are sialic acid-containing glycosphingolipids[6]. Human cells express more than 20 sialyltransferases which transfer sialic acid onto glycolipids or glycoproteins[15]. α-2,3-sialyltransferases (ST3GAL) are a subfamily with 6 enzymes. The extent to which each ST3GAL sialylates glycolipid moiety has yet to be well characterized, for instance, ST3GAL1 sialylates glycoconjugates linked to both lipids and proteins, whereas ST3GAL5 drives sialylation onto lactosylceramide on lipids only[6,207]. Among ganglioside-modifying enzymes, ST3GAL5, also known as GM3 synthase (CMP-*N*-acetylneuraminate: lactosylceramide-α-2,3-*N*-acetylneuraminyltransferase, GM3S), initiates the first step in the biosynthesis of gangliosides by catalyzing the transfer of a sialic acid residue from CMP-sialic acid onto lactosylceramide to form GM3 ganglioside. GM3, a trisaccharide molecule composed of glucose, galactose, and sialic acid, serves as a precursor for other glycosyltransferases which expand the glycan chains, resulting in gangliosides of the a-, b-, and c-series[208] (**Figures 4.1, 4.2**).

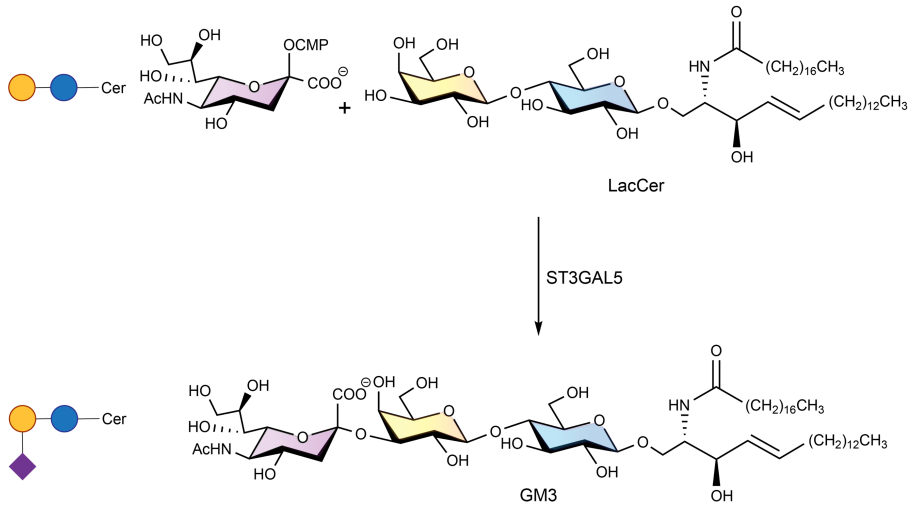

Figure 4.1 GM3 synthesis by ST3GAL5. ST3GAL5 catalyzes the addition of Neu5Ac to lactosylceramide to make GM3 ganglioside via α-2,6-sialic acid linkage.

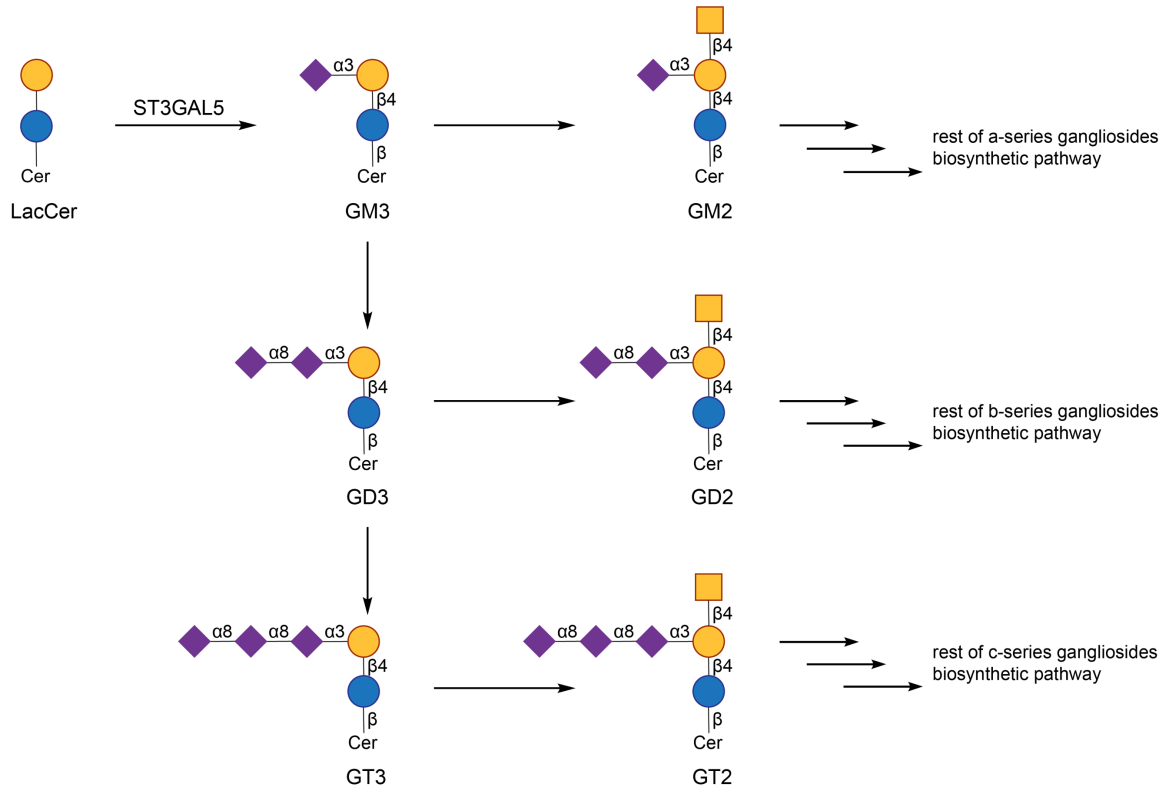

Figure 4.2 ST3GAL5 initiates the biosynthetic pathway of a-, b-, and c-series gangliosides.

ST3GAL5 is known to be associated with metabolic and neurologic disorders. To date, different reports have identified a nonsense mutation in *st3gal5* gene (on chromosome 2p11.2) originally in an Amish family[209] and recently found in children from healthy consanguineous French parents[210], and is called GM3 synthase deficiency (GM3SD). This rare congenital disorder of glycosylation leads to developmental delay, blindness, deafness, and mitochondrial dysfunction [207,211]. In addition, mice lacking *st3gal5*, which is impaired in making GM3, have an increased sensitivity to insulin, reporting GM3 as a negative regulator of insulin receptor signaling[212]. Moreover, the biological function of GM3 ganglioside and its corresponding enzyme, ST3GAL5, have been reported in different cancer types including breast[95], lung[213-215], melanoma[216,217], and bladder[218,219].

microRNA, as an interacting partner of a target transcript, can affect the corresponding protein expression patterns, and consequently, the protein functional outcome in human cells[95,111]. Although it is intriguingly clear that changes in the levels of ST3GAL5 and/ or its resulting catalytic activity, GM3, is associated with different disease states[207,211,212,216,220,221], the post-transcriptional miRNA regulation of ST3GAL5 is poorly studied. In 2014, work from the Mahal laboratory identified a suppressive role for the miR-200 family in tuning the expression of ST3GAL5[95]. Given the recently introduced miRFluR assay, which enables us to study miRNA gene regulation in a high-throughput format[78,130], we decide to expand our current knowledge of ST3GAL5 miRNA regulation via screening the human miRNA interactome for ST3GAL5. The miRFluR assay reveals that ST3GAL5 expression is evenly down- and up-regulated by miRNAs. Further analysis verified that the cellular GM3 content, the product of ST3GAL5, can be regulated by miRNA targeting the ST3GAL5 3'UTR. Taken together, this study uncovers new insights into GM3 synthase regulation by miRNA.

4.3 Results

4.3.1 Comprehensive profiling of miRNA regulatory landscape of ST3GAL5

The most prevalent 3'UTR (995 bp) of ST3GAL5 was cloned downstream of Cerulean reporter protein within the pFmiR plasmid to create pFmiR-ST3GAL5 (**Appendix A**). After analysis with miRFluR assay, 1392 miRNA passed the QC (described in Chapter 2). The data was normalized and a z-score threshold of ±1.965 was applied. I identified 77 miR hits for ST3GAL5 using a z-score cut-off corresponding to the 95% confidence intervals, which contains 31 downregulatory miRNAs (or down-miRs) and 46 upregulatory miRNAs (or up-miRs) (**Figure 4.3**). Of note, our previosuely validated miR hit, down-miR-200b-3p[95], was identified in this

analysis, showing the accuracy of miRFluR assay in identifying the correct miRNA hits for a target gene.

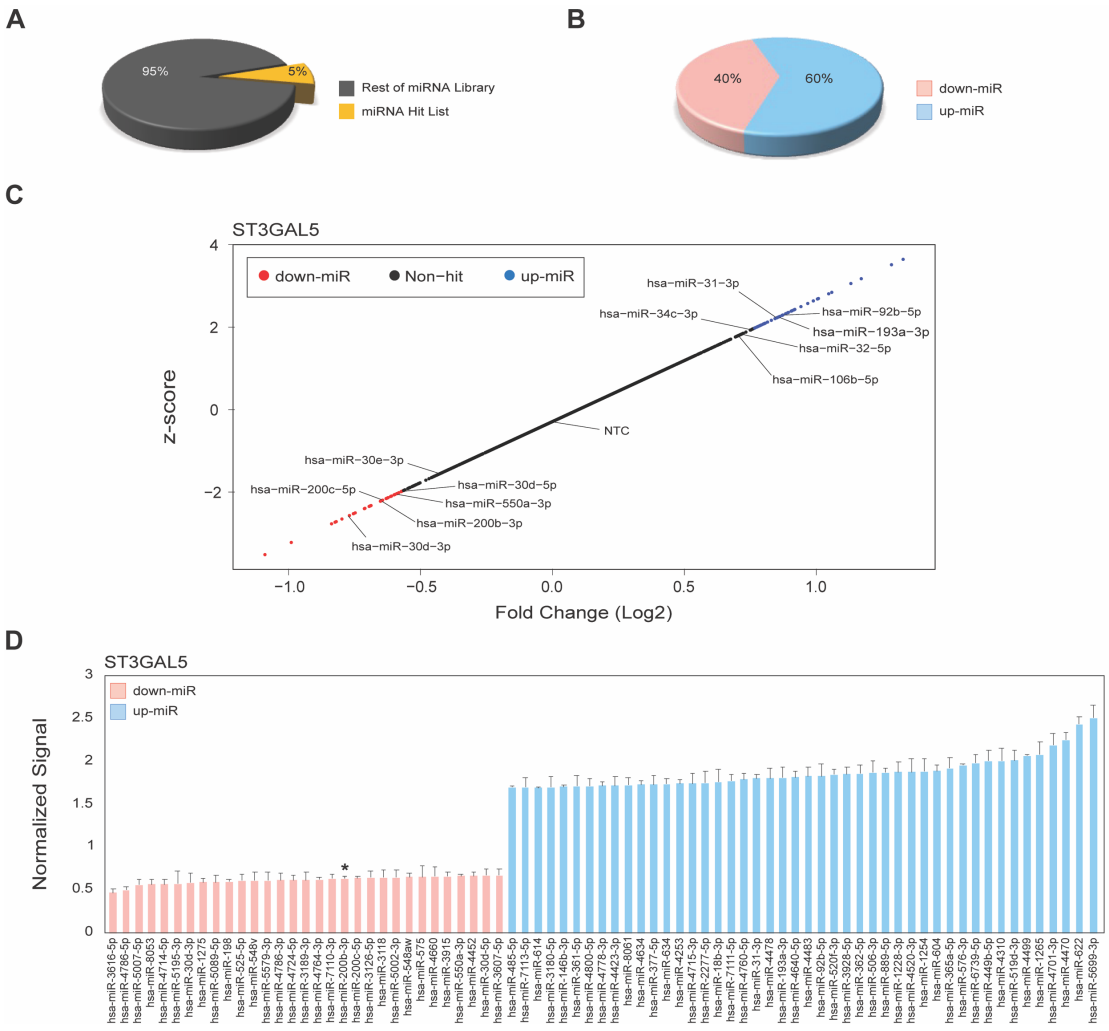

Figure 4.3 ST3GAL5 miRFluR result. (A). Pie chart shows ST3GAL5 miRNA hit list containing 5% of the rest of the miRNA library which passed QC. (B). Pie chart indicates the percentage of down-miR (31 miR hits) and up-miR (46 miR hits) in ST3GAL5 miRNA hit list. (C). Scatter plot indicates post-QC miRNA for ST3GAL5; miRNA in the 95% confidence interval is colored (down-miRs: red, up-miRs: blue) and the tested miRNAs are labelled. (D). Bar chart represents miRNA hit list for ST3GAL5 within 95% confidence interval (* is a known positive control miR-200b-3p for ST3GAL5[95]).

4.3.2 miRNA tune ST3GAL5 expression in two directions: inhibition and upregulation

Non-small lung cancer cell line (NSLC, A549) treatment with TGF-β indicated a fibroblastic appearance and increased migratory capability of cells, and was found to increase ST3GAL5 expression, indicating a promigratory role of this protein in EMT process[95,222]. In this

context, miR-200b-3p was shown to impede EMT by directly targeting ST3GAL5 expression. This work indicates the important role of microRNA in the post-transcriptional regulation of ST3GAL5, and tuning the downstream EMT process[9]. In this Chapter, I tested a select subset of miRNAs (down-miRs: -200c-5p, -550a-3p, 30d-3p, 30d-5p, 30e-3p; up-miRs: -34c-3p, -32-5p, -31-3p, -106b-5p, -193a-3p, -92b-5p) and non-targeting control (NTC, NTC1) in the MDA-MB-231 breast cancer line (**Figure 4.4A-C**), A549 lung cancer line (**Figure 4.4D-F**), and MeWo melanoma cancer line (**Figure 4.4G-I**), where ST3GAL5 expression level is found to be functionally important[214-217]. These miRNAs were chosen due to their biological functions in cancer biology[223-225]. Of note, I used miR-200b-3p as known positive control[9] in Western blot analysis. The Western blot analysis confirms my miRFluR results: down-miRs all inhibit ST3GAL5 expression, and overall, up-miRs upregulate ST3GAL5 protein in all three cell lines. While all down-miRs down-regulate ST3GAL5 expression, I observed more cell line dependency of ST3GAL5 regulation by up-miRs. This cell line dependency is prevalently observed in miRNA-mediated gene regulation which may result from cell-specific miRNA expression and action[226], or other regulatory elements such as RBPs counteracting with miRNA function[149].

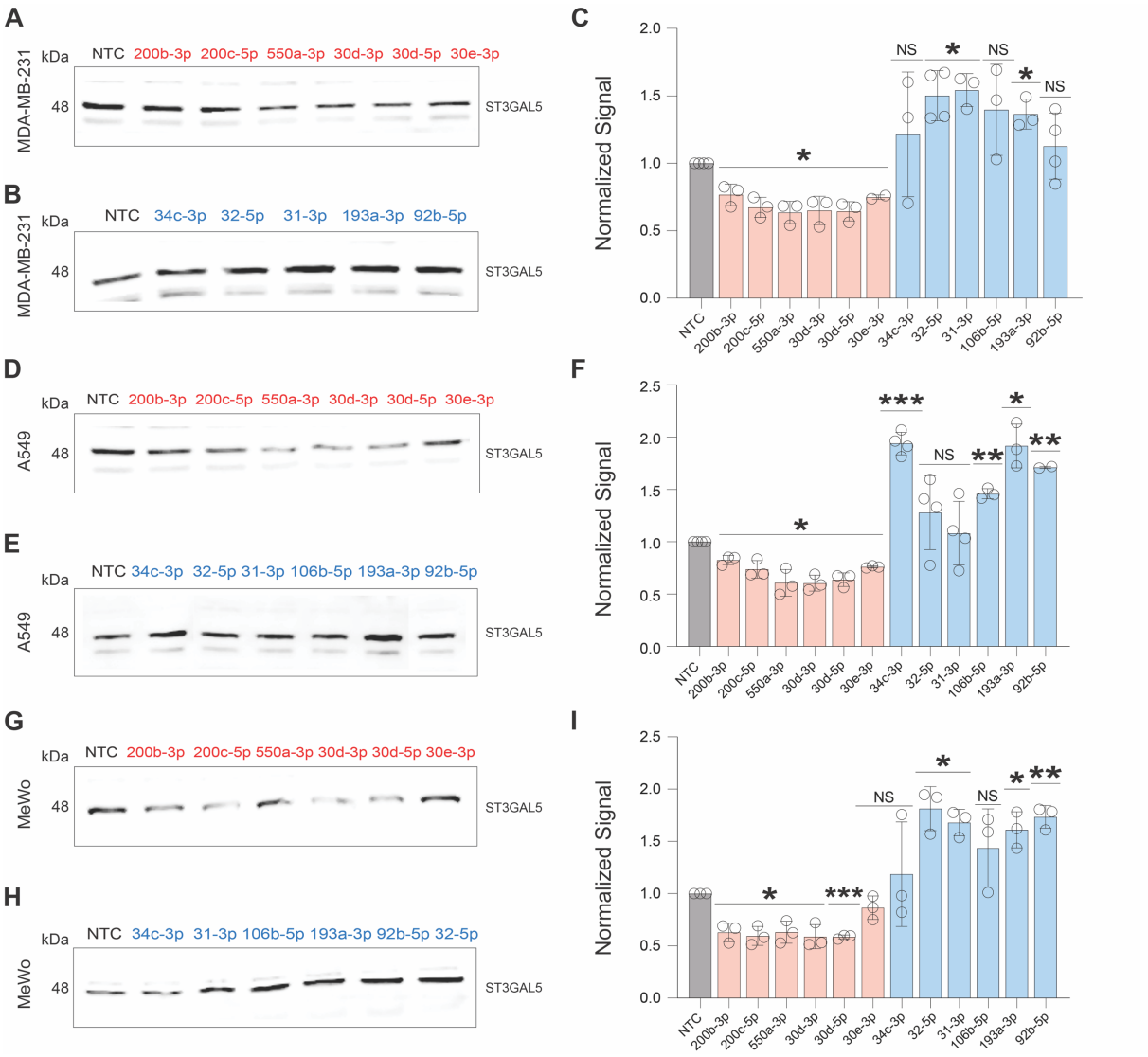

Figure 4.4 miRNA regulation of ST3GAL5 expression in MDA-MB-231, A549, and MeWo cancer cell lines. (A&B, D&E, G&H). Representative Western blots of miRNA-mediated ST3GAL5 expression in MDA-mB-231 (A&B), A549 (D&E), and MeWo (G&H) cells. miRNA mimics (down-miRs: -200b-3p, -200c-5p, -550a-3p, -30d-3p, -30d-5p, -30e-3p; up-miRs: -34c-3p, -32-5p, -31-3p, -106b-5p, -193a-3p, -92b-5p) were transfected into the cells. Western blot analysis was conducted 48 hours post transfection. (C, F, I). Bar charts show three independent biological replicates of Western blot analysis in MDA-MB-231 (C), A549 (F), and MeWo (I). All Western blot samples are normalized over total protein stained with ponceau and NTC. All experiments were performed in biological triplicate. Errors shown are standard

deviations. For Western blot analysis, One sample *t*-test was used to compare miRs to NTC (ns not significant, * $p < 0.05$, ** < 0.01, *** < 0.001).

4.3.3 miRNA regulation of st3gal5 transcript does not always correlates with protein

The miRNA-mediated regulation of *st3gal5* transcript was tested using RT-qPCR quantification analysis in three different cancer cell lines: MDA-MB-231 (**Figure 4.5A**), A549 (**Figure 4.5B**), and MeWo (**Figure 4.5C**). The result shows discrepancies between miRNA-mediated regulation of ST3GAL5 protein and mRNA expression. It is worth noting that although the central dogma tightly binds DNA, RNA, and protein molecules in a sequential manner, the concentration of mRNA and its translation product (protein) are not necessarily aligned with each other. While transcription levels contribute to the protein expression levels, multiple other biological processes involve regulatory molecules including microRNAs that may impact them[227,228].

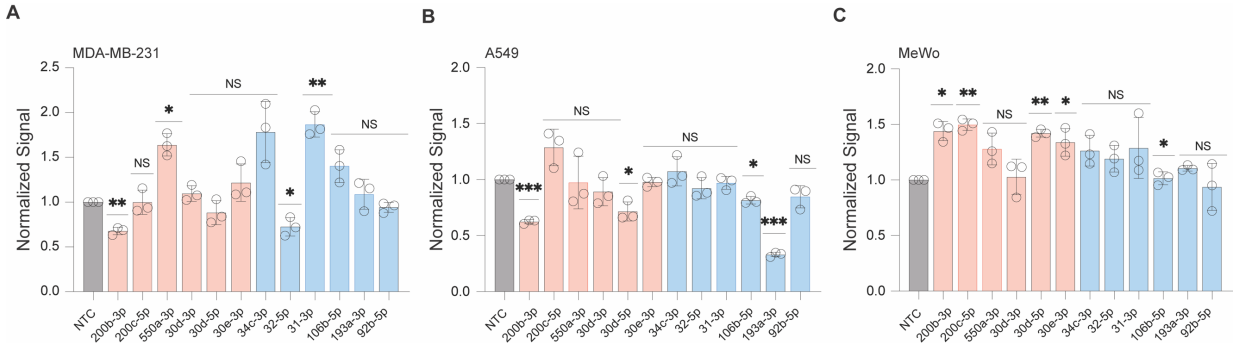

Figure 4.5 RT-qPCR analysis of miRNA-mediated *st3gal5* transcript regulation in cancer cell lines. miRNA mimics (down-miRs: -200b-3p, -200c-5p, -550a-3p, -30d-3p, -30d-5p, -30e-3p; up-miRs: -34c-3p, -32-5p, -31-3p, -106b-5p, -193a-3p, -92b-5p) were transfected to cells. (A-C). Bar charts show RT-qPCR analysis of miRNA-transfected samples in MDA-MB-231 (A), A549 (B), and MeWo (C) cell lines. All RT-qPCR samples were normalized over GAPDH and NTC. All experiments were performed in biological

triplicate. Errors shown are standard deviations. For RT-qPCR analysis, One sample *t*-test was used to compare miRs to NTC (ns not significant, * $p < 0.05$, ** < 0.01, *** < 0.001).

4.3.4 miRNA inhibitors halt endogenous miRNA from controlling ST3GAL5 expression

To corroborate that miRNA mimics reflect the corresponding endogenous miRNA function, I used miRNA Hairpin Inhibitors (or anti-miRs) against select endogenous up-miRs: -32-5p, -31-3p, -193a-3p, and down-miRs: -30d-3p, -30d-5p. The key criteria for an anti-miR to function is a high expression level of the endogenous miRNA in the target cell line. All microRNA selected were highly expressed in MDA-MB-231 cell line[229]. I observed impacts on ST3GAL5 expression upon cell transfection with anti-miRs that corresponds with endogenous activity (**Figure 4.6**).

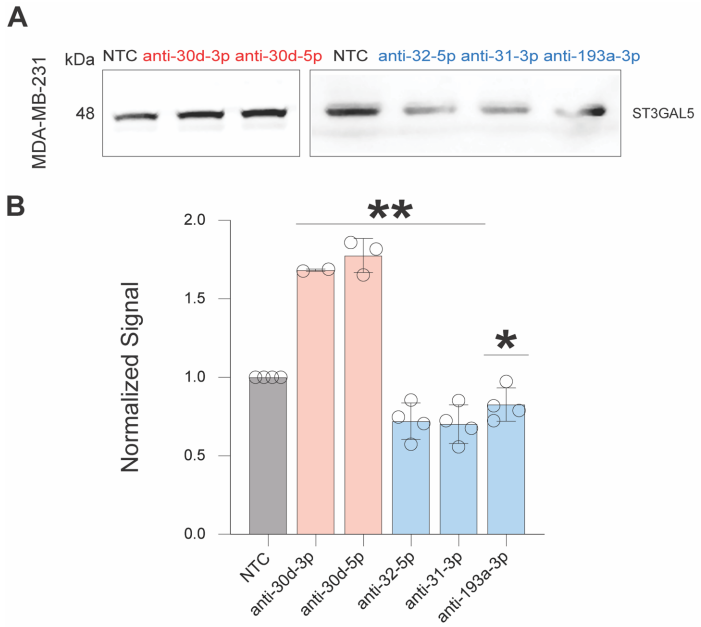

Figure 4.6 Endogenous miRNA inhibition. (A). Representative Western blots of anti-up-miRs (anti-32-5p, anti-31-3p, anti-193a-3p) and anti-down-miRs (anti-30d-3p, anti-30d-5p) in MDA-MB-231 cells. (B). Bar chart shows three independent biological replicates of Western blot analysis shown in (A). All Western blot samples are normalized over total protein stained with ponceau and NTC. The experiment was performed in biological triplicate. Errors shown are standard deviations. For Western blot analysis, One sample *t*-test was used to compare miRs to NTC (* $p < 0.05$, ** < 0.01).

4.3.5 miRNA regulate GM3 epitope via mediating GM3 synthase (ST3GAL5) expression

To assess whether miRNA regulating ST3GAL5 influence GM3 content via ST3GAL5 activity, I tested a subset of miRNAs: down-miRs: -30e-3p, -30d-3p, -30d-5p; up-miRs: -34c-3p, -31-3p, -106b-5p, and two non-targeting controls: NTC1 (used in Western blot and RT-qPCR

experiments as NTC) and NTC2 in MDA-MB-231 and A549 cell lines (**Figure 4.7**). Of note, NTC2 was used as an additional control for NTC1 to confirm that NTC1 does not have synergistic effects on GM3 epitope expression via potentially targeting other glycogenes which may impact GM3 levels. The flow cytometry result showed the same FITC intensities for NTC1 and NTC2, verifying NTC1 as an appropriate control. The cell surface GM3 epitope was stained with FITC-conjugated anti-GM3 antibody and quantified using flow cytometry approach. miR-200b-3p was used as the positive control in the flow cytometry assay, showing 87% and 50% decrease in FITC signal in MDA-MB-231 and A549 cells, respectively.

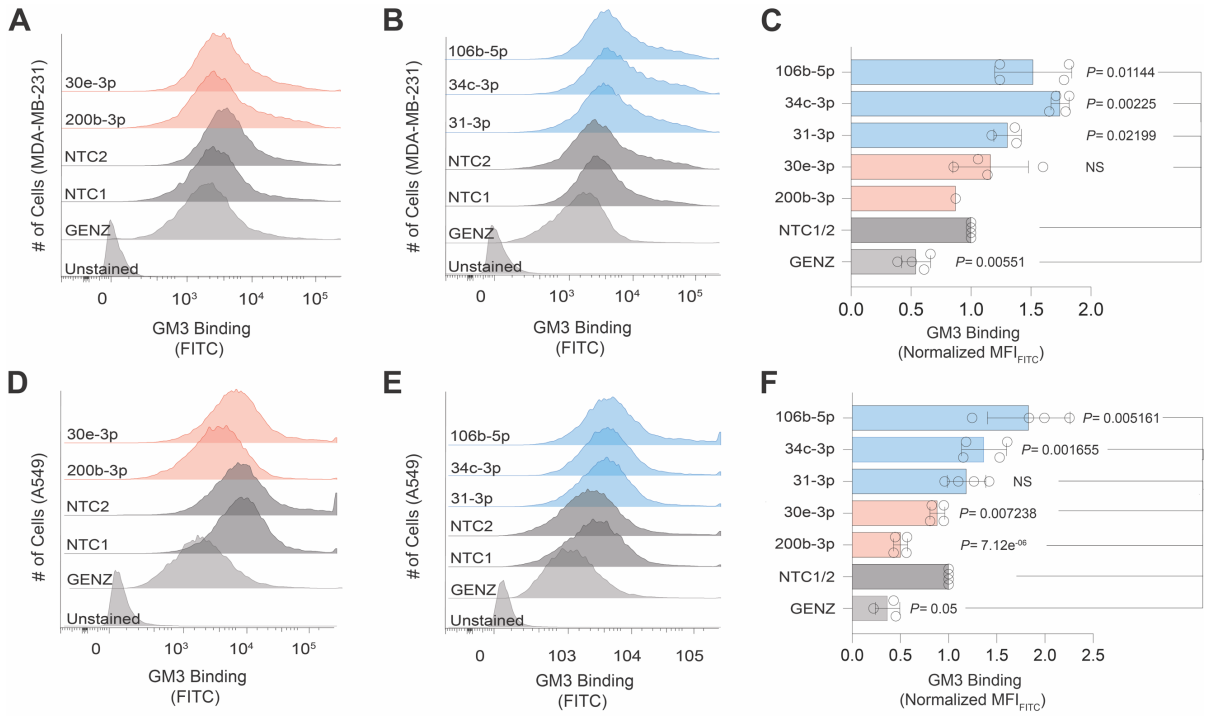

Figure 4.7 miRNA modulation of ST3GAL5 affects GM3 levels in MDA-MB-231 and A549 cell lines. (A&B; D&E). Representative flow cytometry histograms and quantification of GM3 binding in MDA-MB-231 (A&B), A549 (D&E). Cells were transfected with miRNA mimics (down-miRs: -200b-3p, -30e-3p; up-miRs: -34c-3p, -31-3p, -106b-5p) and NTCs (NTC1 and NTC2) for 48 hours. (C&F). Bar graphs show data from replicates shown in (A&B) and (D&E). All samples are normalized over NTC1/2 (average MFI of NTC1 and NTC2). The experiment was performed in biological triplicate. Errors shown are standard

deviations. For Flow cytometry analysis standard *t*-test was used to compare miRs to NTC1/2 (ns not significant).

As a negative control, I used glucosylceramide synthase inhibitor (GENZ) which blocks ganglioside biosynthesis pathway by inhibiting glucosylceramide synthase. Cells treated with GENZ resulted in 50% and 20% reduction in FITC intensity in MDA-MB-231 and A549 cell lines, respectively. The observed GM3 downregulation by the controls (positive control: miR-200b-3p; negative control: GENZ) were stronger in A549 cells than MDA-MB-231 cells. Among down-regulatory miRs identified in this Chapter, only miR-30e-3p was found to downregulate GM3 levels in A549 cell line, whereas other down-miRs do not have impact in either cell lines (**Figure 4.7A, D**). This may be because the cellular GM3 contents can be modulated by other pathways including the ganglioside biosynthetic pathway, wherein cells may preferably express other gangliosides expanded from GM3 precursor (e.g., GM2, GD2). Intriguingly, GM3 epitope is upregulated by the up-miRs: -34c-3p, -31-3p, -106b-5p in both MDA-MB-231 (**Figure 4.7B**) and A549 (**Figure 4.7E**) cells. Overall, this result indicates miRNA-mediated ST3GAL5 regulation can affect cell surface GM3 epitope (**Figure 4.7C, F**).

4.3.6 microRNA impact ST3GAL5 expression via direct interaction with its 3'UTR

Using prediction tools, I identified the predicted binding site for two up-miRs (miR-31-3p, -106b-5p) using RNAhybrid[142], and two down-miRs (miR-30d-3p, -30e-3p) using Targetscan[74] (**Figure 4.8**). In line with Chapter 2[130], the upregulatory miRNA are predicted to bind via non-canonical sites in accordance with RNAhybrid, whereas the predicted down-miR sites by Targetscan are via an 7mer-m8 seed binding pattern[74]. I mutated the predicted miRNA binding sites on 3'UTR within the pFmiR-ST3GAL5 sensor for up- and down-miRs individually. In line with Chapter 2[130], testing the up-miRs WT and mutant sensors via miRFluR assay reveals the accuracy of RNAhybrid in predicting upregulatory miRNA binding sites by abolishing

upregulation upon mutation. Comparing tested WT and mutant sensors for down-miRs also verified the predicted sites for down-miRs binding on ST3GAL5 3'UTR.

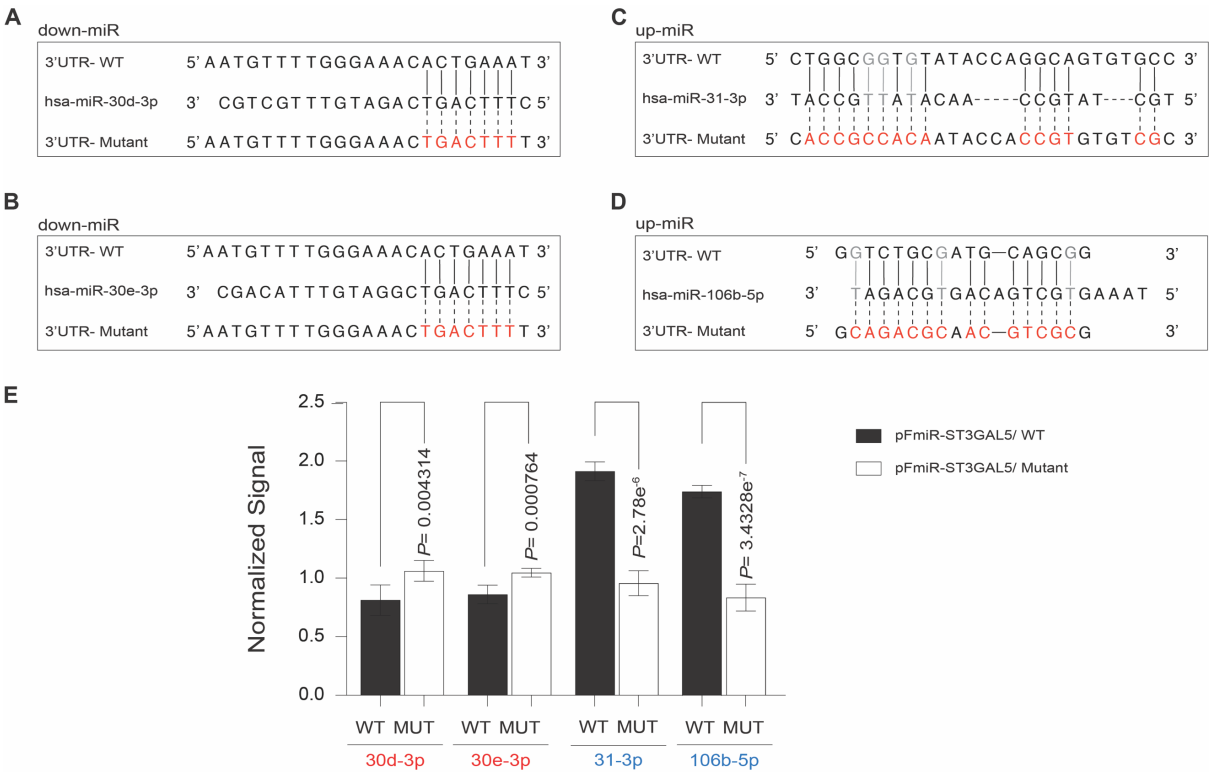

Figure 4.8 miRNA tune ST3GAL5 expression via direct interaction with its 3'UTR. (A-D) Alignment of down-miRs (A: miR-30d-3p; B: miR-30e-3p) and up-miRs (C: miR-31-3p; D: miR-106b-5p) predicted ST3GAL5-3′UTR sites and their corresponding mutants. Mutated residues are shown in red. Wobble interactions are shown in grey. E. Bar graph of data from miRFluR sensors. For each sensor, data was normalized over NTC. A standard *t*-test was used for comparisons. All experiments were performed in biological triplicate, a representative experiment with n = 5 wells is shown.

4.4 Discussion

ST3GAL5 is the enzyme initiating the biosynthesis of the a- , b-, and c-series gangliosides containing epitopes with roles at the crossroad of cancer biology and immunology (e.g., GM2[230,231], GD2[57,232]), as well as those that are mainly associated with other types of disorders including diabetes (e.g., GM3[212,233]) and Alzheimer (e.g., GM1[234,235]). Given that, ST3GAL5 is

one of the key gene whose expression can affect the ganglioside biosynthetic pathway[207,236](**Figure 4.2**).

In this Chapter, the screening of the human miRNAome identified multiple members of the miR-30 family: miRs-30e-3p, -30d-3p, -30d-5p regulating ST3GAL5 expression. The miR-30 family contains five members and six distinct mature miRNAs (miR-30a-3p, -30b-5p, -30c-1, -30c-2, -30d-3p, -30e-3p)[237]. Apart from that, miRNAs are also identified to upregulate ST3GAL5 expression. The miRNA: 3'UTR direct interactions for two down-miRs: -30d-3p and -30e-3p were validated to occur through a shared 7mer-m8 seed binding pattern[74]. Whereas, the upregulatory validated sites for miR-31-3p and miR-106b-5p predicted by RNAhybrid[142] are via non-canonical binding patterns, and do not follow the seed binding rules. This contradicts with the current assumptions, in that miRNA: mRNA direct interaction is primarily mediated by the seed region pairing (nucleotides 2–8 in the 5'-end of miRNA, Section 1.3.2)[74].

High expression levels of different members of the miR-30 family have shown to be associated with the inhibition of tumor growth[238], improved survival rate[225]. This study may suggest another orchestrated regulatory network by cognate miRNA: ST3GAL5 3'UTR (most interestingly, miR-30e-3p, miR-30d-3p, and miR-30d-5p) in pathological states. In addition, the up-miR-106b-5p is highly expressed in breast cancer in comparison with normal tissues and is associated with breast cancer progression[223], promoting migration, invasion, proliferation[239], and poor prognosis in breast cancer patients[240]. Also, miR-106b-5p plays an oncogenic role in lung cancer by promoting cell proliferation and impeding apoptosis[224]. Using the flow cytometry approach, I showed that miRNAs targeting ST3GAL5 can influence the cellular content of ganglioside GM3. The upregulation of ganglioside GM3 has been shown to promote the dimerization and activation of TGF-β receptors, and is positively regulated with cell migration and

EMT-related signaling in TGF-β1-induced lens epithelial cells[241]. Other functional associations of GM3 epitope in signaling pathways are coupled with PI3K/Akt/mTOR pathway (melanoma[216]), the inhibition of epidermal growth factor (EGF) phosphorylation[221,242] (lung cancer[214], bladder cancer[219], epidermoid carcinoma[220]). Given the established roles of other ganglioside epitopes (such as GM2, GD2), which are expanded from GM3 (ST3GAL5 product), in cancer biology[57,230-232], it could be also interesting to explore that to what extent ganglioside pathway regulation is mediated by microRNA via tuning ST3GAL5 expression.

4.5 Conclusion

In 2014, the Mahal laboratory identified ST3GAL5 incorporation to TGF-β–induced EMT process which is post-transcriptionally regulated by miR-200 family[95]. Given the significant roles of ST3GAL5 and resulting gangliosides in various pathological states[57,211,221,231,233], I aimed to study the ST3GAL5 expression regulation by microRNA. Using the high-throughput miRFluR assay[78], I comprehensively mapped the miRNA regulatory landscape of ST3GAL5, identifying two distinct categories of miRNA hits: downregulation and upregulation of ST3GAL5 expression. The examination of the select subset of ST3GAL5 miR hits across different cancer cell lines confirms the bidirectional tuning of the enzyme expression, some of which are verified to occur via direct miRNA: 3'UTR interactions.

Together, this Chapter presents the first comprehensive analysis of miRNA regulation of ST3GAL5 as the key enzyme in the ganglioside pathway. Identifying ST3GAL5 miRNA hit list (contains 5% of whole human miRNAome) opens new avenues to study the regulation of ST3GAL5 expression and potentially ganglioside epitopes in normal physiology and disease states.

4.6 Experimental methods

4.6.1 Cloning

ST3GAL5 3'UTR was amplified via PCR from genomic DNA (gDNA, 10 μg, from MCF-7 cell line) using the primers shown in Table 4.1. The amplicons were cleaned up using a Monarch® PCR & DNA cleanup kit (catalog #: T1030S, NEB). The 3'UTR fragment was then into the cloned restriction sites (AgeI and BsiWI) downstream of Cerulean in the pFmiR-empty backbone[78] using standard ligation protocols (NEB). Plasmid was verified by Sanger sequencing (Molecular Biology Services Unit, University of Alberta). Large-scale endotoxin free DNA preparations were made for sequence-verified construct (pFmiR-ST3GAL5) using Endotoxin-free plasmid DNA purification (Takara Bio USA, Inc., catalog #: 740548). Plasmid map for pFmiR-ST3GAL5 and its 3'UTR sequence can be found in **Appendix A**.

4.6.2 Cell lines

All cell lines (HEK-293T, MDA-MB-231, A549) were purchased directly from the American Type Culture Collection (ATCC). MeWo cell line was a gift from the Hernando laboratory. All cells were cultured using suggested media (HEK-293T & MDA-MB-231: Dulbecco's Modified Eagle Medium (DMEM), 10% FBS; A549: FK-12, 10% FBS; MeWo: DMEM* (catalog # 30-2002), 10% FBS under standard conditions (5% CO_2, 37°C).

4.6.3 miRFluR high-throughput assay

The Human miRIDIAN miRNA mimic Library 21.0 (Dharmacon) was resuspended in ultrapure nuclease-free water (REF#: 10977-015, Invitrogen) and aliquoted into black 384-well, clear optical bottom tissue-culture treated plates (Nunc). Each plate contained three replicate wells of each miRNA in that plate (2 pmol/well). In addition, each plate contained a minimum of 6 wells containing non-targeting controls (NTC). To each well was added target pFmiR plasmid (pFmiR-

ST3GAL5: 30 ng) in 5 µl Opti-MEM (Gibco) and 5 µl of transfection solution (0.1 µl Lipofectamine™ 2000 (catalog #: 11668500, Life Technologies) diluted to 5 µl total volume with Opti-MEM (Gibco), premixed 5 min at room temperature). The mixture was allowed to incubate at room temperature in the plate for 20 min. HEK293T cells (25 µl per well, 400 cells/ µl in phenol red free DMEM supplemented with 10% FBS and Pen/Strep) were then added to the plate. Plates were incubated at 37°C, 5% CO_2. After 48 hours, the fluorescence signals of Cerulean (excitation: 433 nm; emission: 475 nm) and mCherry (excitation: 587 nm; emission: 610 nm) were measured using the clear bottom read option (SYNERGY H1, BioTek, Gen 5 software, version 3.08.01).

4.6.4 Data analysis

I calculated the ratio of Cerulean fluorescence over mCherry fluorescence (Cer/mCh) for each well in each plate. For each miRNA, triplicate values of the ratios were averaged, and the standard deviation (S.D.) obtained. I calculated % error of measurement for each miRNA (100 × S.D./mean). As a quality control measurement (QC), any plates or miRNAs that had high errors in the measurement (median error ±2S.D. across all plates) and/or a high median error of measurement for the plate (>15%) were removed. After QC, 1392 miRNAs were obtained for ST3GAL5 out of 2601 total miRNAs screened for its 3'UTR. The Cer/mCh ratio for each miRNA was then normalized to the non-targeting control miRNA mimic (NTC1) per plate and error was propagated. Data from all plates were then combined and log-transformed z-scores calculated. A z-score of ±1.965, corresponding to a two-tailed *p*-value of 0.05, was used as a threshold for significance. Post-analysis, I identified 77 miRNA hits for ST3GAL5 within 95% confidence interval (**Figure 4.3D and Dataset 4.1 (.xls sheet)**).

4.6.5 Western blot analysis

Western blot analysis was conducted for ST3GAL5 in three cell lines: MDA-MB-231, A549, and MeWo cell lines (down-miRs: miR-200b-3p, miR-200c-5p, miR-550a-3p, miR-30d-3p, miR-30d-5p, miR-30e-3p; up-miRs: miR-34c-3p, miR-31-3p, miR-32-5p, miR-106b-5p, miR-193a-3p, miR-92b-5p). For Western blot analysis, non-targeting control miRNA mimic (NTC1) is used as a control. For all experiments, cells were seeded in six-well plates (50,000 cells/well) and cultured for 24 h in appropriate media. Cells were then washed with Hanks buffered salt solution (HBSS, Gibco) and transfected with miRNA mimics (50 nM mimic, Dharmacon, Horizon Discovery, 5 µl Lipofectamine 2000, Life Technologies in 250 µl OptiMEM). The media was changed to standard media 12 h post-transfection. Cells were then lysed at 48 h post-transfection in cold RIPA lysis buffer supplemented with protease inhibitors (Thermofisher, catalog #: 89900). For Western blot analysis, 30 µg of protein was added to 4X loading buffer with DTT (1 mM), heated at 95°C for 10 min and run on a 10% gel (SDS-PAGE) using standard conditions. Proteins were then transferred from the gel to Polyvinylidene fluoride membrane using iBlot2 Transfer Stacks (PVDF, Invitrogen, catalog number: IB24002) and the iBlot2 transfer device (Invitrogen) using the standard protocol (P_0). Blots were incubated with Ponceau S Solution (Boston BioProducts, catalog # ST-180) for 3 min and the total protein levels were imaged using the protein gel mode (Azure 600, Azure Biosystems Inc.). Blots were blocked with blocking buffer prepared with 5% non-fat dry milk in TBST buffer (TBS buffer plus 0.1% Tween 20), for 30 min at 60 rpm on rocker (LSE platform rocker, Corning) at room temperature. Next, blots were incubated with rabbit polyclonal α-human-ST3GAL5 1° antibody (1:1000 in TBST with 10% blocking buffer, catalog #: ab155671, Abcam). After an overnight incubation at 4°C, blots were washed 1 × rinse and 2 × 50 seconds (sec) wash with 0.1% TBST buffer. A secondary antibody was then added (α-

rabbit IgG-HRP, 1: 6000 in TBST with 10% BSA and incubated for 1 h at room temperature with shaking (60 rpm). Blots were then washed 3 × 45 sec. with 0.1% TBST buffer. Blots were developed using Clarity and Clarity Max Western ECL substrates according to the manufacturer's instructions (Bio-Rad). Membranes were imaged in chemiluminescent mode (Azure 600, Azure Biosystems Inc.). All analysis was done in biological triplicates.

4.6.6 Endogenous miRNA activity validation

miRIDIAN microRNA Hairpin Inhibitors (anti-down-miR: anti-30d-3p, anti-30d-5p: anti-up-miRs: anti-31-3p, anti-32-5p, anti-193a-3p, anti-106b-5p) and miRIDIAN microRNA Hairpin Inhibitor Negative Control (NTC) were purchased from Dharmacon (Horizon Discovery, Cambridge, UK). The selected anti-miRs for ST3GAL5 were tested in MDA-MB-231 cell line. Cells were seeded and incubated as described for Western blot analysis. Cells were transfected with anti-miRNAs (50 nM) using Lipofectamine™ 2000 transfection reagent in OptiMEM following the manufacturer's instructions (Life Technologies). After 12 h media was changed to standard culture media. 48 h post-transfection cells were lysed and analyzed for ST3GAL5 protein levels as previously described. All analysis was done in biological triplicates.

4.6.7 Flow cytometry: GM3 epitope staining

Cells for flow cytometry analysis were transfected with miRNA mimic as previously described. In flow cytometry, I used NTC1 and NTC2 as non-targeting controls. After 48 hours of transfection, samples were trypsin digested (80 µl of 0.25% trypsin per well in 6-well plate format). Up to 1 mL of 1X HBSS was added to remove all the cells from the flask, and cells were pelleted out by centrifugation at 350 × g for 6 min. The cell pellet was resuspended in 1X TBS buffer containing 0.1% BSA and counted using the cell counter. 100 µL of 5×10^5 cells was counted per sample. As a negative control for GM3 epitope staining, I used GENZ in 1:1000 dilution to achieve

a final concentration of 5 μM (catalog #: HY-12744A, Cedarlane). Samples were incubated with anti-GM3 monoclonal antibody 1:20 ratio (Fisher scientific, catalog #: A2582VIAL) in 1X TBS buffer on ice for 25 min in dark. Cells were pelleted out by centrifugation at 350 × g for 5 min. Samples were then resuspended with 100 μL of 1X TBS buffer containing 0.1% BSA and 1:50 ratio of FITC-conjugated Goat anti-Mouse IgM secondary antibody (Thermofisher, REF # 31992) was added to each sample and incubated on ice for 30 min in the dark. Cells were pelleted (350 × g for 5 min) and then resuspended in 400 μl FACS buffer (PBS, 0.1% BSA, 0.1% EDTA, 5 mM).

All samples were analyzed using Fortessa X-20 flow cytometer (Core Facility, Faculty of Medicine and Dentistry, University of Alberta). Experiments are done in a minimum of three biological replicates. Data was analyzed using FlowJo (10.5.3) software (BD Biosciences).

4.6.8 Multi-sites mutagenesis on pFmiR-ST3GAL5

The 3'UTR sequence of ST3GAL5 and the corresponding miRNA sequences (down-miRs: -200b-3p, 200c-5p, -550a-3p, 30d-3p, 30d-5p, 30e-3p; up-miRs: -34c-3p, -31-3p, 32-5p, -106bb-5p, 193a-3p, 92b-5p) were analyzed with either Targetscan[74] or the RNAhybrid tool[142] which calculates a minimal free energy hybridization of target RNA sequence and miRNA. For down-miRs, the miRNA sites predicted by Targetscan were chosen for designing mutant pFmiR-sensors. For up-miRs, the most stable predicted miRNA: mRNA interaction sites by RNAhybrid were selected for designing mutant pFmiR-sensors. Multiple mutation sites were designed, the mutant primers were designed using NEB Base Changer version 1 (https://nebasechangerv1.neb.com) and ordered for synthesis to Integrate DNA Technologies (IDT) which are listed in Table 5.1. Multiple mutation sites were achieved according to protocol for Site Directed Mutagenesis (SDM) using Q5® Site-Directed Mutagenesis kit (NEB, catalog #: E0554S). Amplicons were cleaned up using Monarch PCR & DNA cleanup kit (catalog #: T1030S, NEB). Sequences for the mutant pFmiR-

ST3GAL5 sensors were then verified by sequencing and used in the miRFluR assay as described previously. A minimum of 5-wells were transfected per sensor and the analysis was done in three biological experiments. Data was normalized to the median non-targeting control miRNA mimic (NTC1) used with each sensor.

4.6.9 siRNA knockdown of ST3GAL5

ON-TARGETplus siRNA reagents against ST3GAL5 in a smart pool format and ON-TARGETplus Non-Targeting Control Pool (NTP) were purchased from Dharmacon (Horizon Discovery, CA). MDA-MB-231 cells were seeded in six-well plates (50,000 cells/well) and cultured for 24 h in appropriate media. Cells were then transfected with each of the siRNA pools (25 nM and 50 nM, NTP, ST3GAL5, Dharmacon, Horizon Discovery) using Lipofectamine™ RNAiMAX transfection reagent (catalog#: 13778150, Thermofisher) following the manufacturer's instructions. After 48h, cells were lysed using RIPA lysis buffer supplemented with protease inhibitors (Thermofisher, catalog #: 89900), and lysates were quantified using BCA assay (Micro BCA™ protein assay kit, catalog #: 23235) and were analyzed for Western blot as previously described. Blots were incubated with antibodies and processed as described before. Silencing ST3GAL5 using the siRNA confirmed the antibody signal for specific binding to ST3GAL5 protein on Western blots (**Appendix B**).

Table 4.1 Primer sequences for PCR amplification of WT 3'UTR, RT-qPCR quantification of mRNA, and PCR amplification of mutant 3'UTRs for ST3GAL5.

Primer Name	Sequence (5' → 3')	Sample
a. PCR amplification of ST3GAL5 3'UTR		
ST3GAL5-FWD[a]	AGTCAACCGGTACACAGAAAACCTCAGTTGA	gDNA, MCF-7
ST3GAL5-REV[a]	AGTCACGTACGTTCCTCAAAAGTTTTTATTCTTTTTCATC	gDNA, MCF-7
b. RT-qPCR[a] quantification of ST3GAL5 or GAPDH transcript		
ST3GAL5-FWD	AGAGCCTCAGTCAAGGTTCTGG	Total RNA from MDA-MB-231, A549, and MeWo cell lines
ST3GAL5-REV	GAGGTCATATCCAAAACCCGCC	
GAPDH-FWD	GGTGTGAACCATGAGAAGTATGA	
GAPDH-REV	GAGTCCTTCCACGATACCAAAG	
c. PCR amplification of ST3GAL5 mutant 3'UTRs		
30e-3p-ST3GAL5-MUT-FWD	aactgacttttGAAATCTTCCCAGTATTATAAATTG	pFmiR-ST3GAL5
30e-3p- ST3GAL5-MUT-REV	tcccaaaacattATTCCTGGAAAGGGTGTAC	pFmiR-ST3GAL5
30d-3p- ST3GAL5-MUT-FWD	aactgacttttGAAATCTTCCCAGTATTATAAATTG	pFmiR-ST3GAL5
30d-3p- ST3GAL5-MUT-REV	tcccaaaacattATTCCTGGAAAGGGTGTAC	pFmiR-ST3GAL5
31-3p- ST3GAL5-MUT-FWD	caccgtgtgtcgcAGTTTAAAAAGATGAAAAAGAATAAAAAC	pFmiR-ST3GAL5
31-3p- ST3GAL5-MUT-REV	gtattgtggcggtgGTAGGCATTCAGAAAAGTTTC	pFmiR-ST3GAL5
106b-5p- ST3GAL5-MUT-FWD	acgtcgcgCGTGAGGCCTGGGCTGGT	pFmiR-ST3GAL5
106b-5p- ST3GAL5-MUT-REV	tgcgtctgcCAGTATCAGCAGCAGAGCTACGG	pFmiR-ST3GAL5

[a] FWD, forward; REV, reverse; RT-qPCR, Reverse transcription quantitative polymerase chain reaction.

Chapter 5

Profiling the Human miRNA Interactome of CMAS Reveals miRNA Regulation of Sialic Acid

5.1 Aknowledgment

I would like to warmly thank my undergraduate student, Joseph Reyes for his contributions into Western blot experiments and mutational analysis.

5.2 Introduction

Metabolic reprogramming is a hallmark of cancer. Tumors modify the metabolic phenotypes via rewriting vital metabolites to satisfy cancer growth, progression, and metastasis to distant sites[243-246]. Sialic acid and its metabolic pathway have been shown to be enriched in the metabolic reprogramming of various cancers (e.g., Breast[247,248], colon[249], lung[43,250], ovarian[48], pancreatic[26,36,38], and prostate[45] cancers). It is also an essential nutrient in normal physiology (brain development[251]) and immunology (B-cell survival[252]). Several examples for the functional roles of sialic acid metabolic pathway enzymes (e.g., GNE, NANS) have been described in Section 1.1.1. **C**ytidine **m**onophosphate *N*-**a**cetylneuraminic acid **s**ynthetase (CMAS) is a key enzyme in the sialic acid metabolic pathway, responsible for the biosynthesis of the nucleotide sugar, CMP-sialic acid (CMP-sia)[253]. The nucleotide sugar donor is required for all sialyltransferases (STs) to function by adding CMP-sia onto a glycoconjugate acceptor (**Figure 5.1**). CMAS is the only sialic acid-related enzyme that can activate the cellular pool of sialic acid and provide STs with active substrates for sialylation, suggesting CMAS expression makes major contributions to the cellular sialylation levels[247,248,253]. Knocking down of CMAS has shown sialylation to be essential to the maintenance of breast cancer pathogenicity[247].

High levels of cell surface sialic acid termed "hypersialylation" has emerged as a commonly observed phenotype of tumor microenvironment. This phenotype provides tumor cells with the required biophysical properties (e.g., negative charge of carboxylate group) and regioselectivity via specific sialic acid linkage to a glycoconjugate acceptor Section 1.1.2. Both factors are crucial for recognition by glycan binding proteins (e.g., Siglecs, Selectins), dampening immune cell responses, promoting cancer progression and metastasis via altering cellular adhesion[254-256]. The sialic acid regulatory function in molecular and cellular interactions have been

previously discussed in Section 1.2. The CMP-sia availability of STs can alter the cellular sialylation levels[247]. For example, an increased sialylation is reported in cells treated with Neu5Ac which also resulted in >1.5-fold increase in the transcription of *cmas* and *sialyltransferase*s in compared to untreated cells[257].

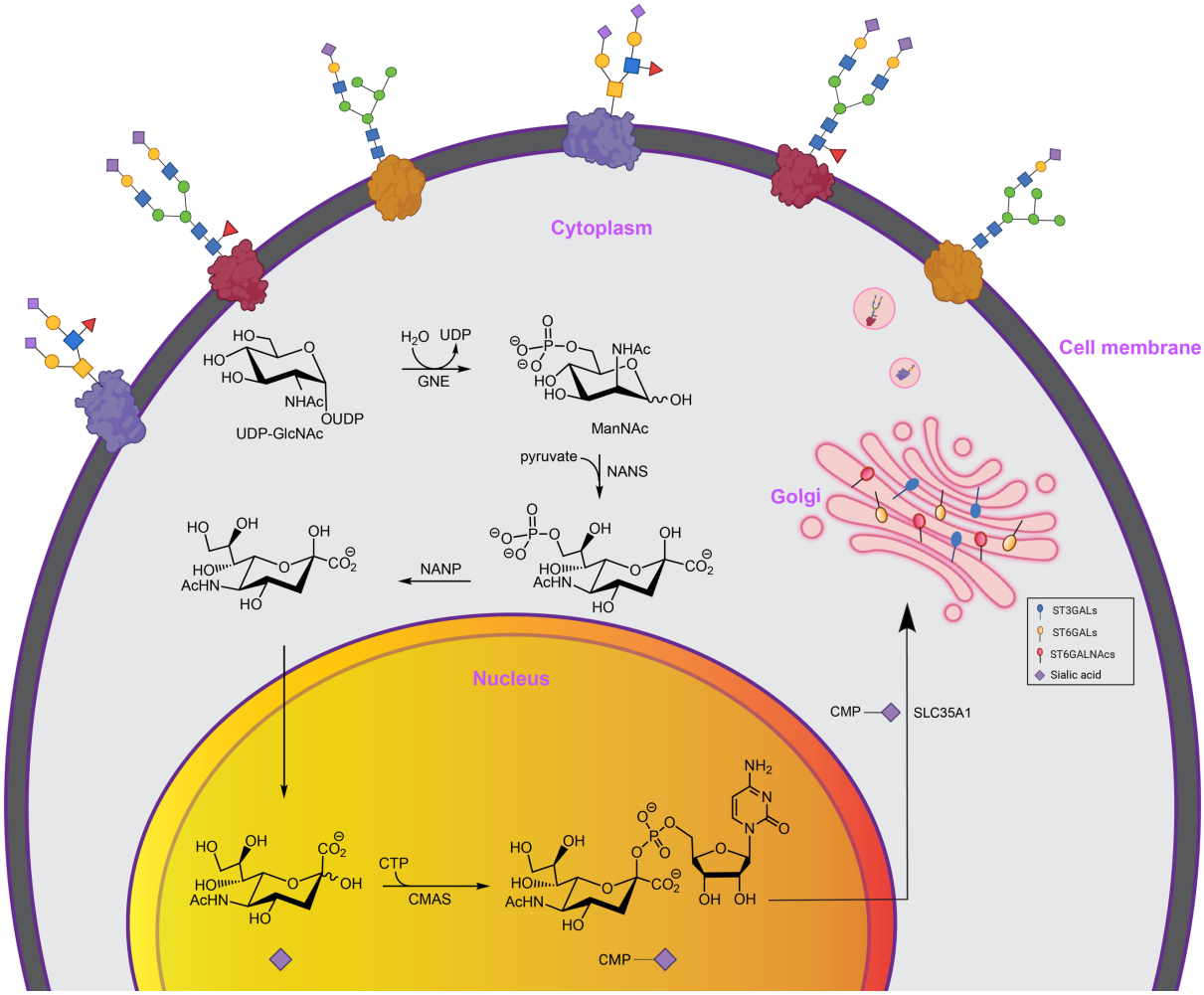

Figure 5.1 Scheme represents sialic acid metabolic pathway. CMAS catalyzes sialic acid activation from sialic acid to CMP-sialic acid inside the nucleus.

Given the impact of CMAS expression level and its product, CMP-sia, in the remodeling of cell surface sialylation, understanding the regulation of this gene may help to understand the regulation of sialic acid. To this end, I used the dual fluorescence ratiometric miRFluR system to investigate the post-transcriptional regulation of CMAS expression by microRNA. In Chapter 2, I

validated that miRNA can modulate gene expression in two distinct directions: inhibition or upregulation of protein expression (**Figure 5.2A**). In this Chapter, using the high throughput miRFluR assay, I comprehensively profiled the miRNA regulatory landscape of CMAS, identifying miRNA that can both down- and up-regulate CMAS expression via direct miRNA: 3'UTR interaction.

5.3 Results

5.3.1 Profiling human miRNA interactome on CMAS 3'UTR using miRFluR assay

To map the miRNA regulatory landscape of CMP-sialic acid synthetase (CMAS), we cloned the most prevalent 3' untranslated region (3'UTR) to create the pFmiR-CMAS sensor (**Figure 5.2**). The 3'UTR length of genes studied so far via miRFluR assay were ≥ 2 kilobases

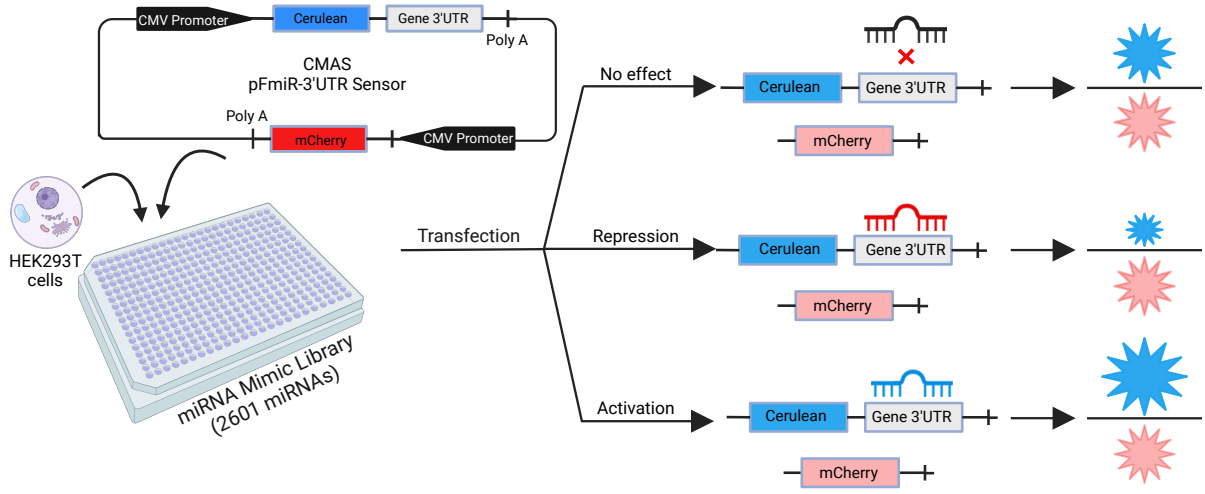

Figure 5.2 Schematic of the miRFluR assay for screening CMAS pFmiR-3'UTR interactome with human miRNAome in HEK293T cells.

(B3GlcT: 2 kb[78], ST6GAL1: 2.75 kb[130], ST6GAL2: 5 kb[130], ST3GAL1: 4.9 kb, ST3GAL2: 2.39 kb, **Appendix A**) except for CD98hc with 190 nucleotides (nt) 3'UTR length (**Appendix A**). The CMAS 3'UTR is relatively short at 357 nt (**Appendix A**). I co-transfected the pFmiR-CMAS

sensor with the miRNA mimic library (Dharmacon, v. 21, 2601 miRs), arrayed in triplicate 384-well plates in HEK293T cells (**Figure 5.2**).

Upon data analysis, I found that the "non-targeting" controls (NTCs) provided with the library were significantly skewed from the median signals, and shifted strongly towards downregulation. Therefore, I tested the NTCs impact on CMAS expression in Western blot analysis of CMAS. My analysis showed that NTCs downregulate CMAS expression. Thus, I chose to median normalize the CMAS dataset (**Figure 5.3A**).

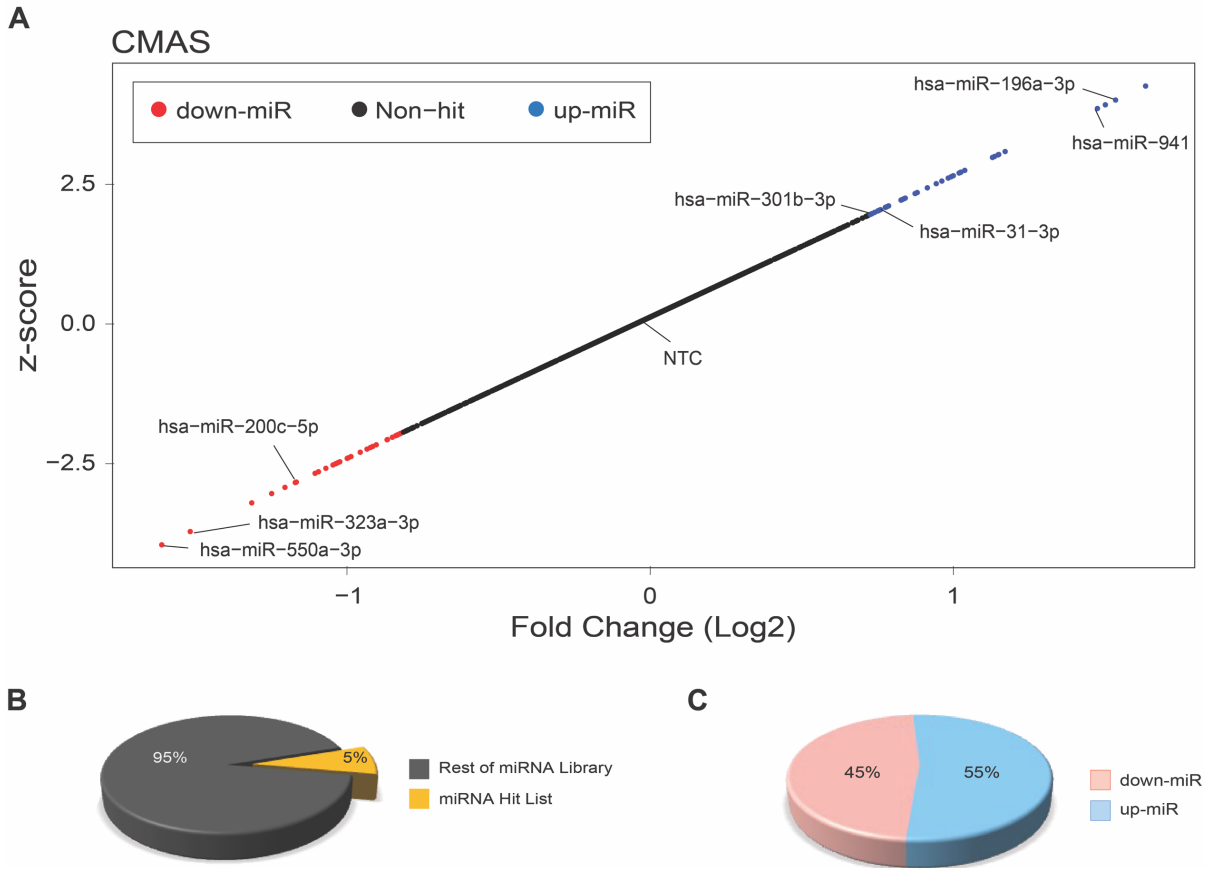

Figure 5.3 Profiling miRNA regulatory landscape of CMAS. (A). Scatter plot indicates post-QC miRNA for CMAS; miRNA in the 95% confidence interval are colored (down-miRs: red, up-miRs: blue) and the tested miRNAs are labeled. (B). Pie chart shows CMAS miRNA hit list containing 5% of miRNA library which passed QC. (C). Pie chart indicates the percentage of down-miR (33 miRNAs) and up-miR (40 miRNAs) in CMAS miRNA hit list.

Post quality control (QC), the CMAS dataset was log_2 transformed and a z-score of ±1.965, corresponding to 95% confidence interval was applied which results in 73 miRNAs as hits for CMAS, representing 5% of miRNA interactions passing QC (**Figure 5.3B**). CMAS miRNA hit list contains 33 downregulatory miRNAs (or down-miRs, 45%, **Figure 5.3C**), and 40 upregulatory miRNAs (or up-miRs, 55%. **Figure 5.3C**).

5.3.2 miRNAs both down- and up-regulate CMAS expression in breast cancer cell lines

A select subset of down-miRs (miR-550a-3p, -323a-3p, -200c-5p) and up-miRs (miR-301b-3p, -31-3p, -196a-3p, -941) were chosen to examine CMAS miRNA hit list over endogenous CMAS expression. Of note, we tested several miRNAs that had no impact on the 3'UTR CMAS sensor, to use as an alternate non-targeting control (NTC). miR-548ay-3p (hereafter NTC1) and miR-625-5p (hereafter NTC2) were chosen as new NTCs with no associations with biological processes[177]. Previous work demonstrated a strong impact of CMAS expression on breast cancer pathogenesis. Thus, I first tested the selected up- and down-miRs in two breast cancer cell lines: MDA-MB-231 (**Figure 5.4A-B**) and MDA-MB-436 (**Figure 5.4D-E**). In line with previous works[78,130], the miRFluR assay accurately identifies cognate miRNA: 3'UTR interactions, showing the select down-miRs are downregulating CMAS expression and up-miRs are increasing CMAS levels in the two cell lines (**Figure 5.4A-B, D-E**). miRNA regulation of CMAS is also assessed for *cmas* transcript expression in MDA-MB-231/436 cells, showing discrepancies between miRNA-mediated gene regulation at transcription and translation levels (**Figure 5.4C and F**). This is consistent with my previous experience (Chapters 2-4) and the literature reports of discrepancies between protein and mRNA levels[78,95,125,126].

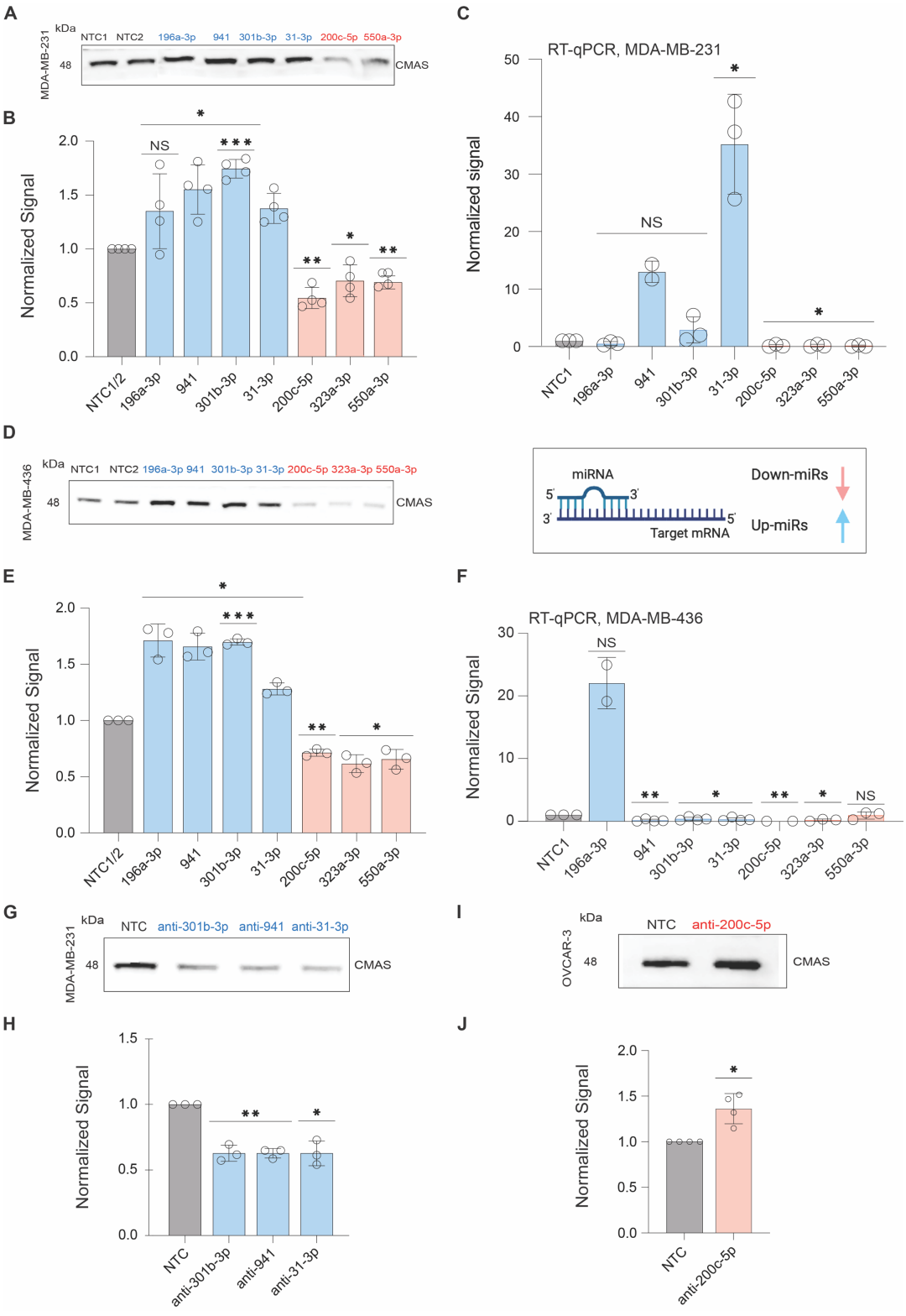

Figure 5.4 miRNA regulation of CMAS expression in breast cancer cell lines. (A&D). Representative blots show Western blot analysis of miRNA-mediated CMAS expression in MDA-mB-231 (A) and MDA-MB-436 (D) cells. miRNA mimics (down-miRs: -200c-5p, -323a-3p, -550a-3p; up-miRs: -196a-3p, -941,

-301b-3p, -31-3p) and NTCs (median controls: NTC1: miR-548ay-3p; NTC2: miR-625-5p) were transfected to the cells. Western blot analysis is conducted 48 hours post transfection. (B&E). Bar graphs show three independent biological replicates of Western blot analysis shown in A and D in MDA-MB-231 (A) and MDA-MB-436 (D) cells. The NTC1/2 is the average of NTC1 and NTC2. (C&F). RT-qPCR quantitative analysis of cmas mRNA expression in MDA-MB-231 (C) and MDA-MB-436 (F). Cells were transfected with the same miRNA mimic listed in A&D and NTC2. (G&I). Representative blots indicate anti-miR inhibiting endogenous miRNA for anti-up-miRs (anti-301b-3p, anti-941, anti-31-3p) in MDA-MB-231 (G) and anti-down-miR-200c-5p in OVCAR-3 (I) cells. NTC (for anti-miR) is used as control. (H&J). Bar graphs show three independent biological replicates of Western blot analysis shown in G and I. All Western blot samples are normalized over total protein stained with ponceau and corresponding NTC. All RT-qPCR samples were normalized over GAPDH and NTC2. Errors shown are standard deviations. For Western blot and RT-qPCR analysis, One sample *t*-test was used to compare miRs to NTCs (ns not significant, * $p < 0.05$, ** < 0.01, *** < 0.001).

To examine the impacts of endogenous miRNA on CMAS expression, I employed miRNA Hairpin Inhibitors (anti-miRs). I chose anti-miRs targeting those miRs for which we have high endogenous expression levels. For this experiment, I used the provided NTC by the Horizon Discovery company for anti-miR, and it does not have any sequence similarity to miRNA mimic NTCs. Three anti-up-miRs (anti-301b-3p, anti-941, anti-31-3p) were transfected in MDA-MB-231 cells and examined via Western blot analysis, resulting in loss of CMAS upregulation (**Figure 5.4G- H**). The endogenous function of down-miR-200c-5p was tested in OVCAR-3 cells by transfecting anti-200c-5p, resulting in loss of downregulation (**Figure 5.4I-J**). This data confirmed the observed up- and down-regulation of CMAS expression comes from endogenous miRNA impacts.

5.3.3 Upregulatory miRNAs for CMAS enriched for pancreatic and lung cancers

To explore the potential involvement of the identified up-miRs in biological pathways, I used miRNA enrichment and annotation database (miEAA, v 2.1)[258]. Running the miRNA enrichment analysis for CMAS upregulatory miRNAs showed a strong signature in cancer biology wherein sialylation is shown to play functional roles[26,36,38] (**Figure 5.5A-B**). Pancreatic cancer and lung cancer were scored as the first and second most enriched cancer types, respectively, for CMAS upregulatory miRNAs (**Figure 5.5C-D**).

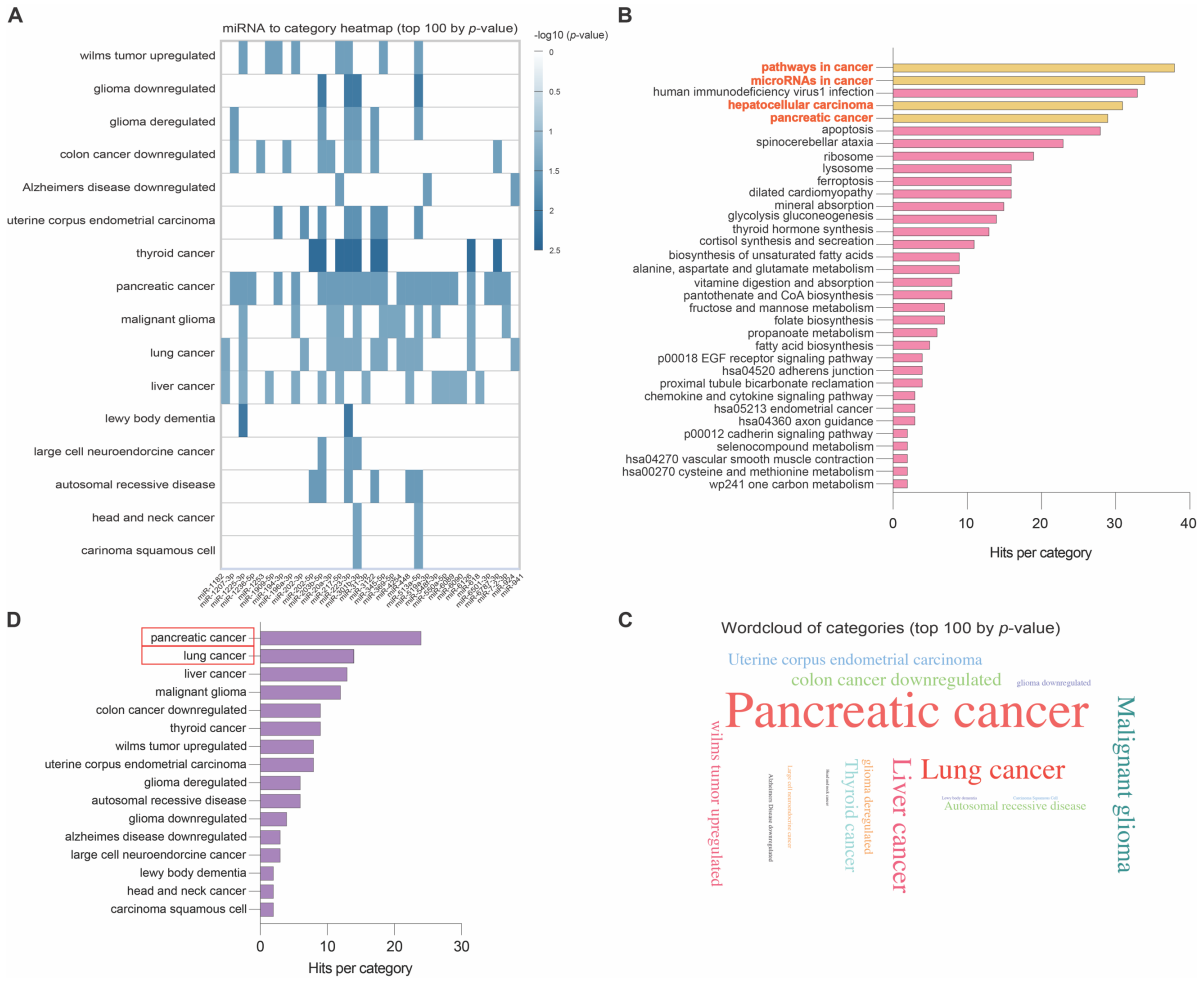

Figure 5.5 Enrichment analysis of upregulatory miRNA for CMAS. The enrichment analysis is conducted by applying $p < 0.05$ using miRNA enrichment analysis and annotation tool (miEAA)[258]. (A). Heat map indicates enrichment of some CMAS upregulatory miRNA in different cancer types. (B). Bar graph shows that CMAS up-miRs are significantly enriched in cancer biology. (C). Bar graph lists cancer types enriched for CMAS up-miRs. (D). Word plot indicates pancreatic, lung, and liver cancers as the first three most enriched cancer types for CMAS up-miRs, respectively.

The CMAS expression level affects the content of all forms of sialylation. Different sialyltransferases and their corresponding sialylation patterns have been reported to play roles in lung and pancreatic cancers. For example, both α-2,6-sialic acid and ST6GAL1, the main enzyme underlying it, are known to play roles in lung cancer and pancreatic cancer progression[26,38,43]. Thus, we narrow our focus upon the examination of miRNA roles in regulating sialic acid regulation in lung and pancreatic cancer cells.

I first analyzed the CMAS expression regulation by transfecting A549 cells with a select subset of down- and up-miRs as listed before (**Figure 5.6**). Overall, I observed the inhibition of CMAS expression by down-miRs, whereas up-miRs upregulated the expression of this enzyme. The miRNA impact on *cmas* transcript levels was also tested. I observed more agreement in the regulatory patterns of CMAS between protein and mRNA levels in A549 cells, indicating higher cell dependency in transcript response than protein.

Among different sialyltransferases, two of them are shown to play roles in lung cancer: ST6GAL1[43] and ST6GALNAc2[250], both are responsible for α-2,6-sialylation. *In vivo* experiments showed that silencing ST6GALNAc2 suppressed breast cancer metastasis to lung in both mouse and human breast cancer models, revealing ST6GALNAc2 metastasis suppressor function[250]. Yuan, Q., and coworkers reported the proinvasive role of α-2,6-sialylation and ST6GAL1 non-small lung cancer cells (A549) *in vitro* and *in vivo*[43]. In this Chapter, I tested the potential impact by miRNA in regulating cell surface α-2,6-sialic acid via targeting CMAS. Thus, I stained A549 cells with the Cy3-SNA lectin and fluorescence signal was visualized using fluorescence microscopy. The fluorescence signal was further quantified using flow cytometry (**Figure 5.6E-G**). The SNA lectin staining showed an increase in α-2,6-sialylation by up-miRs (miR-31-3p, -301b-3p. -196a-3p: ~1.4 fold), whereas the down-miR-200c-5p resulted in a decrease in cell surface α-2,6-sialic acid. To further confirm that the observed miRNA-mediated regulation of α-2,6-sialic acid is via tuning CMAS expression, and not through controlling ST6GAL1 expression, I examined the miRNA impacts on ST6GAL1 expression in A549 cells. The data showed no effects by miRNA on ST6GAL1 expression levels which is in consistent with Chapter 2, where these miRNAs do not pass the applied QC (error threshold, z-score analysis) in miRFluR assay[130] (**Figure 5.6H, I)**.

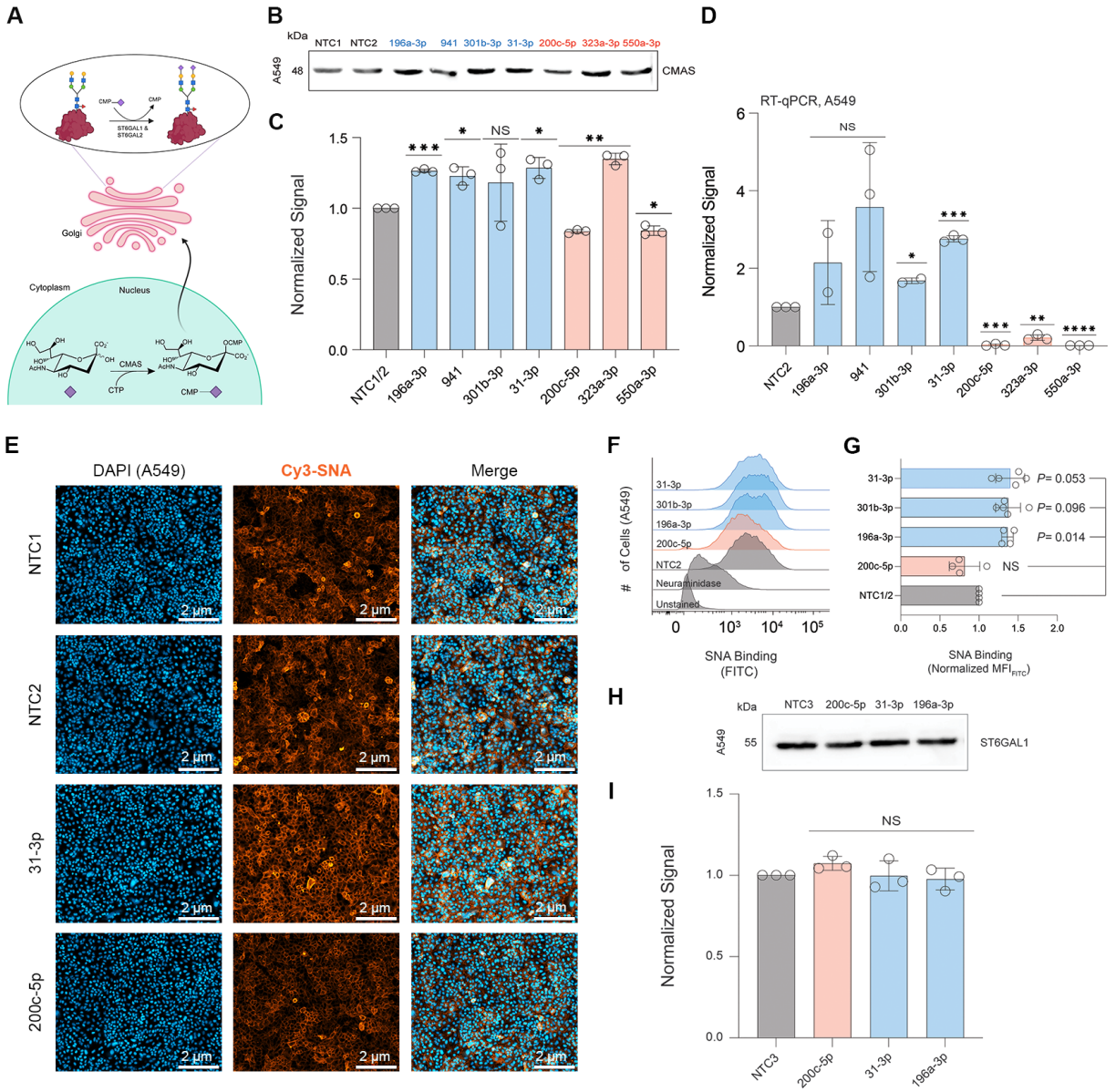

Figure 5.6 miRNA regulation of CMAS expression in A549 cell line. (A) Schematic representation of CMAS function in nucleus and ST6GAL1/2 function in Golgi modifying glycoconjugates with α-2,6-sialylation. (B) Representative blots show Western blot analysis of miRNA-mediated CMAS expression in A549 cells. miRNA mimics (down-miRs: -200c-5p, -323a-3p, -550a-3p; up-miRs: -196a-3p, -941, -301b-3p, -31-3p) or NTCs (median controls: NTC1: miR-548ay-3p; NTC2: miR-625-5p) were transfected to A549 cells. Western blot analysis is conducted 48 hours post transfection. (C). Bar charts shows three independent biological replicates of Western blot analysis shown in B. The NTC1/2 is the average of NTC1 and NTC2. (D). RT-qPCR quantitative analysis of *cmas* mRNA expression in A549 cells transfected with the same miRNA mimic listed in B and NTC2. (E). SNA staining of miRNA (up-miRs: -31-3p, -196a-3p; down-miR-200c-5p) or NTC (for anti-miR) treated cells as in B. (F). Representative flow cytometry histograms and quantification of SNA binding in A549 cells transfected with miRNA mimic. (G). Bar graph shows three biological replicate result of flow cytometry quantification shown in F. (H). Western blot analysis of ST6GAL1 for indicated miRNAs. A549 cells were transfected with same miRNA mimic as listed in E or NTC3 (miRNA mimic non-targeting control for ST6GAL1). (I). Bar graph represents normalized data for three biological replicates. In flow cytometry analysis, paired *t*-test was used to compare

miRs to NTC1/2 and *p*-values are indicated on the graph. All Western blot samples are normalized over total protein stained with ponceau and corresponding NTCs. All RT-qPCR samples were normalized over GAPDH and NTC2. Errors shown are standard deviations. For Western blot and RT-qPCR analysis, One sample *t*-test was used to compare miRs to corresponding NTCs (ns not significant, * $p < 0.05$, ** < 0.01, *** < 0.001).

The endogenous miR-31-3p function in upregulating CMAS expression was further verified via testing the corresponding anti-miR in A549 cells, resulting in loss of CMAS upregulation (**Figure 5.7A**). We also quantified α-2,6-sialic acid levels upon the anti-miR transfection to A549 cells via fluorescence microscopy and flow cytometry. As expected, we observed reduction in SNA binding levels (**Figure 5.7C-D**).

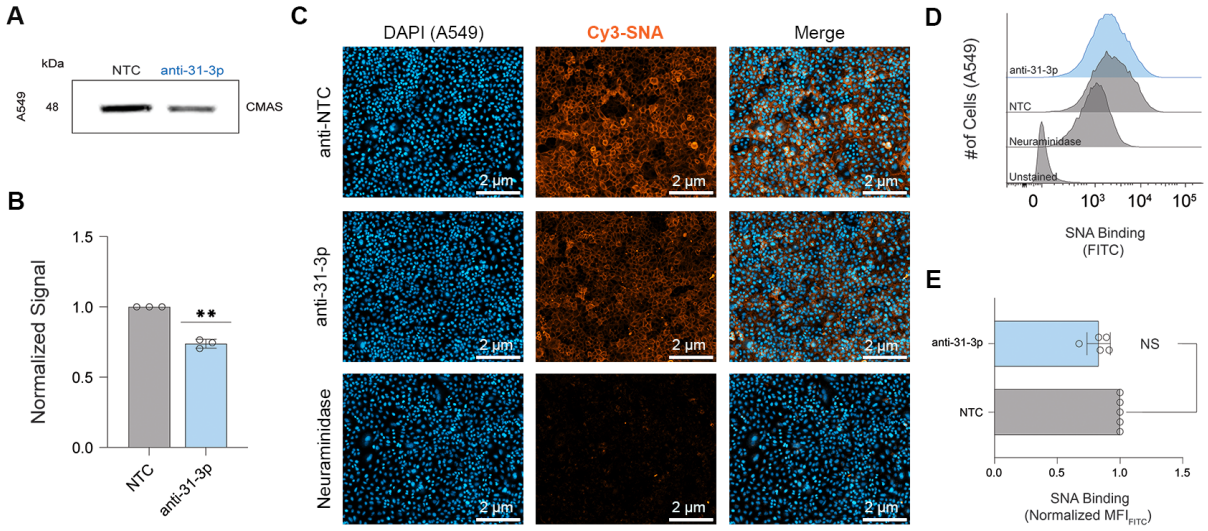

Figure 5.7 Corroboration of endogenous miRNA function in regulating CMAS expression in A549 cell line. (A) Western blot analysis of CMAS for anti-up-miR-31-3p. A549 cells were transfected with anti-miRs or NTC. (B). Bar graph represents normalized data for three biological replicates. (C). SNA staining of anti-up-miR treated A549 cells (NTC, anti-miR-31-3p). (D). Representative flow cytometry histograms and quantification of SNA binding in A549 cells transfected with anti-miRs as in C. (E). Bar graph shows three biological replicate result of flow cytometry quantification shown in D. All experiments were performed in biological triplicate. Errors shown are standard deviations. For Western blot analysis, One

sample *t*-test was used to compare anti-miRs to NTC (ns not significant, ** $p < 0.01$). In flow cytometry analysis, paired *t*-test was used to compare anti-miR to NTC and *p*-values are indicated on the graph.

I tested one down-miR-200c-5p, and two up-miRs: -31-3p and -196a-3p for CMAS expression in SU-86-86, a pancreatic cell line to assess the impact of miRNAs on CMAS

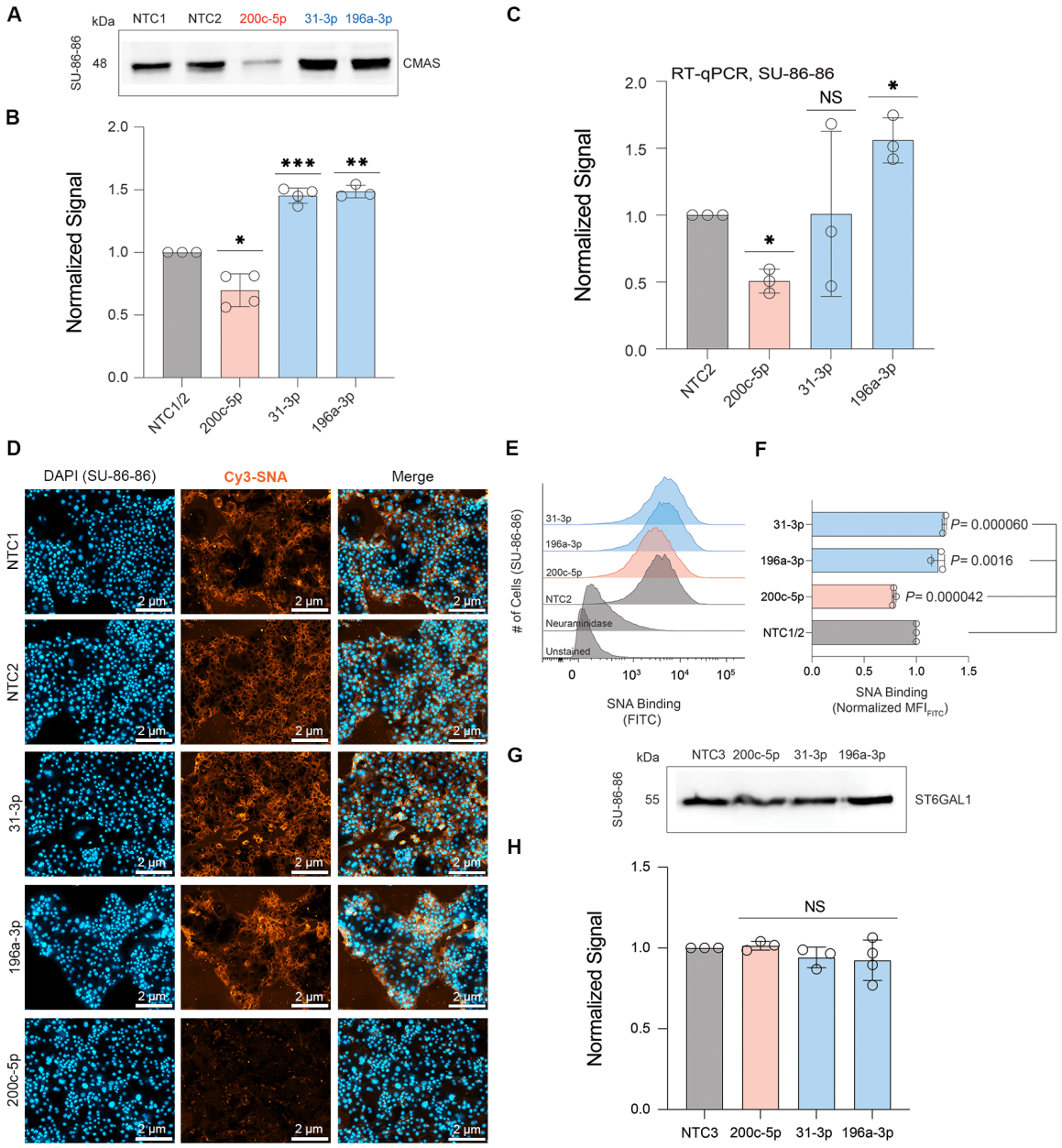

Figure 5.8 miRNA regulation of CMAS expression in SU-86-86 cell line. (A) Representative blots show Western blot analysis of miRNA-mediated CMAS expression in SU-86-86 cells. miRNA mimics (down-miRs: -200c-5p; up-miRs: -196a-3p, -31-3p) or NTCs (median controls: NTC1: miR-548ay-3p; NTC2: miR-625-5p) were transfected to SU-86-86 cells. Western blot analysis is conducted 48 hours post transfection. (B). Bar charts shows three independent biological replicates of Western blot analysis shown

in A. (C). RT-qPCR quantitative analysis of *cmas* mRNA expression in SU-86-86 cells transfected with the same miRNA mimic listed in A or NTC2. (D). SNA staining of miRNA (up-miRs: -31-3p, -196a-3p; down-miR-200c-5p) or NTCs treated cells as in B. (E). Representative flow cytometry histograms and quantification of SNA binding in SU-86-86 cells transfected with miRNA mimic or NTCs treated cells as in B. (F). Bar graph shows three biological replicate result of flow cytometry quantification shown in E. (G). Western blot analysis of ST6GAL1 for indicated miRNAs. SU-86-86 cells were transfected with same miRNA mimic as listed in A or NTC3 (miRNA mimic non-targeting control for ST6GAL1). (H). Bar graph represents normalized data for three biological replicates. In flow cytometry analysis, paired *t*-test was used to compare miRs to NTCs and *p*-values are indicated on the graph. All Western blot samples are normalized over total protein stained with ponceau and corresponding NTCs. All RT-qPCR samples were normalized over GAPDH and NTC2. Errors shown are standard deviations. For Western blot and RT-qPCR analysis, One sample *t*-test was used to compare miRs to corresponding NTCs (ns not significant, * $p < 0.05$, ** < 0.01, *** < 0.001).

expression in pancreatic cancer (**Figure 5.8**). The data indicates the upregulation in CMAS expression by the two up-miRs, whereas miR-200c-5p inhibits CMAS expression. The miRNA impact on *cmas* transcript was examined. To further analyze the sialic acid regulation in pancreatic cancer, we investigate α-2,6-sialic acid regulation by miRNAs targeting the CMAS 3'UTR using SNA staining in SU-86-86 cells. Both fluorescence microscopy and flow cytometry analysis indicated an increase in SNA signal by up-miR-31-3p (~1.2 fold) and up-miR-196a-3p (~1.3 fold) (**Figure 5.8D-F**). The down-miR-200c-5p showed ~20% decrease in SNA intensity. It makes biological sense that CMAS upregulation results in an increased level of α-2,6-sialic acid via providing more of the activated form of sialic acid for ST6GAL1. Since ST6GAL1 is the main enzyme for modifying cell surface with α-2,6-sialic acid, we examine the impact of the miRNA hits for CMAS over ST6GAL1 expression. In line with A549 data for ST6GAL1 expression analysis, I have not observed significant miRNA-mediated regulation for ST6GAL1 (**Figure 5.8G, H**).

5.3.4 CMAS expression is increased via direct miRNA: 3'UTR interaction

Using prediction tools, I identified the predicted binding site for two up-miRs (miRs: -31-3p, -301b-3p) using RNAhybrid[142], and two down-miRs (miRs: -200c-5p, -550a-3p) using Targetscan[74] (**Figure 5.9**). In line with our previous Chapters, the upregulatory miRNA are

predicted to bind via non-canonical sites in accordance with RNAhybrid, whereas the down-miR sites predicted by targetscan have canonical binding patterns. I mutate the predicted miRNA binding sites within the pFmiR-CMAS sensor for each prediction. In line with previous Chapters, mutation of the predicted sites abrogated the impact of the miRNAs.

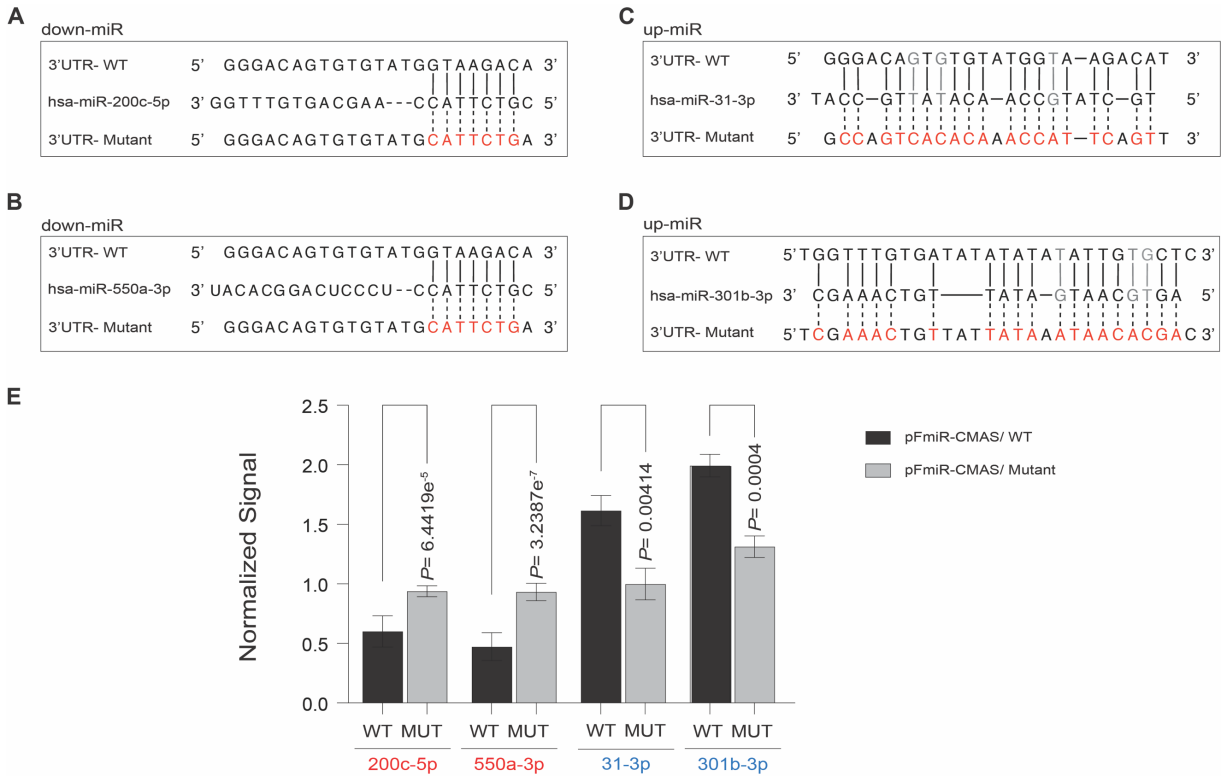

Figure 5.9 Mutational analysis identifies miRNA binding sites on CMAS 3'UTR. A-D. Alignment of down-miRs (A: miR-200c-5p; B: miR-550a-3p) and up-miRs (C: miR-31-3p; D: miR-301b-3p) predicted CMAS-3′UTR sites and their corresponding mutants. Mutated residues are shown in red. Wobble interactions are shown in grey. **E.** Bar graph of data from miRFluR sensors. For each sensor, data was normalized over NTC. A standard *t*-test was used for comparisons. Asll experiments were performed in biological triplicate, a representative experiment with n = 5 wells is shown.

5.4 Discussion

Metabolic reprogramming occurs across cancer development[243-246]. Aberrant expression of STs and CMAS, the sialic acid metabolic pathway enzyme, are considered as a common feature of cancer cells and directly impact cell surface sialic acid content[254]. Interference with sialic acid activation eradicates sialylation, impairing normal physiology (brain development, immune

response) or pathology states (cancer progression, autoimmunity). In mapping miRNA regulatory landscape of CMAS, I identified bidirectional tuning of CMAS expression by miRNA in miRFluR assay. Biological validation verified the expected miRNA impacts on CMAS expression using both miRNA mimic and anti-miRs.

Intriguingly, my enrichment analysis[258] for CMAS *upregulatory* miRNAs identified enrichment for different cancer types: pancreatic cancer, lung cancer, and liver cancer. All three of these malignancies are associated with the increased sialylation patterns drived by different STs. ST6GAL1 and underlying α-2,6-sialylation is the most well-characterized ST in cancer malignancies including these three cancers[26,38,43,99,100]. Work from the Mahal laboratory and others have shown that ST6GAL1 and underlying α-2,6-sialic acid are upregulated in the early-stage of pancreatic ductal adenocarcinoma (PDAC), and promotes PDAC progression [26,38]. In lung cancer, ST6GAL1 and ST6GALNAc2 are the only STs that play two distinct roles. ST6GAL1 upregulation is reported to increase lung cancer proliferation, metastasis, and invasion[43]. Murugaesu, N., *et. al.*, revealed ST6GALNAc2 suppressive role in breast cancer lung metastasis and improved survival in patients with breast cancer[250]. In addition, ST6GAL1 is the only ST reported to be negatively associated with the metastasis capacity of hepatocellular carcinoma (HCC, the most common primary liver cancer)[46]. α-2,6-sialylation of melanoma cell adhesion molecule (MCAM, also known as CD146), by ST6GAL1 masked the galectin-3 interaction site on MCAM[46] whose pro-metastatic function has been reported in HCC[259]. The strong concordance of ST6GAL1 biological roles with the enrichment analysis result from CMAS upregulatory miRNAs in cancer biology aroused my curiosity to examine CMAS expression, α-2,6-sialic acid level, and ST6GAL1 expression in lung (A549) and pancreatic (SU-86-86) cells. My analysis identified miRNAs that impact cell surface α-sialic acid via directly tuning CMAS expression.

Together, this Chapter may provide more evidence for the CMAS expression effects on cellular sialylation levels, herein, α-2,6-sialic acid.

5.5 Conclusion

Sialic acid, the key terminal glycan on cell surface, is known to drive cellular interactions[5,54,99]. Understanding the regulation of sialic acid metabolism may shed light onto sialome reprogramming which occurs across cancer types. In disease states, the rewritten profile of sialosides provides cancer cells with desired interactions with its microenvironment, leading to their growth, progression, and invasion[38,47,95,248]. Among sialic acid biosynthetic pathway enzymes, I comprehensively profiled the miRNA regulatory landscape of CMAS, providing a hit list from human miRNAome as regulators of CMAS expression. I found two distinct miRNA-mediated regulatory patterns: either inhibition or activation of CMAS expression. This Chapter further suggests that miRNA tuning CMAS expression can regulate the ultimate α-2,6-sialylation on the surface of non-small lung and pancreatic cancer cells. This may add more evidence for the CMAS expression levels in impacting the cellular sialylation profile.

5.6 Experimental methods

5.6.1 Cloning

CMAS 3'UTR was amplified via PCR from genomic DNA (gDNA, 10 μg, from HEK293T cell line) using the primers shown in **Table 5.1**. The amplicons were cleaned up using a Monarch® PCR & DNA cleanup kit (catalog #: T1030S, NEB). The 3'UTR fragment was cloned into the pFmiR-empty backbone[78], downstream of Cerulean with the restriction sites: NheI and BamHI, using standard ligation protocols (NEB). Plasmid was verified by Sanger sequencing (Molecular Biology Services Unit, University of Alberta). Large-scale endotoxin free DNA preparations were

made for sequence-verified construct (pFmiR-CMAS) using Endotoxin-free plasmid DNA purification (Takara Bio USA, Inc., catalog #: 740548). Plasmid map for pFmiR-CMAS and its 3'UTR sequence can be found in **Appendix A.**

5.6.2 Cell lines

All cell lines (HEK-293T, MDA-MB-231, MDA-MB-436, OVCAR-3, A549, SU-86-86) were purchased directly from the American Type Culture Collection (ATCC) and cultured using suggested media (HEK-293T & MDA-MB-231: Dulbecco's Modified Eagle Medium (DMEM), 10% FBS; MDA-MB-436: DMEM, 10% FBS, 1 mM sodium pyruvate; OVCAR-3: RPMI-1640, 20% FBS, 0.01 mg/ml bovine insulin; A549: FK-12, 10% FBS; SU-86-86: RPMI-1640, 10% FBS) under standard conditions (5% CO_2, 37°C).

5.6.3 miRFluR high-throughput assay

The Human miRIDIAN miRNA mimic Library 21.0 (Dharmacon) was resuspended in ultrapure nuclease-free water (REF#: 10977-015, Invitrogen) and aliquoted into black 384-well, clear optical bottom tissue-culture treated plates (Nunc). Each plate contained three replicate wells of each miRNA in that plate (2 pmol/well). In addition, each plate contained a minimum of 6 wells containing non-targeting controls (NTC). To each well was added target pFmiR plasmid (pFmiR-CMAS: 30 ng) in 5 µl Opti-MEM (Gibco) and 5 µl of transfection solution (0.1 µl Lipofectamine™ 2000 (catalog #: 11668500, Life Technologies) diluted to 5 µl total volume with Opti-MEM (Gibco), premixed 5 min at room temperature). The mixture was allowed to incubate at room temperature in the plate for 20 min. HEK293T cells (25 µl per well, 400 cells/ µl in phenol red free DMEM supplemented with 10 % FBS and Pen/Strep) were then added to the plate. Plates were incubated at 37°C, 5% CO_2. After 48 hours, the fluorescence signals of Cerulean (excitation:

433 nm; emission: 475 nm) and mCherry (excitation: 587 nm; emission: 610 nm) were measured using the clear bottom read option (SYNERGY H1, BioTek, Gen 5 software, version 3.08.01).

5.6.4 Data analysis

I calculated the ratio of Cerulean fluorescence over mCherry fluorescence (Cer/mCh) for each well in each plate. For each miRNA, triplicate values of the ratios were averaged, and the standard deviation (S.D.) obtained. I calculated % error of measurement for each miRNA (100 × S.D./mean). As a quality control (QC) measurement, I removed any plates or miRNAs that had high errors in the measurement (median error ±2 S.D. across all plates) and/or a high median error of measurement for the plate (>15%). After QC, I obtained data for 1288 miRNAs for CMAS out of 2601 total miRNAs screened for its 3'UTR. The Cer/mCh ratio for each miRNA was then normalized to the median of Cer/mCh ratios within that plate and error was propagated. Data from all plates were then combined and log-transformed z-scores calculated. A z-score of ±1.965, corresponding to a *two*-tailed *p*-value of 0.05, was used as a threshold for significance. Post-analysis we identified 73 miRNA hits for CMAS within 95% confidence interval (**Figure 5.10** and **Dataset 5.1** (.xls sheet)).

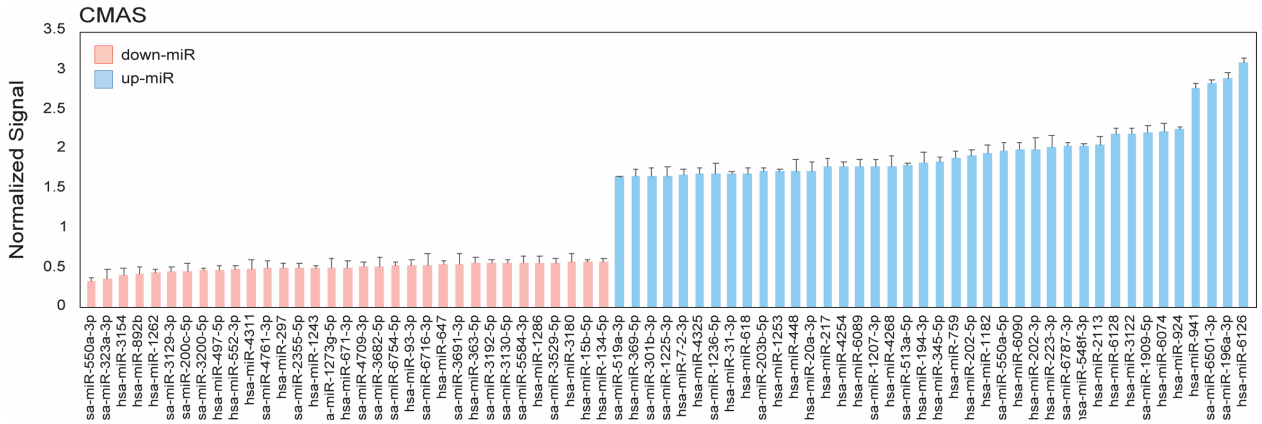

Figure 5.10 Bargraph represents miRNA hit list assay for CMAS resulting from high-throughput miRFluR. Data normalized over median. Error bars represent standard deviation of technical replicates (n=3).

5.6.5 Western blot analysis of CMAS

Western blot analysis was conducted for CMAS in three cell lines: MDA-MB-231, MDA-MB-436, and A549 cell lines (down-miRs: miR-200c-5p, miR-550a-3p, miR-323a-3p; up-miRs: miR-941, miR-196a-3p, miR-301b-3p, miR-31-3p). A small subset of down- and up-miRs was tested in SU-86-86 cell line: down-miR-200c-5p; up-miRs: -31-3p & -196a-3p. For Western blot analysis, 548ay-3p (NTC1) and miR-625-5p (NTC2) are selected as a median control (Cer/mCh ratio ~0.9-1) based on median normalization in miRFluR assay. For all experiments, cells were seeded in six-well plates (50,000 cells/well) and cultured for 24 h in appropriate media. Cells were then washed with Hanks buffered salt solution (HBSS, Gibco) and transfected with miRNA mimics (50 nM mimic, Dharmacon, Horizon Discovery, 5 μL Lipofectamine 2000, Life Technologies in 250 μL OptiMEM). The media was changed to standard media 12 h post-transfection. Cells were then lysed at 48 h post-transfection in cold RIPA lysis buffer supplemented with protease inhibitors (Thermofisher, catalog #: 89900). For Western blot analysis, 30 μg of protein was added to 4x loading buffer with DTT (1 mM), heated at 95°C for 10 min and run on a 10% gel (SDS-PAGE) using standard conditions. Proteins were then transferred from the gel to Polyvinylidene fluoride membrane using iBlot2 Transfer Stacks (PVDF, Invitrogen, catalog number: IB24002) and the iBlot2 transfer device (Invitrogen) using the standard protocol (P_0). Blots were then incubated with Ponceau S Solution (Boston BioProdcuts, catalog #ST-180) for 3 min and the total protein levels were imaged using the protein gel mode (Azure 600, Azure Biosystems Inc.). Blots were blocked with 5% BSA in TBST buffer (TBS buffer plus 0.1% Tween 20) for 30 min at 60 rpm on rocker (LSE platform rocker, Corning) at room temperature. Next, blots were incubated with rabbit polyclonal α-human-CMAS 1° antibody (1:1000 in TBST with

10% BSA, catalog #: HPA039905, Atlas Antibodies). After an overnight incubation at 4℃, blots were washed 1 x rinse and 2 × 30 seconds (sec.) with 0.1% TBST buffer. A secondary antibody was then added (α- rabbit IgG-HRP, 1: 6,000 in TBST with 10% BSA and incubated for 1 h at room temperature with shaking (60 rpm). Blots were then washed 3 × 45 sec. with 0.1% TBST buffer. Blots were developed using Clarity and Clarity Max Western ECL substrates according to the manufacturer's instructions (Bio-Rad). Membranes were imaged in chemiluminescent mode (Azure 600, Azure Biosystems Inc.). All analysis was done in three biological replicates.

5.6.6 Western blot analysis of ST6GAL1

A small subset of down- and up-miRs was tested in A549 and SU-86-86 cell line: down-miR-200c-5p; up-miRs: -31-3p & -196a-3p. For Western blot analysis, miRNA mimic non-targeting control1 (in this Chapter, I labeled it as NTC3) was used to analyze miRNA-mediated ST6GAL1 expression. For all experiments, cells were seeded in six-well plates (50,000 cells/well) and cultured for 24 h in appropriate media. Cells were then washed with Hanks buffered salt solution (HBSS, Gibco) and transfected with miRNA mimics (50 nM mimic, Dharmacon, Horizon Discovery, 5 µl Lipofectamine 2000, Life Technologies in 250 µl OptiMEM). The media was changed to standard media 12 h post-transfection. Cells were then lysed at 48 h post-transfection in cold RIPA lysis buffer supplemented with protease inhibitors (Thermofisher, catalog #: 89900). For Western blot analysis, it was conducted as described in Section 2.6.5.

5.6.7 Endogenous miRNA activity validation

miRIDIAN microRNA Hairpin Inhibitors (anti-down-miR: anti-200c-5p: anti-up-miRs: anti-31-3p, anti-301b-3p, anti-941) and miRIDIAN microRNA Hairpin Inhibitor Negative Control (NTC) were purchased from Dharmacon (Horizon Discovery, Cambridge, UK). The selected anti-miRs for CMAS protein in different cell lines: anti-200c-5p: OVCAR-3 cells; anti-31-3p: MDA-

MB-231 & A549 cells; anti-941 & anti-301b-3p: MDA-MB-231 cells. Each cell line was seeded and incubated as described for Western blot analysis. Cells were transfected with anti-miRNAs, 50 nM using Lipofectamine™ 2000 transfection reagent in OptiMEM following the manufacturer's instructions (Life Technologies). After 12 h media was changed to standard culture media. 48 h post-transfection cells were lysed and analyzed for CMAS protein levels as previously described. All analysis was done in three biological replicates.

5.6.8 RT-qPCR

Total RNA was isolated from cells treated as in Western blot experiments using TRIzol reagent (catalog #: 15596018, Invitrogen) according to the manufacturer's instructions. RNA concentrations were measured using NanoDrop. Isolated total RNA (1 μg) was then reverse transcribed to cDNA using Superscript III Cells Direct cDNA synthesis kit (catalog #: 18080300, Invitrogen). Reverse transcription quantitative PCR (RT-qPCR) was performed using the SYBR Green method and cycle threshold values (Ct) were obtained using an Applied Biosystem (ABI) 7500 Real-Time PCR machine. Values were normalized to the housekeeping gene GAPDH. The primer sequences used for RT-qPCR can be found in **Table 5.1**. All analysis was done in three biological replicates.

5.6.9 Fluorescence microscopy

Cells were seeded onto sterile 22 × 22 glass coverslips placed into 35 mm dishes at a density of 2×10^5 cells/ml in the appropriate media for the cell line as mentioned before. After 24h, cells were transfected with miRNA mimics as previously described (see methods for Western blots). At 48 h post-transfection, cells were washed with PBS (3 × 2 mL) and fixed with 4 % paraformaldehyde for 20 min. Cells were again washed with PBS (3 × 2 mL). Incubate cells with

1% BSA, PBS for 1 hour in the standard condition of incubator (37°C, 5% CO_2). Incubate with Cy3-SNA (SKU #: CL-1303-1, Vector Laboratories) by adding (2 mL total volume, 1:300 (vol: vol) in PBS for 1 hour in standard condition of incubator (37°C, 5% CO_2). Coverslips were then washed (2 mL PBS, 3 x 4 min), and cells were counterstained with Hoechst 33342 (2 mL, 1 µg/mL in PBS, 15 min in incubator). The coverslips were then mounted onto slides with 60 µl of mounting media (90% glycerol in PBS) and imaged with a Zeiss fluorescent microscope (Camera: Axiocam 305 mono, software: ZEN 3.2 pro). Specificity of SNA staining was confirmed by using Neuraminidase (catalog #: P0722L, NEB) prior to Cy3-SNA staining. All analysis was done in three biological replicates.

5.6.10 Flow cytometry: Lectin staining

miRNA or anti-miR transfection to samples for Flow cytometry analysis is prepared with the same method as for Western blot analysis. Post 48 hours-transfection, samples were trypsin digested (80 µL of 0.25% trypsin per well in 6-well plate format). Up to 1 mL of 1X HBSS was added to remove all the cells from the flask, and cells were pelleted out by centrifugation at 350 x g for 6 min. Cell pellets were resuspended in 1X TBS buffer containing 0.1% BSA and were counted using the cell counter. 100 µL of 5×10^5 cells was counted per sample. As a negative control for lectin staining, Neuraminidase (catalog #: P0722L, NEB) sample (is not transfected with miRNA) was trypsin digested and control sample was prepared with Neuraminidase in HBSS: Gibco buffer (catalog #: P0720L, NEB) in 9:1 ratio and incubated at 37°C for 1 hour. 15 µg/ml of FITC-SNA (from Mahal lab) in 1X TBS buffer was added onto each sample and incubated for 25 min at room temperature in dark. Cells were pelleted out by centrifugation at 350 × g for 5 min. Samples were washed with 1X TBS, 0.1% BSA for two times, and centrifuge at 350 × g, 5 min. Samples were resuspended in 400 µl FACS buffer (PBS, 0.1% BSA, 0.1% EDTA, 5 mM).

All samples were analyzed using Fortessa X-20 flow cytometer (Core Facility, Faculty of Medicine and Dentistry, University of Alberta). Experiments are done in a minimum of three biological replicates. Data was analyzed using FlowJo (10.5.3) software (BD Biosciences).

5.6.11 Multi-sites mutagenesis on pFmiR-CMAS

The 3'UTR sequence of CMAS and the corresponding miRNA sequences (down-miRs: -200c-5p, -550a-3p; up-miRs: -31-3p, -301b-3p) were analyzed with either targetscan[74] or the RNAhybrid tool[142] which calculates a minimal free energy hybridization of target RNA sequence and miRNA. For down-miRs, the miRNA sites predicted by targetscan were chosen for designing mutant pFmiR-sensors. For up-miRs, the most stable predicted miRNA: mRNA interaction sites by RNAhybrid were selected for designing mutant pFmiR-sensors. Multiple mutation sites were designed, the mutant primers were designed using NEB Base Changer version 1 (https://nebasechangerv1.neb.com) and ordered for synthesis to Integrate DNA Technologies (IDT) which are listed in **Table 5.1**. Multiple mutation sites were achieved according to protocol for Site Directed Mutagenesis (SDM) using Q5® Site-Directed Mutagenesis kit (NEB, catalog #: E0554S). Amplicons were cleaned up using Monarch PCR & DNA cleanup kit (catalog #: T1030S, NEB). Sequences for the mutant pFmiR-CMAS sensors were then verified by sequencing and used in the miRFluR assay as described previously. A minimum of 5-wells were transfected per sensor and the analysis was done in three biological experiments. Data was normalized to the median control NTC (CMAS: miR-625-5p) used with each sensor.

5.6.12 siRNA knockdown of CMAS

ON-TARGETplus siRNA reagents against CMAS in a smart pool format and ON-TARGETplus Non-Targeting Control Pool (NTP) were purchased from Dharmacon (Horizon

Discovery, CA). SU-86-86 cells were seeded in six-well plates (50,000 cells/well) and cultured for 24 h in appropriate media. Cells were then transfected with each of the siRNA pools (25 nM and 50 nM, NTP, CMAS, Dharmacon, Horizon Discovery) using Lipofectamine™ RNAiMAX transfection reagent (catalog #: 13778150, Thermofisher) following the manufacturer's instructions. After 48h, cells were lysed using RIPA lysis buffer supplemented with protease inhibitors (Thermofisher, catalog #: 89900), and lysates were quantified using BCA assay (Micro BCA™ Protein Assay Kit, catalog #: 23235) and were analyzed for Western blot as previously described. Blots were incubated with antibodies and processed as described before (**Appendix B**).

Table 5.1 Primer sequences for PCR amplification of WT 3'UTR, RT-qPCR quantification of mRNA, and PCR amplification of mutant 3'UTRs for CMAS.

Primer Name	Sequence (5' → 3')	Sample
a. PCR amplification of CMAS 3'UTR		
CMAS-FWD[a]	AGTAAATGCAAGTAAGAACATCATCAAAG	gDNA, HEK-293T
CMAS-REV[a]	CCCCAGATAAATAAAATCCCAACAT	gDNA, HEK-293T
b. RT-qPCR[a] quantification of CMAS or GAPDH transcript		
CMAS-FWD	AGTAAATGCAAGTAAGAACATCATCAAAG	Total RNA from MDA-MB-231, MDA-MB-436, A549, and SU-86-86 cell lines
CMAS-REV	CCCCAGATAAATAAAATCCCAACAT	
GAPDH-FWD	GGTGTGAACCATGAGAAGTATGA	
GAPDH-REV	GAGTCCTTCCACGATACCAAAG	
c. PCR amplification of CMAS mutant 3'UTRs		
200c-5p-CMAS-MUT-FWD	atgcattctgtTGCCCTTCTATTAATAAAAC	pFmiR-CMAS
200c-5p-CMAS-MUT-REV	acacactgtcccCAGATAAATAAAATCCCAACATC	pFmiR-CMAS
550a-3p-CMAS-MUT-FWD	atgcattctgtTGCCCTTCTATTAATAAAAC	pFmiR-CMAS
550a-3p-CMAS-MUT-REV	acacactgtcccCAGATAAATAAAATCCCAACATC	pFmiR-CMAS
31-3p-CMAS-MUT-FWD	aaccattcagttGCCCTTCTATTAATAAAACTAC	pFmiR-CMAS
31-3p-CMAS-MUT-REV	tgtgtgactggcCAGATAAATAAAATCCCAACATC	pFmiR-CMAS
301b-3p-CMAS-MUT-FWD	ataaataacacgacTACTTTTCTCTTTACGCAAG	pFmiR-CMAS
301b-3p-CMAS-MUT-REV	aataacagtttcgaAATCACACTCTCTGTAAC	pFmiR-CMAS

[a] FWD, forward; REV, reverse; RT-qPCR, Reverse transcription quantitative polymerase chain reaction.

Chapter 6

Conclusions and Future Directions

6.1 Acknowledgment

With closing my Ph.D. dissertation, I would like to express my sincere gratitude towards my supervisor, Prof. Lara K. Mahal for being an amazing person and incredibly supportive mentor. It was my tremendous honor to do my Ph.D. under your supervision. Thank you!

I am sincerely grateful for my supervisory committee: Prof. Warren Wakarchuk and Prof. Matthew Macauley for your encourgament and support throughout my Ph.D. marathon. I would like to genuinely acknowledge to the rest of my exam committee: my external referee, Prof. Peter Unrau, my internal referee, Prof. Gulie Gibbs and the chair of my Ph.D. defense, Prof. J. Stryker. Thank you all for your time and expertise.

6.2 Conclusions and future directions

Cell surface sialylation is encoded by a family of at least 20 enzymes, sialyltransferases (STs), which derive specificity in sialylation patterns via creating different linkages (i.e., α-2,3; α-2,6; α-2,8) to acceptor ligands (Gal, GalNAc, Sia). Their diverse tissue expressions give rise to different sialylation patterns across human tissues[260]. Numerous studies show the importance of ST expression levels and corresponding sialylation patterns in normal physiology[5,252] and pathological states including cancer biolgy[5,26,38,47,99,250,254,255], immunology[36,57], and neurodegenerative disorders[208,211,232]. To better understand the regulation of sialylation, I aimed to investigate the miRNA-mediated regulation of sialyltransferases, as drivers of distinct sialylation patterns throughout the human body.

In seeking to address the question, we found a bidirectional tuning by microRNAs[130]. The canonical view of miRNA action is the destabilization of mRNA or inhibition of protein translation[62,204]. To date, protein activation by microRNA has only reported under specific contexts (quiescence state[143,144], in mitochondria[146]), however, our discovery contradicts the current understanding of miRNA function. We indentifed that the upregulatory role of miRNAs (or up-miRs) is via direct miRNA: 3'UTR interactions and does not require those specific conditions observed in previous miRNA-mediated protein activation (non-dividing cells[143,144], without 5'-cap or poly (A) in mitochondria[146]). According to the miR hit lists identified for seven different genes in my Ph.D. dissertation, the extent to which each 3'UTR is hit by up- or down-miRs is target dependent: while ST6GAL1, ST3GAL1 and ST3GAL2 are highly upregulated by miRNAs, ST3GAL5, CMAS, and CD98hc are evenly regulated by up- and down-miRs, and ST6GAL2 is predominantly down-regulated by miRNAs. This suggests that the context of the 3'UTR is a key factor for the extent of up- or down-regulation by miRNAs. For example, secondary structures of

miRNA binding sites, and the strength of miRNA: mRNA patterns may contribute to the levels and directions of miRNA impact. Given that, questions worth asking could be what are the 3'UTR structural impacts on miRNA mode of action. In addition, the recruitment of miRNA to interact with its cognate 3'UTR is drived by the action of complex(es) of proteins including AGO2. The current understaning of RNA binding proteins contributed to miRNA regulatory machinery has yet to be clarified. Now, this question could be asked in two aspects: what are RBPs for downregulatory miRNA? and what are those for upregulatory miRNAs? Are there different protein complexes or RBPs that distinct miRNA modes of actions?

Having determined the miRNA lists targeting seven genes studided in my Ph.D. dissertation, I identified different miRNA:3'UTR pairs whose biological function are dovetailed. For instance, CD98hc and miR-155-5p are both functionally important in the context of cancer biology (e.g., melanoma[159,168,179,180], breast[166,185,261]), immunology (B-cell[82,162] and T-cell[163,189] clonal expansion), and neurodegenerative diseases (e.g., multiple sclerosis[262-264]). In the majority of these biological contexts, the CD98hc upregulation is associated with the more severe or higher stages of disease which are matched with those identified for miR-155-5p. Therefore, it may be worth exploring the potential roles of identified miRNA (e.g., miR-155-5p) in tuning cognate transcript and its protein (e.g., CD98hc) expression.

One important aspect of miRNA biology is its direct effects via interacting with its cognate 3'UTR. It is worth noting that all cognate up-miRNA: 3'UTR binding sites validated throughout this thesis are via non-canonical binding patterns (except up-miR-221-5p for ST6GAL1 that binds via seed region), whereas all validated downregulatory miRNA sites are identified via the seed binding patterns. The predicted binding sites for up- and down-regulatory miRNA may or may not have overlap. For example, in Chapter 2, the majority of predicted sites for up-miRs did not overlap

with those of down-miRs for ST6GAL1, arguing that the observed upregulation is not predominantly via miRNA competition. For those that have overlap, there might be synergistic effects which have yet to be explored. Also, the distribution of up- and down-regulation by miRNA is found to be 3'UTR-dependent: while ST6GAL1, ST3GAL1, and ST3GAL2 are predominantly upregulated by miRNA, ST6GAL2 is mainly downreulated by miRNA. CD98hc, ST3GAL5 and CMAS are approximately evenly up- and down-regulated by miRNA. My Ph.D. dissertation gave rise to different questions regarding miRNA modes of action. One could imagine that miRNA exert the up- versus down-regulation via two distinct machineries which finally impact protein translation. Exploring this hypothesis would help to better understand how miRNA can upregulate protein expression.

Lastly, with the great appreciation of the Mahal laboratory for providing the opportunity for me to delivering my Ph.D. journery to the final station, my Ph.D. defense, it is worth mentioning that I had started investigating miRNA regulatory landscape of more genes such as GNE, SLC35A1, ST6GALNAc5 which are ongoing and will be completed in the future.

References

1 Ashwell, G. & Harford, J. Carbohydrate-specific receptors of the liver. *Annu Rev Biochem* **51**, 531-554 (1982). https://doi.org:10.1146/annurev.bi.51.070182.002531

2 Burnet, F. M. Mucoproteins in relation to virus action. *Physiol Rev* **31**, 131-150 (1951). https://doi.org:10.1152/physrev.1951.31.2.131

3 Klenk, E. Neuraminsäure, das Spaltprodukt eines neuen Gehirnlipoids. *Biological Chemistry* **268**, 50-58 (1941). https://doi.org:10.1515/BCHM2.1941.268.1-2.50

4 Blix, F. G., Gottschalk, A. & Klenk, E. Proposed nomenclature in the field of neuraminic and sialic acids. *Nature* **179**, 1088 (1957). https://doi.org:10.1038/1791088b0

5 Li, F. & Ding, J. Sialylation is involved in cell fate decision during development, reprogramming and cancer progression. *Protein Cell* **10**, 550-565 (2019). https://doi.org:10.1007/s13238-018-0597-5

6 Varki A, C. R., Esko JD, et al., editors. . *Essentials of Glycobiology*. Four edn, (2022).

7 Jaenisch, R. & Bird, A. Epigenetic regulation of gene expression: how the genome integrates intrinsic and environmental signals. *Nat Genet* **33 Suppl**, 245-254 (2003). https://doi.org:10.1038/ng1089

8 Kitamura, N. & Galligan, J. J. A global view of the human post-translational modification landscape. *Biochem J* **480**, 1241-1265 (2023). https://doi.org:10.1042/BCJ20220251

9 Guil, S. & Esteller, M. RNA-RNA interactions in gene regulation: the coding and noncoding players. *Trends Biochem Sci* **40**, 248-256 (2015). https://doi.org:10.1016/j.tibs.2015.03.001

10 Schwarzkopf, M. *et al.* Sialylation is essential for early development in mice. *Proc Natl Acad Sci U S A* **99**, 5267-5270 (2002). https://doi.org:10.1073/pnas.072066199

11 Celeste, F. V. *et al.* Mutation update for GNE gene variants associated with GNE myopathy. *Hum Mutat* **35**, 915-926 (2014). https://doi.org:10.1002/humu.22583

12 Oetke, C., Hinderlich, S., Reutter, W. & Pawlita, M. Epigenetically mediated loss of UDP-GlcNAc 2-epimerase/ManNAc kinase expression in hyposialylated cell lines. *Biochem Biophys Res Commun* **308**, 892-898 (2003). https://doi.org:10.1016/s0006-291x(03)01471-2

13 Giordanengo, V. *et al.* Epigenetic reprogramming of UDP-N-acetylglucosamine 2-epimerase/N-acetylmannosamine kinase (GNE) in HIV-1-infected CEM T cells. *FASEB J* **18**, 1961-1963 (2004). https://doi.org:10.1096/fj.04-2467fje

14 van Karnebeek, C. D. *et al.* NANS-mediated synthesis of sialic acid is required for brain and skeletal development. *Nat Genet* **48**, 777-784 (2016). https://doi.org:10.1038/ng.3578

15 Harduin-Lepers, A. *et al.* The human sialyltransferase family. *Biochimie* **83**, 727-737 (2001). https://doi.org:10.1016/s0300-9084(01)01301-3

16 Li, Y. & Chen, X. Sialic acid metabolism and sialyltransferases: natural functions and applications. *Appl Microbiol Biotechnol* **94**, 887-905 (2012). https://doi.org:10.1007/s00253-012-4040-1

17 Uhlen, M. *et al.* Proteomics. Tissue-based map of the human proteome. *Science* **347**, 1260419 (2015). https://doi.org:10.1126/science.1260419

18 Lundberg, E. *et al.* Defining the transcriptome and proteome in three functionally different human cell lines. *Mol Syst Biol* **6**, 450 (2010). https://doi.org:10.1038/msb.2010.106

19 Morosi, L. G. *et al.* Control of intestinal inflammation by glycosylation-dependent lectin-driven immunoregulatory circuits. *Sci Adv* **7** (2021). https://doi.org:10.1126/sciadv.abf8630
20 Duan, S. & Paulson, J. C. Siglecs as Immune Cell Checkpoints in Disease. *Annu Rev Immunol* **38**, 365-395 (2020). https://doi.org:10.1146/annurev-immunol-102419-035900
21 Svensson, E. C., Soreghan, B. & Paulson, J. C. Organization of the beta-galactoside alpha 2,6-sialyltransferase gene. Evidence for the transcriptional regulation of terminal glycosylation. *J Biol Chem* **265**, 20863-20868 (1990).
22 Milflores-Flores, L., Millan-Perez, L., Santos-Lopez, G., Reyes-Leyva, J. & Vallejo-Ruiz, V. Characterization of P1 promoter activity of the beta-galactoside alpha2,6-sialyltransferase I gene (siat 1) in cervical and hepatic cancer cell lines. *J Biosci* **37**, 259-267 (2012). https://doi.org:10.1007/s12038-012-9194-6
23 Dorsett, K. A., Jones, R. B., Ankenbauer, K. E., Hjelmeland, A. B. & Bellis, S. L. Sox2 promotes expression of the ST6Gal-I glycosyltransferase in ovarian cancer cells. *J Ovarian Res* **12**, 93 (2019). https://doi.org:10.1186/s13048-019-0574-5
24 Smith, B. A. H. *et al.* MYC-driven synthesis of Siglec ligands is a glycoimmune checkpoint. *Proc Natl Acad Sci U S A* **120**, e2215376120 (2023). https://doi.org:10.1073/pnas.2215376120
25 Bojar, D. *et al.* A Useful Guide to Lectin Binding: Machine-Learning Directed Annotation of 57 Unique Lectin Specificities. *ACS Chem Biol* **17**, 2993-3012 (2022). https://doi.org:10.1021/acschembio.1c00689
26 Kurz, E. *et al.* Integrated Systems Analysis of the Murine and Human Pancreatic Cancer Glycomes Reveals a Tumor-Promoting Role for ST6GAL1. *Mol Cell Proteomics* **20**, 100160 (2021). https://doi.org:10.1016/j.mcpro.2021.100160
27 Varki, A. Sialic acids in human health and disease. *Trends Mol Med* **14**, 351-360 (2008). https://doi.org:10.1016/j.molmed.2008.06.002
28 Schnaar, R. L., Gerardy-Schahn, R. & Hildebrandt, H. Sialic acids in the brain: gangliosides and polysialic acid in nervous system development, stability, disease, and regeneration. *Physiol Rev* **94**, 461-518 (2014). https://doi.org:10.1152/physrev.00033.2013
29 Griciuc, A. *et al.* Alzheimer's disease risk gene CD33 inhibits microglial uptake of amyloid beta. *Neuron* **78**, 631-643 (2013). https://doi.org:10.1016/j.neuron.2013.04.014
30 Kaneko, Y., Nimmerjahn, F. & Ravetch, J. V. Anti-inflammatory activity of immunoglobulin G resulting from Fc sialylation. *Science* **313**, 670-673 (2006). https://doi.org:10.1126/science.1129594
31 Anthony, R. M. & Ravetch, J. V. A novel role for the IgG Fc glycan: the anti-inflammatory activity of sialylated IgG Fcs. *J Clin Immunol* **30 Suppl 1**, S9-14 (2010). https://doi.org:10.1007/s10875-010-9405-6
32 Qin, R. *et al.* alpha2,6-Sialylation Is Upregulated in Severe COVID-19, Implicating the Complement Cascade. *ACS Infect Dis* **8**, 2348-2361 (2022). https://doi.org:10.1021/acsinfecdis.2c00421
33 Nguyen, L. *et al.* Sialic acid-containing glycolipids mediate binding and viral entry of SARS-CoV-2. *Nat Chem Biol* **18**, 81-90 (2022). https://doi.org:10.1038/s41589-021-00924-1
34 Lauc, G. *et al.* Loci associated with N-glycosylation of human immunoglobulin G show pleiotropy with autoimmune diseases and haematological cancers. *PLoS Genet* **9**, e1003225 (2013). https://doi.org:10.1371/journal.pgen.1003225

35 Pinho, S. S., Alves, I., Gaifem, J. & Rabinovich, G. A. Immune regulatory networks coordinated by glycans and glycan-binding proteins in autoimmunity and infection. *Cell Mol Immunol* **20**, 1101-1113 (2023). https://doi.org:10.1038/s41423-023-01074-1
36 Rodriguez, E. *et al.* Sialic acids in pancreatic cancer cells drive tumour-associated macrophage differentiation via the Siglec receptors Siglec-7 and Siglec-9. *Nat Commun* **12**, 1270 (2021). https://doi.org:10.1038/s41467-021-21550-4
37 Dube, D. H. & Bertozzi, C. R. Glycans in cancer and inflammation--potential for therapeutics and diagnostics. *Nat Rev Drug Discov* **4**, 477-488 (2005). https://doi.org:10.1038/nrd1751
38 Bhalerao, N. *et al.* ST6GAL1 sialyltransferase promotes acinar to ductal metaplasia and pancreatic cancer progression. *JCI Insight* **8** (2023). https://doi.org:10.1172/jci.insight.161563
39 Wu, Y. *et al.* ST3Gal IV Mediates the Growth and Proliferation of Cervical Cancer Cells In Vitro and In Vivo Via the Notch/p21/CDKs Pathway. *Front Oncol* **10**, 540332 (2020). https://doi.org:10.3389/fonc.2020.540332
40 Deschuyter, M. *et al.* ST3GAL2 knock-down decreases tumoral character of colorectal cancer cells in vitro and in vivo. *Am J Cancer Res* **12**, 280-302 (2022).
41 Agrawal, P., Chen, S., Pablos, A., Jame-Chenarboo, F., Saenz de Vega, E.M., Darvishian, F., Osman, I., Lujambio,A., Mahal, L.K., Hernando,E. Integrated in vivo functional screens and multi-omics analyses identify α-2,3-sialylation as essential for melanoma maintenance. (2024). https://doi.org:10.1101/2024.03.08.584072
42 Pally, D. *et al.* Heterogeneity in 2,6-Linked Sialic Acids Potentiates Invasion of Breast Cancer Epithelia. *ACS Cent Sci* **7**, 110-125 (2021). https://doi.org:10.1021/acscentsci.0c00601
43 Yuan, Q. *et al.* Modification of alpha2,6-sialylation mediates the invasiveness and tumorigenicity of non-small cell lung cancer cells in vitro and in vivo via Notch1/Hes1/MMPs pathway. *Int J Cancer* **143**, 2319-2330 (2018). https://doi.org:10.1002/ijc.31737
44 Jones, R. B. *et al.* Role of the ST6GAL1 sialyltransferase in regulating ovarian cancer cell metabolism. *Glycobiology* **33**, 626-636 (2023). https://doi.org:10.1093/glycob/cwad051
45 Scott, E. *et al.* ST6GAL1-mediated aberrant sialylation promotes prostate cancer progression. *J Pathol* **261**, 71-84 (2023). https://doi.org:10.1002/path.6152
46 Zou, X. *et al.* ST6GAL1 inhibits metastasis of hepatocellular carcinoma via modulating sialylation of MCAM on cell surface. *Oncogene* **42**, 516-529 (2023). https://doi.org:10.1038/s41388-022-02571-9
47 Pietrobono, S. *et al.* ST3GAL1 is a target of the SOX2-GLI1 transcriptional complex and promotes melanoma metastasis through AXL. *Nat Commun* **11**, 5865 (2020). https://doi.org:10.1038/s41467-020-19575-2
48 Wu, X. *et al.* Sialyltransferase ST3GAL1 promotes cell migration, invasion, and TGF-beta1-induced EMT and confers paclitaxel resistance in ovarian cancer. *Cell Death Dis* **9**, 1102 (2018). https://doi.org:10.1038/s41419-018-1101-0
49 Tamura, F. *et al.* RNAi-mediated gene silencing of ST6GalNAc I suppresses the metastatic potential in gastric cancer cells. *Gastric Cancer* **19**, 85-97 (2016). https://doi.org:10.1007/s10120-014-0454-z
50 Zhou, L. *et al.* The beta-galactoside alpha2,6-sialyltranferase 1 (ST6GAL1) inhibits the colorectal cancer metastasis by stabilizing intercellular adhesion molecule-1 via

sialylation. *Cancer Manag Res* **11**, 6185-6199 (2019). https://doi.org:10.2147/CMAR.S208631

51 Zhang, J. *et al.* ST3GAL5-catalyzed gangliosides inhibit TGF-beta-induced epithelial-mesenchymal transition via TbetaRI degradation. *EMBO J* **42**, e110553 (2023). https://doi.org:10.15252/embj.2021110553

52 Bos, P. D. *et al.* Genes that mediate breast cancer metastasis to the brain. *Nature* **459**, 1005-1009 (2009). https://doi.org:10.1038/nature08021

53 Crocker, P. R. *et al.* Siglecs: a family of sialic-acid binding lectins. *Glycobiology* **8**, v (1998). https://doi.org:10.1093/oxfordjournals.glycob.a018832

54 Crocker, P. R., Paulson, J. C. & Varki, A. Siglecs and their roles in the immune system. *Nat Rev Immunol* **7**, 255-266 (2007). https://doi.org:10.1038/nri2056

55 Jame-Chenarboo, Z., Gray, T. E. & Macauley, M. S. Advances in understanding and exploiting Siglec-glycan interactions. *Curr Opin Chem Biol* **80**, 102454 (2024). https://doi.org:10.1016/j.cbpa.2024.102454

56 Schulz, G. *et al.* Detection of ganglioside GD2 in tumor tissues and sera of neuroblastoma patients. *Cancer Res* **44**, 5914-5920 (1984).

57 Theruvath, J. *et al.* Anti-GD2 synergizes with CD47 blockade to mediate tumor eradication. *Nat Med* **28**, 333-344 (2022). https://doi.org:10.1038/s41591-021-01625-x

58 Barondes, S. H. *et al.* Galectins: a family of animal beta-galactoside-binding lectins. *Cell* **76**, 597-598 (1994). https://doi.org:10.1016/0092-8674(94)90498-7

59 Rabinovich, G. A. & Toscano, M. A. Turning 'sweet' on immunity: galectin-glycan interactions in immune tolerance and inflammation. *Nat Rev Immunol* **9**, 338-352 (2009). https://doi.org:10.1038/nri2536

60 Kamerling, J. P. & Vliegenthart, J. F. Identification of O-cetylated N-acylneuraminic acids by mass spectrometry. *Carbohydr Res* **41**, 7-17 (1975). https://doi.org:10.1016/s0008-6215(00)87002-0

61 Visser, E. A. *et al.* Sialic acid O-acetylation: From biosynthesis to roles in health and disease. *J Biol Chem* **297**, 100906 (2021). https://doi.org:10.1016/j.jbc.2021.100906

62 Schmiedel, J. M. *et al.* Gene expression. MicroRNA control of protein expression noise. *Science* **348**, 128-132 (2015). https://doi.org:10.1126/science.aaa1738

63 Denli, A. M., Tops, B. B., Plasterk, R. H., Ketting, R. F. & Hannon, G. J. Processing of primary microRNAs by the Microprocessor complex. *Nature* **432**, 231-235 (2004). https://doi.org:10.1038/nature03049

64 Han, J. *et al.* The Drosha-DGCR8 complex in primary microRNA processing. *Genes Dev* **18**, 3016-3027 (2004). https://doi.org:10.1101/gad.1262504

65 Wilson, R. C. *et al.* Dicer-TRBP complex formation ensures accurate mammalian microRNA biogenesis. *Mol Cell* **57**, 397-407 (2015). https://doi.org:10.1016/j.molcel.2014.11.030

66 Bartel, D. P. MicroRNAs: genomics, biogenesis, mechanism, and function. *Cell* **116**, 281-297 (2004). https://doi.org:10.1016/s0092-8674(04)00045-5

67 Sasaki, T., Shiohama, A., Minoshima, S. & Shimizu, N. Identification of eight members of the Argonaute family in the human genome. *Genomics* **82**, 323-330 (2003). https://doi.org:10.1016/s0888-7543(03)00129-0

68 Fagerberg, L. *et al.* Analysis of the human tissue-specific expression by genome-wide integration of transcriptomics and antibody-based proteomics. *Mol Cell Proteomics* **13**, 397-406 (2014). https://doi.org:10.1074/mcp.M113.035600

69 Meister, G. *et al.* Human Argonaute2 mediates RNA cleavage targeted by miRNAs and siRNAs. *Mol Cell* **15**, 185-197 (2004). https://doi.org:10.1016/j.molcel.2004.07.007
70 Johnson, S. T., Chu, Y., Liu, J. & Corey, D. R. Impact of scaffolding protein TNRC6 paralogs on gene expression and splicing. *RNA* **27**, 1004-1016 (2021). https://doi.org:10.1261/rna.078709.121
71 Elkayam, E. *et al.* Multivalent Recruitment of Human Argonaute by GW182. *Mol Cell* **67**, 646-658 e643 (2017). https://doi.org:10.1016/j.molcel.2017.07.007
72 Nishi, K., Nishi, A., Nagasawa, T. & Ui-Tei, K. Human TNRC6A is an Argonaute-navigator protein for microRNA-mediated gene silencing in the nucleus. *RNA* **19**, 17-35 (2013). https://doi.org:10.1261/rna.034769.112
73 Pfaff, J. *et al.* Structural features of Argonaute-GW182 protein interactions. *Proc Natl Acad Sci U S A* **110**, E3770-3779 (2013). https://doi.org:10.1073/pnas.1308510110
74 Agarwal, V., Bell, G. W., Nam, J. W. & Bartel, D. P. Predicting effective microRNA target sites in mammalian mRNAs. *Elife* **4** (2015). https://doi.org:10.7554/eLife.05005
75 Grimson, A. *et al.* MicroRNA targeting specificity in mammals: determinants beyond seed pairing. *Mol Cell* **27**, 91-105 (2007). https://doi.org:10.1016/j.molcel.2007.06.017
76 Kozomara, A., Birgaoanu, M. & Griffiths-Jones, S. miRBase: from microRNA sequences to function. *Nucleic Acids Res* **47**, D155-D162 (2019). https://doi.org:10.1093/nar/gky1141
77 Wolter, J. M., Kotagama, K., Pierre-Bez, A. C., Firago, M. & Mangone, M. 3'LIFE: a functional assay to detect miRNA targets in high-throughput. *Nucleic Acids Res* **42**, e132 (2014). https://doi.org:10.1093/nar/gku626
78 Thu, C. T., Chung, J. Y., Dhawan, D., Vaiana, C. A. & Mahal, L. K. High-Throughput miRFluR Platform Identifies miRNA Regulating B3GLCT That Predict Peters' Plus Syndrome Phenotype, Supporting the miRNA Proxy Hypothesis. *ACS Chem Biol* **16**, 1900-1907 (2021). https://doi.org:10.1021/acschembio.1c00247
79 Narayan, N. *et al.* Functionally distinct roles for different miR-155 expression levels through contrasting effects on gene expression, in acute myeloid leukaemia. *Leukemia* **31**, 808-820 (2017). https://doi.org:10.1038/leu.2016.279
80 Tili, E., Croce, C. M. & Michaille, J. J. miR-155: on the crosstalk between inflammation and cancer. *Int Rev Immunol* **28**, 264-284 (2009). https://doi.org:10.1080/08830180903093796
81 Kluiver, J. *et al.* BIC and miR-155 are highly expressed in Hodgkin, primary mediastinal and diffuse large B cell lymphomas. *J Pathol* **207**, 243-249 (2005). https://doi.org:10.1002/path.1825
82 Eis, P. S. *et al.* Accumulation of miR-155 and BIC RNA in human B cell lymphomas. *Proc Natl Acad Sci U S A* **102**, 3627-3632 (2005). https://doi.org:10.1073/pnas.0500613102
83 Qin, W., Ren, Q., Liu, T., Huang, Y. & Wang, J. MicroRNA-155 is a novel suppressor of ovarian cancer-initiating cells that targets CLDN1. *FEBS Lett* **587**, 1434-1439 (2013). https://doi.org:10.1016/j.febslet.2013.03.023
84 Nieto, M. A. Epithelial plasticity: a common theme in embryonic and cancer cells. *Science* **342**, 1234850 (2013). https://doi.org:10.1126/science.1234850
85 Peng, F. *et al.* Direct targeting of SUZ12/ROCK2 by miR-200b/c inhibits cholangiocarcinoma tumourigenesis and metastasis. *Br J Cancer* **109**, 3092-3104 (2013). https://doi.org:10.1038/bjc.2013.655

86 Yoon, J. H., Abdelmohsen, K. & Gorospe, M. Functional interactions among microRNAs and long noncoding RNAs. *Semin Cell Dev Biol* **34**, 9-14 (2014). https://doi.org:10.1016/j.semcdb.2014.05.015

87 Bracken, C. P. *et al.* A double-negative feedback loop between ZEB1-SIP1 and the microRNA-200 family regulates epithelial-mesenchymal transition. *Cancer Res* **68**, 7846-7854 (2008). https://doi.org:10.1158/0008-5472.CAN-08-1942

88 Bracken, C. P., Khew-Goodall, Y. & Goodall, G. J. Network-Based Approaches to Understand the Roles of miR-200 and Other microRNAs in Cancer. *Cancer Res* **75**, 2594-2599 (2015). https://doi.org:10.1158/0008-5472.CAN-15-0287

89 Kleaveland, B., Shi, C. Y., Stefano, J. & Bartel, D. P. A Network of Noncoding Regulatory RNAs Acts in the Mammalian Brain. *Cell* **174**, 350-362 e317 (2018). https://doi.org:10.1016/j.cell.2018.05.022

90 Chen, S., Qin, R. & Mahal, L. K. Sweet systems: technologies for glycomic analysis and their integration into systems biology. *Crit Rev Biochem Mol Biol* **56**, 301-320 (2021). https://doi.org:10.1080/10409238.2021.1908953

91 Reily, C., Stewart, T. J., Renfrow, M. B. & Novak, J. Glycosylation in health and disease. *Nat Rev Nephrol* **15**, 346-366 (2019). https://doi.org:10.1038/s41581-019-0129-4

92 Agrawal, P. *et al.* Mapping posttranscriptional regulation of the human glycome uncovers microRNA defining the glycocode. *Proc Natl Acad Sci U S A* **111**, 4338-4343 (2014). https://doi.org:10.1073/pnas.1321524111

93 Liu, H. *et al.* mRNA and microRNA expression profiles of the NCI-60 integrated with drug activities. *Mol Cancer Ther* **9**, 1080-1091 (2010). https://doi.org:10.1158/1535-7163.MCT-09-0965

94 Thu, C. T. & Mahal, L. K. Sweet Control: MicroRNA Regulation of the Glycome. *Biochemistry* **59**, 3098-3110 (2020). https://doi.org:10.1021/acs.biochem.9b00784

95 Kurcon, T. *et al.* miRNA proxy approach reveals hidden functions of glycosylation. *Proc Natl Acad Sci U S A* **112**, 7327-7332 (2015). https://doi.org:10.1073/pnas.1502076112

96 Collins, B. E., Smith, B. A., Bengtson, P. & Paulson, J. C. Ablation of CD22 in ligand-deficient mice restores B cell receptor signaling. *Nat Immunol* **7**, 199-206 (2006). https://doi.org:10.1038/ni1283

97 Hennet, T., Chui, D., Paulson, J. C. & Marth, J. D. Immune regulation by the ST6Gal sialyltransferase. *Proc Natl Acad Sci U S A* **95**, 4504-4509 (1998). https://doi.org:10.1073/pnas.95.8.4504

98 Chakraborty, A. *et al.* ST6GAL1 sialyltransferase promotes acinar to ductal metaplasia and pancreatic cancer progression. *bioRxiv* (2022).

99 Dorsett, K. A. *et al.* Regulation of ST6GAL1 sialyltransferase expression in cancer cells. *Glycobiology* **31**, 530-539 (2021). https://doi.org:10.1093/glycob/cwaa110

100 Garnham, R., Scott, E., Livermore, K. E. & Munkley, J. ST6GAL1: A key player in cancer. *Oncol Lett* **18**, 983-989 (2019). https://doi.org:10.3892/ol.2019.10458

101 Lehoux, S. *et al.* Transcriptional regulation of the human ST6GAL2 gene in cerebral cortex and neuronal cells. *Glycoconj J* **27**, 99-114 (2010). https://doi.org:10.1007/s10719-009-9260-y

102 Krzewinski-Recchi, M. A. *et al.* Identification and functional expression of a second human beta-galactoside alpha2,6-sialyltransferase, ST6Gal II. *Eur J Biochem* **270**, 950-961 (2003). https://doi.org:10.1046/j.1432-1033.2003.03458.x

103 Takashima, S., Tsuji, S. & Tsujimoto, M. Characterization of the second type of human beta-galactoside alpha 2,6-sialyltransferase (ST6Gal II), which sialylates Galbeta 1,4GlcNAc structures on oligosaccharides preferentially. Genomic analysis of human sialyltransferase genes. *J Biol Chem* **277**, 45719-45728 (2002). https://doi.org:10.1074/jbc.M206808200
104 Xu, G. *et al.* Resveratrol Inhibits the Tumorigenesis of Follicular Thyroid Cancer via ST6GAL2-Regulated Activation of the Hippo Signaling Pathway. *Mol Ther Oncolytics* **16**, 124-133 (2020). https://doi.org:10.1016/j.omto.2019.12.010
105 Antony, P. *et al.* Epigenetic inactivation of ST6GAL1 in human bladder cancer. *BMC Cancer* **14**, 901 (2014). https://doi.org:10.1186/1471-2407-14-901
106 Irons, E. E., Punch, P. R. & Lau, J. T. Y. Blood-Borne ST6GAL1 Regulates Immunoglobulin Production in B Cells. *Front Immunol* **11**, 617 (2020). https://doi.org:10.3389/fimmu.2020.00617
107 Chakraborty, A. *et al.* ST6Gal-I sialyltransferase promotes chemoresistance in pancreatic ductal adenocarcinoma by abrogating gemcitabine-mediated DNA damage. *J Biol Chem* **293**, 984-994 (2018). https://doi.org:10.1074/jbc.M117.808584
108 Liu, R. *et al.* Downregulation of ST6GAL2 Correlates to Liver Inflammation and Predicts Adverse Prognosis in Hepatocellular Carcinoma. *J Inflamm Res* **17**, 565-580 (2024). https://doi.org:10.2147/JIR.S437291
109 Xu, L. *et al.* Transcriptional regulation of human beta-galactoside alpha2,6-sialyltransferase (hST6Gal I) gene in colon adenocarcinoma cell line. *Biochem Biophys Res Commun* **307**, 1070-1074 (2003). https://doi.org:10.1016/s0006-291x(03)01314-7
110 Svensson, E. C., Conley, P. B. & Paulson, J. C. Regulated expression of alpha 2,6-sialyltransferase by the liver-enriched transcription factors HNF-1, DBP, and LAP. *J Biol Chem* **267**, 3466-3472 (1992).
111 Bartel, D. P. Metazoan MicroRNAs. *Cell* **173**, 20-51 (2018). https://doi.org:10.1016/j.cell.2018.03.006
112 Lall, S. *et al.* A genome-wide map of conserved microRNA targets in C. elegans. *Curr Biol* **16**, 460-471 (2006). https://doi.org:10.1016/j.cub.2006.01.050
113 Lytle, J. R., Yario, T. A. & Steitz, J. A. Target mRNAs are repressed as efficiently by microRNA-binding sites in the 5' UTR as in the 3' UTR. *Proc Natl Acad Sci U S A* **104**, 9667-9672 (2007). https://doi.org:10.1073/pnas.0703820104
114 Du, B. *et al.* MicroRNA-545 suppresses cell proliferation by targeting cyclin D1 and CDK4 in lung cancer cells. *PLoS One* **9**, e88022 (2014). https://doi.org:10.1371/journal.pone.0088022
115 Peng, Y. & Croce, C. M. The role of MicroRNAs in human cancer. *Signal Transduct Target Ther* **1**, 15004 (2016). https://doi.org:10.1038/sigtrans.2015.4
116 Pinzon, N. *et al.* microRNA target prediction programs predict many false positives. *Genome Res* **27**, 234-245 (2017). https://doi.org:10.1101/gr.205146.116
117 Yun, C. & DasGupta, R. Luciferase reporter assay in Drosophila and mammalian tissue culture cells. *Curr Protoc Chem Biol* **6**, 7-23 (2014). https://doi.org:10.1002/9780470559277.ch130149
118 Boutz, D. R. *et al.* Two-tiered approach identifies a network of cancer and liver disease-related genes regulated by miR-122. *J Biol Chem* **286**, 18066-18078 (2011). https://doi.org:10.1074/jbc.M110.196451

119 Liang, L. *et al.* LncRNA HCP5 promotes follicular thyroid carcinoma progression via miRNAs sponge. *Cell Death Dis* **9**, 372 (2018). https://doi.org:10.1038/s41419-018-0382-7
120 Kleene, R. & Schachner, M. Glycans and neural cell interactions. *Nat Rev Neurosci* **5**, 195-208 (2004). https://doi.org:10.1038/nrn1349
121 Wang, J., Wang, L. & Zhang, C. miR-765 Acts as a Tumor Promoter and Indicates Poor Prognosis in Non-Small Cell Lung Cancer. *Onco Targets Ther* **14**, 4335-4343 (2021). https://doi.org:10.2147/OTT.S284212
122 Zhang, Z. *et al.* Integrating MicroRNA Expression Profiling Studies to Systematically Evaluate the Diagnostic Value of MicroRNAs in Pancreatic Cancer and Validate Their Prognostic Significance with the Cancer Genome Atlas Data. *Cell Physiol Biochem* **49**, 678-695 (2018). https://doi.org:10.1159/000493033
123 Wu, Z., Zhou, L., Ding, G. & Cao, L. Overexpressions of miR-212 are associated with poor prognosis of patients with pancreatic ductal adenocarcinoma. *Cancer Biomark* **18**, 35-39 (2017). https://doi.org:10.3233/CBM-160671
124 Su, A., He, S., Tian, B., Hu, W. & Zhang, Z. MicroRNA-221 mediates the effects of PDGF-BB on migration, proliferation, and the epithelial-mesenchymal transition in pancreatic cancer cells. *PLoS One* **8**, e71309 (2013). https://doi.org:10.1371/journal.pone.0071309
125 Buccitelli, C. & Selbach, M. mRNAs, proteins and the emerging principles of gene expression control. *Nat Rev Genet* **21**, 630-644 (2020). https://doi.org:10.1038/s41576-020-0258-4
126 Vogel, C. & Marcotte, E. M. Insights into the regulation of protein abundance from proteomic and transcriptomic analyses. *Nat Rev Genet* **13**, 227-232 (2012). https://doi.org:10.1038/nrg3185
127 Bojar, D. *et al.* A Useful Guide to Lectin Binding: Machine-Learning Directed Annotation of 57 Unique Lectin Specificities. *ACS Chem Biol* (2022). https://doi.org:10.1021/acschembio.1c00689
128 Shibuya, N. *et al.* The elderberry (Sambucus nigra L.) bark lectin recognizes the Neu5Ac(alpha 2-6)Gal/GalNAc sequence. *J Biol Chem* **262**, 1596-1601 (1987).
129 Cao, L. *et al.* Proteogenomic characterization of pancreatic ductal adenocarcinoma. *Cell* **184**, 5031-5052 e5026 (2021). https://doi.org:10.1016/j.cell.2021.08.023
130 Jame-Chenarboo, F., Ng, H. H., Macdonald, D. & Mahal, L. K. High-Throughput Analysis Reveals miRNA Upregulating alpha-2,6-Sialic Acid through Direct miRNA-mRNA Interactions. *ACS Cent Sci* **8**, 1527-1536 (2022). https://doi.org:10.1021/acscentsci.2c00748
131 Fang, C. *et al.* MiR-488 inhibits proliferation and cisplatin sensibility in non-small-cell lung cancer (NSCLC) cells by activating the eIF3a-mediated NER signaling pathway. *Sci Rep* **7**, 40384 (2017). https://doi.org:10.1038/srep40384
132 Ritchie, W., Flamant, S. & Rasko, J. E. mimiRNA: a microRNA expression profiler and classification resource designed to identify functional correlations between microRNAs and their targets. *Bioinformatics* **26**, 223-227 (2010). https://doi.org:10.1093/bioinformatics/btp649
133 Zhao, L., Jiang, P., Zheng, H., Chen, P. & Yang, M. Downregulation of miR-499a-5p Predicts a Poor Prognosis of Patients With Non-Small Cell Lung Cancer and Restrains the Tumorigenesis by Targeting Fibroblast Growth Factor 9. *Technol Cancer Res Treat* **19**, 1533033820957001 (2020). https://doi.org:10.1177/1533033820957001

134 Nguyen, H. T., Jia, W., Beedle, A. M., Kennedy, E. J. & Murph, M. M. Lysophosphatidic Acid Mediates Activating Transcription Factor 3 Expression Which Is a Target for Post-Transcriptional Silencing by miR-30c-2-3p. *PLoS One* **10**, e0139489 (2015). https://doi.org:10.1371/journal.pone.0139489
135 Gu, Y. *et al.* Suppression of endothelial miR-22 mediates non-small cell lung cancer cell-induced angiogenesis. *Mol Ther Nucleic Acids* **26**, 849-864 (2021). https://doi.org:10.1016/j.omtn.2021.10.003
136 Li, Q., Liu, S., Yan, J., Sun, M. Z. & Greenaway, F. T. The potential role of miR-124-3p in tumorigenesis and other related diseases. *Mol Biol Rep* **48**, 3579-3591 (2021). https://doi.org:10.1007/s11033-021-06347-4
137 Ge, L., Tan, W., Li, G., Gong, N. & Zhou, L. Circ_0026134 promotes NSCLC progression by the miR-3619-5p/CHAF1B axis. *Thorac Cancer* **13**, 582-592 (2022). https://doi.org:10.1111/1759-7714.14301
138 Kozuka, T. *et al.* miR-124 dosage regulates prefrontal cortex function by dopaminergic modulation. *Sci Rep* **9**, 3445 (2019). https://doi.org:10.1038/s41598-019-38910-2
139 Sanuki, R. *et al.* miR-124a is required for hippocampal axogenesis and retinal cone survival through Lhx2 suppression. *Nat Neurosci* **14**, 1125-1134 (2011). https://doi.org:10.1038/nn.2897
140 Place, R. F., Li, L. C., Pookot, D., Noonan, E. J. & Dahiya, R. MicroRNA-373 induces expression of genes with complementary promoter sequences. *Proc Natl Acad Sci U S A* **105**, 1608-1613 (2008). https://doi.org:10.1073/pnas.0707594105
141 Huang, V. in *RNA Activation* (ed Long-Cheng Li) 65-79 (Springer Singapore, 2017).
142 Rehmsmeier, M., Steffen, P., Hochsmann, M. & Giegerich, R. Fast and effective prediction of microRNA/target duplexes. *RNA* **10**, 1507-1517 (2004). https://doi.org:10.1261/rna.5248604
143 Vasudevan, S. & Steitz, J. A. AU-rich-element-mediated upregulation of translation by FXR1 and Argonaute 2. *Cell* **128**, 1105-1118 (2007). https://doi.org:10.1016/j.cell.2007.01.038
144 Vasudevan, S., Tong, Y. & Steitz, J. A. Switching from repression to activation: microRNAs can up-regulate translation. *Science* **318**, 1931-1934 (2007). https://doi.org:10.1126/science.1149460
145 Truesdell, S. S. *et al.* MicroRNA-mediated mRNA translation activation in quiescent cells and oocytes involves recruitment of a nuclear microRNP. *Sci Rep* **2**, 842 (2012). https://doi.org:10.1038/srep00842
146 Zhang, X. *et al.* MicroRNA directly enhances mitochondrial translation during muscle differentiation. *Cell* **158**, 607-619 (2014). https://doi.org:10.1016/j.cell.2014.05.047
147 McGeary, S. E. *et al.* The biochemical basis of microRNA targeting efficacy. *Science* **366** (2019). https://doi.org:10.1126/science.aav1741
148 Liu, J., Liu, Z. & Corey, D. R. The Requirement for GW182 Scaffolding Protein Depends on Whether Argonaute Is Mediating Translation, Transcription, or Splicing. *Biochemistry* **57**, 5247-5256 (2018). https://doi.org:10.1021/acs.biochem.8b00602
149 Bhattacharyya, S. N., Habermacher, R., Martine, U., Closs, E. I. & Filipowicz, W. Relief of microRNA-mediated translational repression in human cells subjected to stress. *Cell* **125**, 1111-1124 (2006). https://doi.org:10.1016/j.cell.2006.04.031
150 Kundu, P., Fabian, M. R., Sonenberg, N., Bhattacharyya, S. N. & Filipowicz, W. HuR protein attenuates miRNA-mediated repression by promoting miRISC dissociation from

the target RNA. *Nucleic Acids Res* **40**, 5088-5100 (2012). https://doi.org:10.1093/nar/gks148

151 Kawasaki, N., Rademacher, C. & Paulson, J. C. CD22 regulates adaptive and innate immune responses of B cells. *J Innate Immun* **3**, 411-419 (2011). https://doi.org:10.1159/000322375

152 Gaziel-Sovran, A. *et al.* miR-30b/30d regulation of GalNAc transferases enhances invasion and immunosuppression during metastasis. *Cancer Cell* **20**, 104-118 (2011). https://doi.org:10.1016/j.ccr.2011.05.027

153 Vaiana, C. A., Kurcon, T. & Mahal, L. K. MicroRNA-424 Predicts a Role for beta-1,4 Branched Glycosylation in Cell Cycle Progression. *J Biol Chem* **291**, 1529-1537 (2016). https://doi.org:10.1074/jbc.M115.672220

154 Kasper, D. M. *et al.* The N-glycome regulates the endothelial-to-hematopoietic transition. *Science* **370**, 1186-1191 (2020). https://doi.org:10.1126/science.aaz2121

155 Zhou, P. *et al.* Large-scale screens of miRNA-mRNA interactions unveiled that the 3'UTR of a gene is targeted by multiple miRNAs. *PLoS One* **8**, e68204 (2013). https://doi.org:10.1371/journal.pone.0068204

156 Chu, Y. *et al.* Argonaute binding within 3'-untranslated regions poorly predicts gene repression. *Nucleic Acids Res* **48**, 7439-7453 (2020). https://doi.org:10.1093/nar/gkaa478

157 Xu, Q. *et al.* miR-221/222 induces pancreatic cancer progression through the regulation of matrix metalloproteinases. *Oncotarget* **6**, 14153-14164 (2015). https://doi.org:10.18632/oncotarget.3686

158 Eulalio, A., Tritschler, F. & Izaurralde, E. The GW182 protein family in animal cells: new insights into domains required for miRNA-mediated gene silencing. *RNA* **15**, 1433-1442 (2009). https://doi.org:10.1261/rna.1703809

159 Agrawal, P., Chen, S., Pablos, A.D.,Jame-Chenarboo, F.,Vega, E.M.S.D.,Darvishian, F.,Osman, I.,Lujambio, A.,Mahal, L.K., Hernando, E. Integrated in vivo functional screens and multi-omics analyses identify a-2,3-sialylation as essential for melanoma maintenance. (2024). https://doi.org:10.1101/2024.03.08.584072

160 Fenczik, C. A. *et al.* Distinct domains of CD98hc regulate integrins and amino acid transport. *J Biol Chem* **276**, 8746-8752 (2001). https://doi.org:10.1074/jbc.M011239200

161 Ip, H. & Sethi, T. CD98 signals controlling tumorigenesis. *Int J Biochem Cell Biol* **81**, 148-150 (2016). https://doi.org:10.1016/j.biocel.2016.11.005

162 Cantor, J. *et al.* CD98hc facilitates B cell proliferation and adaptive humoral immunity. *Nat Immunol* **10**, 412-419 (2009). https://doi.org:10.1038/ni.1712

163 Cantor, J., Slepak, M., Ege, N., Chang, J. T. & Ginsberg, M. H. Loss of T cell CD98 H chain specifically ablates T cell clonal expansion and protects from autoimmunity. *J Immunol* **187**, 851-860 (2011). https://doi.org:10.4049/jimmunol.1100002

164 Cantor, J. M. & Ginsberg, M. H. CD98 at the crossroads of adaptive immunity and cancer. *J Cell Sci* **125**, 1373-1382 (2012). https://doi.org:10.1242/jcs.096040

165 Yagita, H., Masuko, T. & Hashimoto, Y. Inhibition of tumor cell growth in vitro by murine monoclonal antibodies that recognize a proliferation-associated cell surface antigen system in rats and humans. *Cancer Res* **46**, 1478-1484 (1986).

166 Ichinoe, M. *et al.* Prognostic values of L-type amino acid transporter 1 and CD98hc expression in breast cancer. *J Clin Pathol* **74**, 589-595 (2021). https://doi.org:10.1136/jclinpath-2020-206457

167 Kaira, K. *et al.* CD98 expression is associated with poor prognosis in resected non-small-cell lung cancer with lymph node metastases. *Ann Surg Oncol* **16**, 3473-3481 (2009). https://doi.org:10.1245/s10434-009-0685-0
168 Theodosakis, N. *et al.* Integrative discovery of CD98 as a melanoma biomarker. *Pigment Cell Melanoma Res* **29**, 385-387 (2016). https://doi.org:10.1111/pcmr.12464
169 Bajaj, J. *et al.* CD98-Mediated Adhesive Signaling Enables the Establishment and Propagation of Acute Myelogenous Leukemia. *Cancer Cell* **30**, 792-805 (2016). https://doi.org:10.1016/j.ccell.2016.10.003
170 Chandrasekaran, E. V. *et al.* Mammalian sialyltransferase ST3Gal-II: its exchange sialylation catalytic properties allow labeling of sialyl residues in mucin-type sialylated glycoproteins and specific gangliosides. *Biochemistry* **50**, 9475-9487 (2011). https://doi.org:10.1021/bi200301w
171 Priatel, J. J. *et al.* The ST3Gal-I sialyltransferase controls CD8+ T lymphocyte homeostasis by modulating O-glycan biosynthesis. *Immunity* **12**, 273-283 (2000). https://doi.org:10.1016/s1074-7613(00)80180-6
172 Dalziel, M. *et al.* The relative activities of the C2GnT1 and ST3Gal-I glycosyltransferases determine O-glycan structure and expression of a tumor-associated epitope on MUC1. *J Biol Chem* **276**, 11007-11015 (2001). https://doi.org:10.1074/jbc.M006523200
173 Walker, M. R. *et al.* O-linked alpha2,3 sialylation defines stem cell populations in breast cancer. *Sci Adv* **8**, eabj9513 (2022). https://doi.org:10.1126/sciadv.abj9513
174 Hong, Y. *et al.* ST3GAL1 and betaII-spectrin pathways control CAR T cell migration to target tumors. *Nat Immunol* **24**, 1007-1019 (2023). https://doi.org:10.1038/s41590-023-01498-x
175 Lin, C. W. *et al.* Homogeneous antibody and CAR-T cells with improved effector functions targeting SSEA-4 glycan on pancreatic cancer. *Proc Natl Acad Sci U S A* **118** (2021). https://doi.org:10.1073/pnas.2114774118
176 Gómez-Martínez, H., López, A., Gil, M.P., Hernando, E., García-García, F. Novel diagnosis and progression microRNA signatures in melanoma. (2023). https://doi.org:10.1101/2023.10.20.563284
177 Barshir, R. *et al.* GeneCaRNA: A Comprehensive Gene-centric Database of Human Non-coding RNAs in the GeneCards Suite. *J Mol Biol* **433**, 166913 (2021). https://doi.org:10.1016/j.jmb.2021.166913
178 Xia, P. & Dubrovska, A. CD98 heavy chain as a prognostic biomarker and target for cancer treatment. *Front Oncol* **13**, 1251100 (2023). https://doi.org:10.3389/fonc.2023.1251100
179 Ekiz, H. A. *et al.* MicroRNA-155 coordinates the immunological landscape within murine melanoma and correlates with immunity in human cancers. *JCI Insight* **4** (2019). https://doi.org:10.1172/jci.insight.126543
180 Peng, J., Liu, H. & Liu, C. MiR-155 Promotes Uveal Melanoma Cell Proliferation and Invasion by Regulating NDFIP1 Expression. *Technol Cancer Res Treat* **16**, 1160-1167 (2017). https://doi.org:10.1177/1533034617737923
181 Hua, K. *et al.* miR-135b, upregulated in breast cancer, promotes cell growth and disrupts the cell cycle by regulating LATS2. *Int J Oncol* **48**, 1997-2006 (2016). https://doi.org:10.3892/ijo.2016.3405
182 Hossain, A., Kuo, M. T. & Saunders, G. F. Mir-17-5p regulates breast cancer cell proliferation by inhibiting translation of AIB1 mRNA. *Mol Cell Biol* **26**, 8191-8201 (2006). https://doi.org:10.1128/MCB.00242-06

183 Cruz-Munoz, W., Man, S., Xu, P. & Kerbel, R. S. Development of a preclinical model of spontaneous human melanoma central nervous system metastasis. *Cancer Res* **68**, 4500-4505 (2008). https://doi.org:10.1158/0008-5472.CAN-08-0041
184 Stinson, S. *et al.* TRPS1 targeting by miR-221/222 promotes the epithelial-to-mesenchymal transition in breast cancer. *Sci Signal* **4**, ra41 (2011). https://doi.org:10.1126/scisignal.2001538
185 Kong, W. *et al.* Upregulation of miRNA-155 promotes tumour angiogenesis by targeting VHL and is associated with poor prognosis and triple-negative breast cancer. *Oncogene* **33**, 679-689 (2014). https://doi.org:10.1038/onc.2012.636
186 Lee, E. J. *et al.* Expression profiling identifies microRNA signature in pancreatic cancer. *Int J Cancer* **120**, 1046-1054 (2007). https://doi.org:10.1002/ijc.22394
187 Hoang, D. H. *et al.* MicroRNA networks in FLT3-ITD acute myeloid leukemia. *Proc Natl Acad Sci U S A* **119**, e2112482119 (2022). https://doi.org:10.1073/pnas.2112482119
188 Liu, F., Mao, Q., Zhu, S. & Qiu, J. MicroRNA-155-5p promotes cell proliferation and invasion in lung squamous cell carcinoma through negative regulation of fibroblast growth factor 9 expression. *J Thorac Dis* **13**, 3669-3679 (2021). https://doi.org:10.21037/jtd-21-882
189 Schjenken, J. E. *et al.* MicroRNA miR-155 is required for expansion of regulatory T cells to mediate robust pregnancy tolerance in mice. *Mucosal Immunol* **13**, 609-625 (2020). https://doi.org:10.1038/s41385-020-0255-0
190 Costinean, S. *et al.* Pre-B cell proliferation and lymphoblastic leukemia/high-grade lymphoma in E(mu)-miR155 transgenic mice. *Proc Natl Acad Sci U S A* **103**, 7024-7029 (2006). https://doi.org:10.1073/pnas.0602266103
191 Kudo, T. *et al.* Up-regulation of a set of glycosyltransferase genes in human colorectal cancer. *Lab Invest* **78**, 797-811 (1998).
192 Madunic, K. *et al.* Specific (sialyl-)Lewis core 2 O-glycans differentiate colorectal cancer from healthy colon epithelium. *Theranostics* **12**, 4498-4512 (2022). https://doi.org:10.7150/thno.72818
193 Li, D., Zhong, J., Zhang, G., Lin, L. & Liu, Z. Oncogenic Role and Prognostic Value of MicroRNA-937-3p in Patients with Breast Cancer. *Onco Targets Ther* **12**, 11045-11056 (2019). https://doi.org:10.2147/OTT.S229510
194 Lv, Y., Yang, H., Ma, X. & Wu, G. Strand-specific miR-28-3p and miR-28-5p have differential effects on nasopharyngeal cancer cells proliferation, apoptosis, migration and invasion. *Cancer Cell Int* **19**, 187 (2019). https://doi.org:10.1186/s12935-019-0915-x
195 Song, J. *et al.* Let-7i-5p inhibits the proliferation and metastasis of colon cancer cells by targeting kallikrein-related peptidase 6. *Oncol Rep* **40**, 1459-1466 (2018). https://doi.org:10.3892/or.2018.6577
196 Wang, X. *et al.* Circulating exosomal miR-363-5p inhibits lymph node metastasis by downregulating PDGFB and serves as a potential noninvasive biomarker for breast cancer. *Mol Oncol* **15**, 2466-2479 (2021). https://doi.org:10.1002/1878-0261.13029
197 Ribeiro, J. P. *et al.* Characterization of a high-affinity sialic acid-specific CBM40 from Clostridium perfringens and engineering of a divalent form. *Biochem J* **473**, 2109-2118 (2016). https://doi.org:10.1042/BCJ20160340
198 Yu, Y., Yu, F. & Sun, P. MicroRNA-1246 Promotes Melanoma Progression Through Targeting FOXA2. *Onco Targets Ther* **13**, 1245-1253 (2020). https://doi.org:10.2147/OTT.S234276

199 Haynes, B. F. *et al.* Characterization of a monoclonal antibody (4F2) that binds to human monocytes and to a subset of activated lymphocytes. *J Immunol* **126**, 1409-1414 (1981).
200 Mayr, C. Evolution and Biological Roles of Alternative 3'UTRs. *Trends Cell Biol* **26**, 227-237 (2016). https://doi.org:10.1016/j.tcb.2015.10.012
201 Mayr, C. Regulation by 3'-Untranslated Regions. *Annu Rev Genet* **51**, 171-194 (2017). https://doi.org:10.1146/annurev-genet-120116-024704
202 Bartel, D. P. MicroRNAs: target recognition and regulatory functions. *Cell* **136**, 215-233 (2009). https://doi.org:10.1016/j.cell.2009.01.002
203 Helwak, A., Kudla, G., Dudnakova, T. & Tollervey, D. Mapping the human miRNA interactome by CLASH reveals frequent noncanonical binding. *Cell* **153**, 654-665 (2013). https://doi.org:10.1016/j.cell.2013.03.043
204 Bartel, D. P. & Chen, C. Z. Micromanagers of gene expression: the potentially widespread influence of metazoan microRNAs. *Nat Rev Genet* **5**, 396-400 (2004). https://doi.org:10.1038/nrg1328
205 Gurtan, A. M. & Sharp, P. A. The role of miRNAs in regulating gene expression networks. *J Mol Biol* **425**, 3582-3600 (2013). https://doi.org:10.1016/j.jmb.2013.03.007
206 Console, L. *et al.* N-glycosylation is crucial for trafficking and stability of SLC3A2 (CD98). *Sci Rep* **12**, 14570 (2022). https://doi.org:10.1038/s41598-022-18779-4
207 Taniguchi , N., Honke, K., Fukuda, M., Narimatsu, H.,Yamaguchi, Y., Angata, T. *Handbook of Glycosyltransferases and Related Genes*. Second edn, (Springer, 2014).
208 Kolter, T. Ganglioside biochemistry. *ISRN Biochem* **2012**, 506160 (2012). https://doi.org:10.5402/2012/506160
209 Simpson, M. A. *et al.* Infantile-onset symptomatic epilepsy syndrome caused by a homozygous loss-of-function mutation of GM3 synthase. *Nat Genet* **36**, 1225-1229 (2004). https://doi.org:10.1038/ng1460
210 Fragaki, K. *et al.* Refractory epilepsy and mitochondrial dysfunction due to GM3 synthase deficiency. *Eur J Hum Genet* **21**, 528-534 (2013). https://doi.org:10.1038/ejhg.2012.202
211 Li, T. A. & Schnaar, R. L. Congenital Disorders of Ganglioside Biosynthesis. *Prog Mol Biol Transl Sci* **156**, 63-82 (2018). https://doi.org:10.1016/bs.pmbts.2018.01.001
212 Yamashita, T. *et al.* Enhanced insulin sensitivity in mice lacking ganglioside GM3. *Proc Natl Acad Sci U S A* **100**, 3445-3449 (2003). https://doi.org:10.1073/pnas.0635898100
213 Gu, Y. *et al.* Silencing of GM3 synthase suppresses lung metastasis of murine breast cancer cells. *Breast Cancer Res* **10**, R1 (2008). https://doi.org:10.1186/bcr1841
214 Noguchi, M. *et al.* GM3 synthase gene is a novel biomarker for histological classification and drug sensitivity against epidermal growth factor receptor tyrosine kinase inhibitors in non-small cell lung cancer. *Cancer Sci* **98**, 1625-1632 (2007). https://doi.org:10.1111/j.1349-7006.2007.00578.x
215 Tian, L. *et al.* C-Myc-induced hypersialylation of small cell lung cancer facilitates pro-tumoral phenotypes of macrophages. *iScience* **26**, 107771 (2023). https://doi.org:10.1016/j.isci.2023.107771
216 Wang, P. *et al.* GM3 suppresses anchorage-independent growth via Rho GDP dissociation inhibitor beta in melanoma B16 cells. *Cancer Sci* **102**, 1476-1485 (2011). https://doi.org:10.1111/j.1349-7006.2011.01963.x
217 Shimizu, T. *et al.* Tumor hypoxia regulates ganglioside GM3 synthase, which contributes to oxidative stress resistance in malignant melanoma. *Biochim Biophys Acta Gen Subj* **1864**, 129723 (2020). https://doi.org:10.1016/j.bbagen.2020.129723

218 Ouyang, S., Liu, J. H., Ni, Z., Ding, G. F. & Wang, Q. Z. Downregulation of ST3GAL5 is associated with muscle invasion, high grade and a poor prognosis in patients with bladder cancer. *Oncol Lett* **20**, 828-840 (2020). https://doi.org:10.3892/ol.2020.11597
219 Wang, H. *et al.* Antitumor effects of exogenous ganglioside GM3 on bladder cancer in an orthotopic cancer model. *Urology* **81**, 210 e211-215 (2013). https://doi.org:10.1016/j.urology.2012.08.015
220 Kawashima, N., Nishimiya, Y., Takahata, S. & Nakayama, K. I. Induction of Glycosphingolipid GM3 Expression by Valproic Acid Suppresses Cancer Cell Growth. *J Biol Chem* **291**, 21424-21433 (2016). https://doi.org:10.1074/jbc.M116.751503
221 Hakomori, S. I. & Handa, K. GM3 and cancer. *Glycoconj J* **32**, 1-8 (2015). https://doi.org:10.1007/s10719-014-9572-4
222 Guan, F., Handa, K. & Hakomori, S. I. Specific glycosphingolipids mediate epithelial-to-mesenchymal transition of human and mouse epithelial cell lines. *Proc Natl Acad Sci U S A* **106**, 7461-7466 (2009). https://doi.org:10.1073/pnas.0902368106
223 Li, N. *et al.* MiR-106b and miR-93 regulate cell progression by suppression of PTEN via PI3K/Akt pathway in breast cancer. *Cell Death Dis* **8**, e2796 (2017). https://doi.org:10.1038/cddis.2017.119
224 Wei, K. *et al.* MiR-106b-5p Promotes Proliferation and Inhibits Apoptosis by Regulating BTG3 in Non-Small Cell Lung Cancer. *Cell Physiol Biochem* **44**, 1545-1558 (2017). https://doi.org:10.1159/000485650
225 Jamshidi, M. *et al.* High miR-30 Expression Associates with Improved Breast Cancer Patient Survival and Treatment Outcome. *Cancers (Basel)* **13** (2021). https://doi.org:10.3390/cancers13122907
226 Londin, E. *et al.* Analysis of 13 cell types reveals evidence for the expression of numerous novel primate- and tissue-specific microRNAs. *Proc Natl Acad Sci U S A* **112**, E1106-1115 (2015). https://doi.org:10.1073/pnas.1420955112
227 Barrett, L. W., Fletcher, S. & Wilton, S. D. Regulation of eukaryotic gene expression by the untranslated gene regions and other non-coding elements. *Cell Mol Life Sci* **69**, 3613-3634 (2012). https://doi.org:10.1007/s00018-012-0990-9
228 Liu, Y., Beyer, A. & Aebersold, R. On the Dependency of Cellular Protein Levels on mRNA Abundance. *Cell* **165**, 535-550 (2016). https://doi.org:10.1016/j.cell.2016.03.014
229 Kavakiotis, I., Alexiou, A., Tastsoglou, S., Vlachos, I. S. & Hatzigeorgiou, A. G. DIANA-miTED: a microRNA tissue expression database. *Nucleic Acids Res* **50**, D1055-D1061 (2022). https://doi.org:10.1093/nar/gkab733
230 Livingston, P. O. *et al.* Vaccines containing purified GM2 ganglioside elicit GM2 antibodies in melanoma patients. *Proc Natl Acad Sci U S A* **84**, 2911-2915 (1987). https://doi.org:10.1073/pnas.84.9.2911
231 Baz, R. C., Zonder, J. A., Gasparetto, C., Reu, F. J. & Strout, V. Phase I Study of Anti-GM2 Ganglioside Monoclonal Antibody BIW-8962 as Monotherapy in Patients with Previously Treated Multiple Myeloma. *Oncol Ther* **4**, 287-301 (2016). https://doi.org:10.1007/s40487-016-0034-y
232 Majzner, R. G. *et al.* GD2-CAR T cell therapy for H3K27M-mutated diffuse midline gliomas. *Nature* **603**, 934-941 (2022). https://doi.org:10.1038/s41586-022-04489-4
233 Inokuchi, J. GM3 and diabetes. *Glycoconj J* **31**, 193-197 (2014). https://doi.org:10.1007/s10719-013-9516-4

234 Yanagisawa, K. GM1 ganglioside and Alzheimer's disease. *Glycoconj J* **32**, 87-91 (2015). https://doi.org:10.1007/s10719-015-9579-5
235 Yanagisawa, K., Odaka, A., Suzuki, N. & Ihara, Y. GM1 ganglioside-bound amyloid beta-protein (A beta): a possible form of preamyloid in Alzheimer's disease. *Nat Med* **1**, 1062-1066 (1995). https://doi.org:10.1038/nm1095-1062
236 Inokuchi, J. I. & Nagafuku, M. Gangliosides in T cell development and function of mice. *Glycoconj J* **39**, 229-238 (2022). https://doi.org:10.1007/s10719-021-10037-5
237 Chang, T. C. *et al.* Widespread microRNA repression by Myc contributes to tumorigenesis. *Nat Genet* **40**, 43-50 (2008). https://doi.org:10.1038/ng.2007.30
238 Ouzounova, M. *et al.* MicroRNA miR-30 family regulates non-attachment growth of breast cancer cells. *BMC Genomics* **14**, 139 (2013). https://doi.org:10.1186/1471-2164-14-139
239 Li, N. *et al.* MicroRNA-106b targets FUT6 to promote cell migration, invasion, and proliferation in human breast cancer. *IUBMB Life* **68**, 764-775 (2016). https://doi.org:10.1002/iub.1541
240 Zheng, R. *et al.* Prognostic value of miR-106b expression in breast cancer patients. *J Surg Res* **195**, 158-165 (2015). https://doi.org:10.1016/j.jss.2014.12.035
241 Kim, S. J. *et al.* Ganglioside GM3 participates in the TGF-beta1-induced epithelial-mesenchymal transition of human lens epithelial cells. *Biochem J* **449**, 241-251 (2013). https://doi.org:10.1042/BJ20120189
242 Bremer, E. G., Schlessinger, J. & Hakomori, S. Ganglioside-mediated modulation of cell growth. Specific effects of GM3 on tyrosine phosphorylation of the epidermal growth factor receptor. *J Biol Chem* **261**, 2434-2440 (1986).
243 Danzi, F. *et al.* To metabolomics and beyond: a technological portfolio to investigate cancer metabolism. *Signal Transduct Target Ther* **8**, 137 (2023). https://doi.org:10.1038/s41392-023-01380-0
244 Nascentes Melo, L. M., Lesner, N. P., Sabatier, M., Ubellacker, J. M. & Tasdogan, A. Emerging metabolomic tools to study cancer metastasis. *Trends Cancer* **8**, 988-1001 (2022). https://doi.org:10.1016/j.trecan.2022.07.003
245 Shestakova, K. M. *et al.* Targeted metabolomic profiling as a tool for diagnostics of patients with non-small-cell lung cancer. *Sci Rep* **13**, 11072 (2023). https://doi.org:10.1038/s41598-023-38140-7
246 Spratlin, J. L., Serkova, N. J. & Eckhardt, S. G. Clinical applications of metabolomics in oncology: a review. *Clin Cancer Res* **15**, 431-440 (2009). https://doi.org:10.1158/1078-0432.CCR-08-1059
247 Kohnz, R. A. *et al.* Protein Sialylation Regulates a Gene Expression Signature that Promotes Breast Cancer Cell Pathogenicity. *ACS Chem Biol* **11**, 2131-2139 (2016). https://doi.org:10.1021/acschembio.6b00433
248 Teoh, S. T., Ogrodzinski, M. P., Ross, C., Hunter, K. W. & Lunt, S. Y. Sialic Acid Metabolism: A Key Player in Breast Cancer Metastasis Revealed by Metabolomics. *Front Oncol* **8**, 174 (2018). https://doi.org:10.3389/fonc.2018.00174
249 Cornelissen, L. A. M. *et al.* Disruption of sialic acid metabolism drives tumor growth by augmenting CD8(+) T cell apoptosis. *Int J Cancer* **144**, 2290-2302 (2019). https://doi.org:10.1002/ijc.32084
250 Murugaesu, N. *et al.* An in vivo functional screen identifies ST6GalNAc2 sialyltransferase as a breast cancer metastasis suppressor. *Cancer Discov* **4**, 304-317 (2014). https://doi.org:10.1158/2159-8290.CD-13-0287

251 Wang, B. Sialic acid is an essential nutrient for brain development and cognition. *Annu Rev Nutr* **29**, 177-222 (2009). https://doi.org:10.1146/annurev.nutr.28.061807.155515
252 Linder, A. T. *et al.* Sialic acids on B cells are crucial for their survival and provide protection against apoptosis. *Proc Natl Acad Sci U S A* **119**, e2201129119 (2022). https://doi.org:10.1073/pnas.2201129119
253 Sellmeier, M., Weinhold, B. & Munster-Kuhnel, A. CMP-Sialic Acid Synthetase: The Point of Constriction in the Sialylation Pathway. *Top Curr Chem* **366**, 139-167 (2015). https://doi.org:10.1007/128_2013_477
254 Dobie, C. & Skropeta, D. Insights into the role of sialylation in cancer progression and metastasis. *Br J Cancer* **124**, 76-90 (2021). https://doi.org:10.1038/s41416-020-01126-7
255 Filipsky, F. & Laubli, H. Regulation of sialic acid metabolism in cancer. *Carbohydr Res* **539**, 109123 (2024). https://doi.org:10.1016/j.carres.2024.109123
256 Stanczak, M. A. *et al.* Targeting cancer glycosylation repolarizes tumor-associated macrophages allowing effective immune checkpoint blockade. *Sci Transl Med* **14**, eabj1270 (2022). https://doi.org:10.1126/scitranslmed.abj1270
257 Badr, H. A. *et al.* Nutrient-deprived cancer cells preferentially use sialic acid to maintain cell surface glycosylation. *Biomaterials* **70**, 23-36 (2015). https://doi.org:10.1016/j.biomaterials.2015.08.020
258 Aparicio-Puerta, E. *et al.* miEAA 2023: updates, new functional microRNA sets and improved enrichment visualizations. *Nucleic Acids Res* **51**, W319-W325 (2023). https://doi.org:10.1093/nar/gkad392
259 Jiang, G. *et al.* CD146 promotes metastasis and predicts poor prognosis of hepatocellular carcinoma. *J Exp Clin Cancer Res* **35**, 38 (2016). https://doi.org:10.1186/s13046-016-0313-3
260 Varki, A., Esko, J. D. & Colley, K. J. in *Essentials of Glycobiology* (eds A. Varki *et al.*) (2009).
261 Moutabian, H. *et al.* MicroRNA-155 and cancer metastasis: Regulation of invasion, migration, and epithelial-to-mesenchymal transition. *Pathol Res Pract* **250**, 154789 (2023). https://doi.org:10.1016/j.prp.2023.154789
262 Maciak, K., Dziedzic, A., Miller, E. & Saluk-Bijak, J. miR-155 as an Important Regulator of Multiple Sclerosis Pathogenesis. A Review. *Int J Mol Sci* **22** (2021). https://doi.org:10.3390/ijms22094332
263 Wang, L. & Liang, Y. MicroRNAs as T Lymphocyte Regulators in Multiple Sclerosis. *Front Mol Neurosci* **15**, 865529 (2022). https://doi.org:10.3389/fnmol.2022.865529
264 Cantor, J. M. CD98 is a potential target for ablating B cell clonal expansion and autoantibody in multiple sclerosis. *J Neuroimmunol* **274**, 230-233 (2014). https://doi.org:10.1016/j.jneuroim.2014.06.015

Appendix A

Maps and Sequences of pFmiR-3'UTRs

A.1 pFmiR-ST6GAL1 map and ST6GAL1 3'UTR sequence

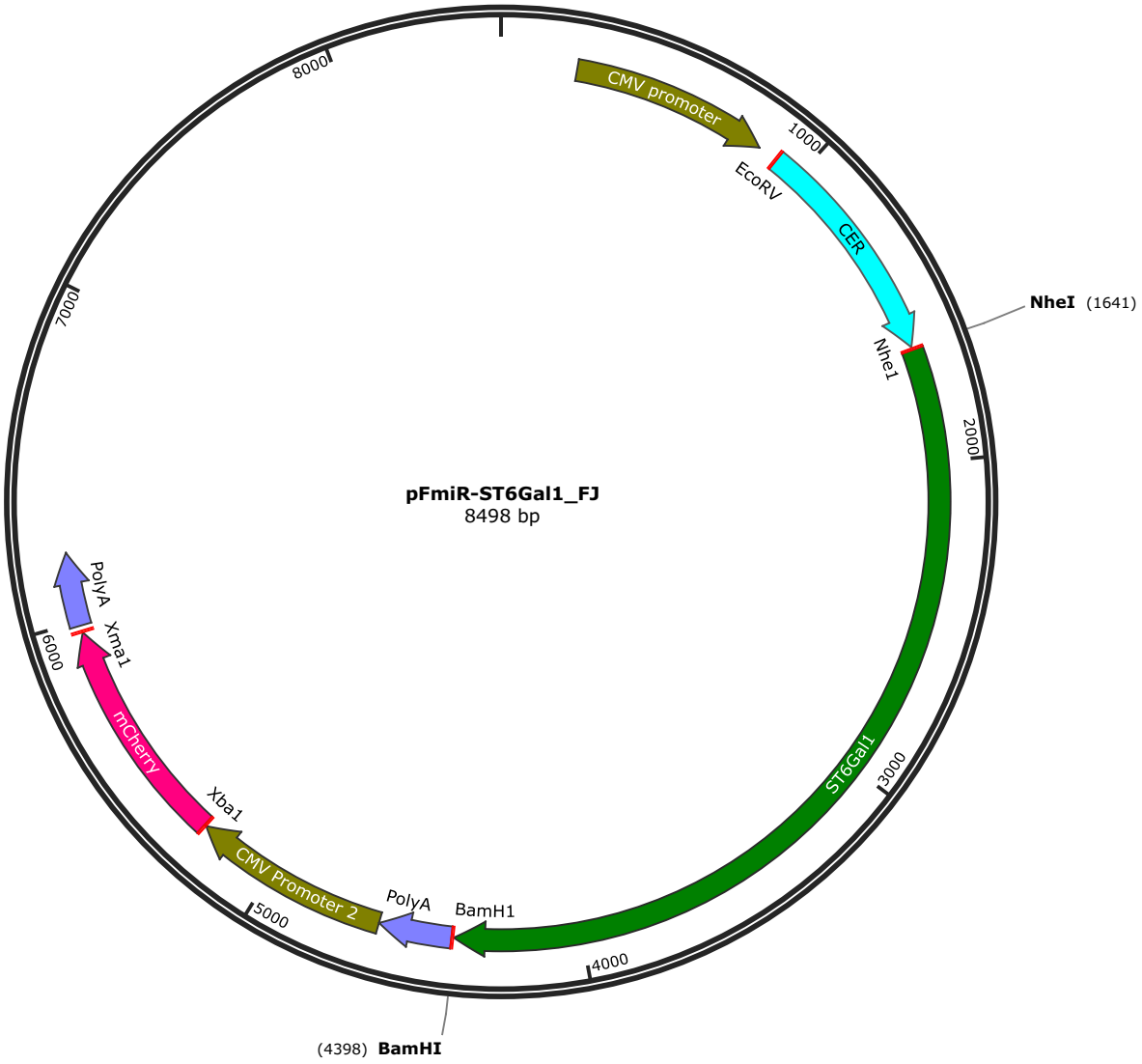

5’GCACAGGCTCCTCACTCTTCTCCATCAGGCATTAAATGAATGGTCTCTTGGCCACCCCAGCCTGGGAAGAACATTTTCCTGAACA
ATTCCAGCCTGCTCCTTTTACTCTAGGGGCCTCTGTCAGCAAGACCATGGGGACTTCAAGAGCCTGTGGTCAGGAAATCAGGTCCA
GCCTTCCCTGTAGCCAGACAGTTTATGAGCCCAGAGCCTCCTGCCACACACATGCACACATATCTAGCATTCTTTCCAGACAGCAT
CCTCCCCGCCTTCCACCTTGGTAGATGCAAGGTCTATCTCTCCCATCAGGGCTGCCAAAGCTGGGCTTTGTTTTTCCCAGCAGAAT
GATGCCATTCTCACAAACCAATGCTCTATATTGCTTGAAGTCTGCATCTAAATATTGATTTCACGTTTTAAAGAAATTCTCTTAAAT
TACAATTGTGCCCAATGCAGGGTGGCTCTGGGGGGCAAGTAGGTGGTACAGGGGATTGGAAACATGCTCCGCGCCTCCAGAGAA
AAGTTGCTCCCGAGGTCCATGCCCCTGGAACGTGTTCCTATCACTCTGGCTGGTTGGGCTGGTCCTTAGACTGGGTGCTTATGATT
AAAGGGTCTTGGTTAGCCCACTTTCCCTCTCCATGTGGAGATGGAAGGTAGAGAAGGATACAGTGTCTATCCTCAAGTTGCTACG
GTTCAGTGAGAGAGGCAGACATCTGAACAGGCAGGTAGGATTCAGTGTGCTCAGTGCACTGGGGATTTGGAGAGAGATGGGCTT
GCTCTCTCTGTGCACCCAGGAGGGCCACGCACTTAAAACTGTGTTTGTGGATCAGAGAAGGCTTTATAGCACAGGGGGCATTCAG
ATGAGTCTTAGAGGAAGAGAAGAAACATGGCAAGCAGATTACATCTGAGCCGTTTGAATTGTGTTTTTCTTTCTTCCCATGTTTAT
TTTCTAAGATCTACCTGAACTTAGAGACTCAAGATATTTTTTTAGGAAACCTCCTACCCATGTCTGAGGTAGCAAGTGCAGCCTCA
CGACAGATACCAGGCAATCCAGAGCCACAAAACGTGATTCCTCCAGGCTCTGCCTGGCCTGACCCTGTCCTGTCAGCTGGGTTTA
CATACCAGTCCCATTCTTCCTTTTCAATACCTACCCCCAAATCTTCTCCTAACCACCATCTGTTTTTTTTTTTTAAAGCATTTTTTGCT
TTAAAAGCATCCTGACCCCAATTTCTTTGAGCTCACGGGCCTTTTGCTGAAGGTCTCTCAGGGTGTAGTGGTGTGGCTCTCTGGAC

TTAACGTCACTCTCAGAGGTCAGAACCTTGGAGATCAGAACTGATTCTCACCAGGTGTGAGAGGTGTGGTAGCAGATTGCAATGC
TCTGCACCTCTTCCTTGCAAGTGAGCAACTTCAGGCTCTCTGGGCAGAGGCTGGCCCACTGTAGTTTGCAGACATGCTCTCCAGAT
GGTTTTACTAAGTCCCCTCTCCCTGATAGGGAATCCTGCTGGACCAGCGCAGCCCTGGTGTGGAGAGGTTAAAAGACTTGCACAG
GATCACCAAGTCATGCTGTAGAGCCAGGATTCCTAGACCCAGGGCTCTGCACTCTCAAGGCTGGCCCCATGTGCTCAAGGGGATC
TAATGTTTGGGCTCCAAACTAACCATCTCGGAGCTGGGCTCCTCATTTACTGCCAAACCCTCAGCTTATGTAGCTAGAAAGGGCCC
TGGAGTGAGAAAGCCTGGATTTTCAAATTGATGCTCCCCTACTGACTAGCTGTGCCACTCTGGGCAAATGCTCTTCCTTGAGCCTG
TTTCCACACCTGTAAAGTGGGGATGATGATCCTATCTCACTGCTTTTGTGAGGATTACAGGAAAGCACCTGTCCTGGCTCTGTACC
TGGCACGTAGTAGGTGCTCAGTTCATGCTGGTTTCCTTCCTGCCTTTAGTAGGGACCTGCTCTGTGCTCACACCTCGGCTGCATGCA
CCCTGCTGTGACGGAGGCTAGTGTGGAAGAGGTCCTGTCCTCAGGGAATTAACTGTCTTATTGGGAGACAACAACTGTCCTCCTTG
GAACACCCAAGAAACCATGCAAAGCAGTGGACAACACAGAACACGCCCTCCTCCTCGCTGCCTGCAGCTCCAATCTGATTCTGCT
TGGGAATGGGCGGAGCACGTGGGCTGCTTAACTGCTGTATAGGACAAGCCCCTTACCCCTCTCTGGGCCCATGAATTCCTGGCTTG
GTTTATGTTCTGATTTGACACACTGATTTTAATCTTCGAATCATGACACTGAGTGCAGAGGAGGTGGCATTCCGACAGCAGGACAT
ACATGTTGGTGTGAAGACTGGGACGACACTGGGTAGAATCTAGTTTTTAATTATTATTAATATAAAGGATCAAATTAATTTAAATA
TGATTCTGAAGTCTACAGAACTTTTAGTTCTGTGCTGTCTATGTGGACACTTTGGTAAAATGCAAATTATGATATGGACGTTATCAT
TGGTCTGGTGAGATGTTTCATATTTGTGACAGTTAATTTAAAAATTATGAGTTAATGCTGCCTGTGTCTATGGGGTTCTGTCTTCTT
TGATAGCCATCTATTCATCTGGATCATGGGACCCTCTCTAATCCTTCCACCAATCAAATAAGCTATTGCTATTGGTTTGGAGTTGAG
ATATCAGTCTCGGAAACTTCTGAAAAATGCTAATAATTACCCAAGGATTATGTCAAATTTTAAAATAAATGTGTGTGTGTTTCTTT
AA 3’

A.2 pFmiR-ST6GAL2 map and ST6GAL2 3'UTR sequence

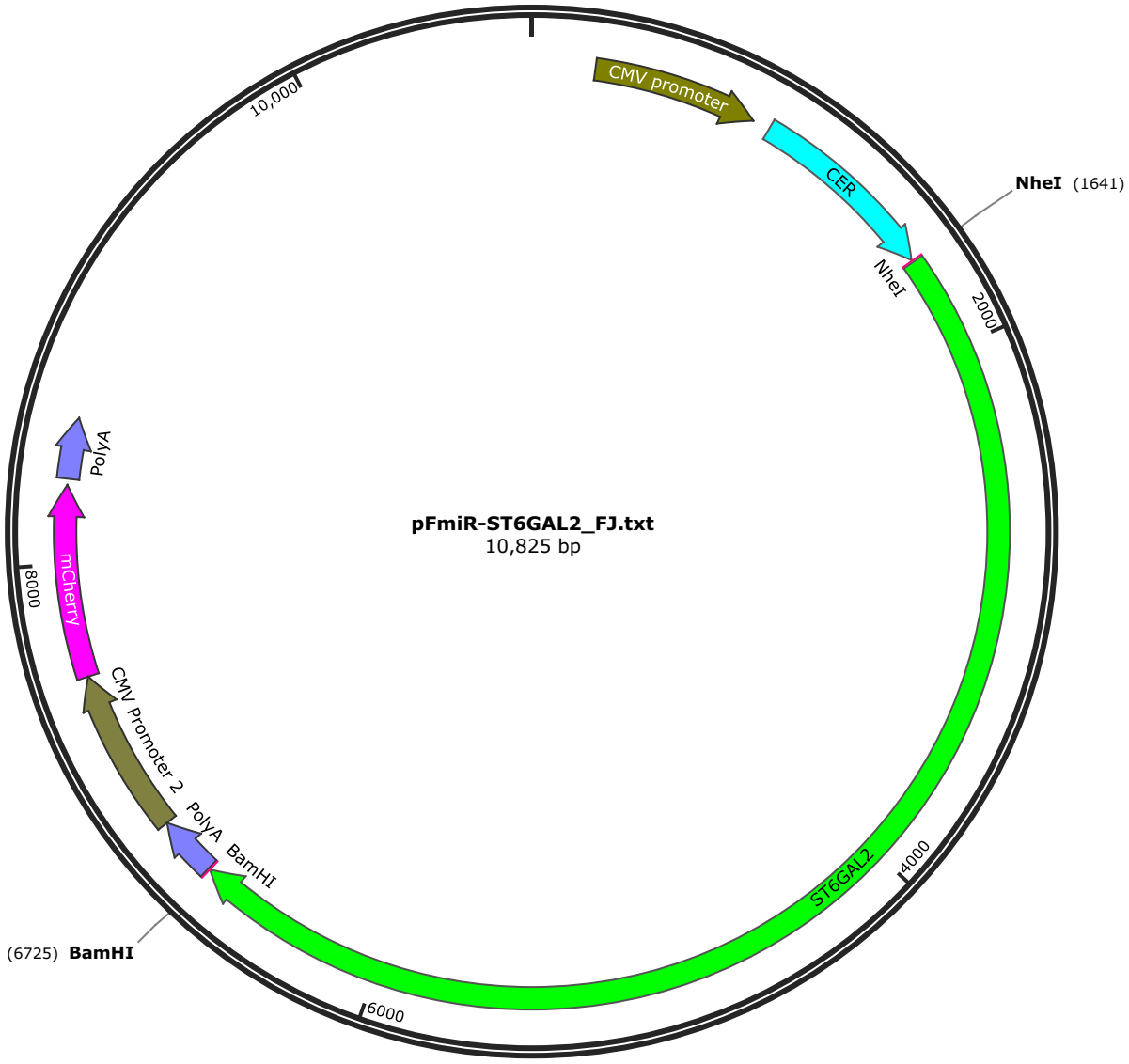

5'AAAGGGTTTCTTGGGAATCAATGTGCAATAAGGTACTACTGTTGTACTCAAAGTCACAAAAGAATACTTGAAGATAGATTTTAG
ACAGTGTAGTTTTGAGTCTTTAAACAGTAATTTAGTGGTGGTCATGATAATCCTTCTCTTTCTAAGCCATTGAGTATGTATTACTGC
TTTGAACATAGAAATGGTTTTTTTAAAAAAATAAGGCTCAAGAAAGATGCAAAACCAAGGATAGCTAGAAAGAAAACACATGTA
TGACCATGGGTATGATACCTCCAGAAATGTTAACAACTTATTCTTCTGCCATGAGTACCCCTCATCAGGGTTGGTTTCAATGACAG
GTTTTGGTGATGTTCCTGACCATATGAAGTGGTTTATGTTTAGAAACATTCAAATTGAGGGACATCATTTACAGCATCGAGTGTGT
CAGTTATACATGCATTCATCATTAAATATCCTAGGTTTTATGACAGACATTGAAATTATCACTCAGATGTGTTTAACAGCAAAAAA
TTCCCAGCACATCCTGGCAAAGGCTTTTATTTCCAACCGTTGCATTCTTCATCTCTGCCTCCCATTGCCCACTGAATGCTTTGCTTTC
TGTGCATCAAGACAGAGTTCTAAAACCAGAAAACATCCATCTTGAAAGGTCCAAGAAAAAGCCAAATTCCATATAGCACCACAG
AGGAGGCCCTTTGTTTCCCTGCAGTATTTCAACCAGGAACATTAGTATCACATCCACCAGGAGGCACATCACTGGCAAGTAACAT
AGAATCACAGGGCTGCAGGTGCCCCTGGACACTCCCCGGTTCTGGCTTTTCTGCCTTGTACCTCCTCACCTGCAGATCTACCCTGC
AGCTTTTGCATAGTCAGTGACACACTTGACAATTGGCACAGCTGTGCTGGGGAAGACGGGAGACACCTTGCTCCTTCCAAACTAG
AAGGAAAGATTTTGGAGCCATCACCCTGTGCTTCTAGGGATGCACGCCTGTCTTTATTATACAGGTTTCTTGCAGGTTTTTATCAGC
CAGTGGGAACTCCACAGTGATGAGCACTGAATCTTCACTAAATCTTCCTACAGACATTTAGGAATCCAGTCCTTGCTTTTGCAGAT
ATGTTTTATGTCAGCAGCATGACAAAGCCATATAATTAAATAATTTATGTGAAAGCATTGCTTATTAACAAGGAAAATATGTAGAT
GCTTCAGAGGGAAAGGCAGCTAGAGGGAAATTTTCATCCCAATATGTTAGCTATATTCAGGGTTGATTTTTTCTTTAATCTCAACT
GTCACTGATACATTGAAAAATTTTTGCTATGAATATAGTGAAACAGAAACATTCTGTAATACCTTAATTAAACATGCTATTATTTC

AATGTATAACCAAAACATATCTCCATGGTACAGTTAAGACTTGTTGCAATGACAATAGCAGCTTAATTAAATGCGTTCTCCCTTGC
AAAATGTATGAATGTCAGGAGAGTTTAGTGGAAAAGTTTTCTTTGTTTCAGGATTGGTTTCTTCTAGACTGTTCTCAGGACTACTTT
CTTGAGCAAGAATGGCTTACAGAGACTGAAGGCTTCTGTTTGGTTAGTCTATTCAGCAGATATGGAGCTGGAAAACAAGACATCT
CCTATAGCTTGCTATAATAGTGAAGGAGAAATTGGAAAGTTTTAATCACAATAATATCCAATAAAAGCCCATTTTGAGAGTTTTGT
TATTAAGTCAATGAGAAGGGATAGGTAACTTTGTCCTATATATTAACTTATGTCTAAATAGACATGGTTAAGCCATGTTCCTTTCT
AATTTCTTTTCTTTTCTTTTTTTTTTTTTTTTTTGAGACAGTCTCTCGCTCTGTCGCCCAGGCTAGAGTGCAGTGGTGCGATCTTGGTT
CACTGCCAGCTCTGCCTCCCACGTTCACACCATTCTCCTGCCTCAGCCTCCTGAGTAGCTGGGGACTACAGGCACCCGCCACCACG
CCCAGCTAATTTTTTGTATTTTTAGTAGAGACAGGGTTTCACCGTGTTAGCCAGGGTGGTCTCGATCTCCTGACCTTGTGATCTGCC
TGCCTCGGCCTCCCAAAGTGATGGGATTATAGGCGTGAGCCACCACCGCGCCCGGTCATTCCTTTCTAATTTCTTGAAAAAACTTT
GTCTTGTCCTTATGTTTACATGTGTGTAATAATTTCAGCAACTCTGGAATGTGGGTGAGGTGGCTGTGGTGGATGAATATTACTCC
CTACCCTCCTTGGATCTTTCTAGATCTTCCAGACCATTAAATGCCCCTGAAGCTCCTTTTATAGTTTTGCAAGTGGATTTACTTGTA
GACATCCTTACTATCCAGCATAATCCCCCTTGGCTGACATGAGAACTTGGTTAGAGGAGAATTTATTGGGGTCAGTGTAAATATTC
AAGTTCAAAAGCCTCAGAACCCAACACTTTAAAGATTTTTAAATGGAATTTTGTCGTAGTCATTGTACTTTTAAAATAGTACTTTC
AGTTTCATTGAGGTTACAAGAAAGACTGAAGAGTACAAAGGAAATTTAGTTACAATTTTTGCATTTATTATGGCCTTAAAGACTCT
TGGGAATCAGGCTCTGTTCAACAGTCAATAAATGTAATACACACATTAATATAGTACTGACTGGGCGTTCTTCTATAAAAGTTTAA
GTTCTTTGGCTTCTAAGAAAATGTTGGGCAGTTACAGTTAACTTGATGACTACTTCTAGTATTAGCCAAATGGGTCCTAAGTGGCA
GCATTTTGCCAGACATTGACTAAATCCTTACATGCCACATTTACTGAATTCCAATAAACATATAGTTCTTCTGTGGAGTAGTTAAC
AGTAAGTGGCAGCTCACTGAATTTCTCCCAGGTTCTGTCTCTTCCAAAATCCTCCATCCTCTCTTATGAAGGGAAGCTGATAAAAA
AAAATCCTCTTGGTGCAAGCTGAAGCTGTTAAGGATTCCTTTTTTCACTCTCAGGACCAACAGACGTTCTTTTGTATTTCAAGATAA
TTTCACCTGTTGTTGTTGTTGTTGTTGTTGTTGTTGTTGTTGTTGTTGTTACAAAGAAACAAATTTTGAGCAGCAATGACAATTC
AACCATATCTAGATTCTCCCTACCTTATTTCTCCAGCCAGTCACACCAGGCAGACGGGTAACCTTTAACAGACCTGGTGTTCTCAT
GGAATACCGATGCTCGTCCCAGGGAGCTGACCTTTCTCACTATGTCCTTATAGAGCTGCTCTTACAGAGAACTTTGTGCTCAGGAC
CAAGGGATGGTCAATTAAAAGTTGCATGTAAGCATCAGGCTTGGATGGGCAAGGGAGGGCTTTTATACATCTTTGAACGACCAGG
TCTTTCCTTGTCTGCCTGAAGGCAGAGCTTCGAGAAACAGCACTTCCCATGTGTCTGGTCCTCTTGGTCTCTCAGCCAGACACTTAA
TCAATCCTGGACTCTCCAGTAGTCCTCAGTCATTGTAGCCATAGCATCTGCAAAAAAAGAAATGCTAAAATAATCATTAGCGTTTT
CAAAATTAGGAAATCAAAGTAGCTGGGTCACTCTCTTACATGTGTATGAGCCAGTTAATTCTGCTGGACAGATCATACTTACGCTG
CTGATTGACTCTTCTGAGCAGTAACACATCTCCTGAATTAATTAGGTAGGTCCCGTTTGGGTGCTTTAAGTGGGATCAGTCTTAGA
TGAGTGCCAGTATGTGATTGAATTTCATACGCACAAATGCCATGATTCAAGTTCTCTCTCCAGTTTTTCTTATAGATCAACACACA
GTACATGTGGTCAGTTACTTGGTTGAATTTCTGCTTAGCTGTGGTAAGAGACAGAGAAAGGGAGTGAGGTGGGACCAGGGGAATT
ATCAGAAAGACATGAGTGAACCTATTGGCCAGGTAGCTTCCAAGTATGTTCTATTGTATTGTCTGTTTTGATTCTGATAGTTTAGA
ACTCTTTCTGATAGTTTAGAACTCTTACCCAGTGGTTACATGACTGATCAAGGCAACTCCATCTGGAAATTAATTGCTTGGGTAAA
ATGTCCCTGAGTTTCAACTTGTCTTTTATCTCTGGATATTCTCTTATGAGATTATTATGCATGTTTCTGTCACATGGGCATTATTTAC
ACACTTGATAAATGAAAGGTATTTCTCTGTCCGTTCAAGGAAATAAAATGTAAGTTCTTGTTTTATTAAATGAATGAAGCCTTTTG
GTTAAAAAAAAAGTAATGTAATATGTTTCTGTTCAAACTTGAGCTAATGACATTTAAGGAATTAAAGACATTGATCTAGTTCTTAG
TATGAAAAGTGTACATGTAGATATAGTTATATAATTGTGTATATACATATCTACACACATGGTTGGTTTTATATTGCTTTTTCATCA
ATATTTTTGACTGAAACCTTTACAATAAATTTTATTTTAATTATGTAACCACTAATATTTTGAGAGAAGGAAGCAAATGTTATATGT
CCTTCTGTTAAAAGAAAAAAAATTCAGTCCTCCGCCAACCGCTTCCCACACACTCATACTCTGCACATCTTGGCTACATTAAAATG
GACTGACAGAATTATTTAAAAGGCACTATGAAGGTAGAACACTACCTTAATATTTTATCCTAGTCAGAAGCCTGATTTAACACTGA
ACTTTGAAGGGAAGCTTAGCTGTAGCTCATGGCTTTCAAAGATTAGAAGAAACATTTACTGGTTCTATGGAAAATAGTCTTCTTGC
TAGGTAGATTGGAAACAAAGAAATTGCATTGGTGGTGTTAAAATCTAACATTTATAACAAATCCTGTTTTATTCTAGATGAAATAC
TTAGACAATTCTTCCAGTGGAAACCAGTGAACTTTTTTAACAGCTTTGGGAATTCTTTTGTATGATAATTTTTAAAATGAAATGTGT
ACTCTTCAAACTAATTAAAGCTTGAAGTTTTCCAGGAGTCGCATTTTAAAAGTGTTTGTACACATTTTAACACTTGGATATTTTCTA
TTTTGGTTTTGTATATTTTTATGTATACACAATGTACAGACTTTTTTCTTGTAAATAAAACATGTTTTCATTTGTCTAGAA3’

A.3 pFmiR-CD98hc map and CD98hc 3'UTR sequence

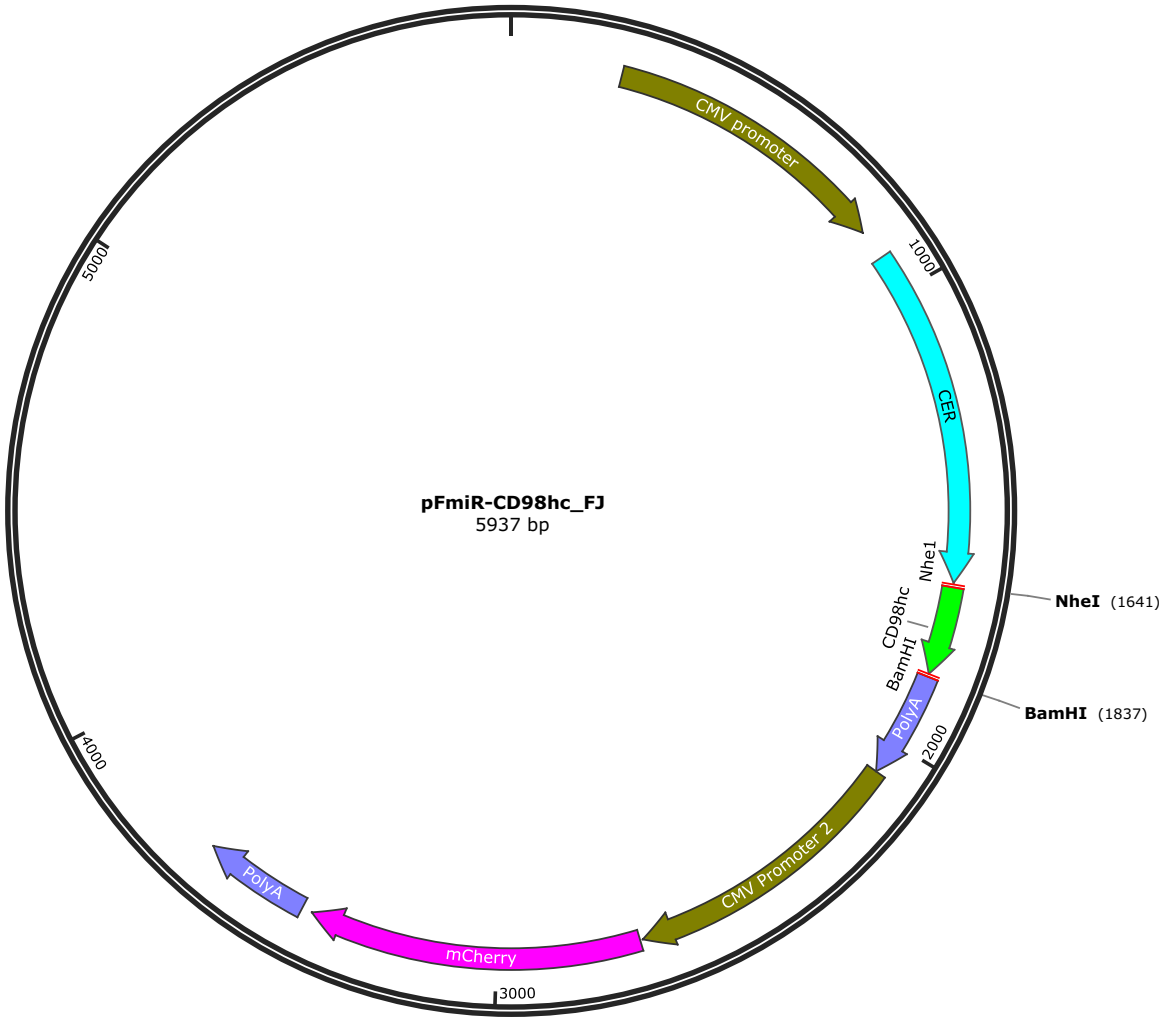

5’CTTCAGCCTGACATGGACCCACTACCCTTCTCCTTTCCTTCCCAGGCCCTTTGGCTTCTGATTTTTCTCTTTTTTAAAAACAAACA
AACAAACTGTTGCAGATTATGAGTGAACCCCCAAATAGGGTGTTTTCTGCCTTCAAATAAAAGTCACCCCTGCATGGTGAAGTCTT
CCCTCTGCTTCTCTCATA3’

A.4 pFmiR-ST3GAL1 map and ST3GAL1 3'UTR sequence

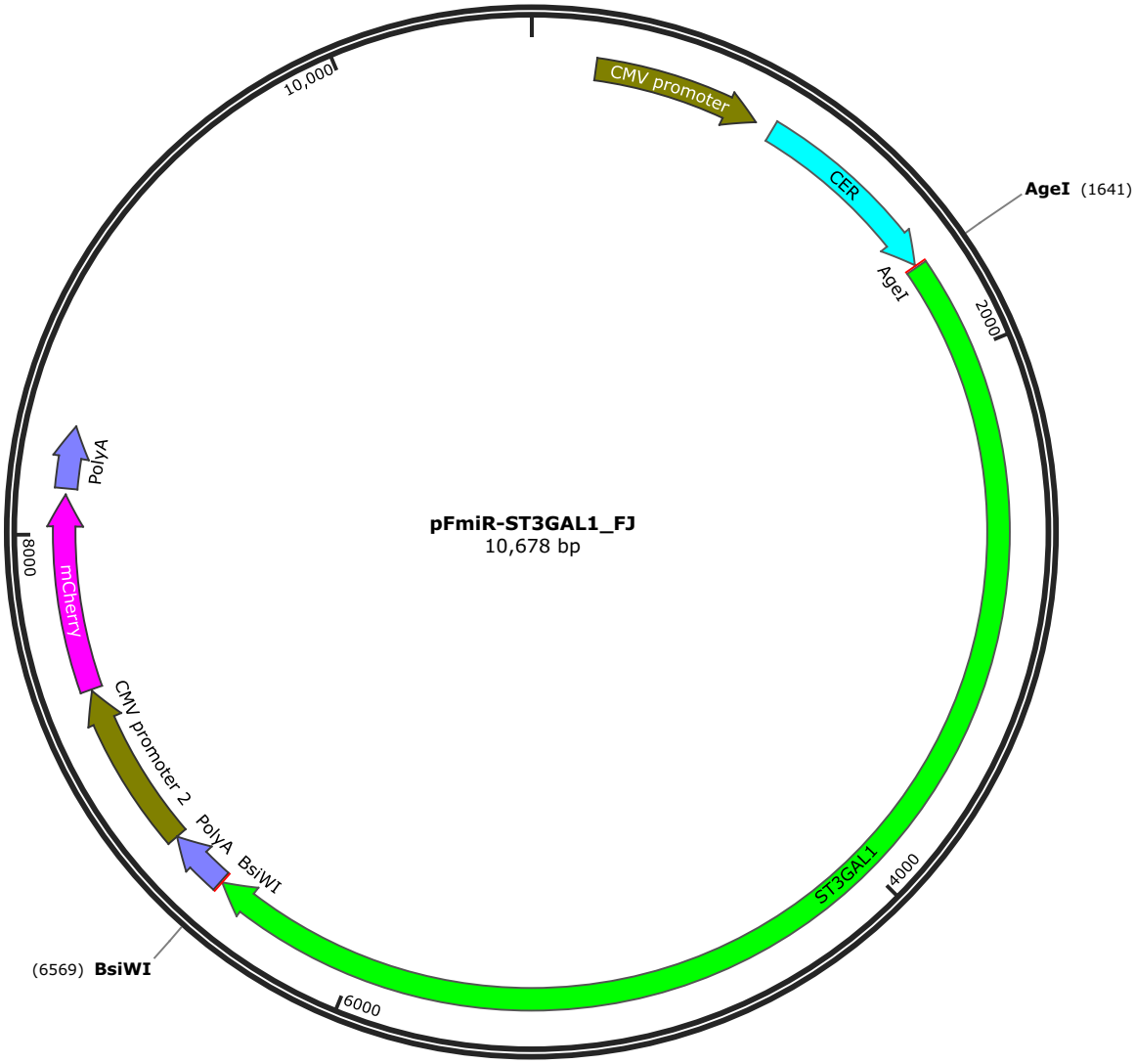

5'CGCAGTGAAGGGCTGAGGATGGACGCACTGTCACACCTCTGCATTTCCAGCCCCAGCATCTTGCTGGAGCCGTTCCATCCCGGA
GCTTGGAGGGGCAGCCTCAGGTGTGTGCCTGGGCACCGCTCACAGCCTCTTGCACCCAGCCGTTGGCAGCATCTACTCAGCAAGG
TCACTAAGCTCTGCCAGCGTGGCAGAGCATGTCTTGGAACCTGTCTTGAGTGGGGACAACGTCCCCCCACTGCTGCCCTAGAGCT
GGGGAGACGCTGGGAAAGGTTCAACCTCCACACACTAAAATCATTTTGGCTCCTGGGGCAAGCTTGGGGAATGAATGTGGAAGAT
GCCTATATTCTGAGAGACAGGACAGTTTCCCAGGAAGATGGGCAGAGACTTGAGTGGCGATTACCTCCAGCACAGAGACGTGCCA
GGCGGTGTTGGCGCTCGGGGCGAGATGCTGCCCTTCTTTGCACGAAGCCTGGCCTCTTGCTTGGCGTGATAACCCTGTCATCTTCC
CAAAGCTCATTTATGAGCCACCAGAGGCTCCTACCCCAAAGATTTTCACAGAAACTTGAGGCCAGGTGCCGTGGCTCACACCTGT
AATCTGAACACTTTGGGAGGCCGAGGCGGGAGGATCACTTGAGCCCAGGAGTTCAAGACCAGCCTGGGCAACATAGTGAGACTC
CTGTCTCTACAAAAATAAAAGATTTAAAAAAATTAGCCAGGCACGGTGGCACACACTTGTAGCCCCAGCTACTAGGGAGGCTGAG
GAGGGAGGATCTCTTGTGCCTAGGAGTTCGAGGCTGCAGTGGGCTGTGATCACACCACTGCACTCCAGCCTGGGCAACAGAGTGA
GACCCTGTCTCTGAAAAAAAAAAAAAAAAGAAAAGAAAAAAAACCCCAAACTTGGCACCGTGTTTCTGACTCCTGCAGATGCCTCT
TCCCAAGCAGTTGTTCCTTTGAGTAGTCAGTCTCATGGTTCTAATCGTGGCGAGAGCGGATCTGACCACTTCCATGTGCCTTTGTAT
TTGGGAAAGAAAAGCATGCATTGGCTGAAATGAAACAAAAGCCCTTACTTGGGAAAAGGGACCCCCACCAGCGGCCCTGCTTGC
TCCGTAGCTGGGAACATCTTTTCTGGTTTCCTGAGCCAGCACCTGAATTGCAACGAAGCTCTGAGGATACTCAAACCACCCAGCA
GTGCGTCAGAATGGAACGTACATTCTCATTCTCAGACTGTTCAATATGGTGCCCGTAACCTCCAAAGCCACACAGGAGGCTGCCA
GCAGCATTTTCCCCAAGGGCCTGAGCTCAGGGTCAAGTCCCTGCTGGCCATCTTGGGGCTGTCACTGGGGGTCTGGGTCAAGGAC

ATCCCAGGAATGGTAACTGCCACATACCTCATCTTCTTACTCCCCAGCTACTCTCTTTTCCTCATTAGCCTTCCTGATTATTTATTGA
TTTCTTTTTTTTATTCAACTGACATTGTTTGCACCCTGGCTCTGTTGGTGGTCCTGGTGTTTTAATGAAGCTTGCCTCACCCAGTAGC
TGGGAAATTAGGTGGGGGTGCTTAAGGGAGGTTTGTAGGAGTCCTCGGACGTGGGATATTGGGGGTATCTAGGGCTTGGATGGTT
TGTGGAATGTCCTCAGCATCCTCCCGTCCCAACCCAACCTTCCTTCTTCCTCATTGTGGACTTGGATTTATTCTCAGGCTAGGAGTC
TCCAAAACTCCGTGAAACCTTATTGCTGCTGGGTGTGGAGTGGAGAGTGACAGGAATGTGGGGGACGGTGATTGTTGGCTCCAGT
TACTAATGTTTAAGCAGAAAAACCACTTTCTTGTTGAAAATATCCCTGAAAAGGTCGCTGCTGCTTTGAGGAGGCGTGACTTTTTC
CTGGTGGAGTGTGACGGAGGCATGGGGCCTGTGCTCCCAGGCTCGGGGGAGCCCCCTCTGCACACGGGGAGGGAGGAACTTGGG
GACATCAGTCATGGGTCACAGGTGGCTTCAGGCCATTCACAAGAGTCCCCGGAAGTTGCGTGCCAAGTTTGGTTTTTTCCCTGAAT
CTCTGCATATGAGCATTTTTCTGGAGAAAGGACCATAGCTTTTATTAGATTCTCAAAGGTTCAGAATGGGGAATGTGTTAAACAAA
CCGAAAACCTGTTTCAGCTTTAAAATCCTCCAAAACTTTAAAGACTTTTCTTTTTTCTGAGAAAGGCTGGTAAATCACTGAGTCAT
CATTCAGAACATACAGCCTCGAAGGGCAGAGCTCACACCCATATATGACGTTAAGAGCTCAACAAATGTTTGTTGAGTGACTGAG
TGACCCCAGGGGCAGACTCCAGATCATCAGACACTGATACAGAGAGCGATGCTATCTCCTCAACTCTCCCTCTTCTCCTAAAAGCT
GAGTCTATATAGGGATGACAGGCTCAGGCTGAGCAGTCGACTTCTCTGGGTTTTGCTGTGTAAGAATAGGTCCCTCAACATGAAG
ATGTGTCTGCGTCTGAGCCAGATGCTGCCTGGGTCGGTTGCCTGGCCTCCGTCTGGTCTCCCTCCCTCCTACTAGGGTGGTCAAGC
TGTGAGATCTCTTCCAGCCTCCAAATCCAGCTTTCCCATTTTACTGATGAGAAAATCAAGGCCACATTGCAGCTGGGTGGGGAGTG
GAGCGTGACAGGCACGGGAGAGGACAGCGATTGTTGACTCTAGTTCCTGATGTTTAATCAGAAAAACCACTTTTCCTGTAGAGCA
CATTTCCTAAAAGGCTGCTGCTGTGTAGGGAGGTGTGGCCTTTTCCTGGTGCAGTGTGAAGGAGGGAAGTGACGGGCAGTCGTGA
ACTGTCTGGGACAGATAGCACAAGTCAGAGTTTGAGCAAAACTAGGGTGTTACCGGCGCTATGTTGAAATTGTCTGGAGGCGGGC
TTTCCCAGCGAGTCTCCATTCAGCATCTGGAAAAAGTGTAACCAGAATGGAGGTGTCTGACTCTCCTGTGCTCTCTCAGCGCCGAG
CTCTAGCTGCAGGCTGCCTGGGTGGCCTTCTCACACCCTCCCGTGCAGGAGACTGCATTTCTCTTTCCCACAGCCCAGCAGATAGC
TCATTGGCTTAGCAATGGGCACTTAACAGAATCCAGTTGTTGCAGCCAGAATTAAATGCACCAGTCTGGCTTAAACCAACTGGAA
CTCATCCCTGGGGTGAAGGTGGCTGGGAATTAGACAAGAGTGTGTGTTAGCCAAAAGGCACATGCATGCTGTCAGCAGGAGAAT
GAGGAGCACTGGTTCTGGGCAGGCAGTGGCAGGGGCTCCCTCAGGCCCCTGATTCCCAGCCCACAGCTCTTTCTACTCTGCAGAC
AGAGTTCCTTGGAGACTGGCCCTGCATTCAGGCAGGGAGCAGAGGGGTCCCTGCCTGCAGCACCCAGAGCTGAACCTGAAGCTAC
AAAGATGGGCTGATGAGGTGGCCCATGAGGTGTCAGCAACATCCCAACCCCCTGGGTCTCCCCAGTGAGTCAGGGCACTGATTTG
CTATAGCTGGAGCTACATGCACCTCTCCTCCCCTCAGCCACCTTTTAGGGGAGAAAGGAGGGCAGATTTGTAACCTCTGGTTCTCT
GCAGGGATCCTGGGCTGGAAGAAAGTTCATAAATGGATGAATGCCTTTTAAAACTCCAGCTTTTCCAAGCATCATTCACCAAAGC
ATTTGGTTAGGCTTAGAGAGAAAAGCTGGATATGAGAAAATAGAATGTAAAATAGGAGGGAAAAAAAAAAAGAAGGTGGAGAG
GGCAGTTAAGATCTGGGTGATTCTTTAGGGAAACGGCTGGTTGAGAGGCTTTGATGGAATCCCATTCTCTGCTGTGGCCAGAAGG
TGGTGCTAGAGGCCAGTCCCACTTGGATGTGACCCTGGCCTCTGCCAGGATTCAAACCACAAAGAACATTTGGAACTGGGATGTT
TGCTTTGAAGCAGCCCGAAAACAAGTGAAAGGAAACCAAGATAACTCTCTCTCCCTCCGCTGGCAAGGATCAAAAATACCTTGTG
CAGGGAAGCCCGAGCCTCGAGGGGCCACTGCCCAGCTAAAGATGACTGGACACCAGCCATGCACCATCAGGAACCAGCACCTGT
CCTCACCCCTGAGAAGAGCCCCGGGGGTATCATTATATCCATCGCAGACATCTGGTTTGCAGCAAATGTGGCTACACGCCATCAG
GATTATCCTGCCCTGTGGACTGGGCTAGCTAGTTTTGAGATAGAGTCAACCTCCCCATTTTTGTTTGTCATGAAAACACCAGCTCCT
GCACCCCTGGGGTGCTACCTGACACCTGTGCAAAGAAAAGGAGGAAAACTTAGAAGAAAAGGCAGAGACAGGCAAGACAGCAT
CTCACAGCTTGTCAGGATCAGGGCATTACCGACTATTTTTTCTTACCAAAAGAGCACTGAATTTCCTAGGGGAAGGTGAGCCACCT
TTACACCTCCTGTCCTCCCTCCCAGCCCGTCAAGCGATCCCATCACCCAGCCTCATCACTCAGCTTCTTCCTAGTACAAAACTGCCA
TCGGTTGTACGTCCTGAGCTGTGGGACGTCAGCTTTAACCCTAGCCTGTCTCAGGGCCTCGCCCTCCAGCCCCCCGCCCCTTAGGG
TGATCGTGGGTTTCTTCCCTTCCTCCTGCACAATCGCTTCCCTTCACTGAATTCCCTTCAAAGCCAAAGTTTCTTGAGCACTTTTTCT
TGTGTGCAGTCTTGTGTGTTTGGGTGTTGGTGTTTTTAAATTTGCTTTCTATTCCCCCCTGCCTCTCTCCATGTCGTTACGCAGCTGA
GCACTGGTTGGGATGCATTCGAATGACTTCAGCAAGATCCTGCTTTCCTCAGCCCCCGCTCTGTTTTATTTATTGTTTAATATTTCC
AATGATCCAAATCAAAGTGAATAAACAAAGAGCTATTTTATTGTT3’

A.5 pFmiR-ST3GAL2 map and ST3GAL2 3'UTR sequence

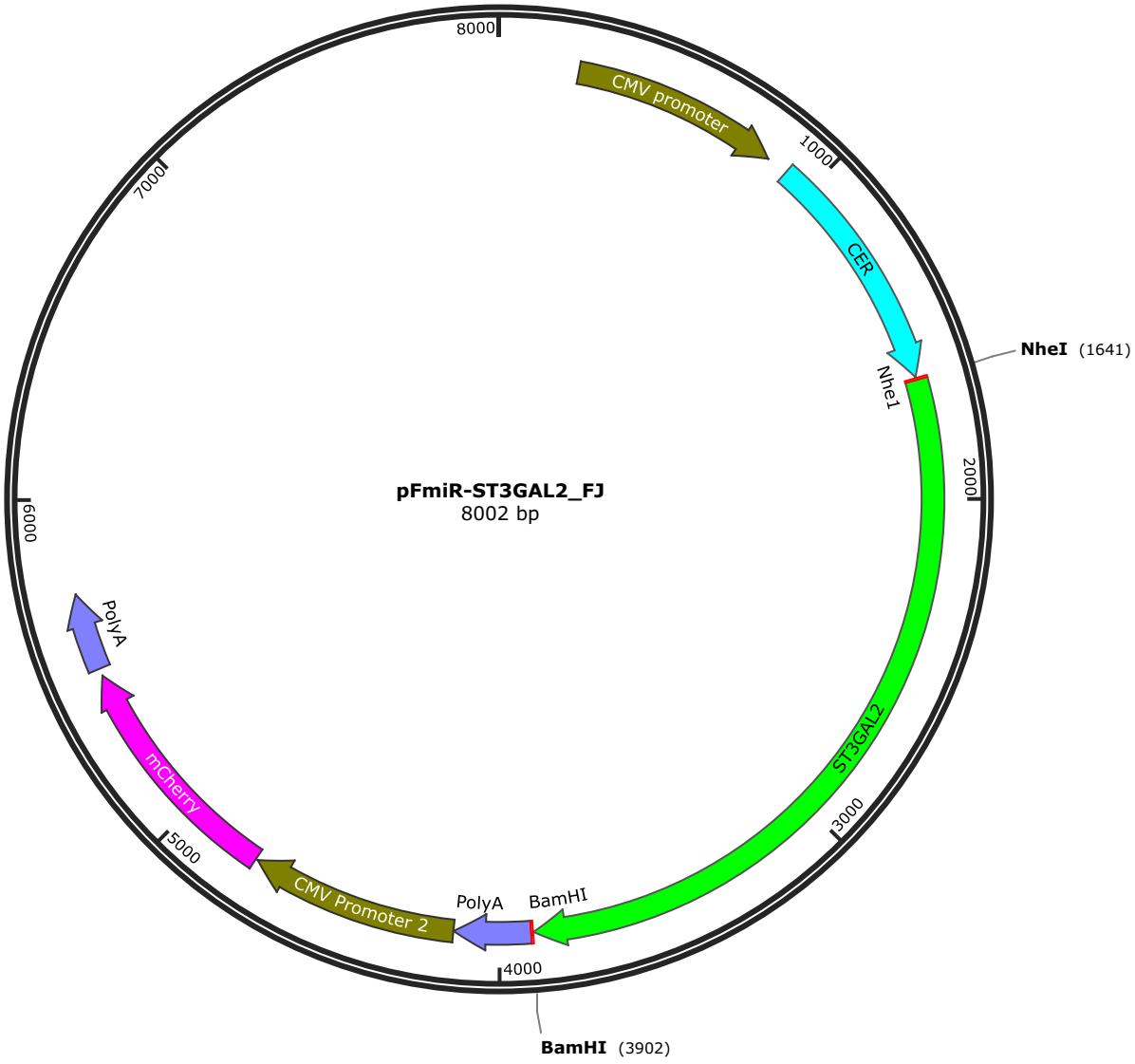

5'GCCGGGCCTCGCCGCGACCCTTCCGGCCCATCTATCGGGCACCGGGGCTCCGGCCCGGGACCCAGGACCAGCAACCCGCGACC
AATCATGCTGCAGCCCAGGGGCGTCTGCTGTGCCCGCCAATCACGAGACTGGGGGACCGGCCGGGCCTGGCACCAATCTGCGCTG
CGGTCGGGCGGAGCTTCTGTTTCTCCCAGCCAATCATGTGACTCAAGGAAAACTTCCGGCGCTGTGTCCAGTCTCCTCCAATCAAT
GGCCTTCGGGGGCGGGCCAGCGGCCGCTCAATCCCCACTCCCTCATGCTTTGGGTTAGGGTTTTCTTTCACGCTTTCTGAGGAGGA
GAGCATGGCGCGGGCCTCGGCGAAGCACTTCCGTCAGCCTCGGGCGGAGGATCGTCTTAGTAGCTGGCCAGACCTGGAGGAGAG
CGGGCGGTCTTTGCGGGCCTCAGGAGATAGGTGGCCGCCCGGCCCCTTTCCCCGCCTGCCCGGATAGGTGCGTGCAGACCCACCA
AAGAAAAGCGGTCGCTGCGGGACCCCCAGTCCCACCTCGGCCGCGCTGTGGGATGGCTGCGCCCCCAGGGCTTCCTGCGTCTCCA
GGAAGCCGGGAGTGGCGCCCTCTGCGGGGTGGGGTGCTCCCGGGCCGAACTCCGGACAGGTGGAGGGGACAGGGCAGAGCTCGA
GGAAGCCCTGTCCCCTTCAGTGCAAGGTGCTGTCACTCACGTGTGCCCTCGACCCTCCCGTTCACCCGCAGCCTTCTCAGCGCCTC
TCCCTGGGCCGGAGGCCTCCTCACCAGCCTACCTGTTGCTCTGGAAAAAAATCCCGTCCCCCGACTCCGTCCCTACCCCCAGTCTT
CGGCCGGCTCTGGCCCCTGGGGAGGGGGCTGCACGGCGGAAGGAGGCTGGCTATGGGCCCGGCTGCCCGCTGCATGTACCTCCTC
CTCCACCCATCGCCTCTTGCCTGGGGGTAACTTTGCCTGGGGCTCATTCTTTGGTTAAGCTGAAGCTGCCGTGGGTGGCCAAACCG
CAGATTCTTTGCAAATTCTGAGCTGGCAGAGCTCGCAGCCGGGAGCCGGCCGGGGAAGAGGAGACTTGCGCGCCGCAAGCCGCC
TGCCTCCACCCTGCTCTCCATCTCCCGCTCTAGAAGGGCTGGGAAGCTCGCGGCCGGGGTTCCACCTGGAAGCTGCTTGCATGGCT

GAACCCAGCTTAGGTCCCTGACGGGGCTGCTGGTGGAATTCTCCCCCTTCGAAGCTGGGGAGGTTTAGGAGGGGGAAGGCTTCTG
TGAAGCTCTCAAACCACTAATAGAGCCCCCTCCCCAACAGTGACGGCGCAGATGCTCCCCCTTTTCTTAGTTGACACCACCAGGCA
GCTTCCTGGCCGTTGGTAGGTTCCTGCAGCTGGCTGAGGGAACAGGGACCGGCAGGGGACTTTGTTAGGGGAGGGTTGGGATGGG
CAGTGGGCCCCTGAAAGTTAATATATTGGAACCTAGCTCGAGTGTCGTTCTTTCCAATTCCGAAAGTAGAAAGAGTAAAAATAGG
GGTGATTGGGGTGGGGTTAGTAGAATGCCTCTCTCAGGGCGCTCCCCCCTCCCCCACCGTTTTAGAGAGCTAGGCCTCAGCCAGTC
TTGCCACTCCCATCTCAGTGCTTCCTGAAGAGGCTGTTTTGAGTGTTGATGAAAAGCAATGCAATTATGCCAAACAGTATTGAGCA
GAATAATTTATTTCTTTTTTTTCTTTTGCTTTAAATCATGAATCCCGCCAGGTACGGTGGCTCACACCTGTCATCCCAGCACTTTGG
GAGGCCAAGGCGGGCGGATTACTTAATACTTAAGGTCAGGAGTTCGAGACCAGCCTGGCCAATATGGTGAAACCTCGTCTCTACC
AAAAAAAAAAAAAAATACAAAAATTAGCCAGGCGCAGTGGTGCGCACCTGTAATCCCAGCTACTTGGAAGGCTGAGGCAGGAGA
ATCCCTTGAACCGAGGAGGCGAAGGTTGCAGTGAGCCGAGATTGTGCCACTGCACTCCAGCCTGGGCGACAGAGCAAGACCCTG
TCTCAAAAAAATTAAATCATGAATCCCCATCCTGGAAGAGGTAGGTCCCAGCATCCAGCCAGATTTTCTGCAATAGTAATTTAAA
CACACTTTTTTATTTCCTTCCCTTTCTGAATTAAAAGGAACAAAAAACTGTCTAGTCCTTCATTGTTCTGAAATGGGCATGATGGAA
GAAGGCGGGTCTGGTAGGATAGCTGTGACTGATAATG 3’

A.6 pFmiR-ST3GAL5 map and ST3GAL5 3'UTR sequence

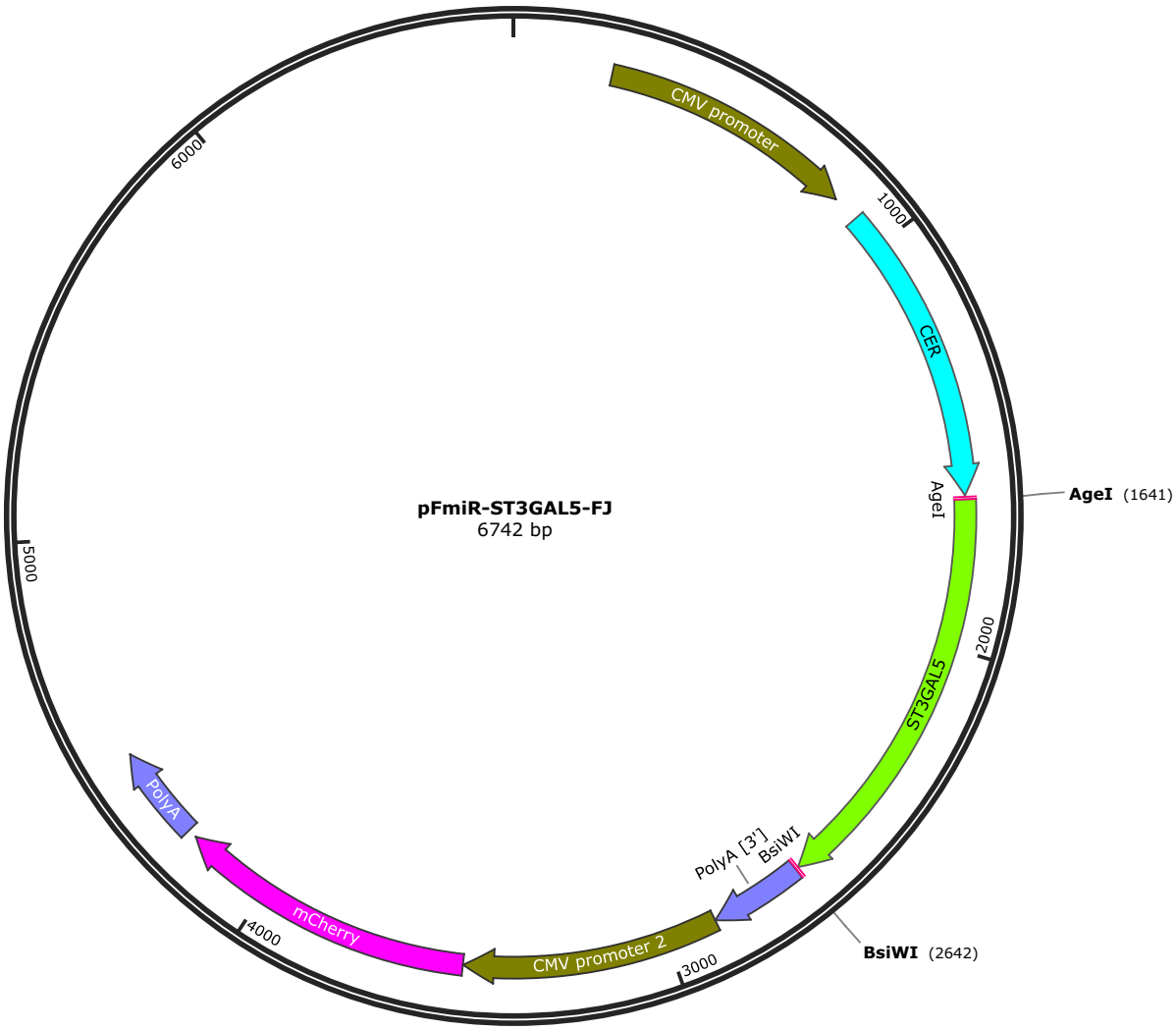

5’ACACAGAAAACCTCAGTTGAAAATGCAACTCTAACTCTGAGAGCTGTTTTTGACAGCCTTCTTGATGTATTTCTCCATCCTGCAGA
TACTTTGAAGTGCAGCTCATGTTTTTAACTTTTAATTTAAAAACACAAAAAAAATTTTAGCTCTTCCCACTTTTTTTTTCCTATTTATTT
GAGGTCAGTGTTTGTTTTTGCACACCATTTTGTAAATGAAACTTAAGAATTGAATTGGAAAGACTTCTCAAAGAGAATTGTATGTAA
CGATGTTGTATTGATTTTTAAGAAAGTAATTTAATTTGTAAAACTTCTGCTCGTTTACACTGCACATTGAATACAGGTAACTAATTGGA
AGGAGAGGGGAGGTCACTCTTTTGATGGTGGCCCTGAACCTCATTCTGGTTCCCTGCTGCGCTGCTTGGTGTGACCCACGGAGGAT

CCACTCCCAGGATGACGTGCTCCGTAGCTCTGCTGCTGATACTGGGTCTGCGATGCAGCGGCGTGAGGCCTGGGCTGGTTGGAGAA
GGTCACAACCCTTCTCTGTTGGTCTGCCTTCTGCTGAAAGACTCGAGAACCAACCAGGGAAGCTGTCCTGGAGGTCCCTGGTCGG
AGAGGGACATAGAATCTGTGACCTCTGACAACTGTGAAGCCACCCTGGGCTACAGAAACCACAGTCTTCCCAGCAATTATTACAAT
TCTTGAATTCCTTGGGGATTTTTTACTGCCCTTTCAAAGCACTTAAGTGTTAGATCTAACGTGTTCCAGTGTCTGTCTGAGGTGACTT
AAAAAATCAGAACAAAACTTCTATTATCCAGAGTCATGGGAGAGTACACCCTTTCCAGGAATAATGTTTTGGGAAACACTGAAATG
AAATCTTCCCAGTATTATAAATTGTGTATTTAAAAAAAAGAAACTTTTCTGAATGCCTACCTGGCGGTGTATACCAGGCAGTGTGCCA
GTTTAAAAAGATGAAAAAGAATAAAAACTTTTGAGGAA3’

A.7 pFmiR-CMAS map and CMAS 3'UTR sequence

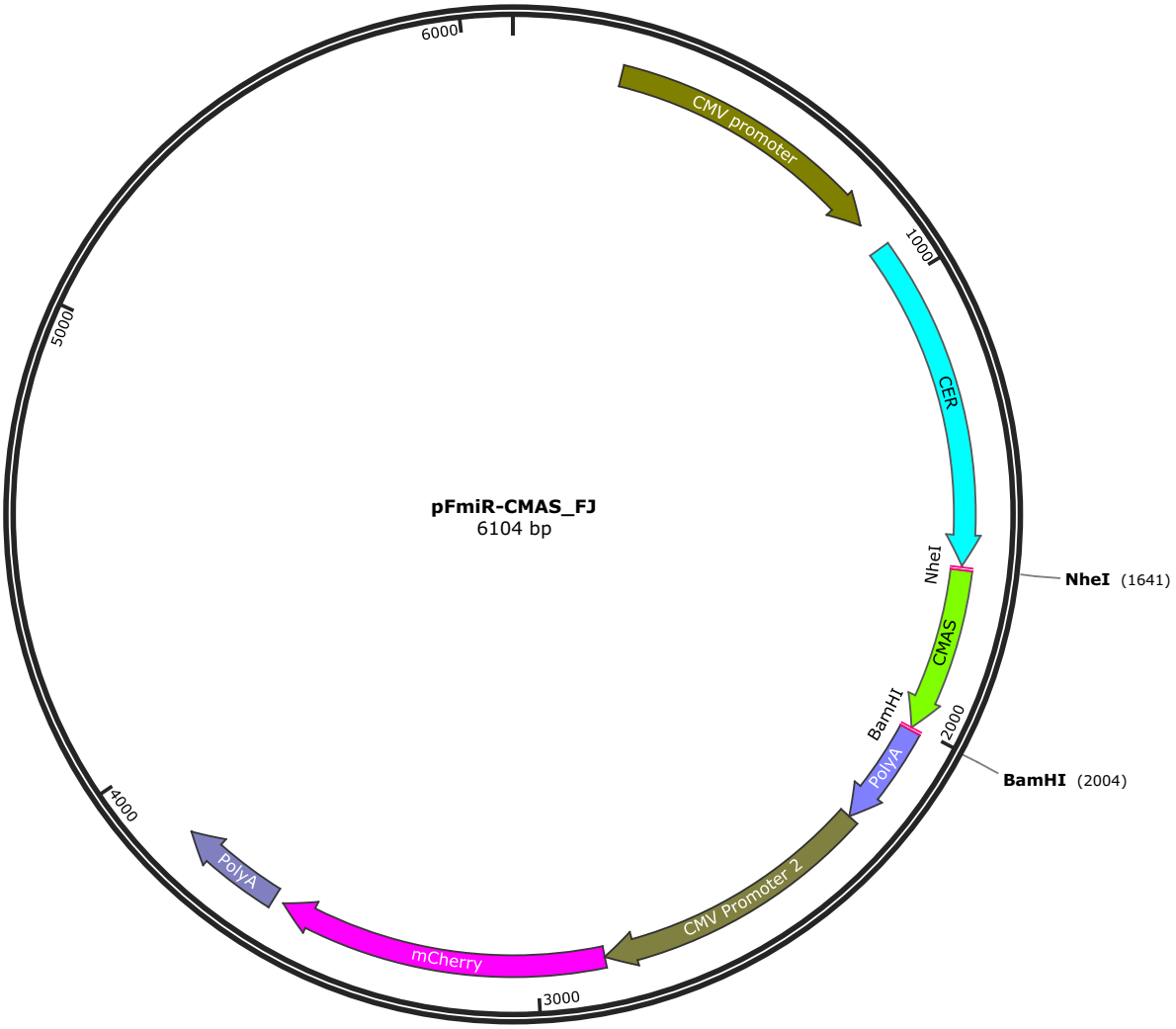

5’AAATTAGCGTAATATTGAGAAAAAAATGATACAGCCTTCTTCAGCCAGTTTGCTTTTATTTTTGATTAAGTAAATTCCATGTTGTAAT
GTTACAGAGAGTGTGATTTGGTTTGTGATATATATATATTGTGCTCTACTTTTCTCTTTACGCAAGATAATTATTTAGAGACTGATTACA
GTCTTTCTCAGATTTTTAGTAAATGCAAGTAAGAACATCATCAAAGTTCACTTTGTATTGTACCCTGTAAAACTGTGTGTTTGTGTGC
TTTCAAAGATGTTGGGATTTTATTTATCTGGGGACAGTGTGTATGGTAAGACATGCCCTTCTATTAATAAAACTACATTTCTCAAACTT
GA3’

Appendix B

Signal Validation for Primary Antibodies

B.1 Anti-ST6GAL1 1° antibody signal validation. a. Ponceau staining. **b**. Whole Western blot for A549 and PANC1 cells treated with siRNA pool against ST6GAL1 or non-targeting pooled (NTP) control.

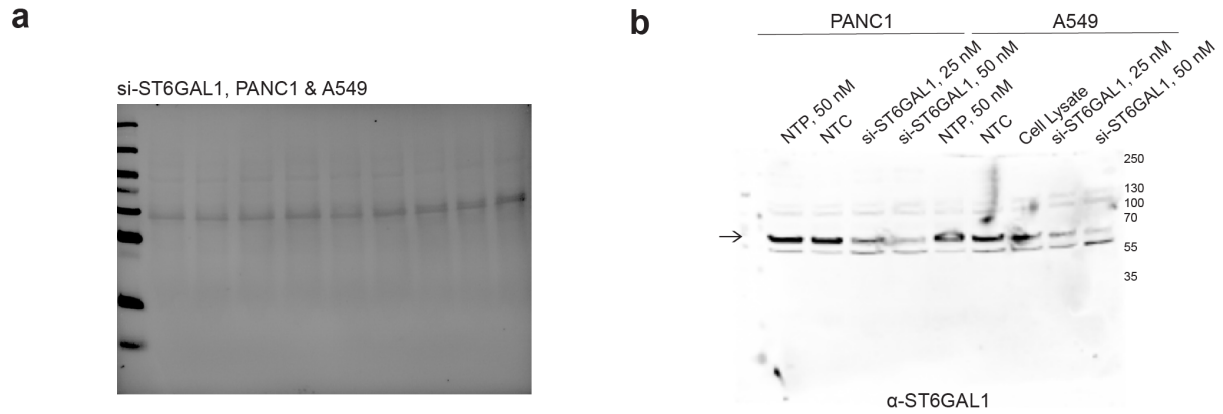

B.2 Anti-CD98hc 1° antibody signal validation. a. Western blot analysis of MeWo cells treated with siRNA pool against CD98hc or NTP. **b**. Quantification of blot shown in a. **c.** Ponceau staining of blot shown in a. **d.** Whole Western blot for data shown a.

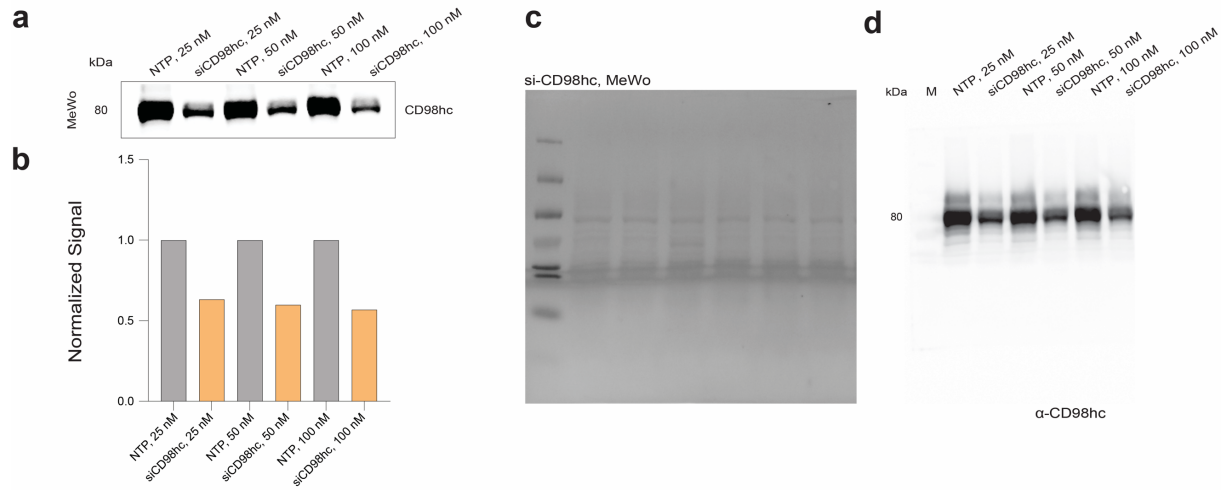

B.3 Anti-ST3GAL1 and anti-ST3GAL2 1° antibodies signal validation. Cells treated with siRNA pools against ST3GAL1 (a-b: HT-29), ST3GAL2 (c-d: MeWo) or NTP. **a, c**. Ponceau

staining of blot shown in b and d. **b, d**. Whole Western blots for HT-29 (b: ST3GAL1) and MeWo (d: ST3GAL2) cells.

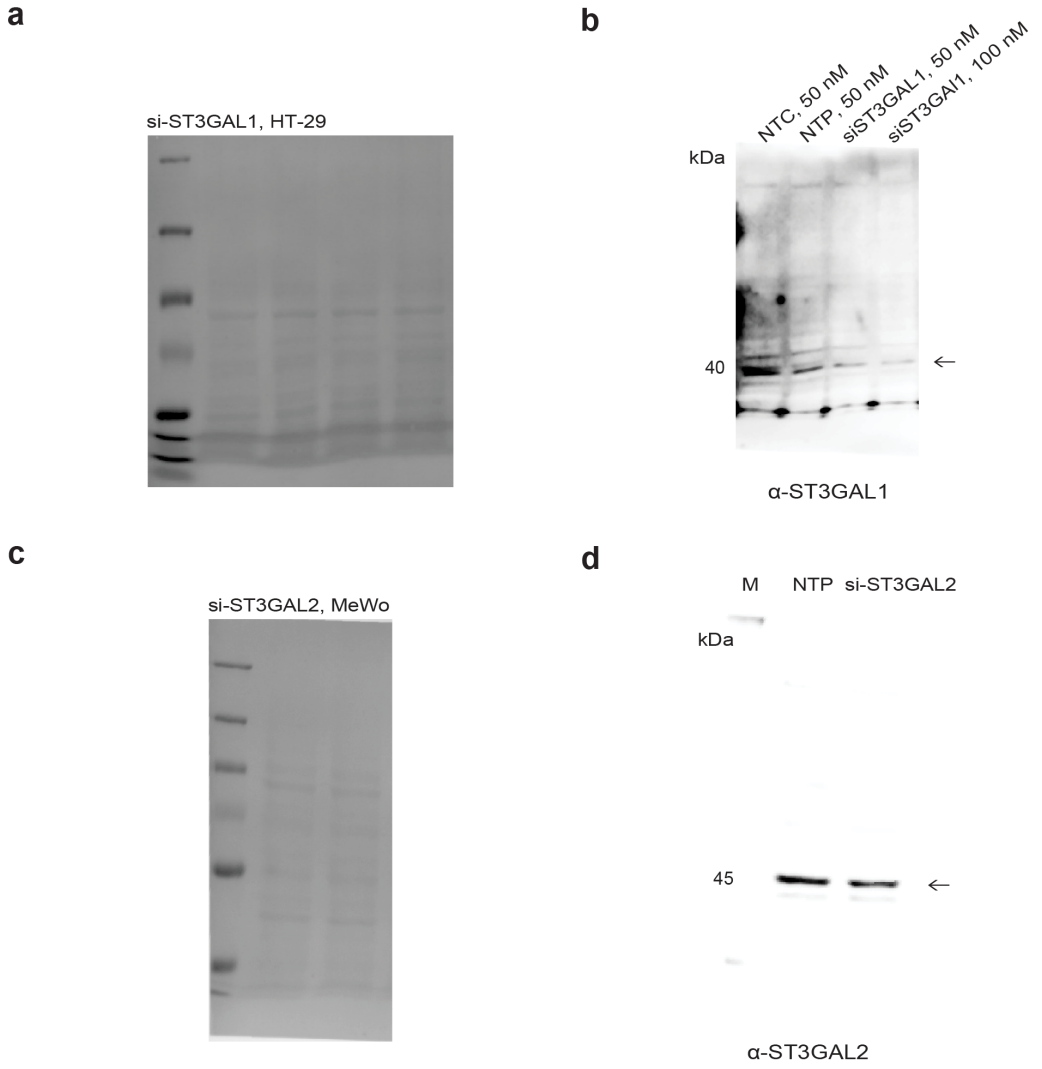

B.4 Anti-ST3GAL5 1° antibody signal validation. a. Western blot analysis of MDA-MB-231 cells treated with siRNA pool against ST3GAL5, NTP or NTC (as controls). **b**. Quantification of blot shown in a. **c,d.** Ponceau staining of blot shown in a. **e, f.** Whole Western blots for data shown a.

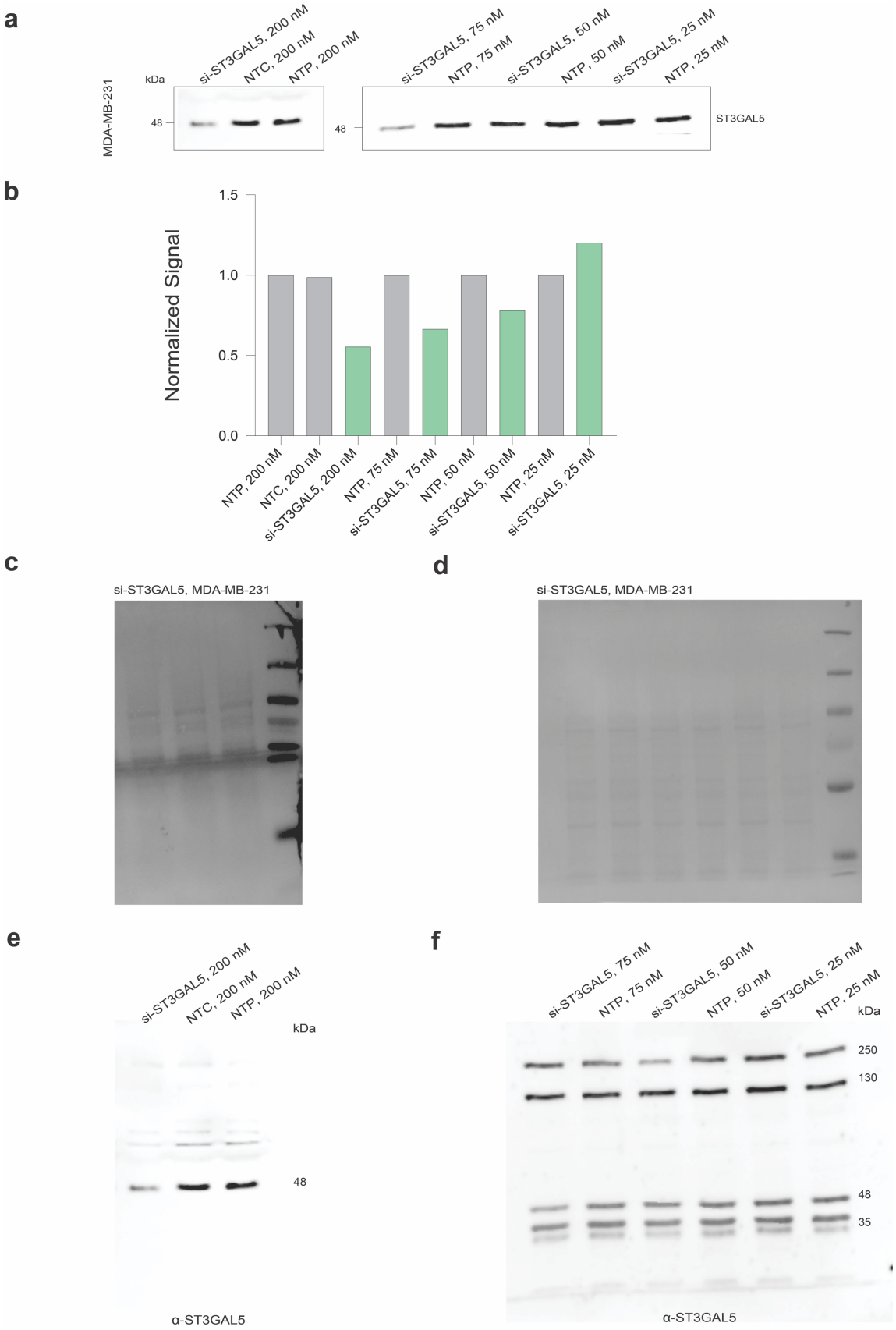
a
si-ST3GAL5, 200 nM
NTC, 200 nM
NTP, 200 nM
si-ST3GAL5, 75 nM
NTP, 75 nM
si-ST3GAL5, 50 nM
NTP, 50 nM
si-ST3GAL5, 25 nM
NTP, 25 nM
kDa
MDA-MB-231
48
48
ST3GAL5
b
Normalized Signal
1.5
1.0
0.5
0.0
NTP, 200 nM
NTC, 200 nM
si-ST3GAL5, 200 nM
NTP, 75 nM
si-ST3GAL5, 75 nM
NTP, 50 nM
si-ST3GAL5, 50 nM
NTP, 25 nM
si-ST3GAL5, 25 nM
c
si-ST3GAL5, MDA-MB-231
d
si-ST3GAL5, MDA-MB-231
e
si-ST3GAL5, 200 nM
NTC, 200 nM
NTP, 200 nM
kDa
48
α-ST3GAL5
f
si-ST3GAL5, 75 nM
NTP, 75 nM
si-ST3GAL5, 50 nM
NTP, 50 nM
si-ST3GAL5, 25 nM
NTP, 25 nM
kDa
250
130
48
35
α-ST3GAL5

B.5 Anti-CMAS 1° antibody signal validation. a. Ponceau staining. **b**. Whole Western blot for SU-86-86 cells treated with siRNA pool against CMAS or NTP.